

Temporal and Spatial Requirements of UBE3A in Angelman Syndrome Pathophysiology



Monica Sonzogni

Temporal and Spatial Requirements of UBE3A in Angelman Syndrome Pathophysiology

Monica Sonzogni

Temporal and Spatial Requirements of UBE3A in Angelman Syndrome Pathophysiology

UBE3A in de pathofysiologie van Angelman syndroom:
Restricties in tijd en plaats

Thesis

to obtain the degree of Doctor from the
Erasmus University Rotterdam
by command of the
rector magnificus

prof. R.C.M.E. Engels

and in accordance with the decision of the Doctorate Board.

The public defence shall be held on
23 September 2020 at 13:30 hrs

by

Monica Sonzogni
born in Bergamo, Italy.

The research described in this thesis was performed at the Department of Neuroscience, Erasmus Medical Center, Rotterdam.

The research of this thesis was financially supported by a fellowship to the author by Associazione Angelman and FROM (Fondazione per la Ricerca Ospedale di Bergamo).

Cover and layout design by Mario Avagliano Trezza

Printing by Ridderprint BV, www.ridderprint.nl

© Monica Sonzogni, 2020.

All rights reserved. No parts of this publication may be reproduced, stored in retrieval system or transmitted in any form by any means without permission of the author or, when appropriate, the scientific journal in which parts of this thesis have been published.

Erasmus University Rotterdam



Doctoral Committee:

Promotor: Prof. dr. Y. Elgersma

Other members: Dr. F.M.S. de Vrij
Prof. Dr. R. Willemsen
Prof. Dr. J.R. Homberg

Copromotor: Dr. B. Distel

Per Emma ed Edoardo

TABLE OF CONTENTS

Preface	9
Chapter 1 - General Introduction	11
Chapter 2 - A behavioral test battery for mouse models of Angelman Syndrome: a powerful tool for testing drugs and novel <i>Ube3a</i> mutants	35
Chapter 3 - (Addendum to Chapter 2) Assessing the potential therapeutic benefits of Gaboxadol treatment in the AS mouse model	77
Chapter 4 - Assessing the requirements of prenatal UBE3A expression for rescue of behavioral phenotypes in a mouse model for Angelman Syndrome	91
Chapter 5 - Delayed loss of UBE3A reduces the expression of Angelman syndrome-associated phenotypes	117
Chapter 6 - Loss of nuclear UBE3A causes electrophysiological and behavioural deficits in mice and is associated with Angelman Syndrome	147
Chapter 7 - General Discussion	207
Appendix	221
Summary	
Samenvatting	
Publications	
Curriculum Vitae	
PhD Portfolio	

Preface

Animal models have been widely used in basic research to address both scientific and clinically relevant questions. This thesis focusses on the use of mouse models to get more insights into the pathophysiology of Angelman Syndrome (AS).

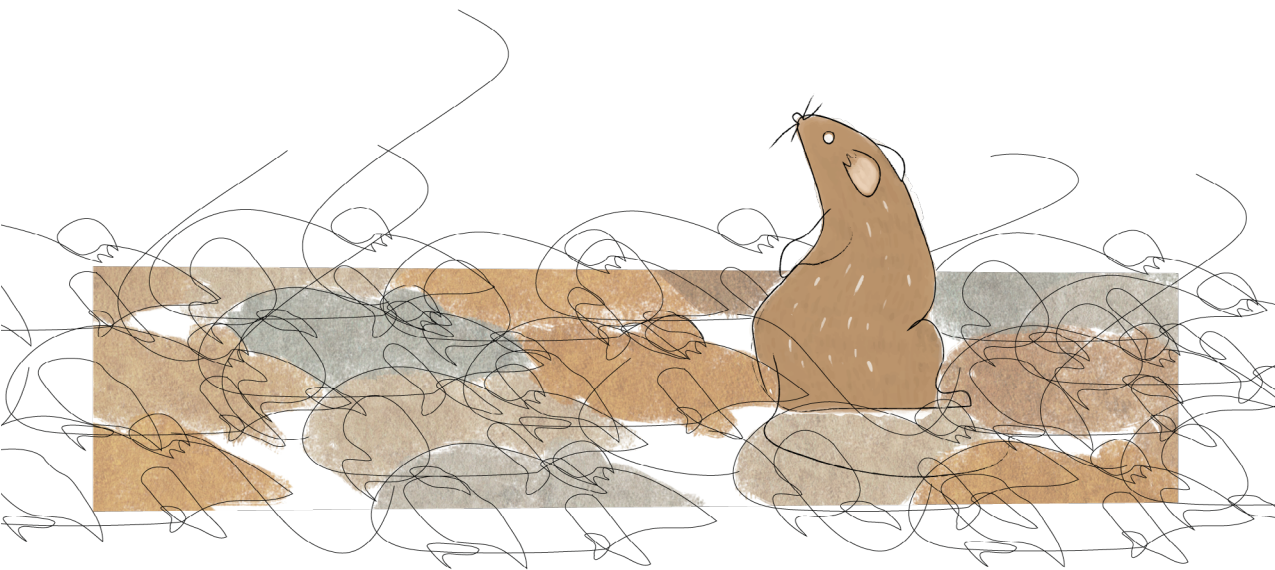
AS is a rare neurodevelopmental disorder, caused by the lack of functional maternal UBE3A gene.

No effective treatments are available yet, but gene reinstatement therapies such as the one that makes use of antisense oligonucleotides (ASO) can be a promising option to treat AS related phenotypes.

This dissertation, taking advantage of the use of a robust set of mouse behavioral tasks, will give insights about when this therapy should start and for how long should last.

And finally, a new viewpoint on the role of UBE3A in AS pathophysiology is given, in which we show that the nuclear localization of UBE3A, rather than its synaptic localization, is critical for normal brain development.

CHAPTER 1
GENERAL INTRODUCTION



Discovery of Angelman Syndrome

Angelman Syndrome (AS) was first discovered in 1965 by the English pediatrician Harry Angelman. He reported three patients with similar characteristics and defined them as puppet children due to their peculiar characteristics, such as flat head, ataxic movements, bouts of laughter and protruding tongue ¹. Excessive laughter and happy-face together with motor deficits are specific behavioral phenotypes that nowadays leads the clinicians to suspect Angelman Syndrome ². Since the discovery of the syndrome, several research labs are trying to elucidate the molecular mechanisms underlying the development of the disease.

Clinical characteristics

AS is considered a rare neurological disorder, with a birth incidence of approximately 1 in 20,000 ^{3,4}. The syndrome is characterized by several clinical features including intellectual disabilities, motor problems, impaired coordination, microcephaly, seizures problems, sleep impairments, lack of speech and high comorbidity with autism spectrum disorders ⁴. First symptoms usually occur during the first year of life, when parents notice the lack of psychomotor activity. By the age of 6 months difficulties in motor coordination are also associated with difficulties in feeding and muscular hypotonia ⁵.

Microcephaly is a characteristic clinical feature which is present in a subset of AS children and that develops during the first 3 years of age ⁶. The occurrence of microcephaly seems to vary not only among populations, for example affecting 80% of the AS Caucasian patients and approximately 37% of the AS Chinese patients ⁷, but also depends on the class of mutation ⁸. This broad spectrum of clinical features makes AS difficult to diagnose, especially during pregnancy when no obvious brain abnormalities are detectable. The fact that the disease appears only during the first years of life might suggest a critical cause present especially in this phase. Seizures usually develop between the first and third year of age and are accompanied by characteristic EEG abnormalities ⁹.

AS develops in early childhood and persists into adulthood. During adolescence an increase of body weight is observed towards obesity, while seizure events ameliorate with age, decreasing in frequency and severity. Moreover, the incidence of death seems to be comparable to neurotypical individuals ¹⁰.

Genetic cause

Several genetic abnormalities involving the integrity of chromosome 15q11-13 have been identified as the cause for AS ¹¹. It was in 1987 that the AS genetic locus was identified in the long arm of chromosome 15 between bands q11 and q13 (15q11-q13) by Magenis et al. (1987)¹² and confirmed later in additional patients harboring chromosome 15q11-q13 deletions ¹³. Interestingly, AS was only observed when the deletion occurred on the maternal copy of chromosome 15 ¹³. This observation was remarkable because it had been previously shown that a deletion of the paternal 15q11-q13 causes Prader-Willi syndrome (PWS), a disorder characterized by several features including cognitive impairments, hyperphagia and obesity ^{14,15}. Two years later, in 1989 these interesting observations were explained by the discovery that chromosome 15q11-q13 is subject to genomic imprinting ¹³, an epigenetic mechanism whereby expression is allele-specific. This biological mechanism allows indeed the silencing of one of the two parental copies.

AS can result from 4 different genetic causes on chromosome 15: *de novo* deletions (large and small) of maternal chromosomal region 15q11.2-q13, encompassing in around 75% of cases the *UBE3A* (Ubiquitin-protein ligase E3A) gene; paternal uniparental disomy of chromosome 15 (1-2%), imprinting defects at the SNRPN methylation site, named Prader Willi Syndrome Imprinting Center (PWS-IC) (1-3%) (see below) and *de novo* or inherited mutations in the maternal *UBE3A* gene (5-10%). The remaining 10% of presumably AS affected children do not harbor genetic variations in the coding sequences of *UBE3A* ^{5,10}.

The severity of the observed phenotypes varies depending on the genes affected with large deletions of the chromosome ¹⁶. Increased susceptibility to seizure events has been reported to be associated to haploinsufficiency of the non-imprinted GABA receptor genes *GABRB3*, *GABRA5* and *GABRG3* ¹⁷. Together with the GABA receptor gene family, the additional deletion of *NIPA1*, *NIPA2*, *CYFIP1* and *GCP5* genes is also conferring an increased risk of autism-like phenotypes, severe language impairment, and seizure events ^{18,19}.

UBE3A gene and its mechanism of imprinting

As previously suggested, the mechanism of imprinting of *UBE3A* plays an important role when it comes to understanding the genetic cause of

Angelman Syndrome. The *UBE3A* gene is biallelically expressed in all the cells of the body, with the exception of neurons in brain (**Figure 1**).

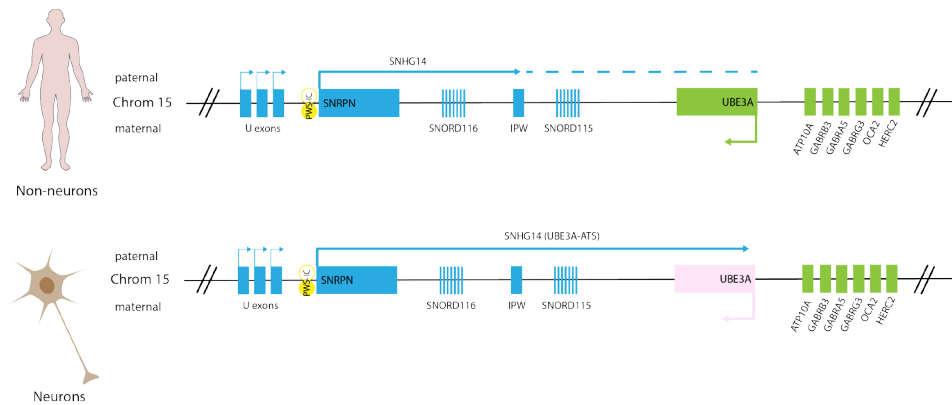


Figure 1. *UBE3A* mechanism of Imprinting.

The differential *UBE3A* mechanism of imprinting in non-neuronal (top) and neuronal cells (bottom) is depicted on the map of human chromosome region 15q11-q13 containing *UBE3A*. Maternally expressed genes are depicted in pink, paternally expressed genes are depicted in blue. Non-imprinted genes are indicated in green. The parent of origin methylation at the maternal Prader-Willi Syndrome Imprinting Center (PWS-IC) is indicated as a yellow full circle; the non-methylation of the paternal PWS-IC is indicated as empty yellow circle.

In neurons, *UBE3A* is expressed only from the maternal allele^{20–24}. As a consequence, AS patients who carry a deletion encompassing the maternal chromosome 15 q11-q13 region, and specifically the *UBE3A* gene, are lacking the *UBE3A* expression in neuronal cells.

The expression of genes on human chromosome 15q11.2-q13, and on the homologous region of mouse chromosome 7, is differentially regulated in maternal and paternal alleles. Indeed, some of these genes, like *SNRPN* and *snRNAs* are expressed exclusively from the paternal chromosome, whereas other genes like *UBE3A* show preferential or tissue-specific expression from either the paternal or maternal chromosome²⁵.

The *SNRPN* promoter is regulated by the activity of the Prader Willi Syndrome Imprinting Center (PWS-IC), which is differentially methylated on the maternal and paternal allele. On the paternal allele, the PWS-IC is not methylated and therefore allows the transcription of the genes under the control of the *SNRPN* promoter. In both human and mouse, we observe the transcription of a long

transcript named *SNHG14* (Small Nucleolar RNA Host gene 14) (>460 kb in human, ~ 1,000 kb in mouse) that includes the *SNRPN* sense transcript, the transcript from which *snoRNAs* are processed, and an antisense transcript with respect to the *UBE3A* locus (*UBE3A-ATS*)²⁰.

In neuronal cells, transcription of *UBE3A-ATS* extends into the *UBE3A* gene and interferes with its transcription on the paternal chromosome, whereas in non-neuronal cells transcription of *SNHG14* does not extend into *UBE3A* and stops at the level of noncoding exons annotated as *IPW* (Imprinted Prader Willi), whose presence is responsible for the restriction of *UBE3A* imprinting in mature neurons²⁶.

The discovery of a significant decrease in *SNHG14* RNA levels around intron 4 of *UBE3A*, which is the same region where the pre-mRNA level of paternal *UBE3A* becomes suppressed, suggested that paternal *UBE3A* is transcriptionally active, and is suppressed during the process of transcription elongation^{27,28}.

Based on these observations, a hypothesis of transcriptional collision has been proposed, in which the two opposing transcriptional complexes for *UBE3A* and *SNHG14* on the paternal chromosome collide with each other around intron 4 of *UBE3A*. The incomplete sense transcript of *UBE3A* is therefore degraded and cannot be processed into a full-length mature mRNA²⁷.

It was only in 2014 that Judson and colleagues investigated the allelic specificity of *Ube3a* expression *in vivo* in neurons and other cell types in the developing brain, including the early postnatal period when AS phenotypes emerge. In their study in mice, they found that neurons downregulate paternal *UBE3A* protein expression as they mature and paternal *UBE3A* expression is detectable until the first postnatal week²⁹. More insight into the paternal *Ube3a* contribution in AS is given in **Chapter 4** of this thesis.

Unsilencing the paternal *UBE3A* gene: a potential therapeutic approach

Since AS cases are caused by lack of *UBE3A*, several research groups aimed to restore *UBE3A* expression by gene therapy or by re-activation of the paternal allele. It was in 2011 that Daily and colleagues³⁰ tried to restore *UBE3A* expression by injection of recombinant adeno-associated virus (AAV) carrying the mouse *Ube3a* (isoform 3) into the hippocampus of AS mice.

The re-expression of *UBE3A* led to the improvement of hippocampus-dependent learning and memory, but no effect on motor dysfunction was

observed³⁰. Despite the high potential of gene therapy, there are a few limits to this approach: first, the limited distribution within the brain; second, the lack of precise control on the level of UBE3A expression; third, we do not know which type of UBE3A isoform we should express (see later for more details about UBE3A isoforms) and fourth, that the effect is permanent. High UBE3A levels are a risk factor for ASD and this in an extremely important aspect to keep in mind in the context of UBE3A reinstatement^{31–33}.

As an alternative, suppression of UBE3A-ATS expression is thought to be a better approach to reactivate the paternal allele. Different options have been investigated in order to unsilence the paternal allele. The first option involves the increase of methylation of the PWS-IC on the paternal allele with the use of specific dietary compounds (such as betaine or acid folic) as a method to reduce UBE3A-ATS expression; increasing the global DNA methylation through dietary supplements, the paternally inherited copy of PWS-IC would become methylated, thereby decreasing the amount of *UBE3-ATS* and with a concomitant increase in paternal *UBE3A* expression. However, these attempts were unsuccessful³⁴.

Another approach has been described by Huang et al. who in 2011 showed that the topoisomerase I inhibitor, topotecan, was able to inhibit the transcriptional elongation of *Ube3a-ATS*, leading to the re-expression of the paternal *Ube3a* allele in AS mice³⁵. However, because of topotecan's lack of specificity and its toxicity its use as treatment has not yet been translated to the clinic.

Later in 2013, Meng et al. developed a new AS mouse model with the insertion of a transcriptional stop cassette resulting in a truncated *Ube3a-ATS* transcript. As a consequence, this led to increased paternal UBE3A expression and at the behavioral level they observed improvement of memory and motor skills²⁸. Almost two years later Meng et al. tested, for the first time, antisense oligonucleotides (ASOs) able to target the *Ube3a-ATS* in AS mice, thus making this approach a possible candidate for AS therapy. With this approach, the hybridization of the ASO to the target RNA led to the activation of RNase H which cleaves the RNA strand of the ASO-RNA heteroduplex resulting in the subsequent degradation of *Ube3a-ATS* RNA, ultimately leading to paternally derived UBE3A protein³⁶. The administration of ASOs would solve most of the limits associated with viral injection, especially in the context of controlling the level and the type (isoform) of UBE3A expression. With this approach the expression of UBE3A remains

tightly regulated avoiding the possibility of having cells reach a level of UBE3A higher than 100% (physiological condition) and falling into the ASD condition.

Interestingly, behavioral experiments performed four weeks after ASO treatment showed a significant improvement in memory in the fear-conditioning paradigm, while abnormal open field behavior or marble burying and accelerating rotarod performances did not benefit from the ASO administration³⁶. One reason for the inefficacy of ASOs in restoring most behavioral phenotypes is the presence of a critical window for UBE3A functionality.

This notion is supported by Santos et al, who in 2015 found that UBE3A reinstatement during the early embryonic stage fully rescued AS-relevant phenotypes. UBE3A reinstatement during adolescence showed a partial rescue of the motor abnormalities, while only hippocampal synaptic plasticity was restored during adulthood³⁷.

Thanks to this study we are now aware that UBE3A exerts its main function during brain development. Because of this, any therapeutic intervention aiming at the restoration of UBE3A expression needs to commence as soon as possible after diagnosis. However, this study did not provide any information about the length of the therapeutic intervention. In other words, for how long does UBE3A expression need to be maintained?

This aspect is addressed in **Chapter 5** of this thesis, giving also more insights about UBE3A function in adulthood. In the study of Santos et al. the critical window of UBE3A was investigated in a mouse model where the paternal *Ube3a* contribution was still intact until the first week of age (as previously suggested by Judson et al, 2014²⁹) and where the reactivated UBE3A expression was coming from a conditional maternal *Ube3a* allele.

Very little is known about the contribution of paternal *Ube3a* during the embryonic phase of brain development when the mechanism of imprinting is not fully active. Because of this, another study investigating the critical window of UBE3A and the function of the paternal allele was undertaken, which is described in **Chapter 4** of this thesis.

UBE3A and the Ubiquitination process

Since the discovery of AS in 1965 researchers have been trying to answer the following questions: what is the real cause of Angelman Syndrome? What are the consequences of missing UBE3A in the brain? What is the function of

UBE3A at the neuronal level?

The *Ube3a* gene encodes the E3 Ubiquitin ligase UBE3A, also known as E6-associated protein (E6-AP). UBE3A was first characterized by Scheffner et al (1993), showing that UBE3A (E6-AP) is an enzyme with ubiquitin ligase activity responsible for the ubiquitination and subsequent degradation of the tumor suppressor protein p53 in HPV infected cells that express the viral E6 protein³⁸. It was a few years later that Kishino et al (1997) discovered the connection between AS and *Ube3a* mutations, reporting the first two frameshift mutations that caused premature termination of translation of the UBE3A protein in 3 individuals diagnosed with AS³⁹.

In the cell, ubiquitin ligases are responsible for the ubiquitination process. In particular, ubiquitination is a post-translational modification that can determine the fate of proteins, like protein degradation by the proteasome or lysosomes, intracellular trafficking, DNA repair and replication and can be seen as a code for intracellular communication⁴⁰. Overall this cellular signaling process involves 3 steps each of which is catalyzed by a specific type of enzyme: E1, E2 and E3⁴¹. In the first step the E1 enzyme activates a single ubiquitin moiety in an ATP-dependent reaction concomitantly linking the C-terminus of the ubiquitin via a thioester bond to the active site cysteine of the E1 enzyme. In the second step, the ubiquitin moiety is transferred to the active site cysteine of the conjugating enzyme E2, thus forming an E2-Ub intermediate. In the final step, the E3 ligase binds both the E2-Ub intermediate and the protein substrate, and catalyzes the transfer of the ubiquitin from the E2 to a specific lysine on the substrate or onto the substrate's first methionine (**Figure 2A**). E3 ligases are generally grouped into three different families: the Really Interesting New Gene (RING); the Homologous to E6AP C terminus (HECT) and the Ring-Between-Ring (RBR) family. Each family member is characterized by at least 2 functional domains, one being responsible for substrate recognition, the other mediating the interaction with the E2/E2-Ub enzyme⁴². UBE3A is one of the over 600 human E3 ubiquitin ligases present in the cell⁴³ and is one of the founding member of the HECT family of E3 ligases. This type of E3 ligase uses a 2-step mechanism to ubiquitinate target proteins. In the first step the ubiquitin moiety bound to the E2 enzyme is transferred to the active site cysteine of the catalytic HECT domain. In the second step the ubiquitin is transferred to a lysine residue on the substrate protein of interest^{42,44} (**Figure 2B**).

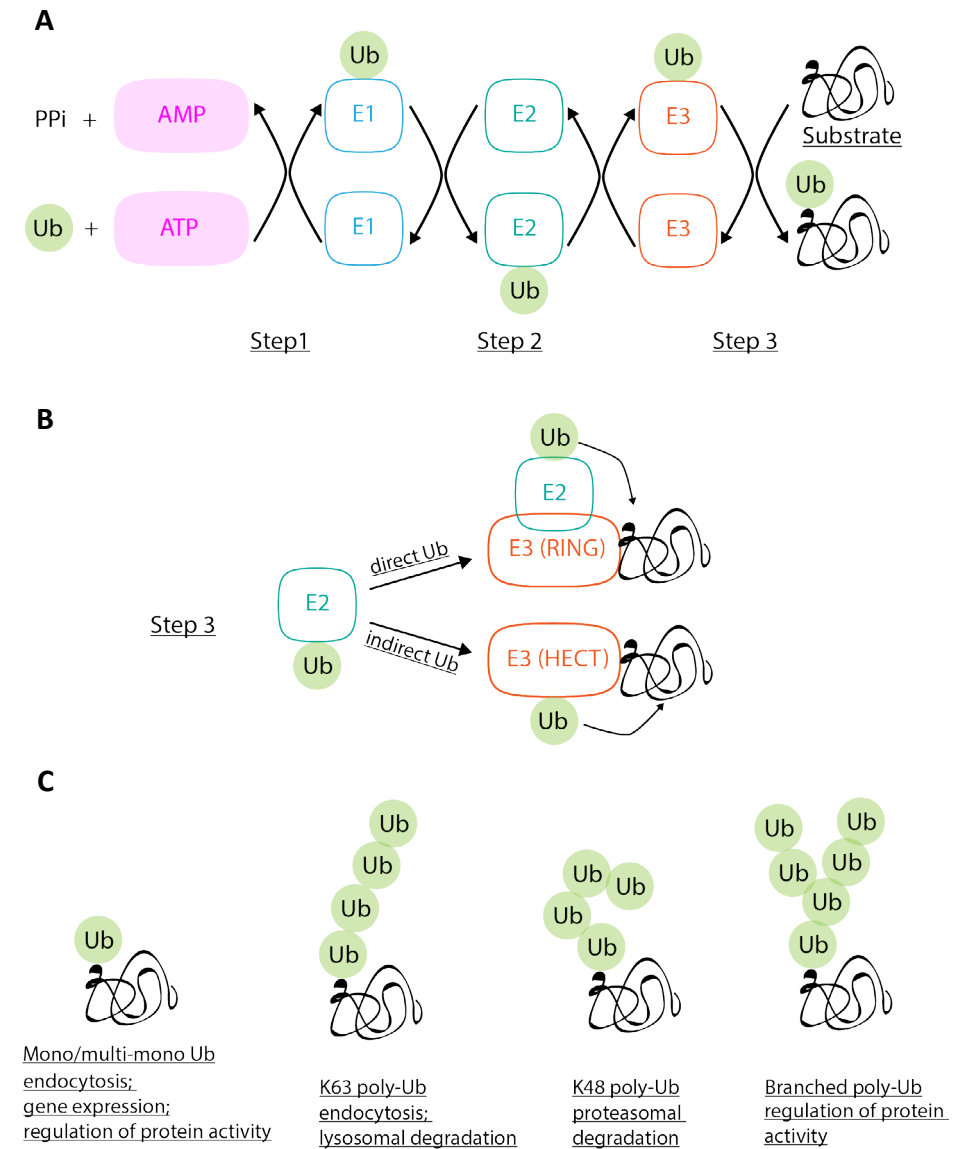


Figure 2. The Ubiquitination process.

A Schematic representation of Ubiquitin activation and transfer to the target protein. **B** In case of RING E3s, an intermediate complex of E3, substrate and E2-Ub is required for the transfer of Ubiquitin to the substrate; in case of HECT E3s, the E2-Ub enzymes transfer Ub first to the active site of E3 prior to transfer to the substrate. **C** Types of ubiquitination products.

Further insight into the catalytic mechanism of UBE3A came from structural studies. In 1999 Huang et al crystallized the UBE3A HECT domain in complex with the E2 conjugating enzyme Ubch7, giving the first insights into the mechanism of ubiquitin transfer from the E2 to the E3 ⁴⁵. Very limited structural information is known for the N terminal half of UBE3A. In 2011 Lemak et al determined the structure of an N-terminal region of UBE3A, which was named Amino-terminal Zn finger of Ube3a Ligase (AZUL) domain. Its structural analysis revealed that the domain forms a Zn binding domain consisting of a helix-loop-helix region where a Zn²⁺ ion is coordinated by four cysteines, and which is highly conserved among UBE3A proteins from different species ⁴⁶. The importance of this conserved domain in the AS pathophysiology is described in **Chapter 6**.

Ubiquitin-dependent and independent function of UBE3A

As previously mentioned, ubiquitination is a fundamental cellular process that regulates the fate of the cell. Ubiquitin is a 76 amino acid protein and the key characteristic are its seven Lys residues that can be ubiquitinated themselves, giving rise to isopeptide-linked ubiquitin chains. Several proteomics studies indicated that in a cell we can observe the co-existence of different types of linkages. The most abundant ones are the Lys48-linked chains and the Lys63 ⁴⁷. In addition, a type of chain independent from the presence of the lysin is the Met1-linked chain, also known as linear chain. This chain consists of ubiquitin moieties attached to the N terminus of the second ubiquitin.

In a cell we can indeed observe not only different types of linkages, but also different types of ubiquitination which regulates the activity of the cell ⁴⁸ (**Figure 2C**). The most well-known and important ones are: mono- or multi mono-ubiquitination (which are usually involved in DNA repair, endocytosis of plasma membrane proteins or chromosome remodeling ⁴⁹) and poly-ubiquitination which is mainly involved in protein degradation and protein trafficking ⁴² depending on the lysine that is used for linking the two ubiquitin moieties in the ubiquitin chain (Lys48 and Lys63, respectively) ⁴⁴.

Given the nature and function of the UBE3A protein, several researchers have tried to investigate which proteins and interactors are misregulated in AS, when the ligase is missing (reviewed in ⁵⁰⁻⁵²). One of these proteins is RING1B. In 2010 Zaaroor-Regev et al., showed that RING1B is a direct target of UBE3A which is first subjected to poly-ubiquitination and then to proteasome

mediated degradation ⁵³. Another up-regulated protein identified in AS mice and a putative UBE3A-interactor is the activity regulated cytoskeleton associated protein (ARC). In 2010, Greer et al suggested that UBE3A regulates synapse development by ubiquitinating ARC, which is a key factor in AMPA receptor endocytosis at excitatory neuron synapses ⁵⁴. However, 3 years later Kunhle et al. (2013) failed to reproduce UBE3A dependent degradation of ARC. They did however show that reduced UBE3A levels led to an increase in estradiol-induced transcription of the ARC gene with subsequent increase in ARC protein levels ⁵⁵. This study then postulated that ubiquitination activity of UBE3A might not be the only key factor in AS pathogenicity, but that the enzyme can have a role in AS unrelated to ubiquitination.

Several studies have suggested a ligase-independent role of UBE3A, especially in transcriptional regulation in the nucleus. Nawaz et al. showed in 1999 that UBE3A was able to act as a co-activator for several steroid hormone receptors, independently from its ubiquitin ligase activity (progesterone, estrogen, androgen and glucocorticoid receptors)⁵⁶. Chromatin immunoprecipitation (ChIP) experiments have indicated that UBE3A is recruited to the estrogen-responsive pS2 promoter and that E6AP is cyclically associated with the pS2 promoter ⁵⁷. Another promoter that has been found associated with and regulated by UBE3A is that of the melanocortin-1-receptor (MC1R) ⁵⁸.

Beside the transcriptional regulation operated through receptor binding, UBE3A has also been reported to target several transcription factors such as PRX1, BMAL1/CLOCK and ESR2, a function that is dependent on its E3 ligase activity ^{51,59,60}. Taken together these data suggest that UBE3A may have a dual function: as a ubiquitin E3 ligase exerting its function in both cytosol and nucleus and as a regulator of gene transcription through receptor binding in the nucleus.

UBE3A subcellular localization and isoforms

The fact that UBE3A exerts its function both in the cytosol and in the nucleus, lead us to investigate where UBE3A exert its main functions and whether AS-associated pathophysiology is related to the function of UBE3A in the nucleus, cytosol or both.

At the cellular level UBE3A protein localizes in pre- and post- synaptic neuronal compartments and in both cytoplasmic and nuclear locations ⁶¹. This synaptic localization may primarily regulate experience-dependent synaptic plasticity ⁶², although our understanding of the diverse roles of ubiquitination

and protein recycling at the synapse is rapidly expanding⁶³. The presence of UBE3A in both cytosolic and nuclear compartments is consistent with its predicted roles in proteasome targeting and transcriptional regulation, and maybe explained by the presence of different isoforms.

In humans we observe three isoforms generated by alternative splicing, displaying unique N-termini, with unknown functional roles⁶⁴ (**Figure 3**).

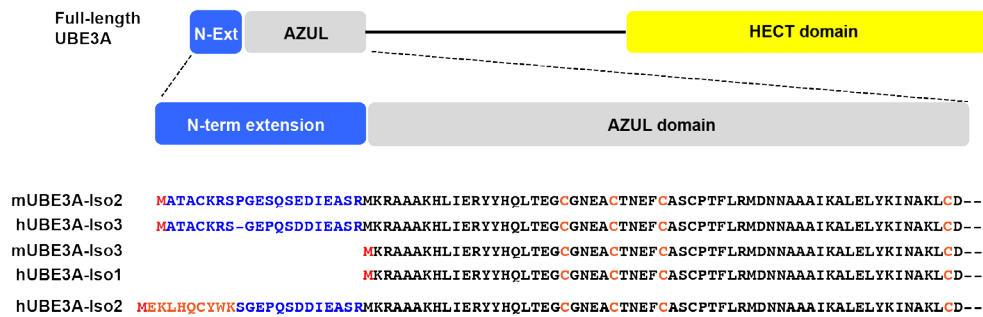


Figure 3: UBE3A mouse and human sequence.

The upper panel shows a schematic representation of mouse and human *UBE3A* depicting the shared AZUL domain and the N-terminal HECT domain. The amino acid sequences of the UBE3A mouse and human isoforms are indicated in the lower panel.

The shortest predicted isoform is the human isoform 1 with a length of 852 amino acids, while the longest one is human isoform 2 with an extra extension of 23 amino acids at the N-terminus. In mice, similar to humans, there are at least three predicted isoforms of UBE3A with distinct amino termini resulting from alternative splicing of the first eight exons of *Ube3a*⁶⁵. Mouse UBE3A isoform 1 makes use of an alternative poly-adenylation site, resulting in a transcript truncated prior to the E3 ligase coding exons. The existence of this isoform, however, is under debate as will be discussed later in **Chapter 6**. Interestingly, mouse isoform 3 is homologous to human isoform 1, while mouse isoform 2 is homologous to human isoform 3, sharing a very similar 21 amino acid N terminus. The first study investigating the function of the different isoforms was conducted by Miao et al., who showed that mouse Isoform 3 mainly localized to the nucleus of neuronal cells, in contrast to mouse isoform 2 which was mainly found in the cytoplasm⁶⁵. In the same study it was shown that mouse isoform 2 corrected the dendritic phenotype in pyramidal neurons⁶⁵. Interestingly, a recent study reported the description

of three children with AS carrying a nearly identical missense mutation that disrupts the translational start site of human UBE3A isoform 1 (homolog of mouse isoform 3) suggesting that human isoform 1 (homologous to mUBE3A mouse isoform 3) is critical to normal development⁶⁶.

Since the discovery of AS, many research groups have attempted to elucidate the function of UBE3A in the brain, and in particular whether the different isoforms each fulfill a separate biological function. The first detailed study on the contribution of the two mouse UBE3A isoforms on AS phenotypes *in vivo* is described in **Chapter 6** of this thesis, giving insights into the importance of UBE3A cellular localization in AS pathophysiology.

AS mouse models and their importance: face validity and construct validity

Neurodevelopmental disorders (NDDs), like Angelman Syndrome, are life-long debilitating illnesses that markedly impair the quality of life. The remarkable genetical and physiological similarities across mammals (like in humans and mice), have prompted researchers to investigate a large range of mechanisms and assess novel therapies in animal models before applying their discoveries to humans. Indeed, animal models can be used to address a variety of scientific questions for studying NDD pathobiology, from basic science to the development and assessment of novel therapies.

An animal model is described as valid if it “resembles the human condition in etiology, pathophysiology, symptomatology and response to therapeutic interventions”. This validity consists of two aspects: the face validity and the construct validity of the animal model. In particular with face validity we refer to the phenotypic similarities between the patient and the animal model condition; with construct validity we refer to the underlying cause of the disease, that should be as similar as possible to be relevant and reliable. There are a number of AS mouse models, *Ube3a* mutants described in the literature where UBE3A is missing (by mutation of a specific exon/intron) or is inactive, that have helped out to reveal the underlying causes of AS phenotypes (**Figure 4**).

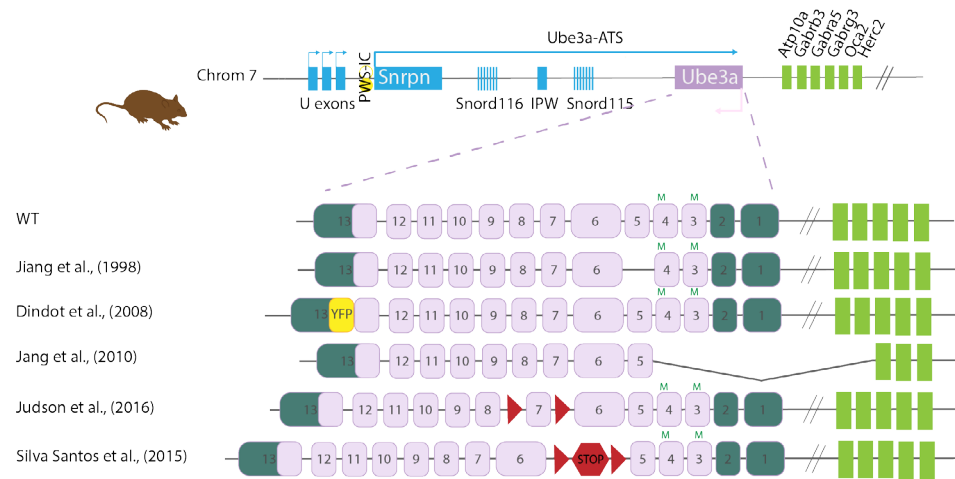


Figure 4: Most commonly used AS mouse models.

The upper panel indicates a schematic representation of mouse chromosome 7 which includes the *Ube3a* gene. The lower panel shows the most used AS mouse models and their schematic genomic structure. In detail, pink squares indicate *Ube3a* expressed exons; red triangles indicate loxP sites; YFP indicates a Yellow Fluorescent Protein positioned in frame at the 3' end of *Ube3a*; red hexagon indicates a transcriptional stop. Adapted from Rotaru et al. (2020)⁶⁷.

Jiang et al., in 1998 by deleting exon 5 of *Ube3a* found out that the phenotypes of mice with maternal deficiency (m-/p+) for *Ube3a* resemble AS patients with motor dysfunction, inducible seizures, and a context-dependent learning deficit⁶⁸.

By using a knock-in mouse model expressing a *Ube3a(YFP)* fusion gene, Dindot et al., (2008) discovered that the maternal *Ube3a(YFP)* allele is preferentially expressed in neurons, and that the fusion protein, UBE3A:YFP (catalytically inactive), is enriched in the nucleus and dendrites⁶¹.

Two years later Jiang et al., (2010) used a chromosomal engineering strategy to generate a mutant AS mouse with a large chromosomal deletion from *Ube3a* to *Gabrb3*, which inactivated the *Ube3a* and *Gabrb3* genes and deleted the *Atp10a* gene⁶⁹. Mice with a large maternal deletion were viable and did not have any obvious developmental defects. Like in the first AS mouse generated by Jang et al., 1998, a number of behavioral experiments have been performed in mice with the large deletion and revealed significant impairment in motor function, learning and memory tasks and

increased spontaneous seizure activity. Moreover, ultrasonic vocalization (USV) recording in newborns revealed that maternal deletion pups emitted significantly more USVs than wild-type littermates. These data suggested an abnormal signaling behavior between mothers and pups that may reflect the abnormal communication behaviors observed in human AS patients. Thus, mutant mice harboring a maternal deletion from *Ube3a* to *Gabrb3* provided an AS mouse model that is molecularly more similar to the chromosomal deletion form of AS in humans than mice which harbor mutations in the only *Ube3a* gene.

As previously reported, Silva Santos et al. (2015), generated the first conditional AS mouse where a floxed stop cassette was inserted in intron 5. In this study they developed an AS model that allows for temporally controlled Cre-dependent induction of the maternal *Ube3a* allele and determined that there are distinct neurodevelopmental windows during which UBE3A restoration can rescue AS-relevant phenotypes. Motor deficits, usually observed in the AS mouse model, were rescued by *Ube3a* gene reinstatement in adolescent mice, whereas anxiety, repetitive behavior, and epilepsy were only rescued when *Ube3a* was reinstated during early development³⁷. These findings suggested that *Ube3a* reinstatement early in development may be necessary to prevent or rescue most AS-associated phenotypes and should be considered in future clinical trial design.

Recently, Judson et al., in 2016 using another conditional mouse model for AS (floxed exon 7 of *Ube3a*) was able to investigate the consequences of the selective UBE3A loss from either GABAergic or glutamatergic neurons, which are largely responsible for orchestrating the balance between excitation and inhibition in cerebral circuits⁷⁰. In this study they suggested that GABAergic, but not glutamatergic, *Ube3a* loss is responsible for mediating the EEG abnormalities and seizures that affect individuals with AS.

Aim of the thesis

Results from studying AS mice have begun to shed light on the pathophysiology of Angelman syndrome and reveal potential therapeutic approaches, which are also the focus of this thesis. The work presented in this thesis touches upon how mouse models can be useful to address several questions relevant to both clinical and fundamental research labs studying one of the many severe neurodevelopmental disorders, one of which is Angelman Syndrome. In **Chapter 2** a description of a battery of behavioral tests is given, that assess

phenotypes in the domains of motor performance, repetitive behavior, anxiety, and seizure susceptibility in AS mice. In this study we evaluate the robustness of these phenotypes when tested in a standardized manner, which can be useful to study not only different therapeutics, but also different AS mouse models.

As described in **Chapter 2** and **3**, we used this behavioral test battery to assess the efficacy of drugs like Minocycline, Levodopa and Gaboxadol which were recently tested in clinical trials of AS.

Another clinically relevant aspect that is addressed in the thesis (using different conditional mouse models and the test battery) is about the optimal time of therapeutic intervention. In particular in **Chapter 4** we further investigated the critical window for therapeutic intervention in AS, giving more insights about the function of the paternal *Ube3a* allele in the disease. Moreover, in **Chapter 5** the length of therapeutic intervention was examined. In other words, how long does UBE3A protein need to be expressed in order to fulfill all its biological functions.

Finally, in **Chapter 6**, with the use of UBE3A isoform specific mouse models it was possible for the first time to understand the importance of UBE3A subcellular localization in the AS pathogenicity.

In summary, the aim of this thesis will be to determine the temporal and (subcellular) spatial role played by the UBE3A protein in relation to Angelman syndrome pathophysiology.

References

1. Hart, H. 'Puppet' children. A report on three cases (1965). *Developmental Medicine and Child Neurology* **50**, 564 (2008).
2. Williams, C. A., Frias, J. L. & Opitz, J. M. The Angelman ("Happy Puppet") syndrome. *American Journal of Medical Genetics* **11**, 453–460 (1982).
3. Mertz, L. G. B. *et al.* Angelman syndrome in Denmark. Birth incidence, genetic findings, and age at diagnosis. *American Journal of Medical Genetics Part A* **161**, 2197–2203 (2013).
4. Williams, C. A. *et al.* Angelman syndrome 2005: Updated consensus for diagnostic criteria. *American Journal of Medical Genetics Part A* **140A**, 413–418 (2006).
5. Van Buggenhout, G. & Fryns, J. P. Angelman syndrome (AS, MIM 105830). *European Journal of Human Genetics* **17**, 1367–1373 (2009).
6. Tan, W. H. *et al.* Angelman syndrome: Mutations influence features in early childhood. *American Journal of Medical Genetics, Part A* **155**, 81–90 (2011).
7. Bai, J. L. *et al.* Molecular and clinical characterization of Angelman syndrome in Chinese patients. *Clinical Genetics* **85**, 273–277 (2014).
8. Bürger, J., Kunze, J., Sperling, K. & Reis, A. Phenotypic differences in Angelman syndrome patients: Imprinting mutations show less frequently microcephaly and hypopigmentation than deletions. *American Journal of Medical Genetics* **66**, 221–226 (1996).
9. Fiumara, A., Pittalà, A., Cocuzza, M. & Sorge, G. Epilepsy in patients with Angelman syndrome. *Italian journal of pediatrics* **36**, 31 (2010).
10. Buiting, K., Williams, C. & Horsthemke, B. Angelman syndrome — insights into a rare neurogenetic disorder. (2016). doi:10.1038/nrneurol.2016.133
11. Chamberlain, S. J. & Lalande, M. Angelman syndrome, a genomic imprinting disorder of the brain. *The Journal of neuroscience : the official journal of the Society for Neuroscience* **30**, 9958–9963 (2010).
12. Magenis, R. E., Brown, M. G., Lacy, D. A., Budden, S. & LaFranchi, S. Is Angelman syndrome an alternate result of del (15) (q11q13)? *Am J Med Genet* **28**, (1987).
13. Knoll, J. H. M. *et al.* Angelman and Prader-Willi syndromes share a common chromosome 15 deletion but differ in parental origin of the deletion. *American Journal of Medical Genetics* **32**, 285–290 (1989).
14. Butler, M. G. & Palmer, C. G. PARENTAL ORIGIN OF CHROMOSOME 15 DELETION IN PRADER-WILLI SYNDROME. *The Lancet* **321**, 1285–1286 (1983).

15. Elena, G., Bruna, C., Benedetta, M., Stefania, D. C. & Giuseppe, C. Prader-Willi Syndrome: Clinical aspects. *Journal of Obesity* **2012**, (2012).
16. Gentile, J. K. *et al.* A neurodevelopmental survey of Angelman syndrome with genotype-phenotype correlations. *Journal of developmental and behavioral pediatrics : JDBP* **31**, 592–601 (2010).
17. Frohlich, J. *et al.* Electrophysiological Phenotype in Angelman Syndrome Differs Between Genotypes. *Biological Psychiatry* **85**, 752–759 (2019).
18. Sahoo, T. *et al.* Microarray based comparative genomic hybridization testing in deletion bearing patients with Angelman syndrome: Genotype-phenotype correlations. *Journal of Medical Genetics* **43**, 512–516 (2006).
19. Sahoo, T. *et al.* Identification of novel deletions of 15q11q13 in Angelman syndrome by array-CGH: Molecular characterization and genotype-phenotype correlations. *European Journal of Human Genetics* **15**, 943–949 (2007).
20. Runte, M. *et al.* The IC-SNURF-SNRPN transcript serves as a host for multiple small nucleolar RNA species and as an antisense RNA for UBE3A. *Human Molecular Genetics* **10**, 2687–2700 (2001).
21. Varon, R. *et al.* SNURF-SNRPN and UBE3A transcript levels in patients with Angelman syndrome. *Human Genetics* **114**, 553–561 (2004).
22. Albrecht, U. *et al.* Imprinted expression of the murine Angelman syndrome gene, Ube3a, in hippocampal and Purkinje neurons. *Nature genetics* **17**, 75–78 (1997).
23. Rougeulle, C., Glatt, H. & Lalande, M. The Angelman syndrome candidate gene, UBE3A/E6-AP, is imprinted in brain. *Nature Genetics* **17**, 14–15 (1997).
24. Vu, T. H. & Hoffman, A. R. Imprinting of the Angelman syndrome gene, UBE3A, is restricted to brain. *Nature Genetics* **17**, 12–13 (1997).
25. Horsthemke, B. & Wagstaff, J. Mechanisms of imprinting of the Prader-Willi/Angelman region. *American Journal of Medical Genetics Part A* **146A**, 2041–2052 (2008).
26. Hsiao, J. S. *et al.* A bipartite boundary element restricts UBE3A imprinting to mature neurons. *Proceedings of the National Academy of Sciences of the United States of America* **116**, 2181–2186 (2019).
27. Meng, L., Person, R. E. & Beaudet, A. L. Ube3a-ATS is an atypical RNA polymerase II transcript that represses the paternal expression of Ube3a. *Human Molecular Genetics* **21**, 3001–3012 (2012).
28. Meng, L. *et al.* Truncation of Ube3a-ATS Unsilences Paternal Ube3a and Ameliorates Behavioral Defects in the Angelman Syndrome Mouse Model. *PLoS Genetics* **9**, (2013).
29. Judson, M. C., Sosa-Pagan, J. O., Del Cid, W. a., Han, J. E. & Philpot, B. D. Allelic specificity of Ube3a expression in the mouse brain during postnatal Development. *Journal of Comparative Neurology* **522**, 1874–1896 (2014).
30. Daily, J. L. *et al.* Adeno-associated virus-mediated rescue of the cognitive defects in a mouse model for Angelman syndrome. *PloS one* **6**, e27221 (2011).
31. Moreno-De-Luca, D. *et al.* Using large clinical data sets to infer pathogenicity for rare copy number variants in autism cohorts. *Molecular Psychiatry* **18**, 1090–1095 (2013).
32. Sanders, S. J. *et al.* Insights into Autism Spectrum Disorder Genomic Architecture and Biology from 71 Risk Loci. *Neuron* **87**, 1215–1233 (2015).
33. Elgersma, Y. A molecular tightrope. *Nature* **526**, 50–51 (2015).
34. Peters, S. U. *et al.* Double-blind therapeutic trial in Angelman syndrome using betaine and folic acid. *American Journal of Medical Genetics, Part A* **152**, 1994–2001 (2010).
35. Huang, H.-S. *et al.* Topoisomerase inhibitors unsilence the dormant allele of Ube3a in neurons. *Nature* **481**, 185–189 (2011).
36. Meng, L. *et al.* Towards a therapy for Angelman syndrome by targeting a long non-coding RNA. *Nature* **518**, 409–12 (2014).
37. Silva-Santos, S. *et al.* Ube3a reinstatement identifies distinct developmental windows in a murine Angelman syndrome model. *Journal of Clinical Investigation* **125**, 2069–2076 (2015).
38. Scheffner, M., Huibregtse, J. M., Vierstra, R. D. & Howley, P. M. The HPV-16 E6 and E6-AP complex functions as a ubiquitin-protein ligase in the ubiquitination of p53. *Cell* **75**, 495–505 (1993).
39. Kishino, T., Lalande, M. & Wagstaff, J. UBE3A/E6-AP mutations cause Angelman syndrome. *Nature Genetics* **15**, 70–73 (1997).
40. Hamilton, A. M., Zito, K., Hamilton, A. M. & Zito, K. Breaking It Down: The Ubiquitin Proteasome System in Neuronal Morphogenesis. *Neural Plasticity* **2013**, 1–10 (2013).
41. Scheffner, M. & Kumar, S. Mammalian HECT ubiquitin-protein ligases: Biological and pathophysiological aspects. *Biochimica et Biophysica Acta - Molecular Cell Research* **1843**, 61–74 (2014).
42. Komander, D. & Rape, M. The Ubiquitin Code. *Annual Review of Biochemistry* **81**, 203–229 (2012).
43. George, A. J., Hoffiz, Y. C., Charles, A. J., Zhu, Y. & Mabb, A. M. A comprehensive

- atlas of E3 ubiquitin ligase mutations in neurological disorders. *Frontiers in Genetics* **9**, (2018).
44. Pickart, C. M. Mechanisms Underlying Ubiquitination. *Annual Review of Biochemistry* **70**, 503–533 (2001).
 45. Huang, L. *et al.* Structure of an E6AP-UbcH7 complex: Insights into ubiquitination by the E2-E3 enzyme cascade. *Science* **286**, 1321–1326 (1999).
 46. Lemak, A., Yee, A., Bezsonova, I., Dhe-Paganon, S. & Arrowsmith, C. H. Zn-binding AZUL domain of human ubiquitin protein ligase Ube3A. *Journal of Biomolecular NMR* **51**, 185–190 (2011).
 47. Swatek, K. N. & Komander, D. Ubiquitin modifications. *Cell Research* **26**, 399–422 (2016).
 48. Haglund, K., Di Fiore, P. P. & Dikic, I. Distinct monoubiquitin signals in receptor endocytosis. *Trends in Biochemical Sciences* **28**, 598–604 (2003).
 49. Hicke, L. Protein regulation by monoubiquitin. *Nature Reviews Molecular Cell Biology* **2**, 195–201 (2001).
 50. Lopez, S. J., Segal, D. J. & LaSalle, J. M. UBE3A: An E3 Ubiquitin Ligase With Genome-Wide Impact in Neurodevelopmental Disease. *Frontiers in Molecular Neuroscience* **11**, 476 (2019).
 51. LaSalle, J. M., Reiter, L. T. & Chamberlain, S. J. Epigenetic regulation of UBE3A and roles in human neurodevelopmental disorders. *Epigenomics* **7**, 1213–1228 (2015).
 52. Sell, G. L. & Margolis, S. S. From UBE3A to Angelman syndrome: a substrate perspective. *Frontiers in Neuroscience* **9**, 1–6 (2015).
 53. Zaaroor-Regev, D. *et al.* Regulation of the polycomb protein Ring1B by self-ubiquitination or by E6-AP may have implications to the pathogenesis of Angelman syndrome. *Proceedings of the National Academy of Sciences of the United States of America* **107**, 6788–6793 (2010).
 54. Greer, P. L. *et al.* The Angelman Syndrome Protein Ube3A Regulates Synapse Development by Ubiquitinating Arc. *Cell* **140**, 704–716 (2010).
 55. Kühnle, S., Mothes, B., Matentzoglou, K. & Scheffner, M. Role of the ubiquitin ligase E6AP/UBE3A in controlling levels of the synaptic protein Arc. *Proceedings of the National Academy of Sciences of the United States of America* **110**, 8888–8893 (2013).
 56. Nawaz, Z. *et al.* The Angelman Syndrome-Associated Protein, E6-AP, Is a Coactivator for the Nuclear Hormone Receptor Superfamily. *Molecular and Cellular Biology* **19**, 1182–1189 (1999).
 57. Ramamoorthy, S. & Nawaz, Z. E6-associated protein (E6-AP) is a dual function coactivator of steroid hormone receptors. *Nuclear receptor signaling* **6**, (2008).
 58. Low, D. & Chen, K.-S. UBE3A regulates MC1R expression: a link to hypopigmentation in Angelman syndrome. *Pigment Cell & Melanoma Research* **24**, 944–952 (2011).
 59. Gossan, N. C. *et al.* The E3 ubiquitin ligase UBE3A is an integral component of the molecular circadian clock through regulating the BMAL1 transcription factor. *Nucleic Acids Research* **42**, 5765–5775 (2014).
 60. Picard, N. *et al.* Phosphorylation of activation function-1 regulates proteasome-dependent nuclear mobility and E6-associated protein ubiquitin ligase recruitment to the estrogen receptor β . *Molecular Endocrinology* **22**, 317–330 (2008).
 61. Dindot, S. V., Antalffy, B. A., Bhattacharjee, M. B. & Beaudet, A. L. The Angelman syndrome ubiquitin ligase localizes to the synapse and nucleus, and maternal deficiency results in abnormal dendritic spine morphology. *Human Molecular Genetics* **17**, 111–118 (2008).
 62. Yashiro, K. *et al.* Ube3a is required for experience-dependent maturation of the neocortex. *Nature Neuroscience* **12**, 777–783 (2009).
 63. Mabb, A. M. & Ehlers, M. D. Ubiquitination in Postsynaptic Function and Plasticity. *Annual Review of Cell and Developmental Biology* **26**, 179–210 (2010).
 64. Yamamoto, Y., Huibregtse, J. M. & Howley, P. M. The human E6-AP gene (UBE3A) encodes three potential protein isoforms generated by differential splicing. *Genomics* **41**, 263–266 (1997).
 65. Miao, S. *et al.* The Angelman syndrome protein Ube3a is required for polarized dendrite morphogenesis in pyramidal neurons. *The Journal of neuroscience : the official journal of the Society for Neuroscience* **33**, 327–33 (2013).
 66. Sadhwani, A. *et al.* Two Angelman families with unusually advanced neurodevelopment carry a start codon variant in the most highly expressed UBE3A isoform. *American Journal of Medical Genetics, Part A* **176**, 1641–1647 (2018).
 67. Rotaru, D. C., Mientjes, E. J. & Elgersma, Y. Angelman Syndrome: From Mouse Models to Therapy. *Neuroscience* (2020). doi:10.1016/j.neuroscience.2020.02.017
 68. Jiang, Y. hui *et al.* Mutation of the Angelman ubiquitin ligase in mice causes increased cytoplasmic p53 and deficits of contextual learning and long-term

- potentiation. *Neuron* **21**, 799–811 (1998).
69. Jiang, Y. H. *et al.* Altered ultrasonic vocalization and impaired learning and memory in Angelman syndrome mouse model with a large maternal deletion from Ube3a to Gabrb3. *PLoS ONE* **5**, e12278 (2010).
70. Judson, M. C. *et al.* GABAergic Neuron-Specific Loss of Ube3a Causes Angelman Syndrome-Like EEG Abnormalities and Enhances Seizure Susceptibility. *Neuron* **90**, 56–69 (2016).

CHAPTER 2

A behavioral test battery for mouse models of Angelman Syndrome: a powerful tool for testing drugs and novel *Ube3a* mutants

**Monica Sonzogni*, Ilse Wallaard*, Sara Silva Santos*, Jenina Kingma,
Dorine du Mee, Geeske M. van Woerden and Ype Elgersma#**

Department of Neuroscience, Erasmus Medical Center, Rotterdam, Netherlands.
ENCORE Expertise Center for Neurodevelopmental Disorders, Erasmus Medical Center, Rotterdam,
Netherlands

* MS, IW and SSS contributed equally to this paper

To whom correspondence should be addressed: y.elgersma@erasmusmc.nl

Molecular Autism, 2018



Abstract

Background

Angelman Syndrome (AS) is a neurodevelopmental disorder caused by mutations affecting UBE3A function. AS is characterized by intellectual disability, impaired motor coordination, epilepsy and behavioral abnormalities including autism spectrum disorder features. The development of treatments for AS heavily relies on the ability to test the efficacy of drugs in mouse models that show reliable, and preferably clinically relevant, phenotypes. We previously described a number of behavioral paradigms that assess phenotypes in the domains of motor performance, repetitive behavior, anxiety, and seizure susceptibility. Here we set out to evaluate the robustness of these phenotypes when tested in a standardized test battery. We then used this behavioral test battery to assess the efficacy of Minocycline and Levodopa, which were recently tested in clinical trials of AS.

Methods

We combined data of eight independent experiments involving 111 *Ube3a* mice and 120 wild-type littermate control mice. Using a meta-analysis, we determined the statistical power of the subtests, and the effect of putative confounding factors, such as the effect of sex and of animal weight on rotarod performance. We further assessed the robustness of these phenotypes by comparing *Ube3a* mutants in different genetic backgrounds, and by comparing the behavioral phenotypes of independently derived *Ube3a* mutant lines. In addition, we investigated if the test battery allowed retesting the same animals, which would allow a within-subject testing design.

Results

We find that the test battery is robust across different *Ube3a* mutant lines, but confirm and extend earlier studies that several phenotypes are very sensitive to genetic background. We further found that the audiogenic seizure susceptibility phenotype is fully reversible upon pharmacological treatment and highly suitable for dose finding studies. In agreement with the clinical trial results, we found that Minocycline and Levodopa treatment of *Ube3a* mice did not show any sign of improved performance in our test battery.

Conclusions

Our study provides a useful tool for preclinical drug testing to identify treatments for Angelman Syndrome. Since the phenotypes are observed in several independently derived *Ube3a* lines, the test battery can also be employed to investigate the effect of specific *Ube3a* mutations on these phenotypes.

Introduction

Angelman Syndrome (AS) is a neurodevelopmental disorder first described in 1965 by Harry Angelman, with a birth incidence of approximately 1:20,000¹.

AS is caused by the functional loss of the maternal allele encoding an E3 ubiquitin protein ligase (UBE3A)². Loss of functional UBE3A results in the core phenotypes of severe intellectual disability, motor coordination deficits, absence of speech and abnormal EEG, as well as in high comorbidity of sleep abnormalities, epilepsy and phenotypes related to autism spectrum³.

Currently, only symptomatic treatments are available for AS, primarily aimed at reducing seizures and improving sleep⁴. The development of targeted treatments for AS heavily relies on the ability to test the efficacy of treatments in mouse models of the disorder. The success of such translational studies depends on three critical factors⁵: (1) high construct validity, (2) high face validity and (3) robustness of the behavioral phenotypes. First, the construct validity (shared underlying aetiology between mouse models and patients) of the AS mouse model is very good, since AS mouse models recapitulate the patient genetics by carrying a mutated *Ube3a* gene specifically at the maternal allele. However, it should be noted that the majority of the AS patients carry a large deletion (15q11-15q13) which encompasses also other genes besides the UBE3A gene, and which may contribute to a more severe phenotype⁶. Second, with respect to face validity (i.e. similarity of phenotypes between patient and the mouse model), the AS mouse model captures many neurological key features of the disorder really well (e.g. epilepsy, motor deficits, abnormal EEG), as well as some of the behavioral abnormalities (abnormal sleep patterns, increased anxiety, repetitive behavior)⁷⁻¹². Robustness of the behavioral phenotypes is the third important aspect to identify novel treatments, as it allows experiments to be sufficiently powered to detect the effect of the treatment, and meanwhile minimizes a Type I error in which a drug is declared effective whereas it is not. Robustness, as well as face validity, also takes into account the sensitivity to genetic background and the extent in which a phenotype is also observed in independently derived mouse models. Notably, almost all behavioral testing described in literature has been performed using the original *Ube3a*^{tm1Alb} mouse strain generated in the Beaudet lab⁷⁻⁹, hence it is unknown to what

extent the reported phenotypes are actually specific to this mouse line. We previously developed a series of behavioral paradigms in the domains of motor performance, anxiety, repetitive behavior and seizure susceptibility, for testing the effect of *Ube3a* gene reinstatement in the inducible *Ube3a*^{mSTOP/p+} (*Ube3a*^{tm1Yelg}) mice¹³. Here we used these paradigms in a highly standardized way, to assess phenotypes in the independently derived *Ube3a*^{tm1Alb} and *Ube3a*^{mE113X/p+} (*Ube3a*^{tm2Yelg}) maternal knock-out strains. We combined data of eight independent experiments across five experimenters and involving 111 *Ube3a*^{tm1Alb} and 120 wild-type littermate control mice. Using a meta-analysis, we determined the statistical power of the different behavioral tests, and the effect of putative confounding factors, such as the effect of sex differences. We further assessed the robustness of these phenotypes by comparing *Ube3a* mutants in different genetic backgrounds. Finally, we employed this behavioral test battery to reassess the efficacy of Minocycline and Levodopa in the AS mouse model. Minocycline is a matrix metalloproteinase-9 inhibitor (MMP9), a tetracycline derivative which possesses antibiotic as well as neuroprotective activity^{14,15}. Its antibiotic properties against both gram-positive and gram-negative bacteria is related to its ability to bind to the bacterial 30S ribosomal subunit, thereby inhibiting protein synthesis¹⁴. Levodopa is the precursor of dopamine, and was shown to be effective in treating Parkinsonism in two adults with Angelman Syndrome¹⁶. Moreover, it is able to reduce CAMK2 phosphorylation¹⁷, which was shown to be increased in a mouse model for Angelman syndrome^{18,19}. Minocycline and Levodopa were previously tested in the AS mouse model and based on the favorable outcome of these preclinical experiments, three clinical trials were performed²⁰⁻²². Unfortunately, none of these drugs showed a significant improvement in AS patients.

Methods

Mouse husbandry and breeding

For this study, we used *Ube3a*^{m-/p+} mice (*Ube3a*^{tm1Alb}; MGI 2181811)⁷ and *Ube3a*^{mE113X/p+} mutants (*Ube3a*^{tm2Yelg}; MGI5911277) as previously described²³. *Ube3a*^{tm1Alb} mice were maintained (>40 generations) in the 129S2 background (full name: 129S2/SvPasCrl) by crossing male *Ube3a*^{m+/p-} mice with female 129S2 wild-type mice. *Ube3a*^{tm2Yelg} mice were maintained (>20 generations) in the C57BL/6J (Charles River) background by crossing male *Ube3a*^{m+/pE113X}

mice with female C57BL/6J wild-type mice. For the seizure susceptibility experiments with $Ube3a^{mE113X/p+}$ animals, this line was backcrossed 8 times in 129S2 by crossing $Ube3a^{pE113X/m+}$ males with 129S2 wild-type females.

For behavioral experiments, female $Ube3a^{tm1Alb} (Ube3a^{m+/p-})$ mice were bred to yield $Ube3a^{m-/p+}$ mice in two different backgrounds: $Ube3a^{m-/p+}$ (AS) mice and their WT littermates in the F1 hybrid 129S2-C57BL/6J background (WT=120, AS=111) and in the 129S2 background (WT=11, AS=16). $Ube3a^{mE113X/p+}$ mice and their WT littermates were generated in the same manner in the F1 hybrid 129S2-C57BL/6J background (WT=10, $Ube3a^{mE113X/p+}$ =10) and in C57BL/6J background (WT=15, $Ube3a^{mE113X/p+}$ =16).

For the seizure susceptibility test we used $Ube3a^{m-/p+}$ (WT=45, AS=114) and $Ube3a^{mE113X/p+}$ mice (WT=4, AS=8) in the 129S2 background.

Mice were housed in individually ventilated cages (IVC; 1145T cages from Techniplast) in a barrier facility. Mice were genotyped when they were 4-7 days old, and re-genotyped at the completion of the experiments. All animals were kept at $22\pm 2^{\circ}\text{C}$ with a 12 hours dark and light cycle, and were tested in the light period, provided with mouse chow (801727CRM(P) from Special Dietary Service) and water *ad libitum*. During behavioral testing, mice were group-housed with 2-4 animals of the same sex per cage. Fighting between males was observed a few times, and in these rare cases, mice were separated and single housed. This was not a reason for exclusion. All mice were single housed during nest building and for the subsequent forced swim test. All animal experiments were conducted in accordance with the European Commission Council Directive 2010/63/EU (CCD approval AVD101002016791).

Behavioral analysis

The weight of the animals was determined a few days before the start of the behavioral analysis. Prior to each test, mice were acclimatized to the testing room for 30 minutes.

All behavioral experiments were performed during the light period of the light/dark cycle. Both male and female mice at the age of 8-12 weeks were used for the experiments. Moreover, we tried to obtain a similar ratio of females/males between the WT and AS groups. Only in the experiments described in **Figure 4** ($Ube3a^{E113X}$ mice in F1 background) and for the epilepsy experiment using $Ube3a^{E113X}$ mice (**Figure 6C**), the female/male ratio between the groups was significantly different ($p < 0.05$; Chi-square test).

All behavioral testing and scoring was performed by experimenters who were blind to genotype and treatment. Behavioral tests were always run in the following order and with a minimal number of days between tests: 1) accelerating rotarod test for 5 consecutive days performed at the same hour every day; 2) 2 days of pause; 3) open field test; 4) 1 day of pause; 5) marble burying test; 6) between 5 to 7 days of pause to allow adaptation to being single caged; 7) nest building test for 5 consecutive days, in which the weight of the nest was assessed at the same hour every day; 8) 2 days of pause; 9) forced swim test.

Accelerating rotarod. Motor function was tested using the accelerating rotarod (4-40 rpm, in 5 minutes; model 7650, Ugo Basile Biological Research Apparatus, Varese, Italy). Mice were given two trials per day with a 45-60 min inter-trial interval for 5 consecutive days (same hour every day). For each day, the average time spent on the rotarod was calculated, or the time until the mouse made 3 consecutive wrapping / passive rotations on the rotarod (latency in seconds). These passive rotations were observed rarely (1-2%) in 129S2 or F1 hybrid 129S2-C57BL/6J mice but rather common in (30%) C57BL/6J mice. Maximum duration of a trial was 5 min.

Open Field test. To test locomotor activity and anxiety, mice were individually placed in a 110 cm diameter circular open field and allowed to explore for 10 min. The light intensity was approximately 25-30 lux measured in the center of the arena. The total distance moved by each mouse in the open arena was recorded by an infrared camera (Noldus® Wageningen, NL) connected to the EthoVision® software (Noldus® Wageningen, NL), and the final outcome is indicated as distance moved in meters. For some groups we also analyzed the time spent in the inner zone (IZ), middle zone (MZ) and outer zone (OZ) (IZ r=25cm, MZ r=40, OZ r=55cm).

Marble burying test. Open makrolon (polycarbonate) cages (50x26x18 cm) were filled with 4 cm of bedding material (Lignocel® Hygenic Animal Bedding, JRS). On top of the bedding material 20 blue glass marbles were arranged in an equidistant 5 x 4 grid and the animals were given access to the marbles for 30 minutes. After the test the mice were gently removed from the cage. Marbles covered for more than 50% by bedding were scored as buried and the outcome measured is the number of buried marbles.

Nest Building test. To measure nest building, mice were single housed for a period of 5 to 7 days before the start of the experiment. Subsequently used nesting material was replaced and 11 grams (11±1) of compressed extra-thick blot filter paper (Bio-rad©) was added to the cage. The amount of the unused nest material was weighed and noted every day for a consecutive of 5 days, each day at the same hour.

Forced swim test. Mice were placed for 6 min in a cylindrical transparent tank (27cm high and 18cm diameter), filled with water (kept at 26±1 degrees Celsius) 15 cm deep. The mouse was first left in the cylinder for 2 minutes to habituate. Immobility during the forced swim test was scored manually (stop-watch) by timing the amount of time the mouse was floating in the water (defined by lack of any movement), and was assessed during the last 4 min of the test. The mouse was considered to be immobile when he ceased to move altogether, making only movements necessary to keep its head above water. The outcome measured is the time in seconds in which the mouse was immobile.

Susceptibility to audiogenic seizures. Because of the different genetic background requirements, an independent cohort of mice was used to test susceptibility to audiogenic seizures. Mice were placed in makrolon (polycarbonate) cages (50x26x18 cm) and audiogenic seizures were induced by vigorously scraping scissors across the metal grating of the cage lid (which creates approximately a 100 dB sound). This noise was generated for 20 seconds, or less if a tonic-clonic seizure developed before that time. Susceptible mice responded with wild running and leaping followed by a tonic-clonic seizure, which typically lasted 10–20 seconds.

Within-subject testing

For the experiment described in **Figure 3**, *Ube3a^{tm1Alb}* mice in F1 hybrid 129S2-C57BL/6J background were subjected to the behavioral test battery for a second time. Once the first battery was completed, female mice that had been single housed for the nest-building test, were placed back together with the original cage mates, while male mice remained separated for the entire second set of behavioral tasks. The second test started four weeks after the first testing was completed.

Drug administration

Vehicle treatment

All animals used for the meta-analysis were treated with vehicle, either by I.P. injection, (max. volume 10 ul/g, Hypodermic-needle 25G x 16 mm (Sterican®/ B-Braun)), Oral gavage (max 10 ul/g, Stainless steel animal feeding tubes 20G x 38 mm (Instech Laboratories)) or by adding to the drinking water.

Minocycline treatment

The adult-treated group consisted of 8-10 week old *Ube3a^{m-/p+}* (n=11 saline; 11 Minocycline) and WT (n=9 saline; 10 Minocycline) littermate control mice in F1 hybrid 129S2-C57BL/6J background. Due to space limitations, only 6 animals per group were used for nest building. Mice were assigned to two treatment groups in such a way that both groups had a comparable distribution of males and females and mutant and wild-type mice. Mice were subjected to daily minocycline or vehicle IP injections (Minocycline hydrochloride, Sigma-Aldrich 45 mg/kg in saline solution), starting three weeks prior to commencing behavioral testing, as previously described^{20,24}. Behavioral testing was started 1.5 hours post-injection, based on the half-life of Minocycline (~ 2h in plasma) and the peak brain levels are reached about 2h after injection²⁵.

For the postnatal-treated group, cages with *Ube3a^{m-/p+}* and WT pups in F1 hybrid 129S2-C57BL/6J background were split in two treatment groups in such a way that both groups had a comparable distribution of males and females and mutant and wild-type mice. The treatment group received minocycline via the lactating dam, which received minocycline through the drinking water (0.2 mg minocycline/ml, supplemented with 1 mg/ml aspartame to counteract the bitter taste and shielded for light)²⁶. This method of administration was shown to yield detectable concentration of minocycline in the blood of adult mice²⁷ and in the breast milk of lactating dams^{28,29}. Once the mice were weaned, they were supplied with the same concentration of minocycline in their drinking water. Assuming a water intake of 1.5 ml/10 g body weight/day³⁰, and assuming an average weight of 25 g/mouse, the average amount of minocycline these mice received is approximately 30 mg/kg/day. The drinking water was refreshed every other day. Treatment continued until all behavioral experiments were completed. The control group received water with aspartame.

Levodopa/Carbidopa treatment

Cages containing *Ube3a^{m-/p+}* and wild-type littermate control mice (8-12 weeks old) in the F1 hybrid 129S2-C57BL/6J background were assigned to two treatment groups in such a way that both groups had 15 wild-type and 15 mutants and a comparable distribution of males and females. Mice in the treatment group received 15 mg/kg Levodopa and 3.75 mg/kg Carbidopa dissolved in saline (Levodopa, Sigma-Aldrich; Carbidopa, Sigma-Aldrich) by IP injection with an injection volume of 10 μ l/g. The untreated group received vehicle injection by IP as described by Tan et al.²¹ The mice were injected 1 hour prior to carrying out the behavioral tasks, during the entire period while partaking in these tests.

Levetiracetam treatment

Ube3a^{m-/p+} mice in the 129S2 background were first tested for audiogenic seizure susceptibility at baseline. Minimally 24 hours later, the mice were again tested for audiogenic seizure susceptibility, this time precisely 1 hour following a single IP injection of Levetiracetam (0-0.5-1-2-10-15 mg/kg; Sigma-Aldrich). The injection volume used is 5 ml/kg and the drug was dissolved in 1% Tween-80 (Sigma-Aldrich) in milliQ water as previously described³¹.

Data analysis

Data was analysed using Excel 2010 (Microsoft) and IBM SPSS software (NY, USA). The open field, marble burying and forced swim test data were analysed using an unpaired T-Test in the untreated experimental groups, and a 2-way ANOVA in Minocycline and Levodopa treated animals (in which we assessed a genotype-treatment interaction). Rotarod and nest building were measured with a repeated measures ANOVA in the untreated experimental groups, or with a multivariate repeated measures ANOVA (assessing significance of interaction of time, genotype and treatment) in the Minocycline and Levodopa experimental groups. We used a *Bonferroni's post hoc test* to detect significant differences in male and female groups. For the within subject experiment we used a paired T-Test for open field, marble burying and forced swim test, while we used a repeated measures factorial ANOVA when analyzing the rotarod and the nest building test. For the audiogenic seizure analysis, a Fisher's exact test was used. The correlation between body weight and maximal performance on the rotarod

test was assessed with a Pearson's correlation test. For the power calculation we performed a priori analysis using G*Power 3.1 software³² with $\alpha=0.05$ and power $(1-\beta) =0.95; 0.90$ or 0.80 . Data is presented as mean \pm SEM in all figures. For all tests, statistical significance was denoted by $p\leq 0.05$ (*), $p< 0.01$ (**), $p<0.001$ (***)

A Chi-square test was performed to test if there were any significant differences in the ratio of females/males between the WT and AS groups.

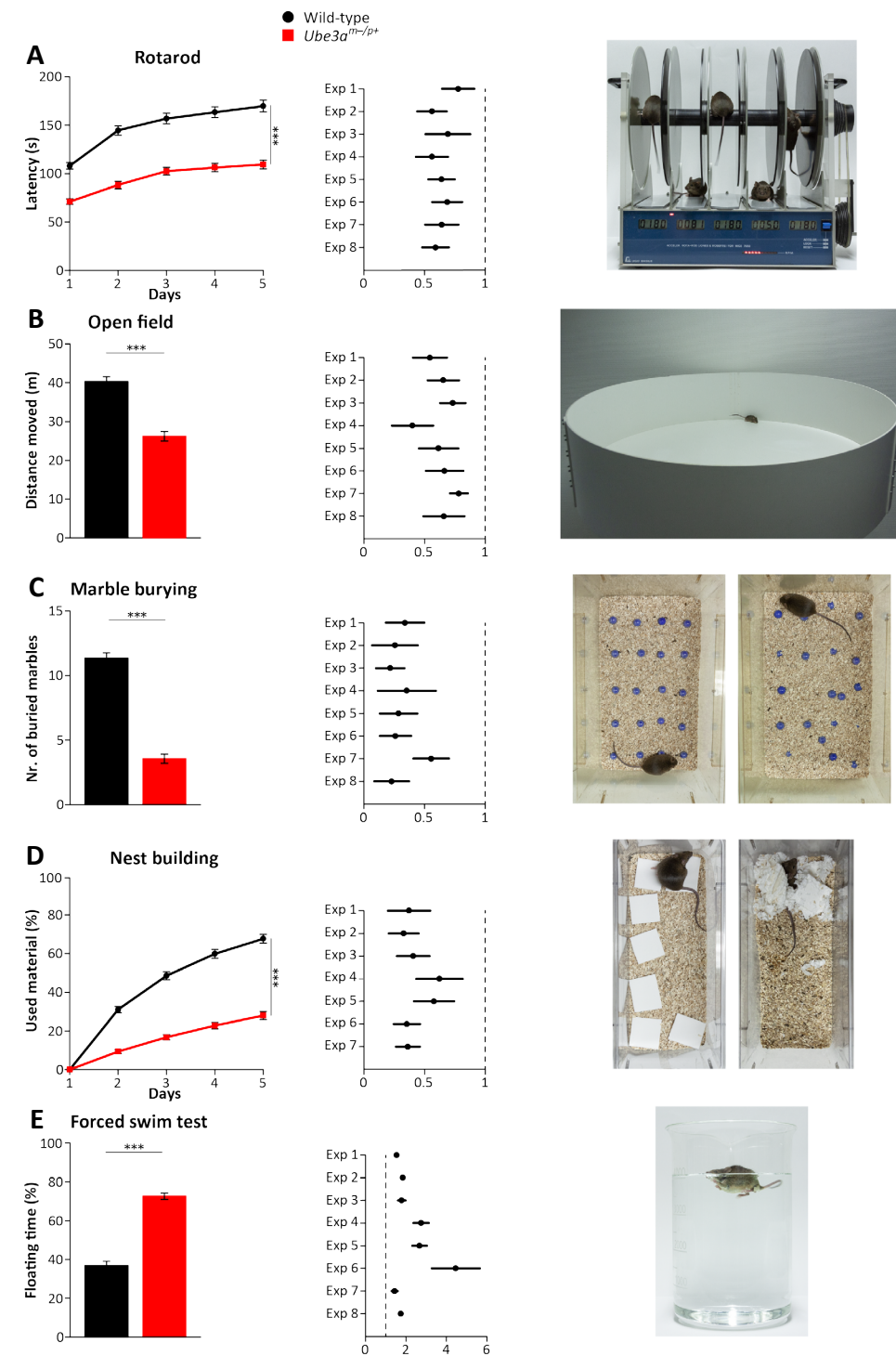
Results

Robust behavioral phenotypes in *Ube3a^{m-/p+}* mice in the F1 hybrid 129S2-C57BL/6J background

We recently developed a number of behavioral tests for testing the effect of gene reinstatement in inducible *Ube3a^{mSTOP/p+}* (*Ube3a^{tm1Yelg}*) mice¹³. These tests can be applied in successive order to assess phenotypes in the domains of motor performance, anxiety, and repetitive behavior. Here we set out to assess the robustness of these phenotypes in an independently derived mouse model of AS, by using F1 hybrid 129S2-C57BL/6J *Ube3a^{m-/p+}* (*Ube3a^{tm1Alb}*) mice⁷, which is the *Ube3a* mouse mutant used for nearly all behavioral studies. We have frequently used this strain to test the efficacy of novel treatments, and combined all data obtained from vehicle treated *Ube3a^{m-/p+}* and wild-type littermate controls in the F1 hybrid 129S2-C57BL/6J background to perform a meta-analysis. In total, this constitutes the combined data of 8 experiments, carried out by 5 experimenters and totaling 111 *Ube3a^{m-/p+}* and 120 wild-type littermate controls (**Table 1; Figure 1**).

Exp.#	Person	WT/MUT (n)	Sex WT f/m MUT f/m (n)	Rotarod (time(s))		Open field (distance(m))		Marble burying (# marbles buried)		Nest building (% material unused)		Forced swim test (% floating)	
				WT mean (sd) Mut mean (sd)	WT mean (sd) Mut mean (sd)	WT mean (sd) Mut mean (sd)	WT mean (sd) Mut mean (sd)	WT mean (sd) Mut mean (sd)	WT mean (sd) Mut mean (sd)	WT mean (sd) Mut mean (sd)			
1	A	15/13	8/7 6/7	128 (42) 96 (32)	41 (14) 22 (11)	11 (4) 4 (3)	14 (25) 79 (18)	53 (23) 83 (7)					
2	A	15/13	5/10 3/10	142 (43) 80 (32)	49 (10) 32 (12)	8 (4) 2 (3)	36 (23) 79 (14)	44 (24) 81 (7)					
3	A	15/13	5/10 3/10	133 (42) 92 (46)	40 (12) 29 (8)	11 (3) 2 (2)	27 (18) 70 (18)	41 (19) 73 (14)					
4	B	21/17 ¹	10/11 7/10	159 (60) 102 (36)	31 (12) 19 (11)	14 (4) 4 (5)	10 (11) 48 (25)	24 (22) 63 (18)					
5	C	9/11 ²	5/4 6/5	163 (49) 91 (37)	25 (6) 10 (7)	12 (5) 4 (5)	48 (27) 69 (12)	28 (24) 76 (8)					
6	D	15/14 ³	4/11 6/8	107 (44) 74 (26)	44 (7) 29 (13)	12 (3) 3 (3)	40 (18) 79 (12)	14 (20) 60 (31)					
7	E	15/15	8/7 7/8	196 (57) 126 (52)	45 (10) 35 (7)	11 (5) 6 (3)	63 (20) 74 (14)	47 (20) 67 (14)					
8	A	15/15 ⁴	7/8 8/7	162 (49) 95 (35)	49 (9) 33 (13)	10 (3) 2 (3)	N/A	47 (20) 88 (9)					

Table 1. Overview of experiments used for the meta-analysis. All experiments were performed using *Ube3a^{tm1Alb}* mice in F1 hybrid 129S2-C57BL/6J background. For all tests shown in this table, we found a significant effect of genotype ($p < 0.05$), except for the nest building test of experiment 8, which was not performed. The table indicates the individual that performed the test battery, the number of wild-type and mutant mice used for each test, the number of females and males used for each experimental group, and the mean and standard deviation of the outcomes obtained. For rotarod we indicated the average performance over the 5 days, while for the nest building we provided the data as measured at day 5. Note that for some of the tests we used a different number of mice (mice were not properly tracked, or a smaller cohort was used for nest building because of space limitations). The adapted n for these experiments is: 1): nest building 13/12, forced swim test 20/17; 2): nest building 6/7; 3): open field 13/14; 4): open field 10/10, nest building not performed.



Individuals with Angelman syndrome show clear motor impairments, and impaired performance on the accelerating rotarod is the most frequently described phenotype in *Ube3a* mice. Indeed, our meta-analysis shows a very robust significant difference between the two genotypes (p<0.001; **Figure 1A**). A power analysis with $\alpha=0.05$; $(1-\beta)=0.95$ showed that this task requires 14 animals per genotype (**Table 2**).

Following 2 days of rest, the same mice were then tested in the open field test. This paradigm is commonly used to assess anxiety in mice. Increased anxiety is commonly observed in individuals with AS³³, as well as individuals with autism spectrum disorder. In this test, we place the mice in an open arena situated in a brightly lit room, and record the distance the mice travel during a 10-minute time span. The measurements of the distance moved in the open arena indicated that AS mice moved significantly less (WT: 40.3 \pm 1.2m; AS: 26.2 \pm 1.2m; p<0.001; **Figure 1B**). A power analysis ($\alpha=0.05$; $(1-\beta)=0.95$) showed that this task requires a minimum number of 21 mice per genotype, which makes this test a relative weak test (**Table 2**). Previous studies reported no significant difference observed between genotypes in the time spent in the inner zone of the open field, which is another measure of anxiety^{8,9}. Our meta-analysis revealed a significant difference between genotypes (p<0.005), but this difference was small (WT: 1.1% versus mutant 0.7% time in inner zone), and a significant effect was only observed in 4 out of the 8 individual experiments (data not shown).

After one day of rest, the same mice were then analyzed in the marble

burying test, a test used to assess repetitive and perseverative behavior as well as anxiety^{34,35}. When exposed to marbles, AS mice show a strongly impaired marble burying behavior compared to WT mice (WT: 11.3±0.4; AS: 3.6±0.3; $p < 0.001$; **Figure 1C**). A power analysis ($\alpha = 0.05$; $(1 - \beta) = 0.95$) showed that 7 animals/group are sufficient for this test, indicating a very robust phenotype (**Table 2**).

After the marble burying task, all mice were single housed for 5-7 days and then analyzed for 5 consecutive days while performing the nest building test. The nest building test assesses the innate behavior of mice to create a nest to maintain body temperature and to find shelter³⁶. AS mice showed a clear phenotype compared to their WT control littermates ($p < 0.001$; **Figure 1D**). As indicated in **Table 2**, the nest building phenotype is quite robust, since it only requires 8 mice ($\alpha = 0.05$; $(1 - \beta) = 0.95$) per group if analyzed over the last day.

Following 2 days of pause, the animals were finally subjected to the forced swim test, in which the mouse is placed in a beaker filled with water, from which the mouse will try to escape by swimming. This test is typically used to test depressive-like behavior in mice³⁷. AS mice showed significant more time floating (instead of swimming) compared to WT mice (WT: 36.8±2.3; AS: 72.6±1.7; $p < 0.001$; **Figure 1E**). The power analysis test showed that this task requires a minimum of 10 mice ($\alpha = 0.05$; $(1 - \beta) = 0.95$).

Taken together, the data indicates that this test battery yields a series of robust behavioral phenotypes that can be obtained in a relative quick manner using a single cohort of mice.

	Wild-type (mean±SD)	Ube3a (mean±SD)	Test	Achieved effect size	Sample size per group $\beta = 0.95$	Sample size per group $\beta = 0.90$	Sample size per group $\beta = 0.80$
Rotarod Time on machine (s)	149±55	95±40	ANOVA	0.56	14	11	9
Open Field Distance moved (m)	40 ±13	26 ±13	T test	1.17	21	17	13
Marble burying (# Marbles buried)	11±4	4 ±4	T test	2.26	7	6	5
Nest building (% used nesting material)	68±23	28 ±19	T test	1.95	8	7	6
Forced swim test (% floating time)	37±25	73 ±18	T test	1.73	10	9	7
Susceptibility to audiogenic seizure (% of animals)	7	98	T test	4.55	3	3	3

Table 2. Achieved power for each behavioral test of the behavioral test battery.

Data provided is based on the experiments using *Ube3a^{tm1Alb}* mice in F1 hybrid 129S2-C57BL/6J background. The table provides the obtained effect size, number of mice needed per genotype for each behavioral test (with power equal to 0.95, 0.90, 0.80) and statistical test used. For rotarod calculations we used the average performance over the 5 days, while for the nest building we used the data of the last test day.

The dependence of sex on the behavioral phenotypes

Angelman syndrome affects both males and females, with no known differences between the sexes. To assess if this is also the case for the *Ube3a* mouse phenotypes described above, we analyzed if there were any significant sex differences. An effect of sex was noted on the rotarod, in which female wild-type and *Ube3a* mice performed significantly better than male wild-type and *Ube3a* mice ($p < 0.001$; **Figure 2A**). Since male mice are heavier than female mice and since *Ube3a*^{m-/p+} mutants show increased weight (**Figure 2F**)^{8,38}, we investigated if the impaired rotarod performance as seen in *Ube3a*^{m-/p+} mutants could be attributed to their increased weight. Hence, we performed a correlation analysis between body weight and time on the rotarod (as measured on the last training day). As shown in **Figure 2G**, no meaningful correlation is observed between body weight and latency to fall in both WT mice and AS mice (WT males Pearson $r = 0.08$, AS males Pearson $r = -0.21$, WT females Pearson $r = 0.35$, AS females Pearson $r = 0.02$), although the correlation observed in WT female mice was just statistically significant ($p < 0.05$), indicating that increased bodyweight actually improves (rather than impairs) rotarod performance. Overall we conclude that the impaired motor performance of *Ube3a*^{m-/p+} mutants on the rotarod is not caused by the increased body weight observed in these mice, but truly reflect differences in motor performance.

We also observed a small effect of sex for the nest building task in which female *Ube3a*^{m-/p+} mutants outperformed the male *Ube3a*^{m-/p+} mutants ($p < 0.05$). A similar tendency was also observed in wild-type mice, but this effect was not significant (**Figure 2B**). Despite the slightly better performance of female *Ube3a*^{m-/p+} mutants, female *Ube3a*^{m-/p+} mutants were still significantly different from wild-type mice ($p < 0.001$).

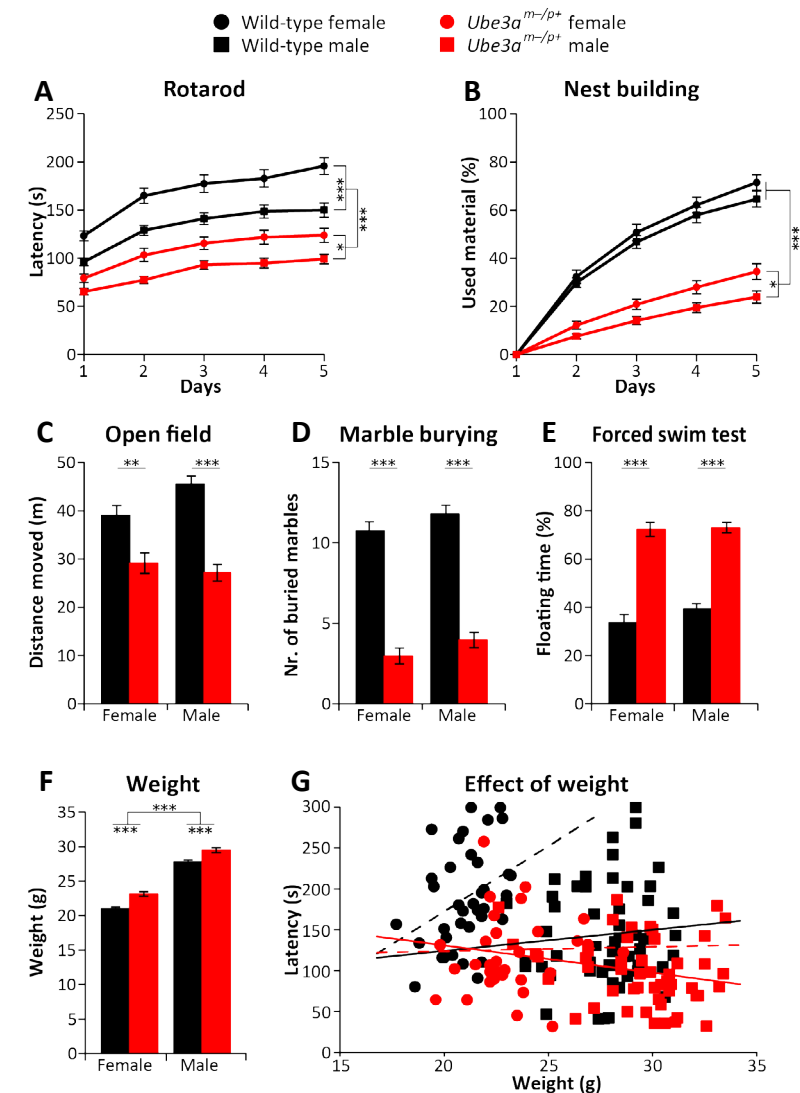


Figure 2. Effect of sex on the behavioral phenotypes of *Ube3a*^{tm1Alb} mice in F1 hybrid 129S2-C57BL/6J background.

A Accelerating rotarod in WT and *Ube3a*^{m-/p+} female mice ($n = 52,46$) and in WT and *Ube3a*^{m-/p+} male mice ($n = 68,65$). **B** Nest building test in WT and *Ube3a*^{m-/p+} female mice ($n = 42,33$) and in WT and *Ube3a*^{m-/p+} male mice ($n = 52,53$). **C** Open field test in WT and *Ube3a*^{m-/p+} female mice ($n = 47,41$) and in WT and *Ube3a*^{m-/p+} male mice ($n = 66,65$). **D** Marble burying test in WT and *Ube3a*^{m-/p+} female mice ($n = 52,46$) and in WT and *Ube3a*^{m-/p+} male mice ($n = 68,65$). **E** Forced swim test in WT and *Ube3a*^{m-/p+} female mice ($n = 52,46$) and in WT and *Ube3a*^{m-/p+} male mice

(n=68,65). **F** Bodyweight in WT and *Ube3a^{m-/p+}* female mice (n=37,33) and in WT and *Ube3a^{m-/p+}* male mice (n=53,50). **G** Pearson correlation test between body weight and latency to fall at day 5 in WT and *Ube3a^{m-/p+}* female mice (n=37,33) and in WT and *Ube3a^{m-/p+}* male mice (n=53,50). Multivariate repeated ANOVA or a 2-way ANOVA was used for statistical comparison. A Bonferroni's post hoc test was used to detect significant differences in behavioral phenotypes of male and female groups. All data represent mean \pm SEM. Significant effects of genotype or sex are indicated as * $p < 0.05$, ** $p < 0.01$, *** $p < 0.001$.

We observed no significant effect of sex in the open field test ($p=0.25$), marble burying test ($p=0.06$) and forced swim test ($p=0.27$; **Figure 2C-E**). Overall these data suggest that the set of behavioral phenotypes observed in AS mice are robust and are not markedly influenced by the sex of the animal. However, given the decreased performance of male mice on the rotarod, mixed cohorts used for rotarod testing should be well balanced with respect to sex to obtain a reliable phenotype.

The behavioral test battery is suitable for within-subject testing design

A within-subject testing design is a powerful design for drug testing purposes, as it allows assessing the efficacy of a drug with considerable fewer animals. Therefore, we investigated whether the behavioral test battery allowed retesting the same animals while maintaining a similar phenotype, which is a prerequisite for applying a within subject design. We subjected 15 *Ube3a^{m-/p+}* mice (*Ube3a^{tm1Alb}*) and 15 WT littermates in the F1 hybrid 129S2-C57BL/6 background to the behavioral test battery, and repeated the test battery after a pause of 4 weeks. As shown in **Figure 3**, performance on the rotarod test, nest building test and forced-swim test was highly similar when the initial test data were compared to the re-testing data. However, performance in the open field test as well as marble burying test was significantly different when this test was performed for the second time (Open field: wild-type initial vs retest $p < 0.001$; *Ube3a^{m-/p+}* initial vs retest $p < 0.001$. Marble burying: wild-type initial vs retest $p < 0.001$; *Ube3a^{m-/p+}* initial vs retest $p < 0.001$; Paired T-test). These differences upon retesting are likely due to the decreased anxiety levels and or habituation of the mice upon re-testing in these paradigms. Importantly, *Ube3a^{m-/p+}* mice remained significant different from wild-type littermates when tested for a second time, with the exception of the marble burying test, which no longer yielded a phenotype upon retesting ($p=0.13$). Hence, we conclude that most tests of the behavioral test battery are suitable for a within-subject design to test the efficacy of a drug.

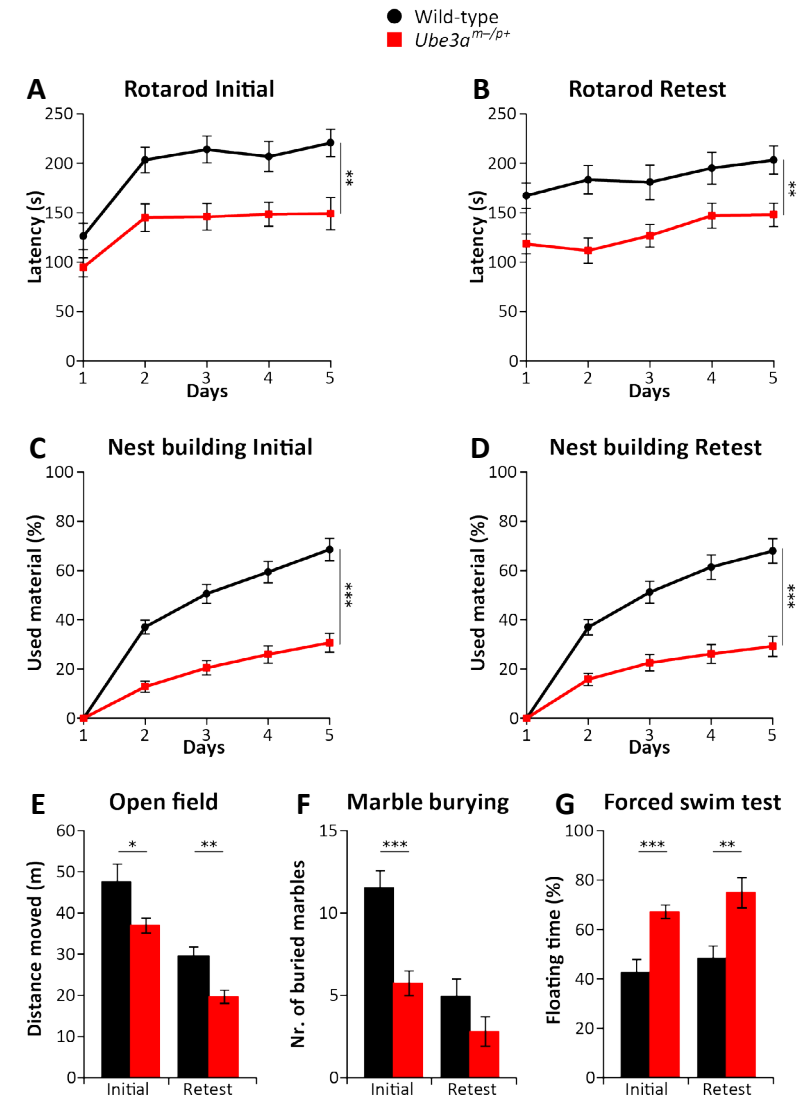


Figure 3. Most behavioral phenotypes are stable upon re-testing *Ube3a^{tm1Alb}* mice in F1 hybrid 129S2-C57BL/6J background.

A,C,E,F,G WT and *Ube3a^{m-/p+}* mice at initial testing and (**B,D,E,F,G**) upon re-testing. A single cohort of 15 wild-type (8 females, 7 males) and 15 *Ube3a^{tm1Alb}* (8 females, 7 males) mice was used for all experiments. A repeated measures ANOVA or T-Test was used for statistical comparison of genotypes, as described in legend of figure 1. All data represent mean \pm SEM. Significant effects of genotype are indicated as * $p < 0.05$, ** $p < 0.01$, *** $p < 0.001$ for genotype significance.

Behavioral phenotypes are also observed in the *Ube3a*^{E113X} mouse model

The results above indicate that the behavioral test battery gives robust phenotypes in the *Ube3a*^{tm1Alb} line as well as in the previously published *Ube3a*^{mSTOP/p+} (*Ube3a*^{tm1Yelg}) line. In order to test the robustness of the battery in a third independently derived *Ube3a* mutant strain, we used the *Ube3a*^{mE113X/p+} (*Ube3a*^{tm2Yelg}) strain, which we recently described²³. As shown in **Figure 4** the *Ube3a*^{mE113X/p+} mutant mice in the F1 129S2-C57BL/6J background, showed again clear impairments on the rotarod ($p < 0.001$), open field test ($p < 0.001$), marble burying test ($p < 0.05$), nest building test ($p < 0.01$), and forced swim test ($p < 0.001$). Taken together, these data suggest that the identified set of behavioral phenotypes in this test battery is present in 3 independently derived *Ube3a* mutant lines.

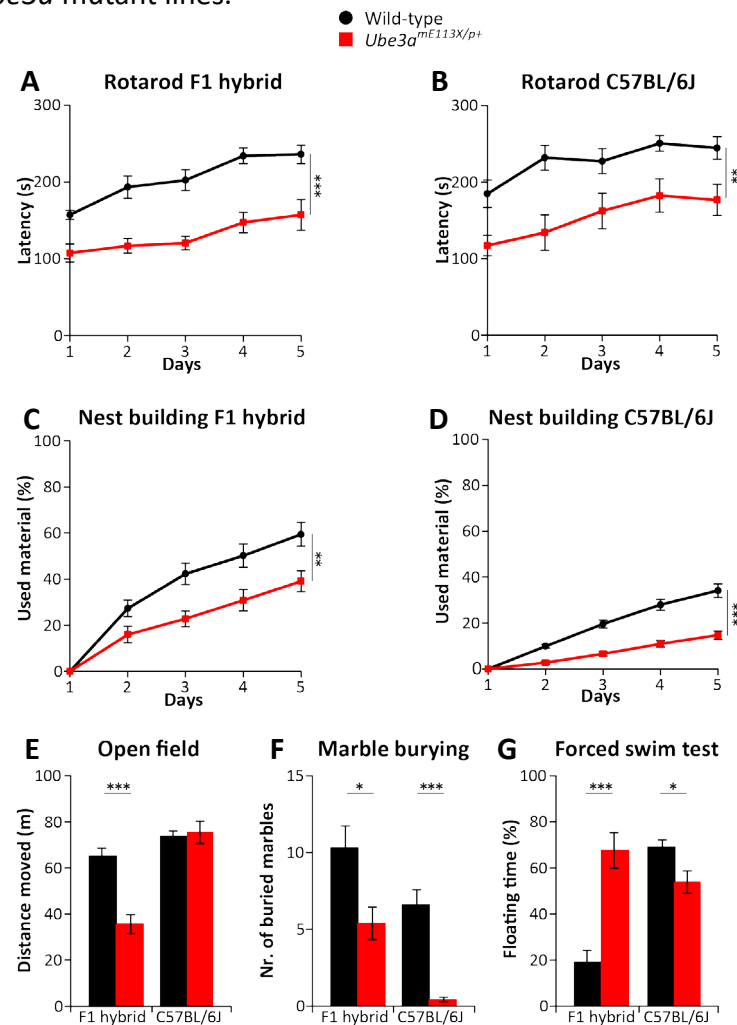


Figure 4. Behavioral testing of *Ube3a*^{mE113X/p+} (*Ube3a*^{tm2Yelg}) mice in the F1 hybrid 129S2-C57BL/6J and the C57BL/6J background.

A,B Accelerating rotarod in WT and *Ube3a*^{mE113X/p+} mice in F1 hybrid 129S2-C57BL/6J and C57BL/6J background. **C,D** Nest building test in WT and *Ube3a*^{mE113X/p+} mice in F1 hybrid 129S2-C57BL/6J and C57BL/6J background. **E,F,G** Open field, marble burying and forced swim test in WT and *Ube3a*^{mE113X/p+} mice in F1 hybrid 129S2-C57BL/6J and C57BL/6J background. For all behavioral tests we used a single cohort of 10 wild-type (1 female, 9 males), 10 *Ube3a*^{mE113X/p+} mice (6 females, 4 males) in F1 hybrid 129S2-C57BL/6J, and 15 wild-type (11 females, 4 males) and 16 *Ube3a*^{mE113X/p+} (*Ube3a*^{tm2Yelg}) (13 females, 4 males) in C57BL/6J background. All data represent mean \pm SEM. A repeated measures ANOVA or T-Test was used for statistical comparison of genotypes, as described in legend of figure 1. Significant effects of genotype are indicated as * $p < 0.05$, ** $p < 0.01$, *** $p < 0.001$.

Mouse genetic background affects the identified AS phenotypes

Previous studies have indicated the importance of the genetic background for certain *Ube3a* phenotypes^{8,9}. To test the importance of the genetic background on the behavioral test battery, we performed the test battery on AS mice on a pure C57BL/6J (**Figure 4**) and 129S2 background (**Figure 5**) instead of the F1 hybrid background. *Ube3a*^{mE113X/p+} mice in C57BL/6J background showed a similar phenotype as *Ube3a*^{mE113X/p+} mutants in the F1 hybrid 129S2-C57BL/6J background with respect to rotarod ($p < 0.01$), marble burying test ($p < 0.001$) and nest building test ($p < 0.001$) (**Figure 4**). No deficit was observed in the open field test ($p = 0.75$). Notably, the *Ube3a*^{mE113X/p+} mice in C57BL/6J background showed a significant phenotype in the forced swim test ($p < 0.05$), however in the opposite direction compared to AS mice in F1 hybrid 129S2-C57BL/6J background.

The test battery was also performed using *Ube3a*^{tm1Alb} mice in the inbred 129S2 background (**Figure 5**). *Ube3a*^{tm1Alb} mice in the 129S2 background did not show any of the phenotypes observed in *Ube3a*^{tm1Alb} mice in the F1 hybrid background, with the exception of the forced swim test ($p < 0.05$), which yielded a similar result as obtained in mice in the F1 hybrid background. Taken together these data confirm and extend previous studies that most AS mouse phenotypes are strongly dependent on the genetic background.

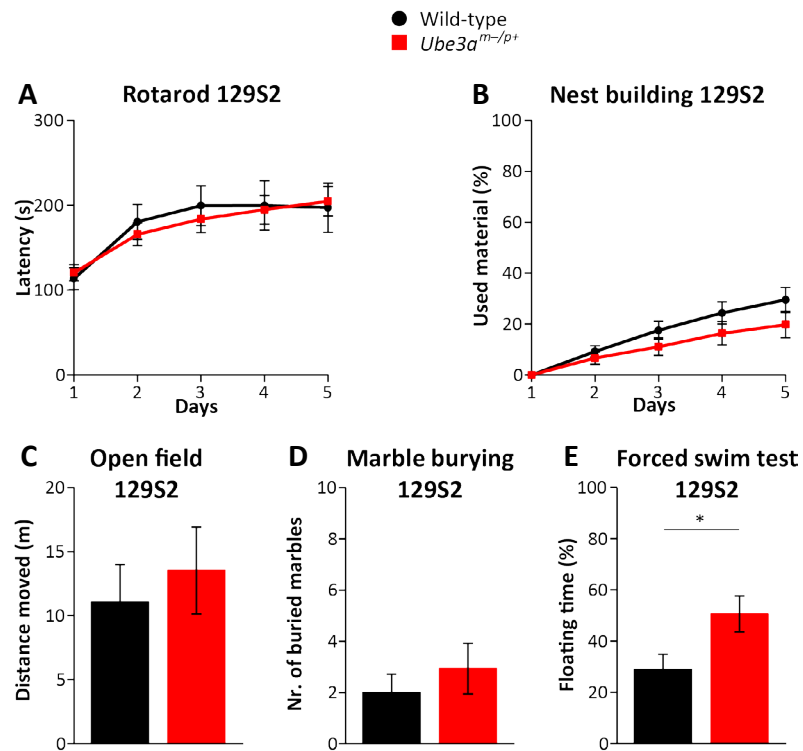


Figure 5. Behavioral testing of *Ube3a^{m-/p+}* (*Ube3a^{tm1Alb}*) mice in the 129S2/SvPasCrl background.

A-E Accelerating rotarod, nest building, open field, marble burying and forced swim test in wild-type and *Ube3a^{tm1Alb}* mice in 129S2/SvPasCrl background (n=11,16)(WT=5 females, 6 males) (*Ube3a^{m-/p+}* = 8 females, 8 males). A repeated measures ANOVA or T-Test was used for statistical comparison of genotypes, as described in legend of figure 1. Significant effects of genotype are indicated as *p<0.05.

Susceptibility to audiogenic seizures

Epilepsy is a common feature of individuals with AS³⁹. We previously showed that *Ube3a^{tm1Alb}* mice as well as *Ube3a^{mSTOP/p+}* (*Ube3a^{tm1Yelg}*) mice are highly susceptible to audiogenic seizures, a phenotype that is specifically observed in mice in the 129S2 background⁷. To investigate the strength of this test in more detail, we performed a meta-analysis of 5 independent experiments with a total of 114 *Ube3a^{m-/p+}* (*Ube3a^{tm1Alb}*) mice and 45 wild-type littermates in the 129S2 background. This analysis showed that this is a very robust phenotype with seizures observed in 98% of *Ube3a^{m-/p+}* mice and in 7% of

the wild-type littermates (p<0.001). The robustness of this test was further confirmed by a power calculation analysis (Table 2).

We tested whether seizures were also present in the *Ube3a^{mE113X/p+}* (*Ube3a^{tm2Yelg}*) line. To that end, we crossed *Ube3a^{pE113X/m+}* females (backcrossed 8 times in 129S2) with 129S2 males. As shown in Figure 6, an audiogenic seizure could be provoked in all *Ube3a^{mE113X/p+}* mutants tested (p<0.001), indicating that this phenotype is observed across 3 independently derived *Ube3a* mutant lines.

We previously demonstrated that the sensitivity to audiogenic seizures can be reversed upon acute treatment with anti-epileptic drugs¹³. Given the high power of this assay, we investigated if this assay is suitable to determine the effective dose of a treatment. To that end, we treated mice with Levetiracetam, a compound that acts as ligand of the synaptic vesicle protein 2A, which is a commonly used anti-epileptic drug for both partial and generalized seizures and which is also often prescribed to individuals with AS^{40,41}. *Ube3a^{m-/p+}* (*Ube3a^{tm1Alb}*) mice in 129S2 background were first assessed for their (baseline) sensitivity to audiogenically evoked seizures without treatment. After establishing that all mice were sensitive, mice received at least one day after baseline testing a single IP dose of Levetiracetam and were tested 1 hour after IP injection. As shown in Figure 6D, a good dose-response curve could be obtained, in which 2 mg/kg Levetiracetam yielded approximately 60% of mice to be resistant to audiogenic seizures. This indicates that this test is highly suitable for quickly determining the effective dose of a treatment.

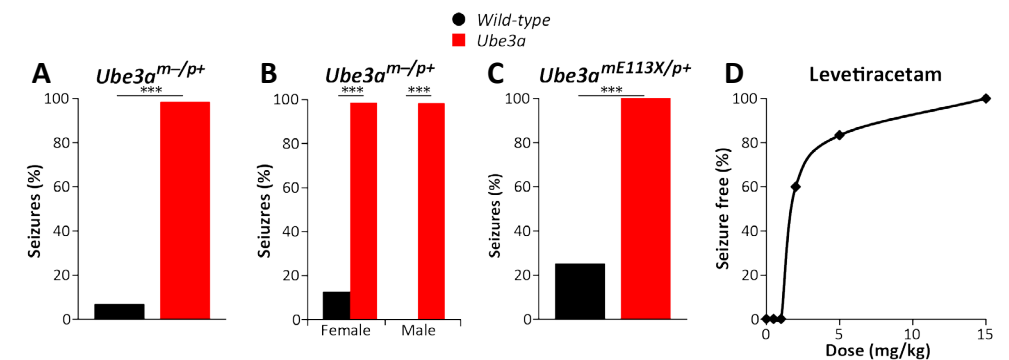


Figure 6. Audiogenic seizure susceptibility of *Ube3a^{m-/p+}* and *Ube3a^{mE113X/p+}* mice in the 129S2/SvPasCrl background.

A Audiogenic seizure susceptibility of WT and *Ube3a^{m-/p+}* mice (n=45,114). **B**

Effect of sex on seizure susceptibility in wild-type and *Ube3a*^{m-/p+} mice (females n=24,62; males n=21,52). **C** Seizure susceptibility in wild-type and *Ube3a*^{mE113X/p+} mice (n=4,8)(WT=3 females, 1 males; *Ube3a*^{mE113X/p+}=1 females, 7 males). **D** Effect of increasing doses of Levetiracetam on epilepsy susceptibility of *Ube3a*^{m-/p+} mice (0 mg/kg, n=12; 0.5 mg/kg, n=6; 1 mg/kg, n=6; 2 mg/kg, n=30; 5 mg/kg, n=30; 15 mg/kg, n=30). Fisher's exact test was used for statistical comparison. ***denotes p<0.001 for genotype significance.

Minocycline treatment does not improve behavioral phenotypes of *Ube3a* mice

It has previously been reported that Minocycline treatment of *Ube3a* animals improves synaptic plasticity as well as motor coordination, which was the basis for an open label study with minocycline in individuals with AS (trial register NCT01531582 and ²⁰), as well as a randomized controlled trial (NCT02056665) ²². Unfortunately, the randomized trial showed no difference between placebo and Minocycline treated individuals ²². To test if Minocycline ameliorated the *Ube3a* mutant phenotypes in our behavioral test battery, we subjected the animals to the same treatment protocol as used for the initial mouse study ²⁰. Adult-treated *Ube3a*^{m-/p+} (*Ube3a*^{tm1Alb}) mice and littermate controls (8-12 weeks of age) in the F1 hybrid 129S2-C57BL/6J background, received daily Minocycline (45 mg/kg) or control saline IP injections starting three weeks prior to behavioral testing. After 3 weeks of daily injections, the mice were sequentially subjected to the behavioral test battery as described above. In contrast to the previous finding (trial register NCT01531582) we did not observe a rescue on the rotarod. We also observed no effect of Minocycline on any of the other tests of the behavioral battery (**Figure 7**; 2-way ANOVA, genotype/treatment interaction p>0.08 in all tests). Notably, prolonged exposure to daily Minocycline injections resulted in yellow deposits over the organs and dullness of the liver (data not shown), confirming previous studies that IP administration of Minocycline is not the best choice of administration ⁴².

Minocycline has also been used to reverse the behavioral deficits of a mouse model of Fragile X ^{26,43}. Notably, in these studies Minocycline treatment was initiated immediately after birth and provided through the drinking water. Since we previously showed that a behavioral rescue of *Ube3a* mice may also depend on the timing of treatment initiation ¹³, we decided to treat *Ube3a* animals immediately after birth, using the same protocol as described for FMRP mice ²⁶. However, also this prolonged postnatal treatment regimen

did not yield a significant behavioral improvement, as none of these tests showed a significant interaction of genotype and treatment (2-way ANOVA, genotype/treatment interaction p>0.16 in all tests) (**Figure 7**).

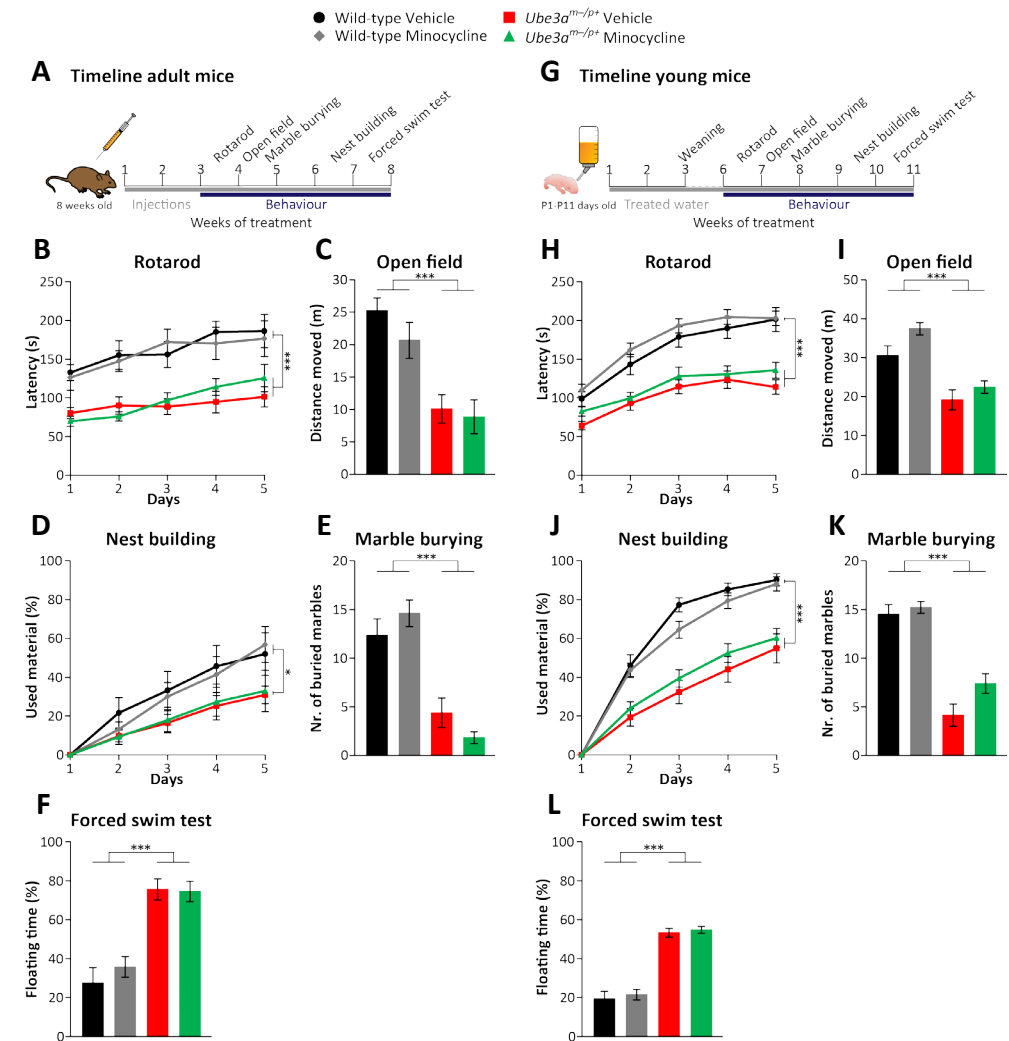


Figure 7. Effect of Minocycline treatment on adult and young *Ube3a*^{tm1Alb} mice in F1 hybrid 129S2-C57BL/6J background.

A Timeline representing Minocycline treatment and behavioral phenotyping of adult *Ube3a*^{m-/p+} mice. **B-F** Effect of Minocycline on adult *Ube3a*^{tm1Alb} mice on the behavioral test battery. Wild-type and *Ube3a*^{m-/p+} (*Ube3a*^{tm1Alb}) vehicle treated adult mice: n= 9,11(WT=5 females, 4 males; *Ube3a*^{m-/p+}=6 females, 5 males), with the exception of the nest building (n=6,7). Minocycline treated wild-type and *Ube3a*^{m-/p+} (*Ube3a*^{tm1Alb}) adult mice: n=10,11 mice (WT=6 females, 4 males;

Ube3a^{m-/p+}=6 females, 5 males), with the exception of the nest building (n=6,6). **G** Timeline representing Minocycline treatment and behavioral phenotyping of young *Ube3a*^{m-/p+} mice. **H-L** Effect of Minocycline on young *Ube3a*^{tm1Alb} mice on the behavioral test battery. Wild-type and *Ube3a*^{m-/p+} (*Ube3a*^{tm1Alb}) vehicle treated young mice: n= 21,17 (WT=11 females, 10 males; *Ube3a*^{m-/p+}=7 females, 10 males), with the exception of the nest building (n=13,12) and the forced swim test (20,17). Minocycline treated wild-type and *Ube3a*^{m-/p+} (*Ube3a*^{tm1Alb}) young mice: n=33,22 mice (WT=20 females, 13 males; *Ube3a*^{m-/p+}=8 females, 14 males), with the exception of the open field (33,21), the marble burying (33,21) and the nest building (n=16,17). A multivariate repeated ANOVA or a 2-way ANOVA was used for statistical comparison in behavioral phenotypes. *p<0.05, ***p<0.001 indicates effect of genotype. In none of the tests we observed an interaction of genotype and treatment.

Levodopa/Carbidopa treatment does not improve behavioral phenotypes of *Ube3a* mice

A recent study showed that treatment of *Ube3a* mice with Levodopa resulted in improvement of their motor skills compared to untreated *Ube3a* mice²¹. Based on this preclinical observation, a placebo-controlled trial of Levodopa was initiated in 55 children between 4 and 12 years diagnosed with AS. Unfortunately, no significant improvement was observed on any the outcomes measured following a 1-year treatment (trial register NCT01281475 and²¹). To test to what extent Levodopa ameliorated the phenotypes of *Ube3a*^{m-/p+} (*Ube3a*^{tm1Alb}) mice in our behavioral battery, we subjected the animals to the same treatment protocol as used for the initial mouse study²¹. *Ube3a*^{m-/p+} and wild-type littermates (8-12 weeks of age) in F1 hybrid 129S2-C57BL/6J background received daily Levodopa/Carbidopa (15 mg/kg Levodopa and 3.75 mg/kg Carbidopa) or control saline IP injections, starting 1 hour prior to behavioral testing. In contrast to the earlier finding²¹, we did not observe a rescue on the rotarod. We also observed no effect of Levodopa treatment on any of the other tests of the behavioral battery (2-way ANOVA, genotype/treatment interaction p>0.17 in all tests) (**Figure 8**).

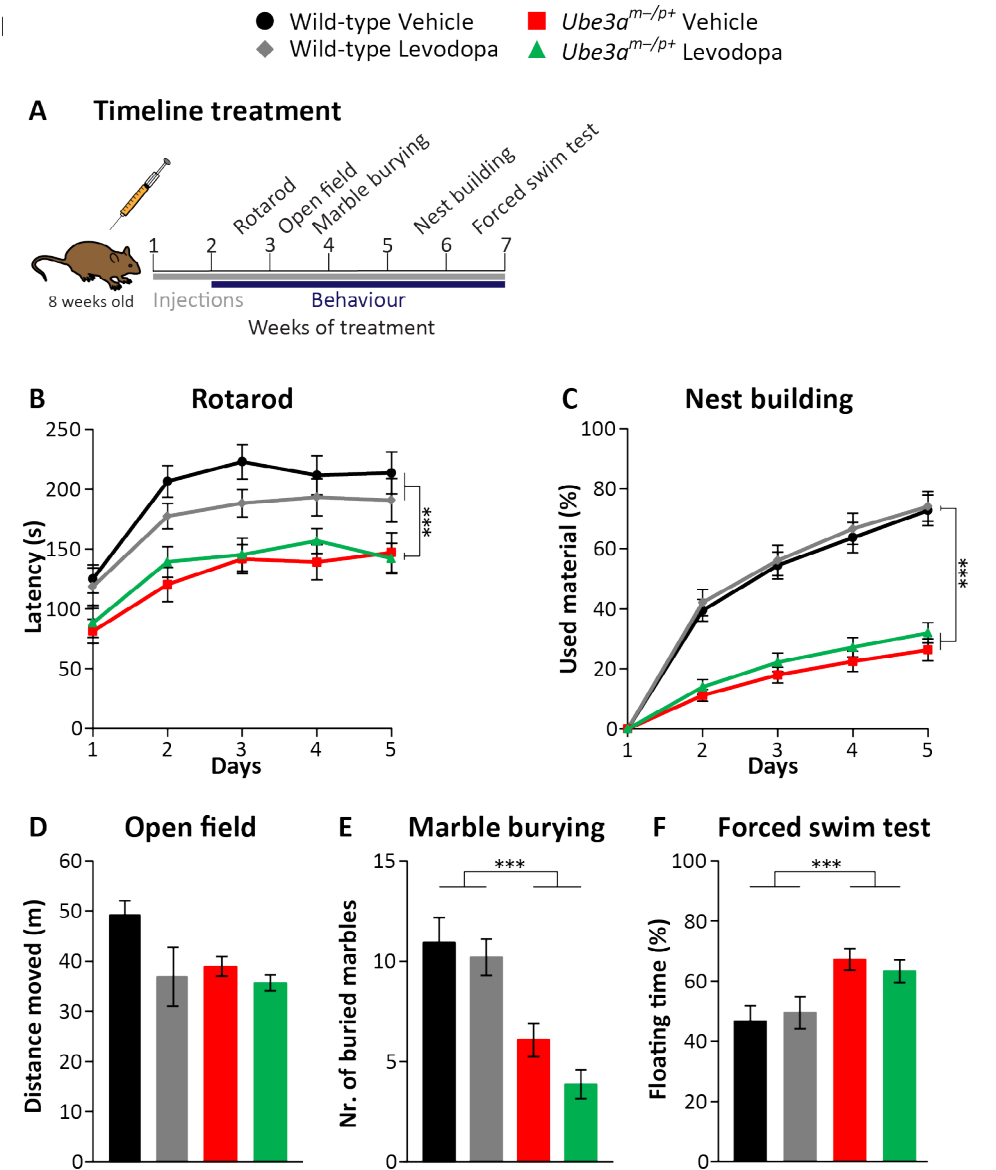


Figure 8. Effect of Levodopa treatment on *Ube3a*^{tm1Alb} mice in F1 hybrid 129S2-C57BL/6J background.

A Timeline representing Levodopa treatment and behavioral phenotyping of *Ube3a*^{m-/p+} mice. **B-F** Effect of Levodopa on the behavioral test battery. Wild-type and *Ube3a*^{m-/p+} (*Ube3a*^{tm1Alb}) vehicle treated mice: n= 15,15 (WT vehicle=8 females, 7 males; *Ube3a*^{m-/p+} vehicle= 7 females, 8 males), Levodopa treated wild-type and *Ube3a*^{m-/p+} (*Ube3a*^{tm1Alb}) mice: n=15,15 mice (WT levodopa=8 females, 7 males; *Ube3a*^{m-/p+} levodopa=6 females, 9 males). A multivariate repeated ANOVA or a 2-way ANOVA was used for statistical comparison in behavioral phenotypes.

*** indicates significant effect of genotype $p < 0.001$. No effect of genotype was observed in the open field test, since Levodopa-treated wild-type mice were similar to *Ube3a* mice. In none of the tests we observed an interaction of genotype and treatment.

Discussion

Robust behavioral phenotypes with high construct and face validity in mouse models of disease, are critical for the identification of novel treatments, and the successful translation of these therapies to clinical trials. These preclinical studies may give us important information about the therapeutic dose, optimal age of treatment and the best outcome measures to be used in a clinical trial. Given the high failure rate of clinical trials aimed at improving cognitive function⁴⁴, it is absolutely critical that the preclinical data is robust (reproducible results across different mutant lines and different experimenters), and that the animal studies have high construct and face validity.

In this study we investigated the robustness of a number of behavioral phenotypes, which we previously described using the inducible *Ube3a*^{mSTOP/p+} (*Ube3a*^{tm1Yelg}) mice¹³. These phenotypes were assessed in two independently derived *Ube3a* lines: in the commonly used *Ube3a*^{tm1Alb} line⁷, and the recently generated *Ube3a*^{mE113X/p+} (*Ube3a*^{tm2Yelg}) line¹³. Recently we have tested 2 additional novel *Ube3a* lines in this test battery with the same results; the *Ube3a*^{tm1.1Bdph} line (MGI:5882092) and a novel (unpublished) *Ube3a* line (*Ube3a*^{em1Yelg}). Thus, taken together a total of five independently derived *Ube3a* lines show phenotypes on all the behavioral tests of the test battery described in this study. In all cases, we used heterozygous *Ube3a* mice in which the mutation was located on the maternally inherited *Ube3a* allele. Therefore we conclude that construct validity is very high. However, since the majority of individuals with AS carries a large chromosomal deletion of the AS critical region (15q11-q13) which encompasses also other genes besides *Ube3a* and which may contribute to a more severe phenotype⁶, it would be of interest to test a mouse model of AS with large maternal deletion¹¹ in our behavioral test battery.

In terms of face validity, we used behavioral paradigms that assess domains of motor performance, anxiety, repetitive behavior and seizure susceptibility, which are all relevant clinical phenotypes of AS. Nevertheless, the clinical translational value of some of our tests (e.g. open field, marble burying,

nest building, and forced swim test) may be limited. Although it is notable that many of our tests involve a strong motor component, we think that it is unlikely that the phenotypes observed in open field, marble burying, nest building and forced swim test are solely related to deficits in the domain of motor functioning. Most notably, we have shown that the critical period for rescuing these phenotypes is distinctly different compared to rescuing the rotarod deficit¹³ (and unpublished data). For instance, we found that gene reactivation in three-week old mice fully rescues the rotarod phenotype, but none of the other phenotypes¹³. It is further noticeable that both WT and mutant mice behave significantly different when tested for a second time in the open field and marble burying test, whereas no significant changes were observed in rotarod performance. This further indicates that the deficits in the open field and marble burying test are indicative of deficits in other domains than motor performance.

An important clinical feature of AS that is lacking in our behavioral test battery, is a paradigm that assesses cognitive function. Despite profound cognitive impairments in individuals with AS, learning deficits in the AS mouse model are rather mild. We and others, have reported learning deficits in AS mice by using the Morris water maze^{8,18,45}. However, this paradigm is very labor intensive and hence less suitable for drug testing. Moreover, we found that a large number of mice are needed to detect significant differences and results varied strongly among experimenters (data not shown). A good learning paradigm that is highly suitable for drug testing is fear conditioning, in which animals are subjected to a single training session in which they are trained to associate a context (training chamber) or cue (tone) with a foot shock. However, we have not been able to get consistent results across experiments and experimenters (data not shown), and varying results are published in literature, with some studies showing a specific deficit in context conditioning^{7,46} and others a specific deficit in cued conditioning⁸ or both⁴⁷⁻⁴⁹. Notably, the two studies that investigated the behavioral deficits of *Ube3a* mice across strains in great detail, showed no context conditioning deficit in *Ube3a* mice in the F1 hybrid 129-C57BL/6J background and C57BL/6J background, and either normal⁹ or impaired⁸ cued fear conditioning in *Ube3a* mice in the C57BL/6J background. Collectively, these studies indicate that this phenotype is rather weak, and hence results obtained with these tests should be interpreted with care.

By combining the data of 8 independent experiments performed by 5

different experimenters, we were able to perform a meta-analysis of 111 *Ube3a*^{m-/p+} (*Ube3a*^{tm1Alb}) and 120 WT littermate mice in the F1 hybrid 129S2-C57BL/6J background and determine the robustness of the phenotypes. In all 8 experiments, we replicated *Ube3a* phenotypes observed on the rotarod, open field test and marble burying test, nest building test and the forced swim test. Deficits of *Ube3a* mice in rotarod performance, open field behavior and marble burying have been reported by many other investigators, and hence our results confirm the robustness of these tests. Impaired nest building behavior and impaired performance in the forced swim test of *Ube3a* mice have not yet been reported by other laboratories, but our study shows that these deficits are also very robust. In fact, a power analysis showed that these tests are among the most robust tests of the behavioral test battery. The open field paradigm was found to have the weakest power.

Our meta-analysis further shows that there is no major effect of sex on the behavioral phenotypes, which is in line with the general notion that such differences are also not present in AS patients. We did however find that female wild-type and mutant mice outperformed male wild-type and mutant mice on the rotarod. Improved performance of female mice on the rotarod has also been reported previously⁵⁰, and emphasizes the need of using well-matched groups when groups of both sexes of *Ube3a* mice are tested on the rotarod. Given that male mice are heavier than female mice, we investigated if the impaired performance of *Ube3a* mice on the rotarod can be attributed to the increased weight of these mutants. However, we found no correlation between weight of the animal and performance on the rotarod. This observation is in line with other studies⁵⁰⁻⁵² and indicates that the reduced performance of *Ube3a* mice on the rotarod represents a *bona fide* impairment in motor performance.

Besides the reproducibility of the observed phenotypes and the high face and construct validity, there are two additional features that make the behavioral test battery for *Ube3a* mice highly useful for drug testing. We show that with the exception of the epilepsy test, all behavioral experiments can be performed with a single cohort of mice, which greatly reduces costs as well as the number of mice needed. In addition, we found that with the exception of the marble burying task, the behavioral test battery can be performed twice with the same cohort while maintaining a phenotype. This makes it possible to test the efficacy of a drug using a within-subject design. We confirmed previous studies that the audiogenic seizure phenotype is a

very powerful test to investigate seizure susceptibility in *Ube3a* mice^{7,13,18}. With this study, this phenotype is now also confirmed in 3 independently derived lines: the commonly used *Ube3a*^{tm1Alb} line⁷, the *Ube3a*^{mSTOP/p+} (*Ube3a*^{tm1Yelg}) line¹³ and the recently generated *Ube3a*^{mE113X/p+} (*Ube3a*^{tm2Yelg}) line²³. Since nearly all *Ube3a* mice show this phenotype compared to less than 10% of wild-type animals, this test has very high power. Moreover, we showed that the phenotype is readily reversible with the anti-epileptic drug Levetiracetam, and that the test is highly suitable for dose finding. The only disadvantage of the audiogenic seizure test, is that it cannot be performed on the same animals as used in the behavioral test battery, since the sensitivity to audiogenic seizures is exclusively observed in *Ube3a* mice in the 129S2 genetic background.

We also observed an effect of genetic background on the tests of the behavioral test battery. *Ube3a* mice in the C57BL/6J background showed a significant phenotype in the rotarod, nest building and marble burying test, but no effect of genotype was observed in the open field test. A significant effect of genotype was found in the forced-swim test, but remarkably, this was in the opposite direction. In contrast, *Ube3a* mice in the 129S2 genetic background showed only a significant deficit in the forced swim test (in the same direction as F1 hybrid mice) and no phenotype on any of the other tests of the behavioral battery. This confirms previous reports that many of the *Ube3a* phenotypes are very sensitive to genetic background and not present in 129 lines^{8,9}. There are however several common findings as well as a few discrepancies between these studies and our study. With respect to the rotarod^{8,9} and marble burying phenotype⁹, our findings that only *Ube3a*-C57BL/6J and *Ube3a*-F1 hybrid mice show a phenotype, are in full agreement with each other (Huang *et al* only tested *Ube3a*-C57BL/6J in the marble burying test). With respect to the open field test (distance travelled), the other two studies also found no phenotype in *Ube3a*-129 mice, but in contrast to our findings they both found a phenotype in *Ube3a*-C57BL/6J mice. One major difference between their and our experimental design, is the time the mice were placed in the open field. Indeed, when we left the *Ube3a*-C57BL/6J mice for 30 minutes in the open field (instead of the 10 minutes we used) we found a nearly significant phenotype in *Ube3a*-C57BL/6J mice ($p=0.06$; data not shown). With respect to percentage of time spent in the inner zone of the open field (which is another measure of anxiety), the other two studies showed no significant effect of genotype in any of

the genetic backgrounds. Our meta-analysis did however reveal a significant difference between genotypes in F1 hybrid mice (WT: 1.1% versus mutant 0.7% time in inner zone; $p < 0.01$), which further indicates that *Ube3a* mutant mice are more anxious. However, we note that the observed difference was small and a significant effect was only observed in 4 out of the 8 individual experiments. Hence this measure is not very robust.

Taken all studies into consideration, it is clear that *Ube3a* mice in the F1 hybrid 129S2-C57BL/6J background show the most robust phenotypes, with the notable exception of the audiogenic seizure susceptibility test, which is strictly seen in *Ube3a*-129S2 mice. The question arises whether the observed differences between *Ube3a* mice in different genetic backgrounds has any translational significance. The lack of phenotypes of *Ube3a*-129S2 mice in most tests could simply reflect the passive/hypoactive phenotype of these mice, resulting in a floor effect. However, it could also be that the AS phenotype is sensitive to genetic background, and that the changes that are observed between individuals with AS are in part caused by genetic modifiers, rather than the nature of the mutation. Detailed studies of individuals with recurrent or similar mutations could provide more insight in that question⁵³. To test the translational value of the behavioral test battery, we decided to re-evaluate the two drugs that previously were tested in clinical trials involving individuals with AS: Minocycline (trial register NCT01531582²⁰ and NCT02056665²²), and Levodopa (trial register NCT01281475²¹). Both drugs were previously shown to rescue the rotarod impairment of *Ube3a* mice (see NCT01531582 for minocycline, and²¹ for Levodopa). In addition, Minocycline rescued the hippocampal LTP deficit of *Ube3a* mice²⁰, whereas Levodopa rescued the increased phosphorylation of CaMK2 observed in *Ube3a* mice²¹. We tested the effect of both drugs on all tests of our behavioral test battery, using the same drug administration protocols as used for the original studies. In addition, we also tested the effect of Minocycline when administered from birth, as previously published for the Fragile X mouse model²⁶. However, in line with the clinical trials, we did not observe any efficacy of these drugs when tested on *Ube3a* mice. Our finding that Minocycline and Levodopa are unable to improve performance on the rotarod is at odds with aforementioned previous preclinical studies. Failure of replication could be due to differences in strains or procedures, although there is full agreement between our labs with respect to performance of *Ube3a* mice on the rotarod and the effects of different genetic backgrounds on this performance⁹. We

think it is more likely that the rotarod experiments used for the preclinical studies were underpowered, as our analysis showed that 14 mice per group are needed for a well-powered rotarod study using two groups. In the Levodopa study, the authors used 6 different treatment groups and only 6 mice per group²¹. Such small sample sizes make the test underpowered, and also very vulnerable for the sex differences that we describe here. Since the details of the rotarod experiments of the Minocycline treatment were not provided (NCT01531582), we cannot comment on these discrepancies.

Conclusions

Here we provided a behavioral test battery with a robust set of well-characterized *Ube3a* phenotypes, which allows researchers to investigate the effects of pharmacological and genetic interventions involving *Ube3a* mice. A standardized set of tests, in combination with a well-defined genetic background, will also be very useful to compare data across laboratories. Moreover, using a standardized behavioral test battery may reduce selective reporting bias⁵⁴. Future studies should reveal how well the results of this behavioral test battery can be replicated between different laboratories in which housing and testing environment is different⁵⁵⁻⁵⁸. In addition, robust tests that capture phenotypes in the domain of cognitive function should be identified and added to this test battery.

Abbreviations

AS: Angelman Syndrome; UBE3A: Ubiquitin-protein ligase E3A; EEG: electroencephalography; WT: Wild-type; Mut: mutant; IP: intraperitoneal.

Declarations

Ethics approval

All animal experiments were conducted in accordance with the European Commission Council Directive 2010/63/EU (CCD approval AVD101002016791).

Consent for publication

All authors have approved the final manuscript and consent for publication.

Availability of data and material

The datasets used and/or analysed during the current study are available from the corresponding author on reasonable request.

Competing interests

The authors declare that they have no competing interests.

Funding

MS was supported by grants from Associazione Angelman and FROM; SSS was supported by Fundação para a Ciência e Tecnologia and Fundação Amélia de Mello and GMW was funded by the Angelman Syndrome Foundation.

Authors' contributions

MS, IW, SSS, JK and DM performed the behavioral experiments. MS, IW, SSS and YE analyzed and interpreted the data. GMW generated the *Ube3a*^{tm2Yelg} mouse model and setup the tracking system. IW made the figures. YE designed the study. MS and YE wrote the manuscript. All authors contributed intellectually to this study, and edited and approved the final manuscript.

Acknowledgements

We thank Linda Koene for advice concerning statistical analysis and generating the figures. We thank Maria Smit and Mireia Bernabé Kleijn for technical assistance with behavioral experiments; Mehrnoush Aghadavoud Jolfaei for genotyping and Minetta Elgersma-Hooisma for mouse colony management and editing of the manuscript.

References

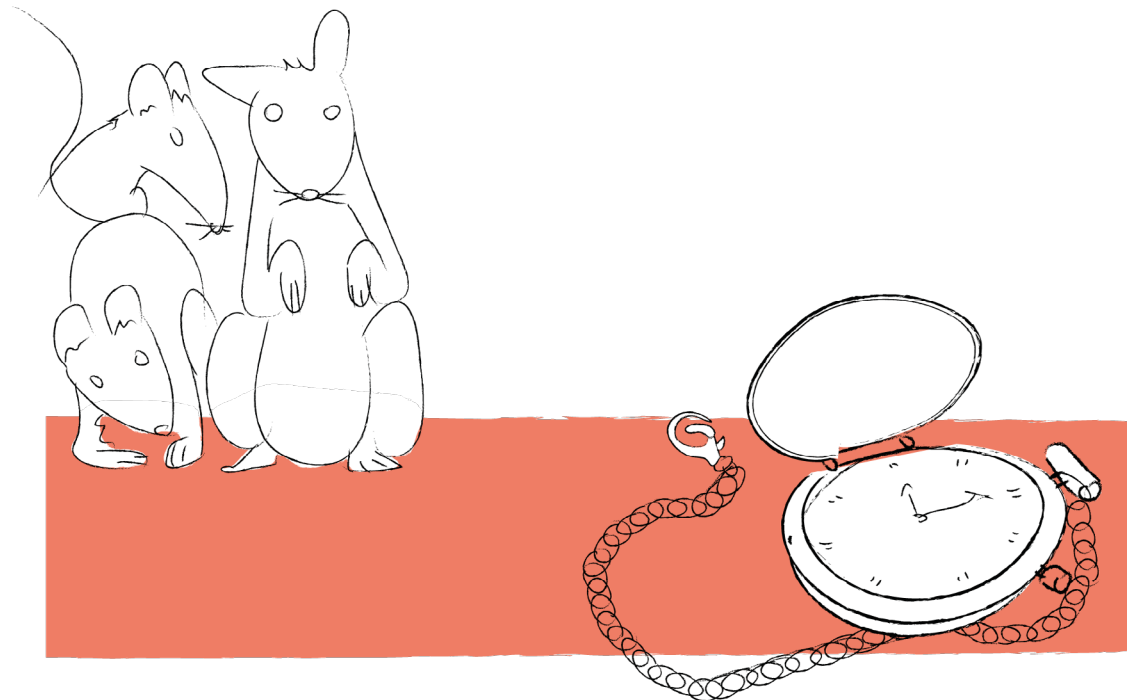
1. Petersen, M. B., Brøndum-Nielsen, K., Hansen, L. K. & Wulff, K. Clinical, cytogenetic, and molecular diagnosis of Angelman syndrome: estimated prevalence rate in a Danish county. *American journal of medical genetics* **60**, 261–262 (1995).
2. Kishino, T., Lalande, M. & Wagstaff, J. UBE3A/E6-AP mutations cause Angelman syndrome. *Nature Genetics* **15**, 70–73 (1997).
3. Williams, C. A. *et al.* Angelman syndrome 2005: Updated consensus for diagnostic criteria. *American Journal of Medical Genetics Part A* **140A**, 413–418 (2006).
4. Tan, W.-H. H. & Bird, L. M. Angelman syndrome: Current and emerging therapies in 2016. *American Journal of Medical Genetics Part C: Seminars in Medical Genetics* **401**, 384–401 (2016).
5. Katz, D. M. *et al.* Preclinical research in Rett syndrome: setting the foundation for translational success. *Disease Models & Mechanisms* **5**, 733–745 (2012).
6. Gentile, J. K. *et al.* A neurodevelopmental survey of Angelman syndrome with genotype-phenotype correlations. *Journal of developmental and behavioral pediatrics : JDBP* **31**, 592–601 (2010).
7. Jiang, Y. hui *et al.* Mutation of the Angelman ubiquitin ligase in mice causes increased cytoplasmic p53 and deficits of contextual learning and long-term potentiation. *Neuron* **21**, 799–811 (1998).
8. Huang, H. S. *et al.* Behavioral deficits in an Angelman syndrome model: Effects of genetic background and age. *Behavioural Brain Research* **243**, 79–90 (2013).
9. Born, H. A. *et al.* Strain-dependence of the Angelman Syndrome phenotypes in Ube3a maternal deficiency mice. *Scientific Reports* **7**, 1–15 (2017).
10. Allensworth, M., Saha, A., Reiter, L. T. & Heck, D. H. Normal social seeking behavior, hypoactivity and reduced exploratory range in a mouse model of Angelman syndrome. *BMC Genetics* **12**, (2011).
11. Jiang, Y. H. *et al.* Altered ultrasonic vocalization and impaired learning and memory in Angelman syndrome mouse model with a large maternal deletion from Ube3a to Gabrb3. *PLoS ONE* **5**, e12278 (2010).
12. Miura, K. *et al.* Neurobehavioral and Electroencephalographic Abnormalities in Ube3aMaternal-Deficient Mice. *Neurobiology of Disease* **9**, 149–159 (2002).
13. Silva-santos, S. *et al.* Ube3a reinstatement identifies distinct developmental

- windows in a murine Angelman syndrome model. *Journal of Clinical Investigation* **125** Silva-s, 1–8 (2015).
14. Garrido-Mesa, N., Zarzuelo, A. & Gálvez, J. Minocycline: Far beyond an antibiotic. *British Journal of Pharmacology* **169**, 337–352 (2013).
 15. Elewa, H. F., Hilali, H., Hess, D. C., Machado, L. S. & Fagan, S. C. Minocycline for short-term neuroprotection. *Pharmacotherapy* **26**, 515–21 (2006).
 16. Harbord, M. Levodopa responsive Parkinsonism in adults with Angelman Syndrome. *Journal of Clinical Neuroscience* **8**, 421–422 (2001).
 17. Brown, A. M., Deutch, A. Y. & Colbran, R. J. Dopamine depletion alters phosphorylation of striatal proteins in a model of Parkinsonism. *The European journal of neuroscience* **22**, 247–56 (2005).
 18. van Woerden, G. M. *et al.* Rescue of neurological deficits in a mouse model for Angelman syndrome by reduction of alphaCaMKII inhibitory phosphorylation. *Nature neuroscience* **10**, 280–282 (2007).
 19. Weeber, E. J. *et al.* Derangements of hippocampal calcium/calmodulin-dependent protein kinase II in a mouse model for Angelman mental retardation syndrome. *The Journal of neuroscience : the official journal of the Society for Neuroscience* **23**, 2634–2644 (2003).
 20. Grieco, J. C. *et al.* An open-label pilot trial of minocycline in children as a treatment for Angelman syndrome. *BMC neurology* **14**, 232 (2014).
 21. Tan, W. H. *et al.* A randomized controlled trial of levodopa in patients with Angelman syndrome. *American Journal of Medical Genetics, Part A* 1–9 (2017). doi:10.1002/ajmg.a.38457
 22. Ruiz-Antorán, B. *et al.* Randomized Clinical Trial, Placebo Compared To Evaluate The Efficacy And Safety of Minocycline In Angelman Syndrome (A-Manece Study). *Clinical Therapeutics* **37**, e154–e155 (2015).
 23. Wang, T., van Woerden, G. M., Elgersma, Y. & Borst, J. G. G. Enhanced Transmission at the Calyx of Held Synapse in a Mouse Model for Angelman Syndrome. *Frontiers in Cellular Neuroscience* **11**, 1–19 (2018).
 24. Grieco, J. Minocycline Treatment and the Necessity to Develop a Novel Outcome Measure for Children with Angelman Syndrome. *Graduate Theses and Dissertations* (2015).
 25. Andes, D. & Craig, W. A. Animal model pharmacokinetics and pharmacodynamics: a critical review. *International Journal of Antimicrobial Agents* **19**, 261–268 (2002).
 26. Bilousova, T. V. *et al.* Minocycline promotes dendritic spine maturation and improves behavioural performance in the fragile X mouse model. *Journal of Medical Genetics* **46**, 94–102 (2009).
 27. Lee, C. Z. *et al.* Dose–Response Effect of Tetracyclines on Cerebral Matrix Metalloproteinase-9 after Vascular Endothelial Growth Factor Hyperstimulation. *Journal of Cerebral Blood Flow & Metabolism* **26**, 1157–1164 (2006).
 28. Lin, S. *et al.* Minocycline blocks bilirubin neurotoxicity and prevents hyperbilirubinemia-induced cerebellar hypoplasia in the Gunn rat. *European Journal of Neuroscience* **22**, 21–27 (2005).
 29. Luzzi, P. *et al.* Effects of treatments on inflammatory and apoptotic markers in the CNS of mice with globoid cell leukodystrophy. *Brain Research* **1300**, 146–158 (2009).
 30. Zutphen, L. F. M. van., Baumans, V. & Beynen, A. C. *Principles of laboratory animal science : a contribution to the humane use and care of animals and to the quality of experimental results.* (Elsevier, 2001).
 31. Florek-Luszczki, M., Wlaz, A. & Luszczki, J. J. Interactions of levetiracetam with carbamazepine, phenytoin, topiramate and vigabatrin in the mouse 6 Hz psychomotor seizure model – A type II isobolographic analysis. *European Journal of Pharmacology* **723**, 410–418 (2014).
 32. Kiel, C., Faul, F., Erdfelder, E., Lang, A. G. & Buchner, A. G* Power 3: A flexible statistical power analysis program for the social, behavioral, and biomedical sciences. *Behavior research methods* **39**, 175–191 (2007).
 33. Pelc, K., Cheron, G. & Dan, B. Behavior and neuropsychiatric manifestations in Angelman syndrome. **4**, 577–584 (2008).
 34. Kedia, S. & Chattarji, S. Marble burying as a test of the delayed anxiogenic effects of acute immobilisation stress in mice. *Journal of Neuroscience Methods* **233**, 150–154 (2014).
 35. Angoa-Pérez, M., Kane, M. J., Briggs, D. I., Francescutti, D. M. & Kuhn, D. M. Marble Burying and Nestlet Shredding as Tests of Repetitive, Compulsive-like Behaviors in Mice. *Journal of Visualized Experiments* 1–7 (2013). doi:10.3791/50978
 36. Jirkof, P. Burrowing and nest building behavior as indicators of well-being in mice. *Journal of Neuroscience Methods* **234**, 139–146 (2014).
 37. Can, A. *et al.* The Mouse Forced Swim Test. *Journal of Visualized Experiments* 4–8 (2011). doi:10.3791/3638
 38. Meng, L. *et al.* Truncation of Ube3a-ATS Unsilences Paternal Ube3a and Ameliorates Behavioral Defects in the Angelman Syndrome Mouse Model. *PLoS Genetics* **9**, (2013).

39. Fiumara, A., Pittalà, A., Cocuzza, M. & Sorge, G. Epilepsy in patients with Angelman syndrome. *Italian journal of pediatrics* **36**, 31 (2010).
40. Weber, P. Levetiracetam in nonconvulsive status epilepticus in a child with angelman syndrome. *Journal of Child Neurology* **25**, 393–396 (2010).
41. Thibert, R. L. *et al.* Epilepsy in Angelman syndrome: A questionnaire-based assessment of the natural history and current treatment options. *Epilepsia* **50**, 2369–2376 (2009).
42. Fagan, S. C. *et al.* Optimal delivery of minocycline to the brain: Implication for human studies of acute neuroprotection. *Experimental Neurology* **186**, 248–251 (2004).
43. Rotschafer, S. E., Trujillo, M. S., Dansie, L. E., Ethell, I. M. & Razak, K. A. Minocycline treatment reverses ultrasonic vocalization production deficit in a mouse model of Fragile X Syndrome. *Brain Research* **1439**, 7–14 (2012).
44. van der Vaart, T., Overwater, I. E., Oostenbrink, R., Moll, H. A. & Elgersma, Y. Treatment of Cognitive Deficits in Genetic Disorders. *JAMA Neurology* **72**, 1052 (2015).
45. Daily, J. L. *et al.* Adeno-associated virus-mediated rescue of the cognitive defects in a mouse model for Angelman syndrome. *PloS one* **6**, e27221 (2011).
46. Hethorn, W. R. *et al.* Reelin supplementation recovers synaptic plasticity and cognitive deficits in a mouse model for Angelman syndrome. *The European journal of neuroscience* **41**, 1372–80 (2015).
47. Baudry, M. *et al.* Ampakines promote spine actin polymerization, long-term potentiation, and learning in a mouse model of Angelman syndrome. *Neurobiology of Disease* **47**, 210–215 (2012).
48. Sun, J. *et al.* UBE3A Regulates Synaptic Plasticity and Learning and Memory by Controlling SK2 Channel Endocytosis. *Cell reports* **12**, 449–61 (2015).
49. Sun, J. *et al.* mTORC1–S6K1 inhibition or mTORC2 activation improves hippocampal synaptic plasticity and learning in Angelman syndrome mice. *Cellular and Molecular Life Sciences* **73**, 4303–4314 (2016).
50. Kovács, A. D. & Pearce, D. A. Location- and sex-specific differences in weight and motor coordination in two commonly used mouse strains. *Scientific Reports* **3**, 1–7 (2013).
51. Cook, M. N., Bolivar, V. J., McFadyen, M. P. & Flaherty, L. Behavioral differences among 129 substrains: Implications for knockout and transgenic mice. *Behavioral Neuroscience* **116**, 600–611 (2002).
52. McFadyen, M. P., Kusek, G., Bolivar, V. J. & Flaherty, L. Differences among eight inbred strains of mice in motor ability and motor learning on a rotarod. *Genes, Brain and Behavior* **2**, 214–219 (2003).
53. Abaied, L. *et al.* A novel UBE3A truncating mutation in large Tunisian Angelman syndrome pedigree. *American Journal of Medical Genetics Part A* **152A**, 141–146 (2010).
54. Tsilidis, K. K. *et al.* Evaluation of Excess Significance Bias in Animal Studies of Neurological Diseases. *PLoS Biology* **11**, e1001609 (2013).
55. Mineur, Y. S. & Crusio, W. E. Behavioral effects of ventilated micro-environment housing in three inbred mouse strains. *Physiology & Behavior* **97**, 334–340 (2009).
56. Richter, S. H., Garner, J. P. & Würbel, H. Environmental standardization: cure or cause of poor reproducibility in animal experiments? *Nature Methods* **6**, 257–261 (2009).
57. Flint, J. *et al.* A simple genetic basis for a complex psychological trait in laboratory mice. *Science* **269**, 1432–1435 (1995).
58. Mandillo, S. *et al.* Reliability, robustness, and reproducibility in mouse behavioral phenotyping: a cross-laboratory study. *Physiological genomics* **34**, 243–55 (2008).

CHAPTER 4

Assessing the requirements of prenatal UBE3A expression for rescue of behavioral phenotypes in a mouse model for Angelman Syndrome



**Monica Sonzogni¹, Peipei Zhai^{1,2}, Edwin J. Mientjes¹, Geeske M. van Woerden¹,
Ype Elgersma^{*1}**

¹ Department of Neuroscience and the ENCORE Expertise Center for Neurodevelopmental Disorders,
Erasmus MC University Medical Center, Rotterdam, 3015 CN, The Netherlands

² Department of Neurology, The First Affiliated Hospital of Henan University, No.357, Ximendajie
Street, Kaifeng City, Henan Province, China

*Correspondence: y.elgersma@erasmusmc.nl

Provisionally accepted for Molecular Autism

Abstract**Background**

Angelman Syndrome (AS) is a rare neurodevelopmental disorder caused by the loss of functional ubiquitin protein ligase E3A (UBE3A). In neurons, UBE3A expression is tightly regulated by a mechanism of imprinting which suppresses the expression of the paternal *UBE3A* allele. Promising treatment strategies for AS are directed at activating paternal *UBE3A* gene expression. However, for such strategies to be successful, it is important to know when such a treatment should start, and how much UBE3A expression is needed for normal embryonic brain development.

Methods

Using a conditional mouse model of AS, we further delineated the critical period for UBE3A expression during early brain development. *Ube3a* gene expression was induced around the second week of gestation and mouse phenotypes were assessed using a behavioral test battery. To further investigate the requirements of embryonic UBE3A expression, we made use of mice in which the paternal *Ube3a* allele was deleted.

Results

We observed a full behavioral rescue of the AS mouse model phenotypes when *Ube3a* gene reactivation was induced around the start of the last week of mouse embryonic development. We found that full silencing of the paternal *Ube3a* allele was not completed till the first week after birth, but that deletion of the paternal *Ube3a* allele had no significant effect on the assessed phenotypes.

Limitations

Direct translation to human is limited, as we do not precisely know how human and mouse brain development aligns over gestational time. Moreover, many of the assessed phenotypes have limited translational value, as the underlying brain regions involved in these tasks is largely unknown.

Conclusions

Our findings provide further important insights in the requirements of UBE3A expression during brain development. We found that loss of up to

50% of UBE3A protein during prenatal mouse brain development does not significantly impact the assessed mouse behavioral phenotypes. Together with previous findings, our results indicate that the most critical function for mouse UBE3A lies in the early postnatal period between birth and P21.

Keywords

Angelman Syndrome; UBE3A; mouse-model; behavior; critical period; ASO therapy.

Background

Angelman Syndrome (AS) is a neurodevelopmental disorder characterized by distinct features such as severe intellectual disability, absence of speech, jerky movements, hyperactivity, seizures and EEG abnormalities¹. The genetic cause underlying AS became apparent when a deletion of chromosome 15q11-q13 was identified on the maternally inherited allele^{2,3}. In contrast, the deletion of the paternal 15q11-q13 locus causes Prader-Willi Syndrome (PWS), a disorder characterized by obesity and hyperphagia. The discovery of neuronal imprinting of chromosome 15q11-q13 explained the occurrence of two distinct disorders associated with the same deletion². Kishino and colleagues (1997) later identified the ubiquitin protein ligase E3A (UBE3A) gene as the causal gene for AS⁴.

Imprinting of UBE3A is regulated by the expression of an antisense RNA (*UBE3A-ATS*), which is expressed from the paternally inherited chromosome in the brain^{5,6}. No effective therapy is currently available for AS, but the discovery of UBE3A-ATS dependent silencing of paternal *UBE3A*, opened the door to pursue a treatment that involves the reactivation of the paternal gene^{7,8}. Clinical trials that use antisense oligonucleotides (AONs/ASOs) to activate paternal *UBE3A* expression in individuals with AS have recently been initiated and offer a promising approach for treating AS.

For the clinical success of a paternal *UBE3A* gene reactivation approach, it is essential to know if UBE3A is critical for early brain development. If so, such a therapy might have to be given at or even before birth⁹. To address this question, we previously generated an inducible *Ube3a* mouse line which contains a transcriptional 'STOP-cassette' flanked by LoxP sites (*Ube3a*^{tm1Yelg}; from hereon called *Ube3a*^{LSL}) allowing UBE3A expression after Cre-mediated deletion of the STOP cassette¹⁰. By restoring UBE3A expression at different time points, we observed that an early therapeutic intervention is needed to rescue the majority of AS phenotypes¹⁰. Specifically, we found that inducing *UBE3A* gene expression around the first embryonic day of development results in a full rescue of all phenotypes, whereas inducing *UBE3A* gene expression at P21 only rescued motor coordination. Neonatal gene reactivation resulted in a limited behavioral rescue, but these results should be interpreted with care, as we did not manage to get full gene reinstatement in newborn mice. Hence, the precise critical window for obtaining a full behavioral rescue in a mouse model of AS remains undetermined.

It is important to realize that both *Ube3a* alleles are expressed during early (prenatal) brain development as paternal *Ube3a* gene silencing is not complete until the first few days *after* birth¹¹. Thus, if normal brain development requires both copies of *Ube3a* to be active, this offers an explanation why *Ube3a* gene reactivation after birth showed limited success in mice. To specifically address the importance of bi-allelic *UBE3A* expression before birth, one can use mice in which the paternal allele is mutated, whereas the maternal gene is normally expressed. Mice lacking a functional copy of maternal *Ube3a* (*m⁻/p⁺*; 'AS' mice) exhibit a number of robust phenotypes, including phenotypes that are directly relevant to AS^{10,12-16}, but very few studies have investigated the effect of deleting the paternal *Ube3a* allele. Paternal loss of *Ube3a* expression affects the development of the cerebellum¹², but this does not have an impact on the motor performance^{12,13,17,18}. These findings are in line with a study that showed a limited role of the cerebellum in AS mice on these tasks¹⁹. However, it has been reported that deletion of both *Ube3a* alleles in mice affects licking behavior in a different way compared to maternal *Ube3a* deletion¹⁷ which could suggest specific changes in cerebellar function. Moreover, loss of paternal *Ube3a* gene expression caused increased seizure propensity¹², a phenotype that is highly relevant to AS individual's clinical outcome.

The aim of this study is to further delineate the requirement of UBE3A expression during prenatal brain development. To address this, we used two approaches. First, we investigated a conditional mouse model of AS in which maternal *Ube3a* expression is reactivated before the last week of mouse embryonic development. Second, we investigated the importance of paternal *Ube3a* expression during prenatal brain development.

Methods

Mouse breeding

We made use of *Ube3a*^{L^{SL}} (*Ube3a*^{tm1^{Yelg}}; MGI:5704099) mice as previously described¹⁰. These mice were maintained in the 129S2 background (full name: 129S2/SvPasCrl) by crossing male 129S2 *Ube3a*^{m+/p^LSL} mice with 129S2 females. For the behavioral experiments we used mice in the B6129S2F1 background, which were generated as described below. To generate embryonic reactivation of *Ube3a* at E12.5, 129S2 *Ube3a*^{m+/p^LSL} female mice were crossed with Nestin-Cre expressing male mice (Tg(Nes-cre)1Kln; MGI:2176173)²⁰ in the C57BL/6J background (Charles River Laboratories). This breeding yielded 4 experimental groups in a B6129SF1 background: WT mice with and without *Cre*, and *Ube3a*^{m^LSL/p+} mice with and without *Cre*.

To test paternal *Ube3a* contribution we made use of *Ube3a*^{tm1^{Alb}} mice (MGI 2181811)¹² and *Ube3a*^{E113X} mutants (*Ube3a*^{tm2^{Yelg}}; MGI5911277)²¹. *Ube3a*^{tm1^{Alb}} mice were maintained (>40 generations) in the 129S2 background by crossing male *Ube3a*^{m+/p-} mice with female 129S2 wild-type mice. *Ube3a*^{tm2^{Yelg}} mice were maintained (>20 generations) in the C57BL/6J (Charles River) background by crossing male *Ube3a*^{m+/p^{E113X}} mice with female C57BL/6J wild-type mice. To generate mice lacking *Ube3a* on either the maternal or paternal or both alleles, we crossed female *Ube3a*^{tm1^{Alb}} mice were crossed with male *Ube3a*^{tm2^{Yelg}} mice. This breeding yielded 4 experimental groups: WT mice, heterozygous *Ube3a*^{m+/p-} mice, *Ube3a*^{m-/p+} (AS) mice and homozygous *Ube3a*^{m-/p-} mice.

Mouse husbandry

All mice were group-housed in a barrier facility, in cages that were individually ventilated (IVC; 1145T cages from Techniplast). Mice were genotyped when they were 4-7 days old, and re-genotyped at the completion of the experiments. All animals were kept at 22±2°C with a 12 hours dark and light cycle, and provided with mouse chow (801727CRM(P) from Special Dietary Service) and water *ad libitum*. During behavioral testing, mice remained group-housed, except during the nest building test and subsequent forced swim test.

Behavioral test battery

All behavioral experiments were performed during the light period of the

light/dark cycle. Both male and female mice were used between 8-12 weeks of age. Mice were acclimatized to the testing room for 30 minutes before each behavioral performance. All behavioral testing and scoring were performed by an experimenter blind to genotype. Behavioral tests were precisely performed as previously described¹⁴ and as listed below:

Accelerating rotarod. Motor capabilities were tested by placing the mice on the accelerating rotarod (4-40 rpm, in 5 minutes; model 7650, Ugo Basile Biological Research Apparatus, Varese, Italy). Mice were tested twice a day with a 45-60 min inter-trial interval for 5 consecutive days (same hour every day). For each day, the average time spent on the rotarod was calculated, or the time until the mouse made 3 consecutive wrapping/passive rotations on the rotarod (latency in seconds). Maximum duration of a trial was 5 min.

Reversed rotarod. Motor capabilities in the *Ube3a* paternal deficient line were tested by placing the mice on the accelerating rotarod (4-40 rpm, in 5 minutes; modified model 7650, Ugo Basile Biological Research Apparatus, Varese, Italy) in such a way that they are walking backwards. Mice were tested twice a day with a 45-60 min inter-trial interval for 5 consecutive days (same hour every day). For each day, the average time spent on the rotarod was calculated, or the time until the mouse made 3 consecutive wrapping/passive rotations on the rotarod (latency in seconds). Maximum duration of a trial was 5 min.

Open Field test. In this test, which is useful to test locomotor activity and anxiety, mice were individually placed in a brightly lit 110 cm diameter circular open field (25 lux in the middle of the arena) and allowed to explore the space for 10 min. The total distance moved by each mouse in the open arena was recorded by an infrared camera (Noldus® Wageningen, NL) connected to the EthoVision® software (Noldus® Wageningen, NL), and the outcome measure indicated as distance moved in centimeters.

Marble burying test. Open makrolon (polycarbonate) cages (50x26x18 cm) were provided with 4 cm of bedding material (Lignocel® Hygenic Animal Bedding, JRS). On top of the bedding material 20 blue glass marbles were placed in an equidistant 5 x 4 grid and the animal was placed in this cage for 30 minutes. The outcome measure is the number of buried marbles, which

were scored as buried when covered more than 50% by bedding material.

Nest Building test. Mice were single housed for a period of 5 to 7 days before the start of the experiment. Successively, the used nesting material was replaced with around 11 grams (11±1) of compressed extra-thick blot filter paper (Bio-rad®). The amount of the unused nest material was weighed and noted daily for a consecutive of 5 days, each day at the same hour.

Forced swim test. Mice were placed in a cylindrical transparent tank (27cm high and 18 cm diameter), filled with water (26±1 degree Celsius) 15 cm deep for 6 min. The outcome measured is the time in seconds in which the mouse was immobile. The latency of immobility was only assessed during the last 4 min of the test. The mouse was considered to be immobile when it stopped moving, making only movements necessary to keep its head above water.

Western blot analysis

To assess UBE3A expression, brain tissues were dissected and immediately stored in liquid nitrogen. The lysates were made by homogenization in lysis buffer (10 mM Tris-HCl, pH 6.8, 2.5% SDS, 2 mM EDTA) and supplemented with protease and phosphatase inhibitor cocktail (Sigma-Aldrich). 20 µg of protein lysate was loaded on 4-12% SDS-PAGE gel (Bio-Rad) and transferred on nitrocellulose membranes to be then incubated with anti-UBE3A antibody (E8655 Sigma-Aldrich; 1:1000) and anti-actin antibody (MAB1501R, Millipore; 1: 20 000). Briefly, membranes were blocked in 4% TBS milk solution for 1 hour at room temperature and incubated at 4°C over-night, rotating end over end, with the primary antibody dissolved in 2% TBS-T milk solution. The day after, membranes were washed 3 times for 10 minutes with TBS-T and incubated with the secondary antibody, a fluorophore-conjugated goat anti-mouse antibody (IR Dye 800CW, Westburg; 1:15 000), dissolved in 2% TBS-T milk solution for 1 hour. At the end of the incubation, membranes were washed 3 times for 10 minutes with TBS and the resulting blots were analyzed and quantified using a LI-COR Odyssey Scanner and Odyssey 3.0 software.

Immunofluorescent and immunohistochemical staining

Mice were sedated with 0.15 ml Nembutal (60 mg/kg), transcardially

perfused and the brains were post-fixed with 4% paraformaldehyde in sodium phosphate buffer (PB) for 2 h. After incubation in 10% sucrose (in 0.1 M Phosphate buffer) overnight, brains were embedded in a sucrose/gelatin mixture (10 and 12%, respectively). Brain sections were cut on a microtome (SM2000R; Leica Microsystems, Rijswijk, Netherlands) at a thickness of 40µm and treated with peroxidase when the immunohistochemical staining was applied (H₂O₂). The brain sections were then washed in PBS and incubated for 1 h in blocking buffer containing 10% horse serum, 0.5% Triton X-100 in PBS. Subsequently, sections were incubated for 48–72 h in 2% normal horse serum, 0.5% Triton X-100 incubation buffer in PBS with primary antibody (mouse anti-E6AP, clone 3E5 Sigma–Aldrich; 1:750). The secondary antibody (anti-mouse HRP, P0447 Dako; 1:200) was detected by 3,3-diaminobenzidine (DAB) as the chromogen, and DAB sections were imaged using a Nanozoomer scanner.

In case of immunofluorescent stainings, after the primary antibody incubation, sections were washed with PBS and the secondary antibody was added (anti-mouse Alexa 488, Jackson ImmunoResearch Labs, 1:200 diluted) in PBS containing 2% NHS and 0.5% Triton X-100. After 1–2 h incubation of the secondary antibody at room temperature, sections were washed in PB (0.05 M), mounted on and covered using Mowiol (Sigma-Aldrich). All images were acquired using the LSM700 confocal microscope (Zeiss).

Statistical analysis

All data were statistically analyzed using IBM SPSS software, and P values <0.05 were considered significant. Statistical analysis was performed using univariate ANOVA or 2 way-repeated measures ANOVA with Bonferroni's post hoc comparison.

Results

Characterization of the Nestin-CRE conditional AS mouse model

Previously we generated the inducible *Ube3a^{LSL}* line containing a floxed transcriptional ‘STOP-cassette’ enabling UBE3A expression upon Cre-mediated deletion¹⁰. A partial rescue of behavioral phenotypes was observed when UBE3A expression was induced at postnatal day 1 (P1). However, since we achieved normal UBE3A gene expression in only 30% of the cells, a failure to rescue certain behaviors could also be attributed to a failure to induce gene expression in all cells. To further zoom in on this critical period for UBE3A functioning, we investigated if reactivation of *Ube3a* around the onset of the third week of mouse pregnancy would rescue AS phenotypes, thereby further narrowing down the critical window of UBE3A expression for full behavioral rescue. We took advantage of the Nestin-Cre line, in which Cre expression is under the control of the Nestin promoter²⁰, and crossed this line with the *Ube3a^{LSL}* line¹⁰, resulting in *Ube3a^{LSL}/Cre⁺* (Cre-positive) and *Ube3a^{LSL}/Cre⁻* (Cre-negative) control mice. Nestin is an intermediate filament protein that is known as a neural stem/progenitor cell marker^{22–24}. Since the Nestin promoter becomes active around E12.5²⁵, we estimated that sufficient Cre expression to mediate deletion of the STOP cassette, and to induce expression of UBE3A protein at wild-type levels would be reached around the start of the third week of mouse embryonic brain development. Indeed, Western blot analysis of brain UBE3A protein levels confirmed normal UBE3A protein levels in *Ube3a^{LSL}/Cre⁺* mice at E15, whereas no expression of maternal UBE3A expression was observed in these mice at E9 (Figure 1). Consistent with the expression profile of Nestin, immunohistochemical stainings of adult *Ube3a^{LSL}/Cre⁺* mice confirmed that UBE3A gene expression was obtained throughout the brain.

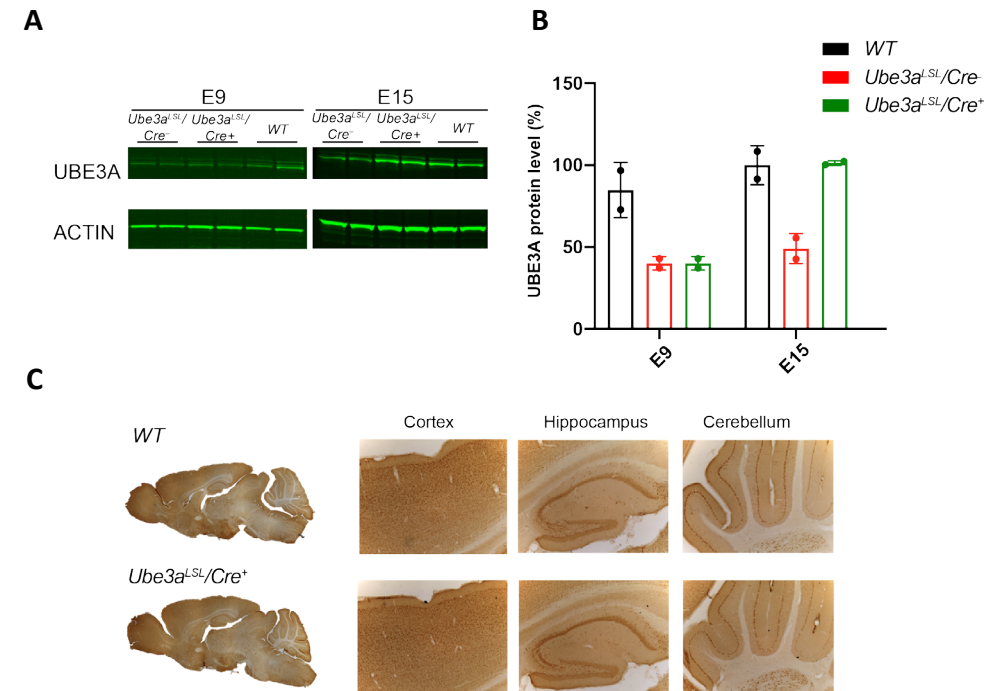


Figure 1. Successful maternal *Ube3a* gene activation upon Nestin-Cre mediated deletion of the transcriptional STOP cassette.

A-B Western blot data and UBE3A quantification from total lysates of E9 and E15 brains of *Ube3a^{LSL}/Cre⁺*, *Ube3a^{LSL}/Cre⁻* mice and WT littermates normalized to WT E15 levels. Bars depict mean \pm SD (n=2 per genotype, per time point) **C** Immunohistochemical UBE3A staining of sections of brains from adult WT and *Ube3a^{LSL}/Cre⁺* mice.

UBE3A gene reactivation around the third week of mouse embryonic development prevents the manifestation of AS phenotypes

After the biochemical validation of the new AS mouse line, we subjected wild-type mice, *Ube3a^{LSL}/Cre⁺* and *Ube3a^{LSL}/Cre⁻* control mice to a well-characterized and robust behavioral testing battery^{10,14}. Since the wild-type mice with and without Cre were not significantly different from each other we pooled these two groups to have more statistical power. *Ube3a^{LSL}/Cre⁻* control mice showed a significant deficit in all tasks except the open field task (p= 0.16) for which we previously showed that this is the weakest phenotype and for which we calculated that a sample size of 21 mice per

group is required for sufficient power ($1 - \beta = 0.95$)¹⁴. In contrast, *Ube3a^{LSL}/Cre⁺* mice in which UBE3A expression was induced around the start of the last week of mouse embryonic development, were not significantly different from wild-type mice on rotarod, nest building, marble burying and the forced swim test. This indicates that activating the maternal *Ube3a* allele around the onset of the last week of mouse embryonic development is sufficient to prevent the development of these phenotypes (**Figure 2B, Additional file 1: Table 1**).

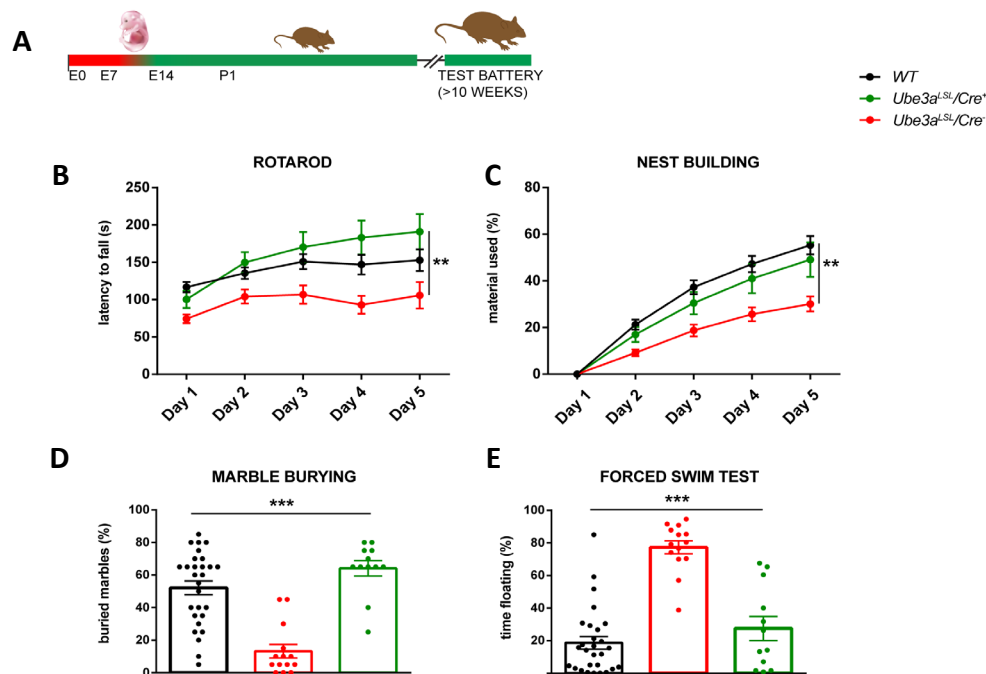


Figure 2. Behavioral testing of *Ube3a^{LSL/+}* mice show a full rescue of most AS-like behavioral phenotypes.

A Schematic representation of *Ube3a* gene reactivation during mouse embryonic development around two weeks of gestation and time point of behavioral testing. **B-F** Accelerating rotarod test, nest building test, marble burying test and forced-swim test in WT and *Ube3a^{LSL/+}* mice (WT=28, *Ube3a^{LSL/-}*=14, *Ube3a^{LSL/+}*=12). A repeated measures ANOVA or Univariate ANOVA was used for statistical comparison of genotypes. Asterisk indicate significant effects of genotype: * $P < 0.05$; ** $P < 0.01$; *** $P < 0.001$

Assessing paternal *Ube3a* expression during brain development

From the Western blot analysis of **Figure 1**, it is clear that at E9, approximately 50% of UBE3A is still present in *Ube3a^{LSL}/Cre⁻* mice. Given that the *Ube3a^{LSL}/Cre⁻* mice and *Ube3a^{LSL}/Cre⁺* mice show similar UBE3A levels, and that the Nestin promoter is not yet active at that time point, this protein must be derived from the paternal allele. Indeed, it has been shown that imprinting of the paternal allele is not completed till the first week after birth¹¹. To investigate specifically the contribution of the maternal and paternal *Ube3a* allele during early brain development, we performed a Western blot on total brain lysates isolated from WT and AS (*Ube3a^{m/+}*) mice at E14, E17, P1, P7, P14, P21 and adult mice. The values obtained from AS mice yielded the values of paternal UBE3A expression. The amount of UBE3A derived from the maternal allele was calculated by subtracting the UBE3A values measured in AS mice from the total UBE3A amount as observed in wild-type mice. The analysis shows that while total UBE3A levels are relatively constant throughout development, UBE3A is entirely bi-allelically expressed at E14 (**Figure 3A**). Only after birth does the paternal allele get fully silenced.

Contribution of paternal *Ube3a* expression to the behavioral phenotypes

We have previously shown for different *Ube3a* mutants that our behavioral testing battery is very sensitive to mutations affecting maternal *Ube3a* gene expression^{10,14,26,27}. Given the observation that the paternal allele is highly expressed throughout prenatal brain development (**Figure 3**), we wondered whether loss of paternal *Ube3a* expression (*Ube3a^{m+/p-}* mice) would also cause behavioral phenotypes on these tests. In fact, by making use of these *Ube3a^{m+/p-}* mice, we are effectively mimicking a *Ube3a* gene reinstatement experiment which resembles AS mice in which we induce *Ube3a* gene activation around birth (see **Figure 3B** for a graphical representation of this model).

Besides analyzing the effect of loss of paternal gene expression, we also wondered whether loss of both paternal and maternal *Ube3a* expression (*Ube3a^{m-/p-}*) would worsen the behavioral phenotype compared to mice in which only the maternal *Ube3a* allele is deleted.

In order to disentangle the functional role of the maternal and paternal allele, we made use of two distinct *Ube3a* mutants that both cause loss of *Ube3a* expression: the commonly used *Ube3a^{m-/p+}* mice in which exon 5 is deleted

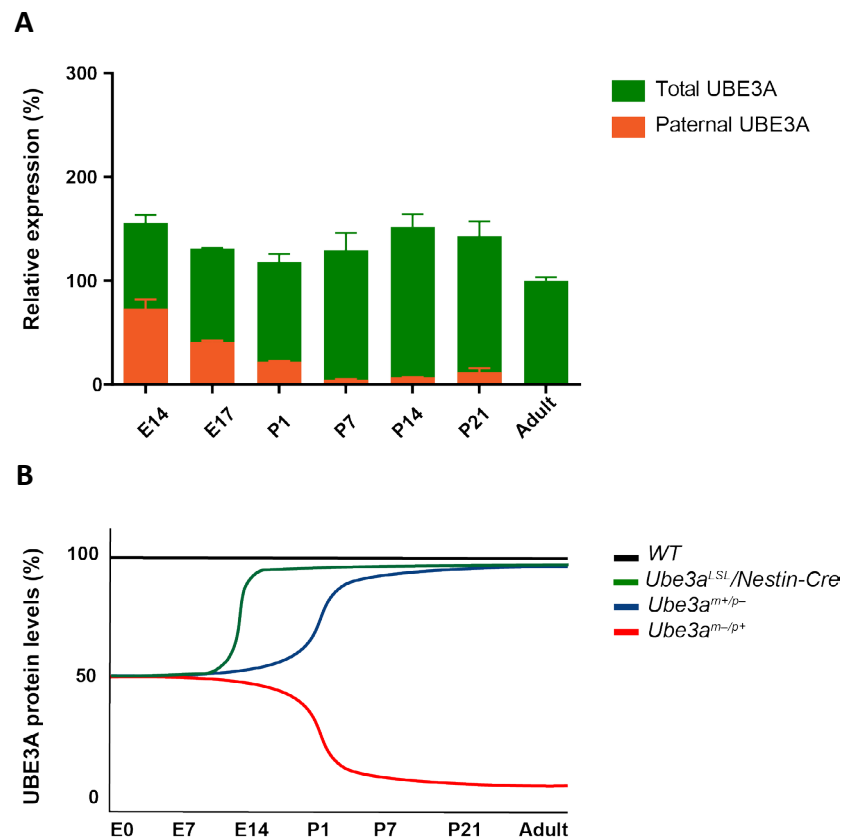


Figure 3. Silencing of the paternal *Ube3a* gene is not completed till after birth.

A UBE3A quantification in total lysates of brains isolated from WT and AS mice at E14 (n=8,5), E17 (n=2,2), P1 (n=6,3), P7 (n=5,5), P14 (n=4,3), P21 (n=3,2) and adult mice (n=2). The values obtained from AS mice yielded the values of paternal UBE3A expression. The amount of UBE3A derived from the maternal allele was calculated by subtracting the UBE3A values measured in AS mice from the total UBE3A amount as observed in wild-type mice. All values were normalized against UBE3A levels in adult WT mice. Error bars represent mean \pm SEM.

B Schematic representation of UBE3A levels in WT, *Ube3a^{LSL}/Nestin-Cre*, *Ube3a^{m+/p-}* and *Ube3a^{m-/p+}* mice, indicating that *Ube3a^{m+/p-}* can effectively be used as a UBE3A reinstatement model in which UBE3A levels are restored to normal levels after birth.

(*Ube3a^{tm1Alb}*; ¹²) and the *Ube3a^{E113X}* mutant (*Ube3a^{tm2Yelg}*; ²¹) which carries a premature stop codon in exon 5. Both lines were shown to be similarly affected in all tasks of the behavioral testing battery ¹⁴. Crossing these two lines with each other allowed us to determine whether the paternal or maternal allele was mutated in heterozygous offspring. This breeding yielded 4 experimental groups: WT mice, heterozygous *Ube3a^{m+/p-}* mice, *Ube3a^{m-/p+}* mice and homozygous *Ube3a^{m-/p-}* mice.

Immunofluorescent staining of brains derived from adult mice of these 4 experimental groups shows that the expression of UBE3A in mice lacking the paternal allele (*Ube3a^{m+/p-}* mice) is comparable to wild-type mice (**Figure 4A**). In contrast, adult mice lacking maternally derived UBE3A (*Ube3a^{m-/p+}* mice) show very low levels of UBE3A immunoreactivity, and even less staining was observed in the double mutants in which both maternal and paternal *Ube3a* alleles (*Ube3a^{m-/p-}* mice) are mutated (**Figure 4A**). This was further confirmed by Western blot analysis of cortex, hippocampus, striatum and cerebellum (**Figure 4B**). In liver and lung, heterozygous *Ube3a^{m+/p-}* and *Ube3a^{m-/p+}* mice show comparable UBE3A expression, approximately 50% compared to wild-type levels. This confirms bi-allelic *Ube3a* expression outside the brain, and moreover, that both *Ube3a* mutant lines similarly affect *Ube3a* gene expression.

The four experimental groups were then subjected to the behavioral test battery as described above. However, given the effect of paternal gene deletion on cerebellar maturation ¹², we used the more difficult reversal rotarod task rather than the standard rotarod testing to increase the sensitivity of this task. *Ube3a^{m-/p+}* mice lacking the maternal allele showed a significant phenotype on all tests compared to wild-type littermate control mice. (**Figure 5, Additional file 1: Table 1**). *Ube3a^{m+/p-}* mice lacking an active paternal *Ube3a* gene showed a tendency to display reduced performance compared to wild-type mice on all tests, but this never reached statistical significance. Similarly, *Ube3a^{m-/p-}* mutants in which both the maternal and paternal *Ube3a* allele were deleted, showed a tendency to impaired performance compared to *Ube3a^{m-/p+}* mice lacking only the maternal allele, but again this never reached statistical significance. This suggests that lack of paternal gene expression throughout prenatal brain development does not have a measurable effect on the phenotypes tested.

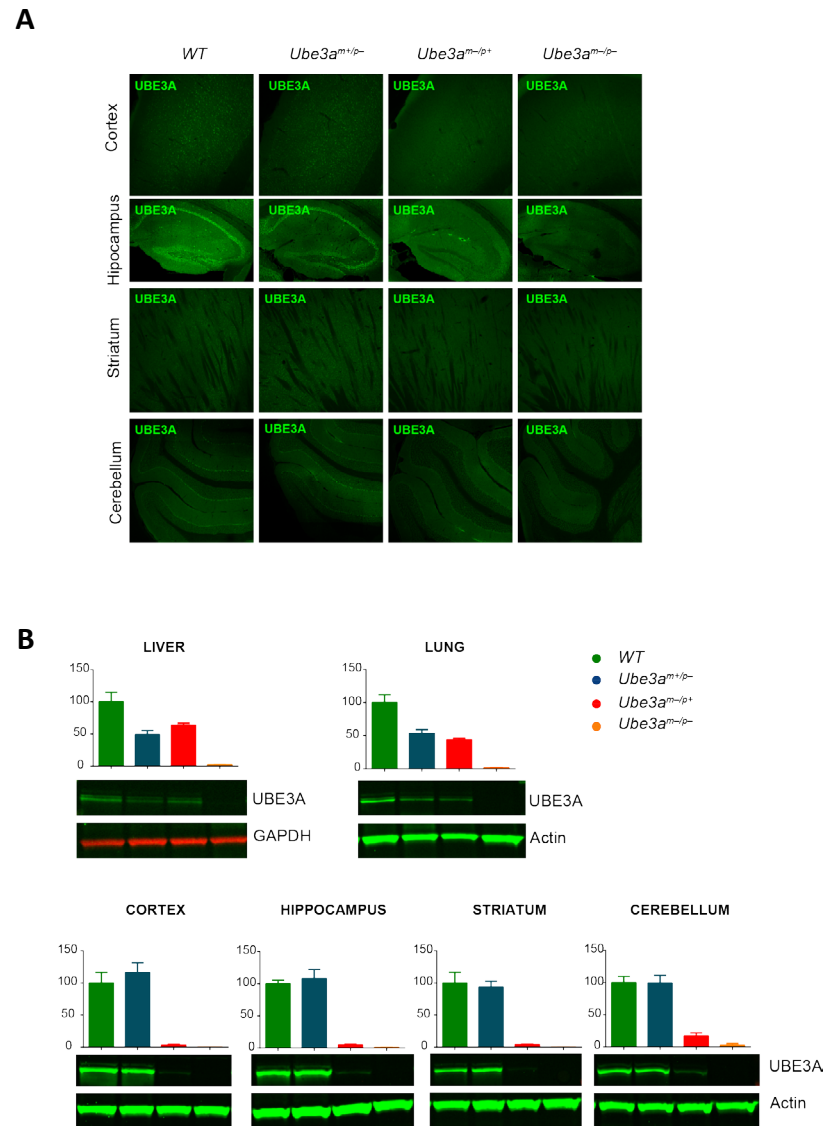


Figure 4. UBE3A expression in WT, *Ube3a*^{m+/p-} mice, *Ube3a*^{m-/p+} mice, and *Ube3a*^{m-/p-} mice.

A Immunofluorescent staining of sections of cortex, hippocampus, striatum and cerebellum of brains isolated from adult WT, *Ube3a*^{m+/p-} mice, *Ube3a*^{m-/p+} mice, and *Ube3a*^{m-/p-} mice.

B Western blotting and UBE3A quantification in peripheral (liver and lung) and non-peripheral (cortex, hippocampus, striatum and cerebellum) areas. Error bars represent mean \pm SEM.

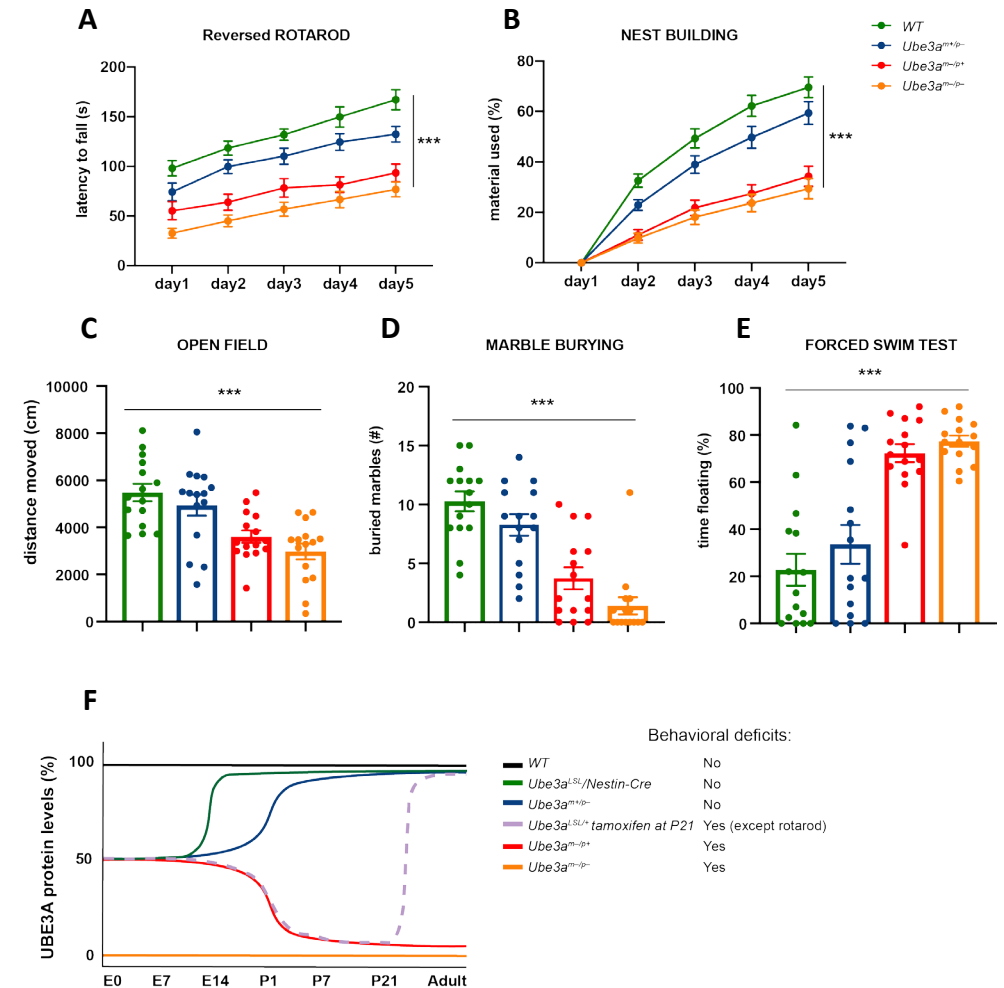


Figure 5. Limited function of the *Ube3a* paternal allele in the development of AS-like behavioral phenotypes.

A-E Accelerating rotarod, nest building, open field, marble burying and forced swim test in WT, *Ube3a*^{m+/p-}, *Ube3a*^{m-/p+} and *Ube3a*^{m-/p-} mice (n=15 per genotype). A repeated measures ANOVA or Univariate ANOVA was used for statistical comparison of genotypes. Asterisks indicate significant effects of genotype $p < 0.001$. Error bars represent mean \pm SEM.

F Schematic representation of several *Ube3a* lines used for studying the critical period, which indicates that the critical window of rescuing behavioral deficits in AS mice by gene reinstatement lies around birth and P21. Each curve depicts the level of UBE3A protein in WT, *Ube3a*^{LSL}/*Nestin-Cre*, *Ube3a*^{m+/p-}, *Ube3a*^{m-/p+} and *Ube3a*^{m-/p-} mice (this study) over time. In addition, we included the previously published result of *Ube3a*^{LSL} mice crossed with the inducible *Cag-Cre*^{ERT} line in which gene reactivation was induced by tamoxifen injection at P21¹⁰. The presence of behavioral phenotypes has been indicated for each mouse line.

Discussion

The purpose of this study was to further delineate the requirement of UBE3A expression during prenatal brain development. In order to address this question, we took advantage of a conditional mouse model of AS, in which the maternal *Ube3a* allele is reactivated around the onset of the third week of mouse embryonic development. In addition, we investigated the importance of expressing the paternal *Ube3a* allele during prenatal brain development, especially in terms of its contribution to the AS established phenotypes.

By reactivating *Ube3a* around the onset of the last week of mouse embryonic development, we were able to rescue all behavioral phenotypes in which AS mice were affected. These findings further narrow down the previously identified critical window for therapeutic intervention¹⁰. In our previous study¹⁰, we identified a critical window for *Ube3a* reinstatement that lies between E0-P21. In this study, early embryonic reinstatement of *Ube3a* (E0) prevented AS phenotypes across different behavioral domains from developing. In contrast, postnatal reinstatement (P0-P21) rescued only few of the previously reported test battery phenotypes¹⁰. Our results are now suggesting that the critical window for complete reversal of behavioral phenotypes can be narrowed down from the period around birth to P21 (**Figure 5F**).

We showed that during mouse embryonic development, UBE3A is expressed from both alleles. We found that around E14, expression is still entirely bi-allelic, and full silencing of the paternal allele has not been achieved until the first week after birth, which is in line with previous findings¹¹. To further investigate the requirements of embryonic UBE3A expression levels, we made use of *Ube3a*^{m+/p-} mice in which the paternal *Ube3a* allele was mutated. In these mice, UBE3A protein levels were reduced to 50% during the first two weeks of embryonic brain development, and increased up to 80% of WT levels around birth. Analysis of these mice showed a tendency of decreased performance on all tests, but the effects were small and did not reach statistical significance. Hence, 50% of UBE3A protein is sufficient for normal prenatal brain development. Moreover, these experiments suggest that the critical period for UBE3A-dependent brain development starts after

birth (**Figure 5F**).

Limitations

Our study has two major limitations. The first limitation is that we do not know how well the requirements for UBE3A expression during mouse brain development aligns with human brain development. The AS murine model has been widely used in the biomedical AS field to investigate potential therapeutic approaches, but despite the similarities between mouse and human, mice obviously have a much shorter lifespan compared to humans and timing of brain development and systems level functioning is very different. Several studies tried to investigate how we can correlate the two species in terms of brain development and function^{28,29}. When we align major developmental milestones, such as time to the weaning period or the age to attain puberty, one human year equals approximately 57 mouse days, and 4 mouse days, respectively²⁹. A more elaborate comparison that includes brain anatomical milestones as well as major behavioral milestones indicates that mouse P1 compares to early second trimester in human^{28,29}. But if we aim to draw a parallel in identifying the best period for a behavioral rescue, it is particularly important to look at the critical periods underlying the development of sensory pathways, language and higher cognitive functions^{30,31}. The best-understood critical periods controlling specific attributes of primary sensory modalities in animals, are the representation of different tones in the auditory cortex or left versus right eye inputs in the visual cortex³¹. For this last case, the critical period for acquiring binocular vision closes around 4 weeks of age in mice, while in humans it remains open till 7 years of age³². All together these studies indicate that it remains highly uncertain how we can precisely correlate the newly identified critical window to the human condition. But regardless of these limitations, our study suggests that early postnatal intervention is likely to be most successful to rescue AS related phenotypes, and that the UBE3A gene plays a critical role in perinatal mouse brain development, but less so in adult mice²⁶.

The second limitation is that most of the behavioral tests we used have limited clinical value. With the exception of the rotarod, we do not know what brain areas are underlying the deficits in the open field test, marble burying test, nest building test and forced swim test. These measures were

selected because we have previously shown that they give robust phenotypes in different lines of AS mice and different genetic backgrounds^{10,14,26,27}. In addition we have previously calculated the power of these tests¹⁴. From that study we know that we were underpowered to see a significant effect in the open field, which was indeed the case for the first set of experiments using the *Ube3a*^{LSL}/Nestin-cre mice.

A minor limitation of our study is that although we did not find an effect of paternal *Ube3a* gene deletion, all tests showed a tendency in the same direction. Hence, we cannot exclude a small effect, meaning that for optimal embryonic mouse brain development expression of both alleles is required. But nevertheless, our data implies that by losing 50% of protein expression before birth, the effect on the mouse behavioral phenotypes that we assessed is at best small.

Conclusion

Our findings provide further important information about the requirements of *Ube3a* expression during brain development. Taken together with our previous studies^{10,26}, our findings have further defined the critical period for obtaining a full behavioral rescue by *Ube3a* gene reinstatement strategies, and show that this period lies just after birth and before P21¹⁰ in AS mice (**Figure 5F**). In addition, we show that loss of up to 50% of UBE3A protein during embryonic mouse brain development does not significantly impact the assessed mouse behavioral phenotypes.

List of abbreviations

AS: Angelman Syndrome; UBE3A: Ubiquitin-protein ligase E3A; WT: Wild-type; PWS: Prader-Willi Syndrome; AON/ASO: Antisense-oligonucleotide.

Declarations

Ethics approval

All animal experiments were conducted in accordance with the European Commission Council Directive 2010/63/EU (CCD approval AVD101002016791).

Consent for publication

All authors have approved the final manuscript and consent for publication.

Availability of data and materials

The datasets used and/or analyzed during the current study are available from the corresponding author on reasonable request.

Competing interest

The authors declare that they have no competing interests.

Funding

YE was funded by a NWO-ZoN-MW grant. MS was supported by grants from Associazione Angelman and FROM. PZ was funded by the Chinese Scholarship Council (CSC).

Authors' contributions

MS and PZ performed the behavioral experiments. MS, PZ, EJM and GMW provided the histological and biochemical characterization of the used AS mouse lines. MS and YE analyzed and interpreted the data. YE designed the study. MS and YE wrote the manuscript. All authors contributed intellectually to this study, and edited and approved the final manuscript.

Acknowledgments

We thank Mehrnoush Aghadavoud Jolfaei for genotyping and Minetta Elgersma-Hooisma for mouse colony management.

References

1. Williams, C. A. *et al.* Angelman syndrome 2005: Updated consensus for diagnostic criteria. *American Journal of Medical Genetics Part A* **140A**, 413–418 (2006).
2. Knoll, J. H. M. *et al.* Angelman and Prader-Willi syndromes share a common chromosome 15 deletion but differ in parental origin of the deletion. *American Journal of Medical Genetics* **32**, 285–290 (1989).
3. Magenis, R. E., Brown, M. G., Lacy, D. A., Budden, S. & LaFranchi, S. Is Angelman syndrome an alternate result of del (15) (q11q13)? *Am J Med Genet* **28**, (1987).
4. Kishino, T., Lalande, M. & Wagstaff, J. UBE3A/E6-AP mutations cause Angelman syndrome. *Nature Genetics* **15**, 70–73 (1997).
5. Rougeulle, C., Glatt, H. & Lalande, M. The Angelman syndrome candidate gene, UBE3A/E6-AP, is imprinted in brain. *Nature Genetics* **17**, 14–15 (1997).
6. Meng, L., Person, R. E. & Beaudet, A. L. Ube3a-ATS is an atypical RNA polymerase II transcript that represses the paternal expression of Ube3a. *Human Molecular Genetics* **21**, 3001–3012 (2012).
7. Meng, L. *et al.* Towards a therapy for Angelman syndrome by targeting a long non-coding RNA. *Nature* **518**, 409–12 (2014).
8. Huang, H.-S. *et al.* Topoisomerase inhibitors unsilence the dormant allele of Ube3a in neurons. *Nature* **481**, 185–189 (2011).
9. Zylka, M. J. Prenatal Treatment Path for Angelman Syndrome and Other Neurodevelopmental Disorders. (2019). doi:10.1002/aur.2203
10. Silva-Santos, S. *et al.* Ube3a reinstatement identifies distinct developmental windows in a murine Angelman syndrome model. *Journal of Clinical Investigation* **125**, 2069–2076 (2015).
11. Judson, M. C., Sosa-Pagan, J. O., Del Cid, W. a., Han, J. E. & Philpot, B. D. Allelic specificity of Ube3a expression in the mouse brain during postnatal Development. *Journal of Comparative Neurology* **522**, 1874–1896 (2014).
12. Jiang, Y. hui *et al.* Mutation of the Angelman ubiquitin ligase in mice causes increased cytoplasmic p53 and deficits of contextual learning and long-term potentiation. *Neuron* **21**, 799–811 (1998).
13. Miura, K. *et al.* Neurobehavioral and Electroencephalographic Abnormalities in Ube3a Maternal-Deficient Mice. *Neurobiology of Disease* **9**, 149–159 (2002).
14. Sonzogni, M. *et al.* A behavioral test battery for mouse models of Angelman syndrome: a powerful tool for testing drugs and novel Ube3a mutants. *Molecular autism* **9**, 47 (2018).
15. Huang, H. S. *et al.* Behavioral deficits in an Angelman syndrome model: Effects of genetic background and age. *Behavioural Brain Research* **243**, 79–90 (2013).
16. Born, H. A. *et al.* Strain-dependence of the Angelman Syndrome phenotypes in Ube3a maternal deficiency mice. *Scientific Reports* **7**, 1–15 (2017).
17. Heck, D. H., Zhao, Y., Roy, S., LeDoux, M. S. & Reiter, L. T. Analysis of cerebellar function in Ube3a-deficient mice reveals novel genotype-specific behaviors. *Human molecular genetics* **17**, 2181–9 (2008).
18. Mulherkar, S. A. & Ranjan Jana, N. Loss of dopaminergic neurons and resulting behavioural deficits in mouse model of Angelman syndrome. (2010). doi:10.1016/j.nbd.2010.08.002
19. Bruinsma, C. F. *et al.* Dissociation of locomotor and cerebellar deficits in a murine Angelman syndrome model. *Journal of Clinical Investigation* **125**, 4305–4315 (2015).
20. Tronche, F. *et al.* Disruption of the glucocorticoid receptor gene in the nervous system results in reduced anxiety. (1999).
21. Wang, T., van Woerden, G. M., Elgersma, Y. & Borst, J. G. G. Enhanced Transmission at the Calyx of Held Synapse in a Mouse Model for Angelman Syndrome. *Frontiers in Cellular Neuroscience* **11**, 1–19 (2018).
22. Palmer, T. D., Willhoite, A. R. & Gage, F. H. Vascular niche for adult hippocampal neurogenesis. *Journal of Comparative Neurology* **425**, 479–494 (2000).
23. Alvarez-Buylla, A., García-Verdugo, J. M. & Tramontin, A. D. A unified hypothesis on the lineage of neural stem cells. *Nature Reviews Neuroscience* **2**, 287–293 (2001).
24. Suzuki, S., Namiki, J., Shibata, S., Mastuzaki, Y. & Okano, H. The neural stem/progenitor cell marker nestin is expressed in proliferative endothelial cells, but not in mature vasculature. *Journal of Histochemistry and Cytochemistry* **58**, 721–730 (2010).
25. Liang, H., Hippenmeyer, S. & Troy Ghashghaei, H. A Nestin-cre transgenic mouse is insufficient for recombination in early embryonic neural progenitors. *Biology Open* **1**, 1200–1203
26. Sonzogni, M. *et al.* Delayed loss of UBE3A reduces the expression of Angelman syndrome-associated phenotypes. *Molecular Autism* **10**, 23 (2019).
27. Avagliano Trezza, R. *et al.* Loss of nuclear UBE3A causes electrophysiological and behavioral deficits in mice and is associated with Angelman syndrome.

Nature Neuroscience **22**, 1235–1247 (2019).

28. Workman, A. D., Charvet, C. J., Clancy, B., Darlington, R. B. & Finlay, B. L. Modeling transformations of neurodevelopmental sequences across mammalian species. *Journal of Neuroscience* **33**, 7368–7383 (2013).
29. Dutta, S. & Sengupta, P. Men and mice: Relating their ages. *Life Sciences* **152**, 244–248 (2016).
30. Hensch, T. K. Critical period plasticity in local cortical circuits. *Nature Reviews Neuroscience* **6**, 877–888 (2005).
31. Hensch, T. K. & Bilimoria, P. M. Re-opening Windows: Manipulating Critical Periods for Brain Development. *Cerebrum : the Dana forum on brain science* **2012**, 11 (2012).
32. Levelt, C. N. & Hübener, M. Critical-Period Plasticity in the Visual Cortex. *Annual Review of Neuroscience* **35**, 309–330 (2012).

Supplemental information

Ube3a mouse model	behavioral test	dependent variable	test statistic	directionality	independent variables	test statistic value (df)	p value F test	post-hoc test for effect of genotype	p-value (Bonferroni)
Ube3a (LSL) x NES-CRE	rotarod	latency to fall (s)	2-way repeated measure ANOVA	2 sided	Genotype Time Genotype*Time	F(2,51)=6.387 F(1,947,99,29)=16.421 F(3,894,99,29)=2.295	p<0.01 p<0.001 p=0.066	WT	p<0.05 p=0.791
	marble burying	% buried marbles	univariate ANOVA	2 sided	Genotype	F(2,51)=25.80	p<0.001	WT	p<0.001 p=0.248
	nest building	used nesting material (%)	2-way repeated measure ANOVA	2 sided	Genotype Time Genotype*Time	F(2,51)=7.57 F(1,29,85,766)=204.6 F(2,579,65,766)=6.25	p<0.01 p<0.001 p<0.01	WT	p<0.01 p=0.801
	forced swim test	floating time (%)	univariate ANOVA	2 sided	Genotype	F(2,51)=38.75	p<0.001	WT	p<0.001 p=0.648
	reversed rotarod	latency to fall (s)	2-way repeated measure ANOVA	2 sided	Genotype Time Genotype*Time	F(3,56)=25.729 F(2,775,155,328)=77.113 F(8,32,155,328)=2.12	p<0.001 p<0.001 p=0.121	WT Ube3a m-/p- Ube3a m+/p-	p<0.001 p=0.334 p=0.074 p<0.001
	open field	distance moved (cm)	univariate ANOVA	2 sided	Genotype	F(3,56)=10.317	p<0.001	Ube3a m-/p- Ube3a m+/p-	p<0.01 p=1 p=1 p<0.01
Ube3a x Ube3a	marble burying	% buried marbles	univariate ANOVA	2 sided	Genotype	F(3,56)=22.684	p<0.001	WT Ube3a m-/p- Ube3a m+/p-	p<0.001 p=0.350 p=0.620 p<0.001
	nest building	used nesting material (%)	2-way repeated measure ANOVA	2 sided	Genotype Time Genotype*Time	F(3,56)=22.859 F(1,323,74,073)=437.87 F(8,32,155,328)=18.765	p<0.001 p<0.001 p<0.001	WT Ube3a m-/p- Ube3a m+/p-	p<0.001 p=1 p=0.156 p<0.001
	forced swim test	floating time (%)	univariate ANOVA	2 sided	Genotype	F(3,56)=22.563	p<0.001	WT Ube3a m-/p- Ube3a m+/p-	p<0.001 p=1 p=1 p<0.001

Additional file 1 (XLS). Table 1.

Summary of the statistical tests used for the behavioral paradigms performed on each experimental group.

CHAPTER 5

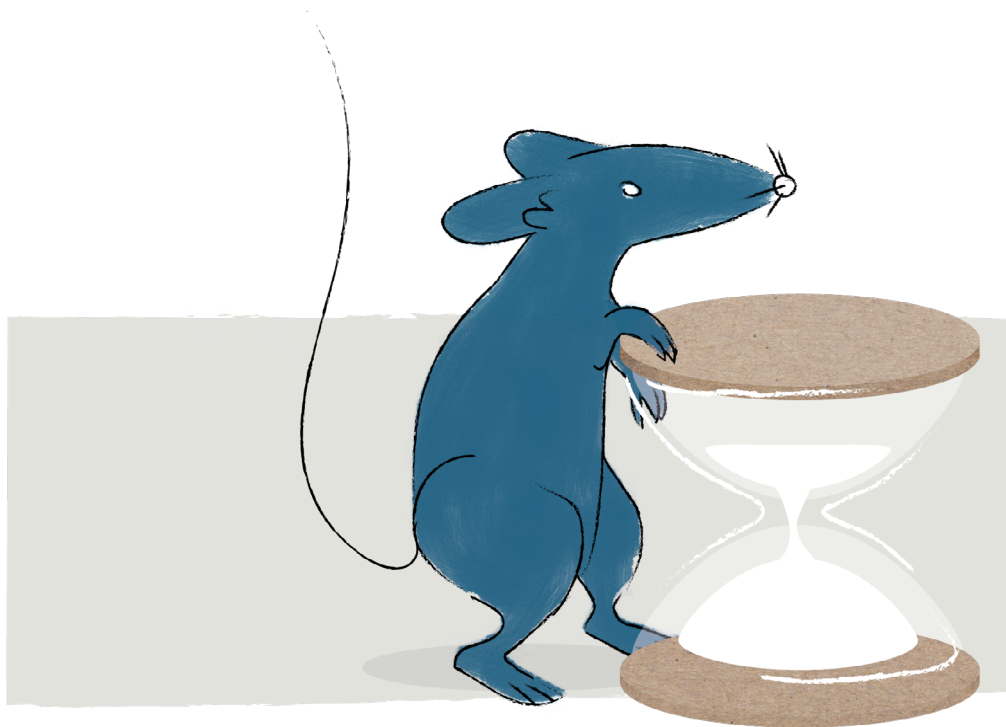
Delayed loss of UBE3A reduces the expression of Angelman syndrome-associated phenotypes

**Monica Sonzogni¹, Johanna Hakonen¹, Mireia Bernabé Kleijn¹, Sara Silva-Santos¹,
Matthew C. Judson², Benjamin D. Philpot², Geeske M. van Woerden¹,
Ype Elgersma^{1*}**

¹ Department of Neuroscience and the ENCORE Expertise Center for Neurodevelopmental Disorders,
Erasmus MC University Medical Center, Rotterdam, 3015 CN, The Netherlands

² Neuroscience Center, Department of Cell Biology and Physiology, and Carolina Institute for
Developmental Disabilities, University of North Carolina, Chapel Hill, North Carolina Institute, USA

*Correspondence: y.elgersma@erasmusmc.nl



Abstract

Background

Angelman syndrome (AS) is a severe neurodevelopmental disorder caused by mutations affecting *UBE3A* gene expression. Previous studies in mice revealed distinct critical periods during neurodevelopment in which reactivation of *Ube3a* gene expression can prevent the onset of behavioral deficits. Whether UBE3A is required for brain function throughout life is unknown. Here we address the importance of maintaining UBE3A expression after normal brain development.

Findings

Using a conditional mouse, we deleted the *Ube3a* gene at three ages spanning brain maturation. We assessed the consequences of *Ube3a* gene deletion by testing the mice in behavioral tasks previously shown to produce robust phenotypes in AS model mice. Early embryonic deletion of *Ube3a* recapitulated all behavioral deficits of AS mice. In contrast, *Ube3a* gene deletion at 3 or 12 weeks of age did not have a significant effect on most behavioral tasks, and did not increase seizure sensitivity.

Conclusions

Taken together, these results emphasize that UBE3A critically impacts early brain development, but plays a more limited role in adulthood. Our findings provide important considerations for upcoming clinical trials in which UBE3A gene expression is reactivated, and suggest that even transient UBE3A reinstatement during a critical window of early development is likely to prevent most adverse Angelman syndrome phenotypes. However, sustained UBE3A expression into adulthood is probably needed for optimal clinical benefit.

Introduction

Loss of the maternally inherited *UBE3A* allele results in Angelman syndrome (AS), a severe neurodevelopmental disorder, which is characterized by severe intellectual disability, motor coordination deficits, absence of speech, abnormal EEG, and behavioral deficits¹. *UBE3A* gene dosage also appears to be critical with respect to autism spectrum disorder (ASD)². Previous studies showed that there is up to 50% ASD comorbidity in AS individuals³⁻⁵, while overdosage of *UBE3A*, due to copy number variation of the 15q11-13 region, is among the highest genetic risk factors for ASD, accounting for up to 0.4% of all cases^{6,7}. Since duplication of the maternal locus is highly associated with pathogenicity⁷⁻¹⁰, it is likely that *UBE3A* (the only maternally expressed gene in this locus), is the major effector of ASD outcome. Indeed, duplications of just the *UBE3A* gene, as well as a gain-of-function *UBE3A* point mutation that renders UBE3A enzymatically hyperactive, have been linked to severe forms of ASD¹¹⁻¹⁴.

One of the most promising approaches for developing a treatment for AS is based on the activation of the epigenetically-silenced paternal *UBE3A* gene. Paternal *UBE3A* is silenced in neurons by a long non-coding *UBE3A-ATS* transcript, which can be activated by either using anti-sense oligonucleotides (ASOs) that target degradation of this transcript, or by topoisomerase inhibitors that interfere with the transcription of the *UBE3A-ATS*¹⁵⁻¹⁷. These *UBE3A* reinstatement approaches are particularly attractive since they restore UBE3A protein levels without risking over-expression.

Using an inducible *Ube3a* mouse model in which gene expression was genetically reinstated at different time points of brain development, we revealed distinct critical windows during brain development in which *Ube3a* needs to be reactivated to achieve an optimal behavioral rescue¹⁸. This suggests that early therapeutic intervention is needed for *UBE3A* reinstatement therapy to be fully effective. However, these results also pose a new question: to what extent is UBE3A expression required *after* brain development, and should treatment be continued after brain development has taken place?

To address this question, we made use of a conditional mouse model for AS that enabled us to delete the *Ube3a* gene at any desired time point. We found that early embryonic deletion of *Ube3a* recapitulated phenotypes that were previously described for AS mice¹⁹. In contrast, behavioral

deficits were mostly absent when the *Ube3a* gene was deleted in young (3 weeks) or fully adult (12 weeks) mice. These results emphasize that most phenotypes observed in AS mice reflect developmental deficits. Continued UBE3A expression beyond the completion of brain development may not be required for normal performance on most behavioral tasks.

Methods

Mouse breeding

We made use of the *Ube3a^{flox}* (*Ube3a^{tm1.1Bdph}*, MGI:5882092) mice as previously described²⁰. These mice were maintained in the C57BL/6J (Charles River Laboratories) background by crossing male B6.*Ube3a^{m+/plox}* mice with C57BL/6J females. For the behavioral experiments we used mice in the B6129S2F1 background, which were generated as described below. To generate embryonic deletion of *Ube3a*, B6.*Ube3a^{m+/plox}* female mice were crossed with CAG (CMV early enhancer/chicken actin promoter) CRE-expressing male mice [MGI:2176435; Tg(CAG-cre)13Miy; in the manuscript referred to as *Cre^{embryo}*] in the 129S2/SvPasCrl background (Charles River Laboratories)²¹. This breeding yielded 4 experimental groups in a B6129SF1 background: WT mice with and without CRE, and *Ube3a^{mlox/p+}* mice with and without CRE.

To allow temporal control of *Ube3a* deletion at 3 and 12 weeks of age, B6.*Ube3a^{m+/plox}* female mice were crossed with homozygous 129S2*Cre^{ERT}* [MGI:2182767; Tg(CAG-CRE/Esr1*)5Amc/J, also referred to as Tg(CAG-CRE-ERT2)] male mice²². This breeding yielded 2 experimental groups in a 129S2B6F1 background: WT mice with the CAGcre/Esr1 allele, and *Ube3a^{mlox/p+}* mice with the CAGcre/Esr1 allele.

For the seizure susceptibility experiments we used mice in the 129S2/SvPasCrl background. To that end, B6.*Ube3a^{mlox/p+}* mice were backcrossed for 4-5 generations in the 129S2/SvPasCrl background. Female 129S2.*Ube3a^{m+/plox}* mice were crossed with either Tg(CAG-CRE) or *Cre^{ERT}* male mice in the congenic 129S2/SvPasCrl background (backcrossed >20 generations).

Mouse husbandry

All mice were group-housed in a barrier facility, in cages that were individually ventilated (IVC; 1145T cages from Techniplast). Mice were genotyped when they were 4-7 days old, and re-genotyped at the completion of the experiments. All animals were kept at 22±2°C with a 12 hours dark and light cycle, and provided with mouse chow (801727CRM(P) from Special Dietary Service) and water *ad libitum*. During behavioral testing, mice remained group-housed, except during the nest building test and subsequent forced swim test.

Tamoxifen treatment and randomization

Three or twelve week-old Cre^{ERT};Ube3a^{mfllox/p+} transgenic mice and their wild type littermates (both sexes) received tamoxifen to induce Cre-mediated deletion of the *Ube3a* gene. Tamoxifen (Sigma-Aldrich) was diluted in vegetable (sunflower) oil at a concentration of 20 mg/ml as previously described^{18,22,23} and as recommended by the Jackson Laboratories²⁴. For five consecutive days, each mouse received 0.10 mg tamoxifen per gram body weight daily by intraperitoneal (IP) injection. The control group received daily IP injections of sunflower oil for 5 consecutive days (vehicle). Injection of either tamoxifen or vehicle were randomly assigned to the mice and the experimenter was blind to genotype.

Behavioral test battery

All behavioral experiments were performed during the light period of the light/dark cycle. Both male and female mice were used at the ages indicated in the text. Mice were acclimatized to the testing room for 30 minutes before each behavioral performance. All behavioral testing and scoring were performed by an experimenter blind to genotype. Behavioral tests were precisely performed as previously described^{18,19} and as listed below:

Accelerating rotarod. Motor capabilities were tested by placing the mice on the accelerating rotarod (4-40 rpm, in 5 minutes; model 7650, Ugo Basile Biological Research Apparatus, Varese, Italy). Mice were tested twice per day with a 45-60 min inter-trial interval for 5 consecutive days (same hour every day). For each day, the average time spent on the rotarod was calculated, or the time until the mouse made 3 consecutive wrapping / passive rotations on the rotarod (latency in seconds). Maximum duration of a trial was 5 min.

Open Field test. In this test, which is useful to test locomotor activity and anxiety, mice were individually placed in a brightly lit 110 cm diameter circular open field (25 lux in the middle of the arena) and allowed to explore the space for 10 min. The total distance moved by each mouse in the open arena was recorded by an infrared camera (Noldus® Wageningen, NL) connected to the EthoVision® software (Noldus® Wageningen, NL), and the final outcome is indicated as distance moved in centimeters.

Marble burying test. Open makrolon (polycarbonate) cages (50x26x18 cm)

were provided with 4 cm of bedding material (Lignocel® Hygenic Animal Bedding, JRS). On top of the bedding material 20 blue glass marbles were placed in an equidistant 5 x 4 grid and the animals were free to access to the marbles for 30 minutes. Once the time was run out, the mice were gently removed from the cage. The outcome measured is the number of buried marbles, which were scored as buried when covered more than 50% by bedding material.

Nest Building test. Mice were single housed for a period of 5 to 7 days before the start of the experiment. Successively, the used nesting material was replaced with around 11 grams (11±1) of compressed extra-thick blot filter paper (Bio-rad®). The amount of the unused nest material was weighed and noted daily for a consecutive of 5 days, each day at the same hour.

Forced swim test. Mice were placed in a cylindrical transparent tank (27cm high and 18cm diameter), filled with water (26±1 degrees Celsius) 15 cm deep for 6 min. The outcome measured is the time in seconds in which the mouse was immobile. The latency of immobility was only assessed during the last 4 min of the test. The mouse was considered to be immobile when it stopped moving, making only movements necessary to keep its head above water.

Susceptibility to audiogenic seizures. Mice were placed in makrolon (polycarbonate) cages (50x26x18 cm) and audiogenic seizures were induced by vigorously scraping scissors across the metal grating of the cage lid (which creates approximately a 100 dB sound). This noise was generated for 20 seconds, or less if a tonic-clonic seizure developed before that time. Susceptible mice responded with wild running and leaping followed by a tonic-clonic seizure, which typically lasted 10–20 seconds.

Western blot analysis and immunohistochemistry

Mice were sacrificed at 20-25 weeks of age, for subsequent analysis. For Western blots analysis, approximately 20µg of protein lysate were loaded on 4-12% SDS-PAGE gel (Bio-Rad) and transferred on nitrocellulose membranes to be then incubated with anti-UBE3A antibody (E8655 Sigma-Aldrich; 1:1000) and anti-actin antibody (MAB1501R, Millipore; 1: 20 000).

Briefly, membranes were blocked in 4% TBS milk solution for 1 hour at room temperature and incubated at 4°C over-night, rotating end over end, with the primary antibody dissolved in 2% TBS-T milk solution. The day after membranes were washed 3 times for 10 minutes with TBS-T and incubated with the secondary antibody, a fluorophore-conjugated goat anti-mouse antibody (IR Dye 800CW, Westburg; 1:15 000), dissolved in 2% TBS-T milk solution for 1 hour. At the end of the incubation, membranes were washed 3 times for 10 minutes with TBS and the resulting blots were analyzed and quantified using a LI-COR Odyssey Scanner and Odyssey 3.0 software.

For immunohistochemistry, mice were sedated with 0.15 ml Nembutal (60 mg/kg), transcardially perfused and the brains were post-fixed with 4% paraformaldehyde in sodium phosphate buffer (PB) for 2 h. After incubation in 10% sucrose (in 0.1 M Phosphate buffer) overnight, brains were embedded in a sucrose/gelatin mixture (10 and 12%, respectively). Brain sections were cut on a microtome (SM2000R; Leica Microsystems, Rijswijk, Netherlands) at a thickness of 40µm and treated with peroxidase (H₂O₂). The brain sections were then washed in PBS and were incubated for 1 h in blocking buffer containing 10% horse serum, 0.5% Triton X-100 in PBS. Subsequently, sections were incubated for 48–72 h in 2% normal horse serum, 0.5% Triton X-100 incubation buffer in PBS with primary antibody (mouse anti-E6AP, clone 3E5 Sigma–Aldrich; 1:750). The secondary antibody (anti-mouse HRP, P0447 Dako; 1:200) was detected by 3,3-diaminobenzidine (DAB) as the chromogen, and DAB sections were analyzed and photographed using Nanozoomer scanner.

Statistics

All data were statistically analyzed using IBM SPSS software, and P values less than 0.05 were considered significant. Statistical analysis was performed using univariate ANOVA (Kruskal-Wallis statistic test when data were non-normally distributed) or 2 way-repeated measures ANOVA with Bonferroni's and Dunnet/Mann-Whitney U test post hoc comparison. See the **Additional files** for more details.

Results

To elucidate the importance of continued UBE3A expression after early brain development, we took advantage of a conditional *Ube3a*^{mflox/p+} mouse

model²⁰ that enabled us to delete the maternal *Ube3a* gene at any desired time point. We first crossed female *Ube3a*^{mflox/p+} mice with a constitutive Cre-expressing mouse line²¹. This resulted in full, early embryonic deletion of the maternal *Ube3a* allele, and a consequent depletion of neuronal UBE3A protein expression in cortex, hippocampus, striatum and cerebellum, similar to what has been observed for the *Ube3a*^{m-/p+} AS mouse model¹⁸ (**Figure 1, Additional file 1-3: Table S1, Figure S1, Table S2**).

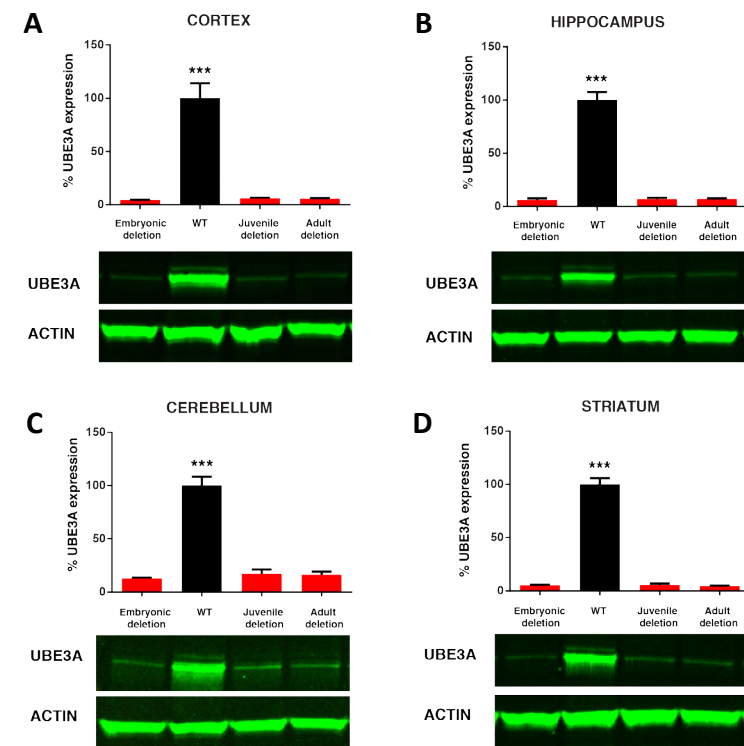


Figure 1. Loss of UBE3A expression upon juvenile and adult *Ube3a* gene deletion.

UBE3A Western blot analysis of wild-type mice and mice in which the *Ube3a* gene deletion is induced at 3 weeks ('juvenile deletion') or at 12 weeks 'adult deletion'. Mice were sacrificed between 22–25 weeks of age. The analysis shows that loss of UBE3A expression in cortex (A), hippocampus (B), cerebellum (C), and striatum (D) of these mice is comparable to mice in which the *Ube3a* gene is absent throughout development ('embryonic deletion') (N=3 per genotype). Data shown are means with SEM. See methods and **Additional file 1** for statistical tests.

Next we demonstrated that Cre^{embryo};*Ube3a*^{mflox/p+} faithfully recapitulate

the phenotypes that we previously established to be present in three independent AS mouse models^{18,19} (Figure 2, Additional file 4-6: Table S3, Figure S2, Table S4). These behavioral phenotypes are in the domains of motor function, anxiety and repetitive behaviors, and were selected to fulfill the following criteria: (1) Large effect sizes to allow multiple comparisons within and between cohorts, (2) reproducible phenotypes across multiple AS lines, (3) phenotypic penetrance in AS mice of different ages, and (4) tolerance of different experimenters. Moreover, these tests can all be performed in a single cohort of mice using a highly standardized (and optimized) method¹⁹. Having established that *Ube3a*^{mfllox/p+} mice phenocopy other AS lines tested in our behavioral test battery, we investigated the importance of continued UBE3A expression in these behavioral paradigms, after early brain development and into adulthood. To that end, we crossed female *Ube3a*^{mfllox/p+} mice with a tamoxifen inducible Cre line (Cre^{ERT})²². *Ube3a* gene deletion was induced by IP injection of tamoxifen in juvenile mice at 3 weeks of age, and in adult mice at 12 weeks of age (Figure 2). Western blot analysis of mice sacrificed at approximately 20-25 weeks, showed that overall UBE3A protein levels in cortex, hippocampus, and striatum of Cre^{ERT}; *Ube3a*^{mfllox/p+} mice closely resembled UBE3A levels of brains in which *Ube3a* was deleted embryonically (Figure 1; See also Additional file 7, 8: Figure S3, S4; Additional file 3: Table S2). Immunohistochemistry confirmed tamoxifen-induced *Ube3a* gene deletion throughout the brain (Additional file 7, 8: Figure S3, S4). Having ascertained that tamoxifen efficiently deleted the maternal *Ube3a* gene, we assessed the behavioral phenotypes of these Cre^{ERT}; *Ube3a*^{mfllox/p+} mice, minimally 7 weeks after gene deletion. This extended time period between gene deletion and testing not only allowed full clearance of UBE3A protein, but also allowed the neurons and neuronal networks to adapt to the loss of UBE3A expression, ensuring that any observed phenotypes were due to permanent consequences of UBE3A loss.

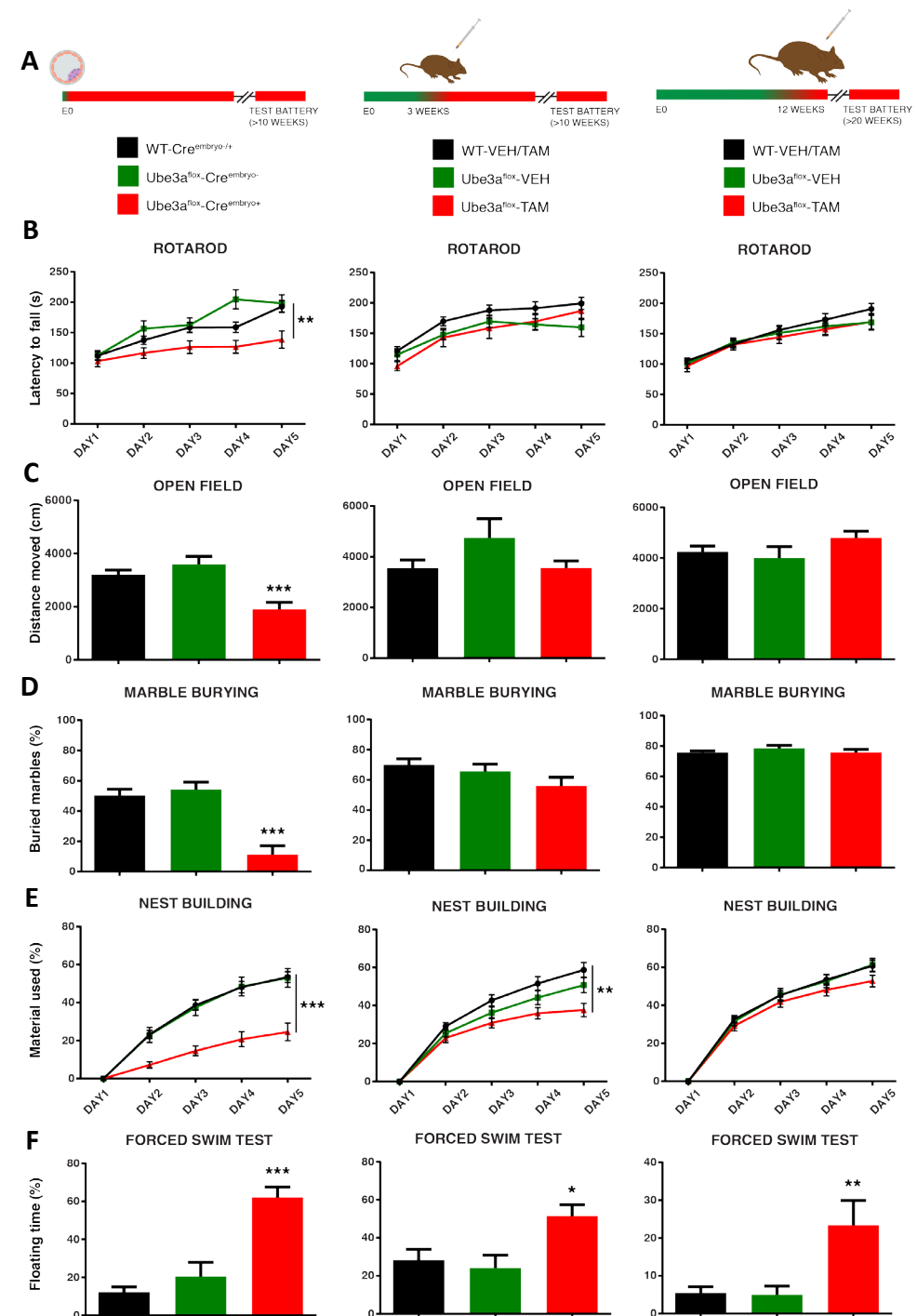


Figure 2. *Ube3a* gene deletion in juvenile and adult mice does not recapitulate the phenotypes observed in embryonically deleted *Ube3a* mice.

A Schematic depicting *Ube3a* gene deletion at early embryonic age, juvenile age (3 weeks) and adult age (12 weeks). **B-F** Behavioral tasks performed with *Cre^{embryo};Ube3a^{mfllox/p+}* and *Cre^{ERT};Ube3a^{mfllox/p+}* mice. Juvenile and adult *Ube3a* gene deletion results in deficits in the forced swim test. Asterisks indicate the effect of genotype. Wild-type (WT) mice in the *Cre^{embryo};Ube3a^{mfllox/p}* group represent combined data of Cre positive and Cre negative animals (Embryonic deletion: N for WT-Cre^{embryo}- / WT-Cre^{embryo}+ / *Ube3a^{mfllox/p+}*-Cre^{embryo}- / *Ube3a^{mfllox/p+}*-Cre^{embryo}+ mice= 15/group) Wild-type mice (WT) in the juvenile and adult-treated gene deletion group represent combined data of tamoxifen and vehicle-treated wild-type mice (Juvenile deletion: N for WT-OIL/ WT-TAM / *Ube3a^{mfllox/p+}*-VEH/ *Ube3a^{mfllox/p+}*-TAM mice= 11, 13, 14, 16)(Adult deletion: N for WT-OIL/ WT-TAM / *Ube3a^{mfllox/p+}*-VEH/ *Ube3a^{mfllox/p+}*-TAM mice= 15/group). Data shown are means with SEM. See methods and Additional file 4 for statistical tests.

Maternal *Ube3a* gene deletion in adult (12 week old) mice resulted in impaired forced-swim test behavior. Surprisingly however, performance in the accelerating rotarod, open field, nest building, and marble burying paradigms was not affected (**Figure 2, See also Additional file 5: Figure S2**). This indicates that these behaviors and their supporting neural circuits do not depend on continued UBE3A expression during adulthood¹⁸. Importantly, the lack of phenotypic penetrance in these tests is not caused by the age of testing (approximately 20-22 weeks), since we have previously shown that these phenotypes are still clearly present in AS mice aged 28 weeks¹⁸. Moreover, a retrospective analysis of several studies in our laboratory in which mice aged > 20 weeks were included, showed a strong phenotype on all these tests (**Additional file 9: Figure S5**).

For experiments in which *Ube3a* gene deletion was induced in juvenile mice at 3 weeks of age, we chose again to delay behavioral testing for a minimum of 7 weeks to allow the brain to respond to the gene deletion. Consequently, the age of testing was similar between juvenile deletion and embryonic deletion mice (*Cre^{embryo};Ube3a^{mfllox/p+}*), allowing for a direct comparison between these groups. Maternal *Ube3a* gene deletion in juvenile mice resulted in a significant impairment in the forced-swim test, highlighting once more the necessity of continued UBE3A expression for normal performance on this test. In addition, these mice also showed an impairment in the nest-building task. Since this phenotype was not present in mice in which *Ube3a* gene deletion was induced at 12 weeks of age, this result indicates that the neuronal network supporting performance in the nest-building task is not yet fully developed at 3 weeks of age. Surprisingly, none of the other tests

revealed impairments, suggesting that by three weeks of age, the brain has already developed to such an extent that UBE3A protein is no longer required for normal performance of most behaviors.

Most individuals with AS suffer from epilepsy. We have previously shown that AS mice in the 129S2 background exhibit exaggerated susceptibility to audiogenic seizures, which can be suppressed by modulating CAMK2 activity as well as by anti-epileptic drugs^{18,19,25}. This phenotype is not age dependent as it is readily observed in AS mice tested between 8-28 weeks old^{18,19}. We tested sensitivity to audiogenic seizures in 129S2-backcrossed *Ube3a^{mfllox/p+}* mice in which the *Ube3a* gene was deleted embryonically, at 3 weeks of age or in adulthood. Early embryonic deletion of the *Ube3a* gene rendered all (15/15) *Cre^{embryo};Ube3a^{mfllox/p+}* mice susceptible to audiogenic seizures. In contrast, neither juvenile (0/8) nor adult *Ube3a* gene deletion (0/16) resulted in mice that were sensitive to audiogenic seizures. This indicates that the sensitivity to audiogenic seizure is exclusively dependent on the presence or absence of UBE3A during early brain development¹⁸.

Discussion

The purpose of this study was to assess the role of the *Ube3a* gene in the mature brain, with the specific goal of gaining insight into whether UBE3A reinstatement therapies must be sustained throughout life for maximal efficacy in treating AS. In order to address this question, we took advantage of the conditional *Ube3a^{mfllox/p+}* mouse model²⁰, crossed with either a constitutive Cre-expressing mouse line (*Cre^{embryo}*)²¹ or with a tamoxifen inducible Cre line (*Cre^{ERT}*)²², to allow deletion of the *Ube3a* gene at distinct times during brain development.

By deleting *Ube3a* during early embryogenesis, we were able to reproduce all the behavioral deficits observed in various AS mouse models, highlighting the usefulness of this mouse model and the robustness of these phenotypes^{18,19}. These results further confirm the critical role of UBE3A during brain development, as we established previously¹⁸. In contrast, we observed limited phenotypic penetrance upon *Ube3a* deletion at 3 weeks or 12-weeks of age. We observed no deficits in motor coordination (rotarod), explorative behavior and anxiety (open field), or repetitive behavior and anxiety (marble burying). Nor did we evince a predisposition toward epilepsy as assessed by the audiogenic seizure provocation test. These results cannot be explained

by the age of the mice at the time of testing: juvenile deletion mice were the same age at testing as $Cre^{embryo};Ube3a^{mlox/p+}$ mice in which the gene was deleted embryonically. Moreover, AS mice older than 20 weeks of age continue to exhibit robust phenotypes on these tasks, as we demonstrated both here and in a previous study¹⁸.

Our results corroborate findings from our reciprocal *Ube3a* reinstatement studies¹⁸, leading us to conclude that the circuits underlying these behaviors are brought online during the perinatal period, and are well established by weaning. In contrast, it appears that circuits supporting nest-building behavior are not yet fully mature at three weeks of age, since deletion of *Ube3a* at this age (but not at 12 weeks) still results in a significant deficit. Notably, irrespective of the age of the mice, deletion of *Ube3a* always caused a deficit in the forced swim test paradigm, suggesting that the requisite circuits must sustain UBE3A expression for normal performance on this task.

Limitations

Our study has several limitations. First of all, it is possible that tamoxifen-induced postnatal *Ube3a* gene deletion does not occur in all cells. Our Western blot analysis shows no significant differences between UBE3A protein levels in mice with an embryonic *Ube3a* deletion compared to mice with a postnatal deletion of *Ube3a*. But this does not rule out the possibility that a small percentage of neurons did not undergo *Ube3a* gene deletion following tamoxifen treatment, and that *Ube3a* expression in a small subset of cells is sufficient to maintain normal behavioral function. A second limitation is that we did not assess behaviors related to learning and memory. Individuals with AS show severe intellectual deficits, but as discussed previously¹⁹, AS mouse models do not show robust learning deficits in our hands. Hence, we cannot exclude that normal learning and memory requires UBE3A to be present at a time when learning takes place. Finally, the face validity of some of our behavioral tests is quite limited (*e.g.* marble burying and nest building), as we do not know the underlying circuits and the relevance of these circuits to human AS phenotypes.

Conclusions

Our findings underscore the critical role of UBE3A for normal brain development, and suggest that most AS behavioral phenotypes arise from the absence of UBE3A during embryonic or early postnatal development. Our results also demonstrate that while expression of UBE3A in the mature brain may not be required for the acquisition and performance of most tests investigated in this study, certain behaviors do depend on continued UBE3A expression. Hence, our study indicates that there is likely to be clinical benefit by having enduring UBE3A reinstatement. Although we do not know how the first three weeks of postnatal brain development in mice translates to human brain development, our results suggest that even transient UBE3A reinstatement during a critical window of early development is likely to prevent most adverse Angelman syndrome phenotypes. Taken together these results emphasize the need to start *Ube3a* gene reactivation therapies early in life, and to sustain reactivation into adulthood for optimal effect.

Abbreviations

AS: Angelman syndrome; UBE3A: Ubiquitin protein ligase E3A; ASD: Autism Spectrum Disorder; ASO: antisense oligonucleotides; UBE3A-ATS: Ubiquitin protein ligase E3A antisense transcript; CAMK2: Ca²⁺/calmodulin-dependent protein kinase 2; WT: wild-type.

Declarations**Ethical approval**

All animal experiments were conducted in accordance with the European Commission Council Directive 2010/63/EU (CCD approval AVD101002016791).

Consent for publication

Not applicable.

Availability of data and material

The datasets used and/or analysed during the current study are available from the corresponding author on reasonable request.

Competing interests

Y.E. B.D.P and M.C.J. have received money from pharmaceutical companies for consultation and/or drug testing studies regarding Angelman syndrome.

Funding

This work was supported by a grant from the Angelman Syndrome Foundation (ASF) to YE and BDP. BDP was also supported by NIH grant R01HD093771. MS was supported by a grant from Associazione Angelman and FROM. GvW was supported by ASF. SSS was supported by Fundação para a Ciência e Tecnologia and Fundação Amélia de Mello.

Author contributions

MS, JH, MBK and SSS performed behavioral, molecular and immunostaining experiments. MS analyzed the data and performed statistical analysis. MCJ and BDP generated the floxed mice. GvW provided training and technical advice. YE and MS designed and coordinated the investigations. YE, MS, MCJ and BDP wrote the manuscript. The final version of the manuscript was

approved by all authors.

Acknowledgments

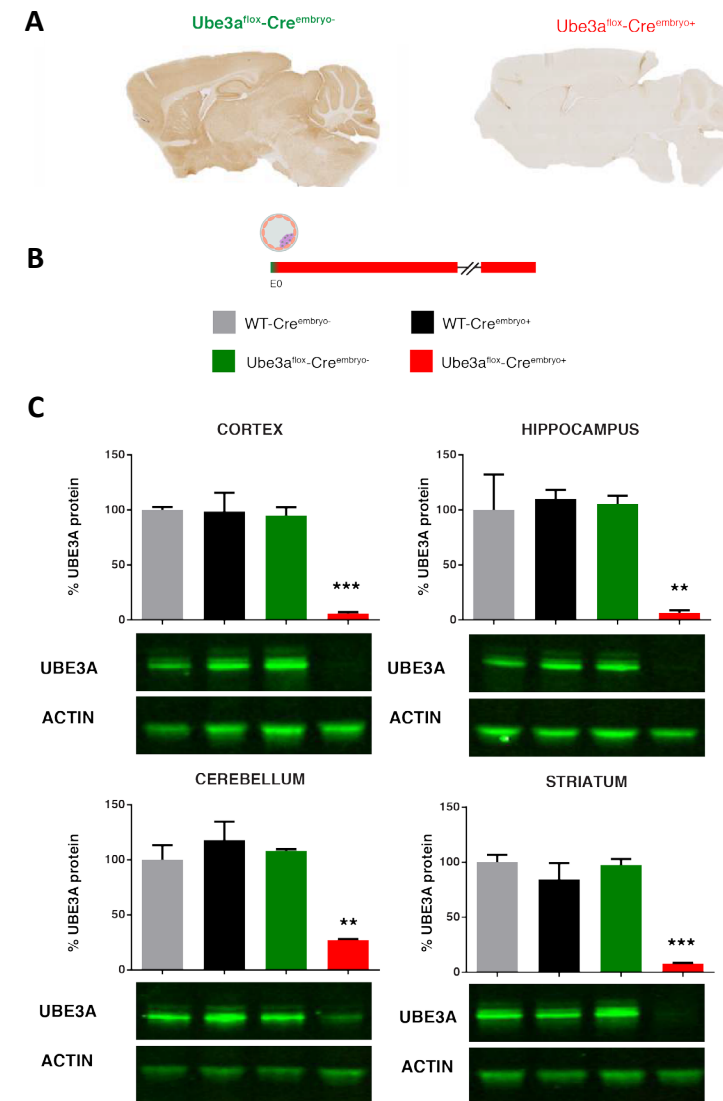
We thank Mehrnoush Aghadavoud Jolfaei for genotyping, Minetta Elgersma for mouse colony management and seizure susceptibility experiments, Ilse Wallaard for technical assistance, and Caroline Bruinsma and Edwin Mientjes for supervision and technical advice.

References

1. Buiting, K., Williams, C. & Horsthemke, B. Angelman syndrome—insights into a rare neurogenetic disorder. *Nature Reviews Neurology* **12**, 584–593 (2016).
2. Elgersma, Y. A molecular tightrope. *Nature* **526**, 50–51 (2015).
3. Trillingsgaard, A. & Østergaard, J. R. Autism in Angelman Syndrome. *Autism* **8**, 163–174 (2004).
4. Moss, J. & Howlin, P. Autism spectrum disorders in genetic syndromes: Implications for diagnosis, intervention and understanding the wider autism spectrum disorder population. *Journal of Intellectual Disability Research* **53**, 852–873 (2009).
5. Peters, S. U., Horowitz, L., Barbieri-Welge, R., Taylor, J. L. & Hundley, R. J. Longitudinal follow-up of autism spectrum features and sensory behaviors in Angelman syndrome by deletion class. *Journal of Child Psychology and Psychiatry* **53**, 152–159 (2012).
6. Moreno-De-Luca, D. *et al.* Using large clinical data sets to infer pathogenicity for rare copy number variants in autism cohorts. *Molecular Psychiatry* **18**, 1090–1095 (2013).
7. Sanders, S. J. *et al.* Insights into Autism Spectrum Disorder Genomic Architecture and Biology from 71 Risk Loci. *Neuron* **87**, 1215–1233 (2015).
8. Cook, E. H. *et al.* Autism or Atypical Autism in Maternally but Not Paternally Derived Proximal 15q Duplication. *Am. J. Hum. Genet* **60**, (1997).
9. Isles, A. R. *et al.* Parental Origin of Interstitial Duplications at 15q11.2–q13.3 in Schizophrenia and Neurodevelopmental Disorders. *PLoS genetics* **12**, e1005993 (2016).
10. Finucane, B. M. *et al.* 15q Duplication Syndrome and Related Disorders. *GeneReviews*[®] (University of Washington, Seattle, 1993).
11. Hogart, A., Wu, D., LaSalle, J. M. & Schanen, N. C. The comorbidity of autism with the genomic disorders of chromosome 15q11.2–q13. *Neurobiology of Disease* **38**, 181–191 (2010).
12. Urraca, N. *et al.* The interstitial duplication 15q11.2–q13 syndrome includes autism, mild facial anomalies and a characteristic EEG signature. *Autism research : official journal of the International Society for Autism Research* **6**, 268–79 (2013).
13. Noor, A. *et al.* 15q11.2 Duplication Encompassing Only the UBE3A Gene Is Associated with Developmental Delay and Neuropsychiatric Phenotypes. *Human Mutation* **36**, 689–693 (2015).
14. Yi, J. J. J. *et al.* An Autism-Linked Mutation Disables Phosphorylation Control of UBE3A. *Cell* **162**, 795–807 (2015).
15. Meng, L. *et al.* Towards a therapy for Angelman syndrome by targeting a long non-coding RNA. *Nature* **518**, 409–12 (2014).
16. Huang, H.-S. *et al.* Topoisomerase inhibitors unsilence the dormant allele of Ube3a in neurons. *Nature* **481**, 185–189 (2011).
17. King, I. F. *et al.* Topoisomerases facilitate transcription of long genes linked to autism. *Nature* **501**, 58–62 (2013).
18. Silva-santos, S. *et al.* Ube3a reinstatement identifies distinct developmental windows in a murine Angelman syndrome model. *Journal of Clinical Investigation* **125** *Suppl 1*, 1–8 (2015).
19. Sonzogni, M. *et al.* A behavioral test battery for mouse models of Angelman syndrome: a powerful tool for testing drugs and novel Ube3a mutants. *Molecular autism* **9**, 47 (2018).
20. Judson, M. C. *et al.* GABAergic Neuron-Specific Loss of Ube3a Causes Angelman Syndrome-Like EEG Abnormalities and Enhances Seizure Susceptibility. *Neuron* **90**, 56–69 (2016).
21. Sakai, K. & Miyazaki, J. A Transgenic Mouse Line That Retains Cre Recombinase Activity in Mature Oocytes Irrespective of the Cre Transgene Transmission. *Biochemical and Biophysical Research Communications* **237**, 318–324 (1997).
22. Hayashi, S. & McMahon, A. P. Efficient Recombination in Diverse Tissues by a Tamoxifen-Inducible Form of Cre: A Tool for Temporally Regulated Gene Activation/Inactivation in the Mouse. *Developmental Biology* **244**, 305–318 (2002).
23. Gu, B. *et al.* Ube3a reinstatement mitigates epileptogenesis in Angelman syndrome model mice. *The Journal of Clinical Investigation* **129**, 163–168 (2019).
24. Intraperitoneal Injection of Tamoxifen for Inducible Cre-Driver Lines. Available at: <https://www.jax.org/research-and-faculty/resources/cre-repository/tamoxifen>. (Accessed: 20th March 2019)
25. van Woerden, G. M. *et al.* Rescue of neurological deficits in a mouse model for Angelman syndrome by reduction of alphaCaMKII inhibitory phosphorylation. *Nature neuroscience* **10**, 280–282 (2007).

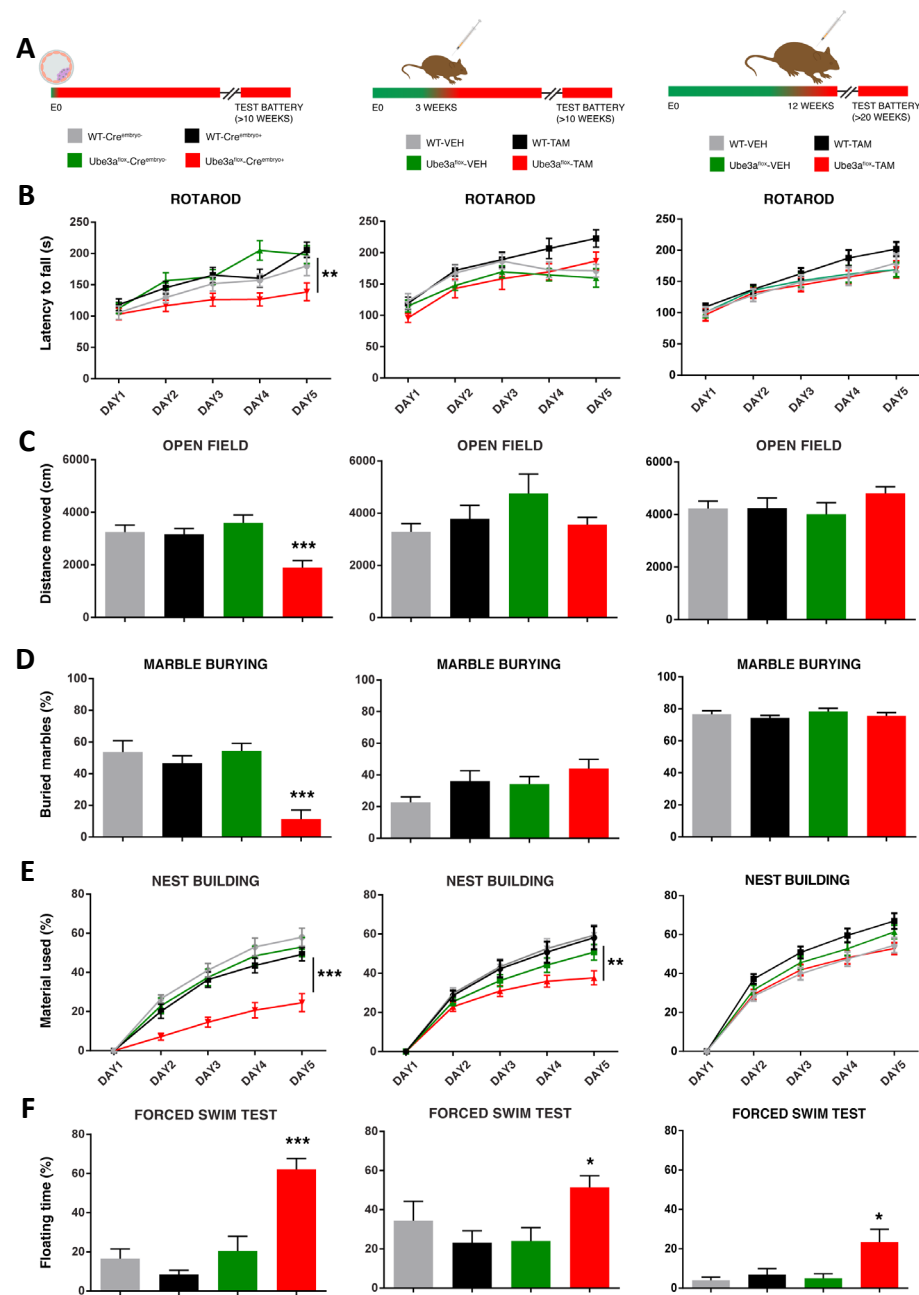
Supplementary Information

Additional file 1, 3, 4, 6 of this Chapter are available at the following DOI link: 10.1186/s13229-019-0277-1.



Additional file 2 (PDF). Figure S1 Deletion of UBE3A during embryogenesis.

A Whole brain immunohistochemical stainings indicate reduced UBE3A protein levels in *Ube3a^{lox}-Cre^{embryo}+* mice compared to *Ube3a^{lox}-Cre^{embryo}-* control mice. **B** *Ube3a* gene deletion upon CRE activation driven by the Cag promoter during embryogenesis. **C** Western blot data indicate reduced UBE3A protein levels in *Ube3a^{lox}-Cre^{embryo}+* mice compared to control groups. Number of mice used for the western blot analysis is n=3 per genotype. Data shown are mean (±SEM). See Additional file 3 (Supplemental Table S2) for statistical analysis and the sample sizes.



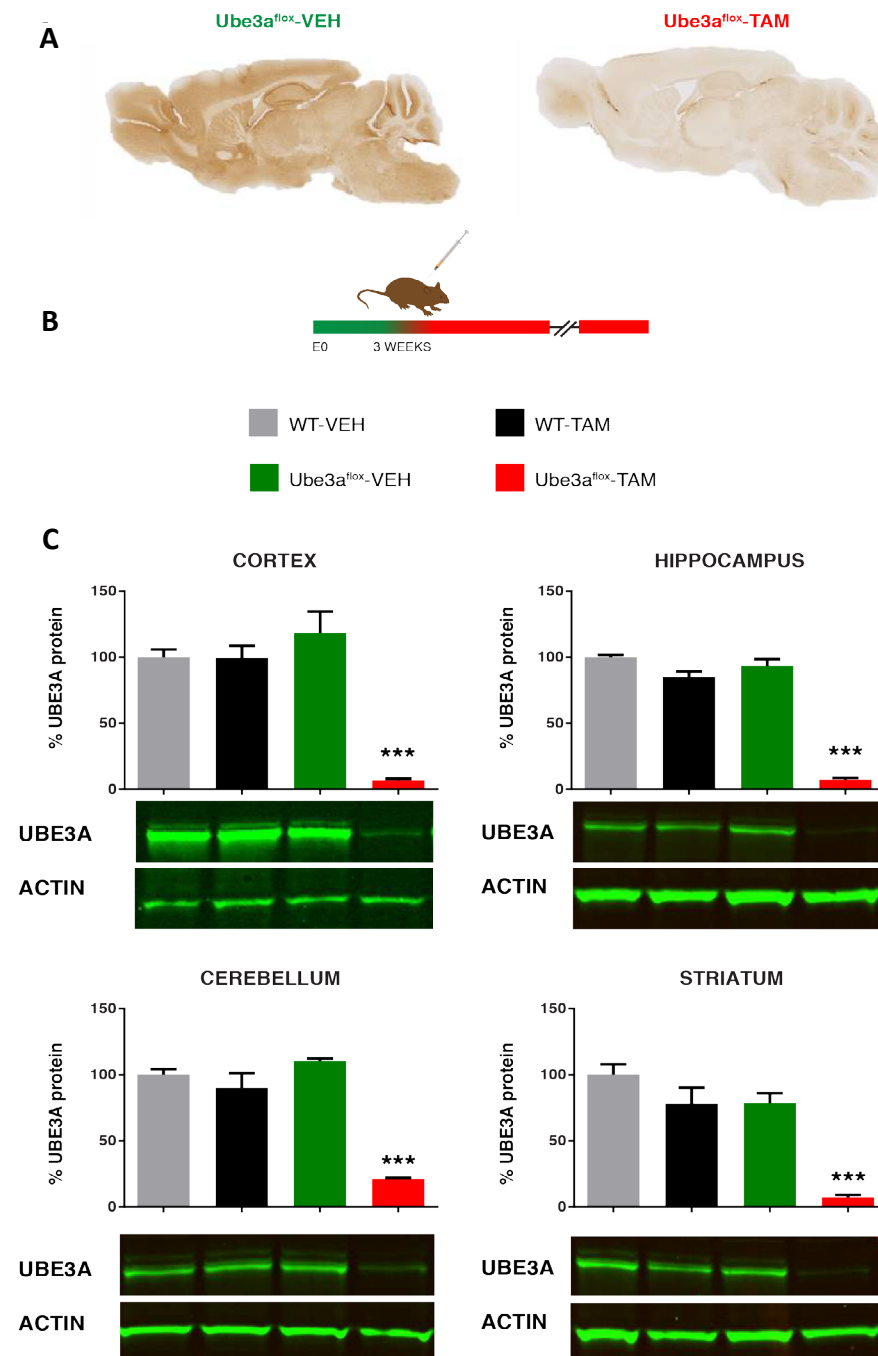
Additional file 5 (PDF). Figure S2. Supplemental figure 2. *Ube3a* gene deletion in juvenile and adult mice does not recapitulate the phenotypes observed in embryonically deleted *Ube3a* mice.

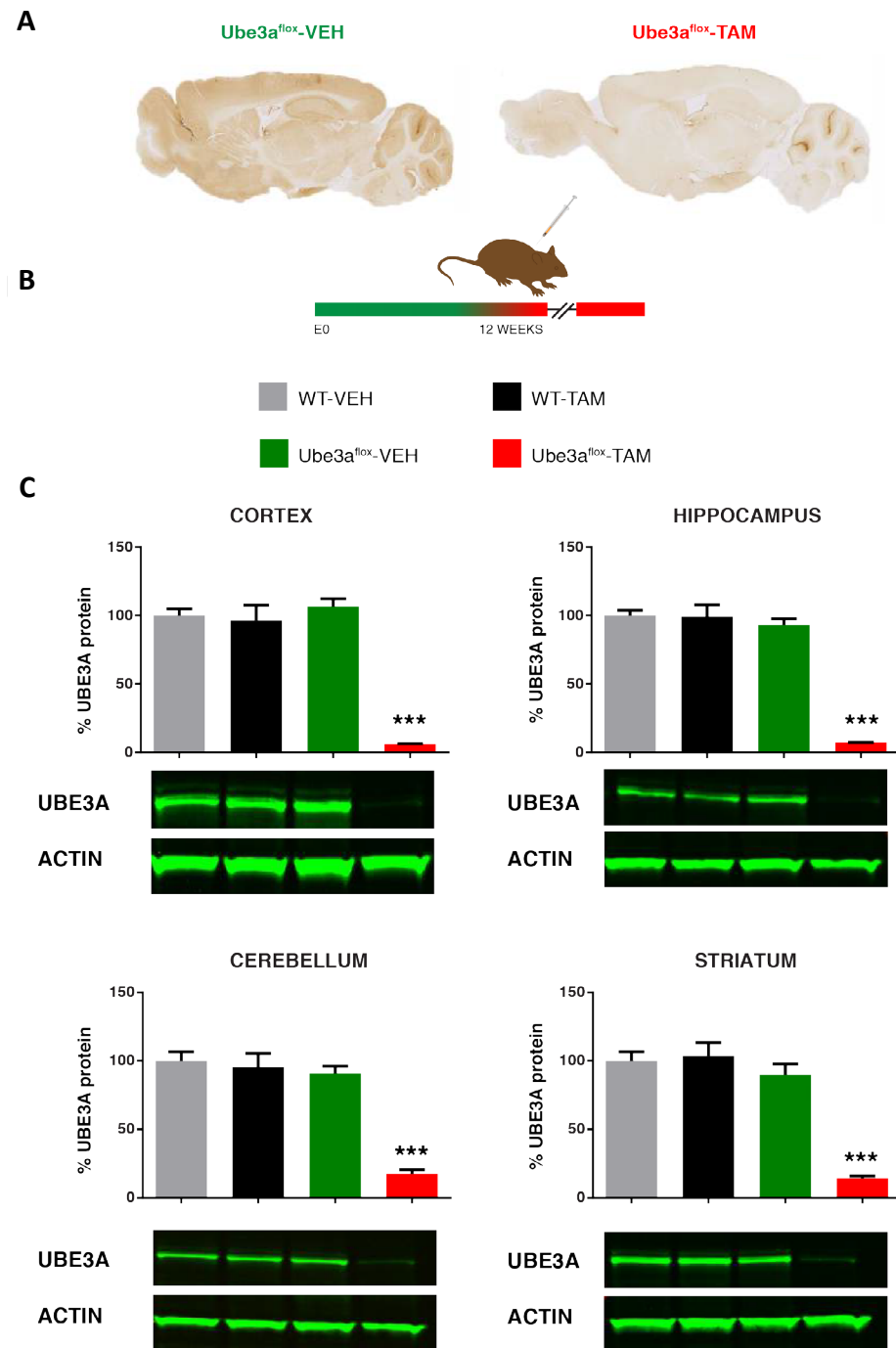
A Schematic depicting *Ube3a* gene deletion at early embryonic age, juvenile

age (3 weeks) and adult age (12 weeks). **B-F** Behavioral tasks performed with *Cre^{embryo};Ube3a^{mlox/p+}* (N for WT-*Cre^{embryo}-* / WT-*Cre^{embryo}+* / *Ube3a^{mlox/p+}-Cre^{embryo}-* / *Ube3a^{mlox/p+}-Cre^{embryo}+* mice= 15/group) and *Cre^{ERT};Ube3a^{mlox/p+}* mice (Juvenile deletion: N for WT-OIL/ WT-TAM/ *Ube3a^{mlox/p+}-VEH*/ *Ube3a^{mlox/p+}-TAM* mice= 11, 13, 14, 16; Adult deletion: N for WT-OIL/ WT-TAM/ *Ube3a^{mlox/p+}-VEH*/ *Ube3a^{mlox/p+}-TAM* mice= 15/group). Juvenile and adult *Ube3a* gene deletion results in deficits in the forced swim test. Asterisks indicate the effect of genotype. Data shown are means with SEM. See methods and **Additional file 6** for statistical tests and sample size.

Additional file 7 (PDF). Figure S3. Supplemental figure 3. Deletion of UBE3A in young mice.

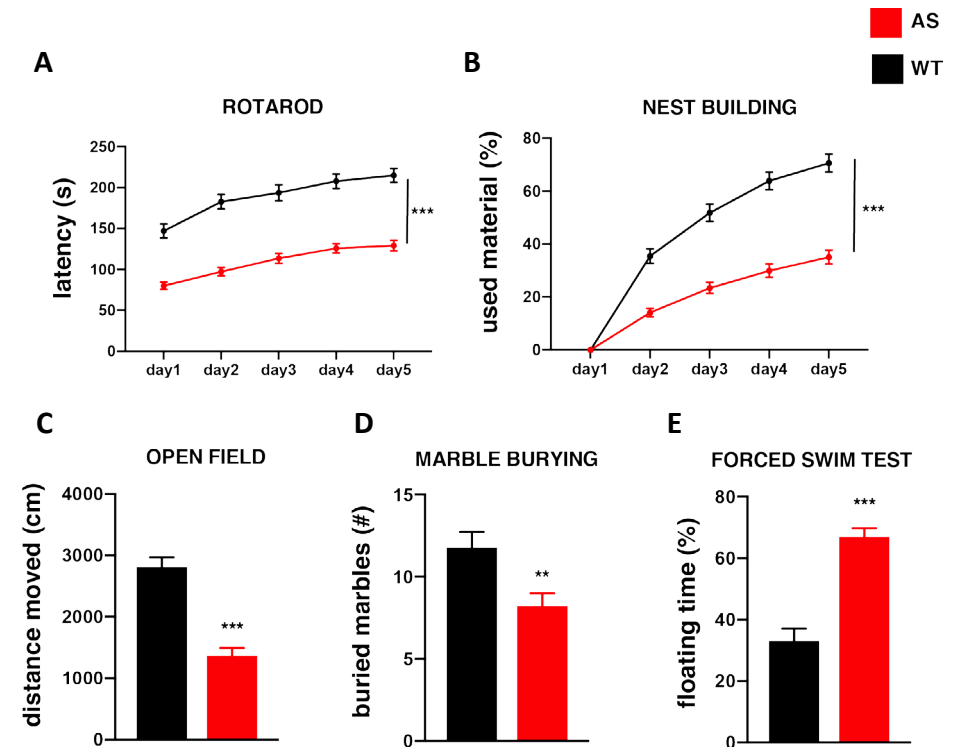
A Immunohistochemical staining indicate reduced UBE3A protein levels in *Ube3a^{fllox}-TAM* mice compared to *Ube3a^{fllox}-VEH* control group. **B** *Ube3a* gene deletion induced at 3 weeks of age upon CRE activation by tamoxifen injection. **C** Western blot data indicate reduced UBE3A protein levels in *Ube3a^{fllox}-Cre^{embryo+}* mice compared to control groups. Number of mice used for the western blot analysis is n=3-4 per genotype. Data shown are mean (\pm SEM). See Supplemental Table S2 for statistical analysis and the sample sizes.





Additional file 8 (PDF). Figure S4. Supplemental Figure 4. Deletion of UBE3A in adult mice.

A Immunohistochemical stainings indicate reduced protein levels of UBE3A in *Ube3a*^{lox}-TAM mice compared to *Ube3a*^{lox}-VEH control group. **B** *Ube3a* gene deletion at 12 weeks of age upon CRE activation by tamoxifen injection. **C** Western blot data indicate reduced UBE3A protein levels in *Ube3a*^{lox}-*Cre*^{embryo+} mice compared to control groups. Number of mice used for the western blot analysis is n=3/genotype. Data shown are mean (±SEM). See Supplemental Table S2 for statistical analysis and the sample sizes.



Additional file 9 (PDF). Figure S5. Behavioural test battery in mice older than 20 weeks of age.

A Accelerating rotarod in wild-type (WT) and AS mice (n=51, 67). **B** Nest building test in WT and AS mice (n=39, 45). **C** Open field test in WT and AS mice (n=36, 57). **D** Marble burying test in WT and AS mice (n=47, 62). **E** Forced swim test in WT and AS mice (n=37, 60). All data represent mean ± SEM. A repeated measures ANOVA or t-test (or Mann Whitney U test for nonparametric data) was used for statistical comparison. All tests show a significance effect of genotype (***) p<0.001).

Loss of nuclear UBE3A causes electrophysiological and behavioural deficits in mice and is associated with Angelman Syndrome

**Rossella Avagliano Trezza^{1,2,3,8}, Monica Sonzogni^{2,3,8}, Stijn N. V. Bossuyt^{1,8},
F. Isabella Zampeta^{2,3}, A. Mattijs Punt^{2,3}, Marlene van den Berg¹,
Diana C. Rotaru^{2,3,8}, Linda M.C. Koene^{2,3,8}, Shashini T. Munsh i⁴,
Jeffrey Stedehouder⁴, Johan M. Kros⁵, Mark Williams⁶, Helen Heussler⁷,
Femke M. S. de Vrij⁴, Edwin J. Mientjes^{2,3}, Geeske M. van Woerden^{2,3},
Steven A. Kushner^{3,4}, Ben Distel^{1,2,3,9*}, Ype Elgersma^{2,3,9*}**

¹Department of Medical Biochemistry, Amsterdam UMC, University of Amsterdam, Amsterdam, 1105AZ, The Netherlands

²Department of Neuroscience, Erasmus MC University Medical Center, Rotterdam, 3015 CN, The Netherlands

³ENCORE Expertise Center for Neurodevelopmental Disorders, Erasmus MC University Medical Center, Rotterdam, 3015 CN, The Netherlands

⁴Department of Psychiatry, Erasmus MC University Medical Center, Rotterdam, 3015 CN, The Netherlands

⁵Department of Pathology, Erasmus MC University Medical Center, Rotterdam, 3015 CN, The Netherlands

⁶Mater Research Institute, The University of Queensland, Woolloongabba; Faculty of Medicine, The University of Queensland, St Lucia, Queensland, Australia

⁷Mater Research Institute, The University of Queensland, Woolloongabba; Child Development Program, Queensland Children's Hospital, South Brisbane; Child Health Research Centre, The University of Queensland, South Brisbane, Queensland, Australia

⁸These authors contributed equally

⁹These senior authors contributed equally

*Correspondence: y.elgersma@erasmusmc.nl; b.distel@amc.uva.nl



Abstract

Mutations affecting ubiquitin-ligase UBE3A cause Angelman Syndrome (AS). Although most studies focus on the synaptic function of UBE3A, we show that UBE3A is highly enriched in the nucleus of mouse and human neurons. We found that the two major isoforms of UBE3A exhibit a highly distinct nuclear versus cytoplasmic subcellular localization. Both isoforms undergo nuclear import through direct binding to PSMD4/RPN10, but the amino-terminus of the cytoplasmic isoform prevents nuclear retention. Mice lacking the nuclear UBE3A isoform recapitulate the behavioural and electrophysiological phenotypes of *Ube3a*^{m-/p} mice, whereas mice harbouring a targeted deletion of the cytosolic isoform are unaffected. Finally, we identified AS-associated UBE3A missense mutations that interfere with either nuclear targeting or nuclear retention of UBE3A. Taken together, our findings elucidate the mechanisms underlying the subcellular localization of UBE3A, and indicate that the nuclear UBE3A isoform is the most critical for AS pathophysiology.

Introduction

Angelman syndrome (AS) is a severe neurodevelopmental disorder, affecting 1:20,000 individuals. The primary symptoms of AS include intellectual disability, motor dysfunction, absence of speech, treatment-refractory epilepsy and distinctive behavioural features. AS is caused by loss-of-function of the maternally inherited *UBE3A* allele, which encodes a HECT E3 ubiquitin ligase^{1,2,3}. Given that the loss of UBE3A affects synaptic function (*e.g.*^{4,5}), most efforts have focused on identifying synaptic UBE3A targets (*e.g.*⁶⁻⁸), but the critical substrates responsible for AS pathophysiology remain unknown. However, recent studies showed that UBE3A localizes to the nucleus as well as to synapses^{9,10-13}, and it is notable that many of the putative targets are predominantly nuclear^{1,2}.

The *UBE3A* gene encodes distinct isoforms that are generated by differential splicing^{6,14} (**Figure 1A; Supplementary Figure 1A,B**). In this study we focus on the two murine UBE3A isoforms that have highly-conserved human homologs: mouse UBE3A isoform 2 and 3 (**Figure 1A**). Mouse UBE3A isoform 2 (mUBE3A-Iso2) (homologous to human UBE3A isoform 3; hUBE3A-Iso3), is referred to as the long UBE3A isoform because of its 21 amino acid N-terminal extension. Mouse UBE3A isoform 3 (mUBE3A-Iso3) (homologous to human UBE3A isoform 1; hUBE3A-Iso1), lacks this N-terminal extension⁶ (**Figure 1A**). A previous study showed that the long UBE3A mouse isoform (mUBE3A-Iso2) has a predominantly cytosolic localization whereas the short isoform (mUBE3A-Iso3) is mainly nuclear¹¹. Mouse *Ube3a* Isoform 1 is a non-coding transcript, which has been suggested to play a role in brain development¹⁵, but this transcript is very low expressed in mice and absent in human (**Supplementary Figure 1**).

The nuclear localization of mUBE3A-Iso3 raises two important questions: (1) how is nuclear localization of UBE3A achieved and (2), is nuclear UBE3A required for normal neurodevelopment? Here, we found that PSMD4/S5a/RPN10 is responsible for targeting UBE3A to the nucleus by binding to the AZUL domain of UBE3A. Once inside the nucleus, mUBE3A-Iso2 is actively transported back to the cytoplasm, whereas the short mUBE3A-Iso3 is retained within the nucleus. Using newly generated isoform-specific *Ube3a* mice, we establish the critical importance of nuclear UBE3A in AS-related phenotypes. This is consistent with our discovery that certain AS-linked missense mutations interfere with either nuclear targeting or retention of

UBE3A. Taken together our studies uncover a complex regulation of UBE3A targeting to the nucleus, and suggest that nuclear UBE3A plays an important role in normal neurodevelopment.

Results

UBE3A is highly enriched in the nucleus of mature human and mouse neurons

We first assessed the subcellular distribution of UBE3A in mouse primary hippocampal neurons, human iPSC-derived neurons, and human post-mortem prefrontal cortex (PFC) (**Figure 1**). We found that UBE3A was highly enriched in the nucleus of mouse and human cultured neurons, as well as in human post-mortem brain.

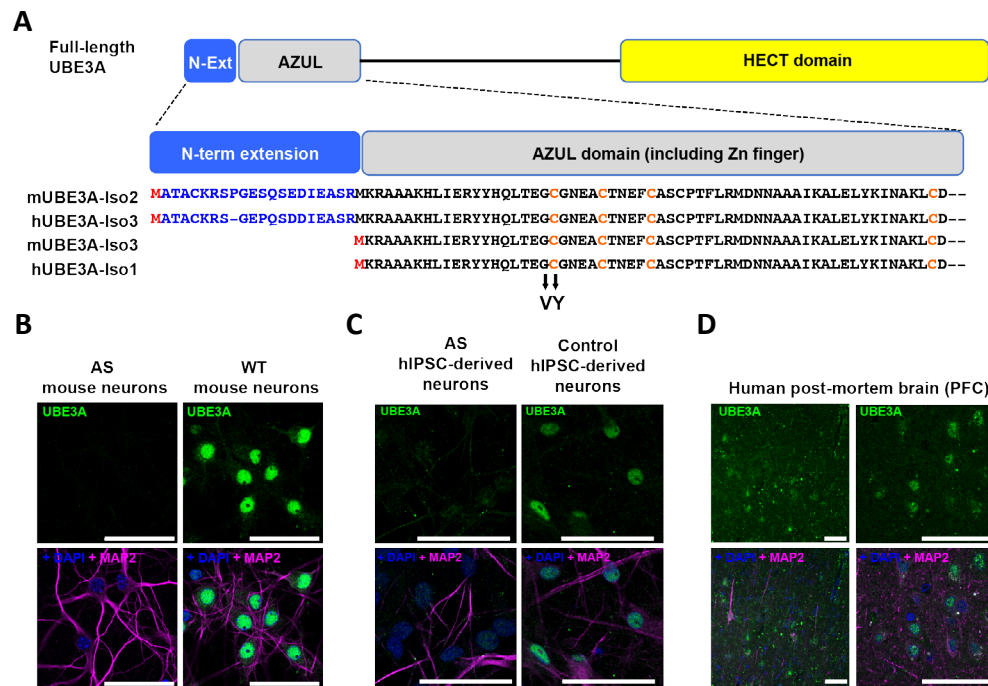


Figure 1. UBE3A is enriched in the nucleus of mature human and mouse neurons.

A Top: Schematic representation of the UBE3A protein and its functional domains. Depicted are the N-terminal extension of UBE3A mouse isoform 2 (mUBE3A-Iso2) and human isoform 3 (hUBE3A-Iso3) (blue), the N-terminal Zn-binding AZUL domain (grey), and the C-terminal HECT domain (yellow). **Bottom:** Amino acid sequence alignment of the N-termini of only the isoforms that are

expressed in both mice and human: the longer mUBE3A-Iso2 (NP_035798.2) and hUBE3A-Iso3 (NP_001341434.1) proteins, and the predominantly expressed shorter mUBE3A-Iso3 (NP_001029134.1) and hUBE3A-Iso1 (NP_001341455.1) proteins. The translational start sites (methionines) of the isoforms are depicted in red. The obligatory cysteine residues involved in the Zn²⁺ coordination (Cys21, Cys26, Cys31 and Cys60) are indicated in orange. Arrows indicate the p.Gly20Val and p.Cys21Tyr missense mutations in the AZUL domain as identified in AS patients (numbering refers to mUBE3A-Iso3/ hUBE3A-Iso1 reference sequence). **B** Localization of mUBE3A (green; upper panels) in DIV7 (*days in vitro*) mouse hippocampal neurons derived from E16.5 *Ube3a*^{m-/p+} (AS) and wild-type (WT) embryos. Lower panels: overlay of UBE3A with MAP2 (pink) and DAPI (blue). Representative images from a minimum of 3 independent cultures of neurons derived from an average of 5 embryos with similar results obtained. **C** Localization of hUBE3A in iPSC derived neurons from an AS patient and a neurotypical control, stained after 6 weeks of differentiation for UBE3A, MAP2 and DAPI. Representative images from a minimum of 3 independent neuronal cultures derived from 1 AS iPSC line and 2 independent control iPSC lines with similar results obtained. **D** hUBE3A localization in post-mortem tissue obtained from prefrontal cortex (PFC) of an adult individual, stained for UBE3A, MAP2 and DAPI. Representative images from a minimum of 3 brain sections derived from 2 neurotypical individuals with similar results obtained. **B-D**, scale bar: 50 μ m.

A previous study showed that the longer mUBE3A-Iso2 is localized to the cytosol while the shorter mUBE3A-Iso3 is mainly nuclear¹¹. This suggests that the localization of mouse UBE3A is regulated by differential isoform expression and implies that the shorter isoform is predicted to be the predominant isoform in mouse and human neurons. We used SDS-PAGE gradient gels to separate the UBE3A isoforms, and determined their levels by semi-quantitative Western blotting (**Figure 2A**; **Supplementary Figure 2A**; Note that the identity of these bands is confirmed in brain samples from isoform specific mutant mice, as shown in **Figure 7B**). Quantification of the isoform specific bands on the Western blots revealed that the (short) mUBE3A-Iso3 represents approximately 75-80% of the total UBE3A protein present in mouse brain. Comparable values were found for the short human isoform (hUBE3A-Iso1) in human post-mortem brain (**Supplementary Figure 1B**), indicating that the short isoform is indeed the predominant UBE3A protein isoform in the brain in both species. Moreover, we found that the protein ratio of these two UBE3A isoforms does not change during development (**Figure 2B**).

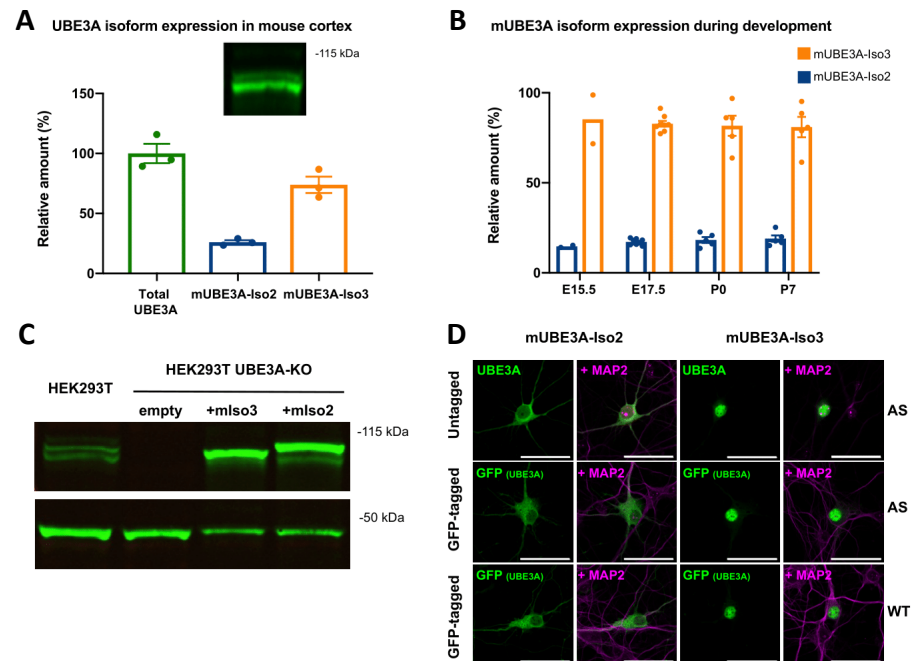


Figure 2. Mouse UBE3A localization is dictated by the 3A isoforms.

A Quantification of mUBE3A-Iso2 and mUBE3A-Iso3 in mouse cortical lysates (n=3 animals, bars represent mean values \pm SEM). Inset shows a representative UBE3A immunoblot in which the mUBE3A-Iso2 and mUBE3A-Iso3 proteins are separated. The image has been cropped from a full Western blot and vertically stretched to allow separation and quantification of the bands (See Supplemental Figure 2A) **B** Quantification of mUBE3A-Iso2 (blue) and mUBE3A-Iso3 (yellow) during mouse cortical development: Embryonic day (E)15.5 (n=2 animals) and E17.5 (n=8 animals, and Postnatal day (P)0 (n=5 animals), and P7 (n=5 animals) Bars represent mean values \pm SEM. **C** Immunoblot analysis of heterologously expressed mUBE3A isoforms in HEK293T^{UBE3A-KO} cells. The first lane shows endogenous UBE3A expression in untransfected HEK293T cells. For visualization purposes only 50% of lysates of mUBE3A-Iso3 and mUBE3A-Iso2 expressing cells were loaded compared to the untransfected cells. The image has been cropped from a full Western blot (See Supplemental Figure 2B) **D** Localization of mUBE3A isoforms in hippocampal neurons derived from E16.5 *Ube3a*^{m-/p+} (AS) and wild-type (WT) embryos. Neurons were transfected with mUBE3A-Iso2 and mUBE3A-Iso3 without a tag (upper panels) or with mUBE3A-Iso2 and mUBE3A-Iso3 tagged at their C-termini with GFP (lower 2 panels). Neurons were stained for UBE3A (green, upper panels) together with MAP2 (pink, all panels) and DAPI (blue, all panels). UBE3A-GFP expression was detected by direct fluorescence. Scale bar: 50 μ m.

Nuclear localization of UBE3A requires the N-terminal AZUL domain

To study the mechanism by which UBE3A is targeted to the nucleus, we generated mUBE3A-Iso2 and mUBE3A-Iso3 expression vectors, and validated them using HEK293T^{UBE3A-KO} cells (**Figure 2C, Supplementary Figure 2B**). When transfected into primary hippocampal cultures, the long isoform (mUBE3A-Iso2) exhibited a cytosolic localization, while the short isoform (mUBE3A-Iso3) was predominantly localized to the nucleus (**Figure 2D**). Importantly, the same subcellular distribution was observed upon expression of GFP (green fluorescent protein)-tagged or non-tagged constructs, and the localization was similar in *Ube3a* knockout compared to WT neurons. This indicates that the localization is not affected by the tag or by the presence of endogenous UBE3A (**Figure 2D**).

Next, we sought to identify the sequences that are responsible for the nuclear localization of the short UBE3A isoform. The size of mUBE3A-Iso3-GFP (~125 kDa) is close to the passive diffusion limit of the nuclear pore¹⁶; together with our observation that mUBE3A-Iso3-GFP is localized almost exclusively to the nucleus, this strongly suggests that mUBE3A-Iso3 contains sequences for active transport to the nucleus. Moreover, a recent study suggested that UBE3A forms oligomers¹⁷, the size of which would greatly exceed the limit for passive nuclear import. However, none of the available *in silico* algorithms yielded any evidence of a high confidence nuclear localization sequence (NLS) in UBE3A.

Since mUBE3A-Iso2 and mUBE3A-Iso3 differ only in their N-terminal sequences, we searched for the nuclear targeting domain by constructing deletion mutants lacking an increasingly larger portion of the N-terminus of mUBE3A-Iso3 while fully preserving the integrity of the HECT domain. Deletion of amino acids 1-76 encompassing the Zn-finger (AZUL) domain¹⁸ (UBE3A-Iso3- Δ AZUL) resulted in an exclusively cytosolic localization of UBE3A in both primary neurons and HEK293T cells, indicating that the AZUL domain is required for nuclear localization (**Figure 3**). To test whether the AZUL domain of UBE3A acts as a *bona fide* nuclear localization signal, we fused amino acids 1-76 of UBE3A to 6xGFP. The size of the 6xGFP (~162 kDa) is too large to passively diffuse into the nucleus¹⁹, and hence this provides a stringent test of *bona fide* NLS function. Whereas the NLS-6xGFP protein

showed exclusively nuclear labeling, the AZUL-6xGFP construct showed cytosolic labeling. When full-length mUBE3A-Iso3 was fused to 6xGFP, the protein was found in both the cytosol and nucleus (**Figure 3**). Together, these data indicate that the AZUL domain is necessary, but not sufficient to mediate nuclear localization of UBE3A.

Cytosolic localization of mUBE3A-Iso2 is determined by nuclear export

Since the AZUL domain that is required for nuclear localization is present in both mUBE3A-Iso2 and mUBE3A-Iso3, we hypothesized that the N-terminal extension of mUBE3A-Iso2 (which is the only sequence difference between these isoforms; **Figure 1A**), either interferes with nuclear import, or alternatively, mediates export back to the cytoplasm. To distinguish between these possibilities, we used Leptomycin B to inhibit active nuclear export of proteins to the cytoplasm²⁰. To validate Leptomycin B treatment under our experimental conditions, we used a control construct consisting of a fusion between GFP, NLS, and NES. In untreated HEK293T cells the NES-NLS-GFP construct is predominantly cytosolic because of the strong NES, but upon blocking nuclear export with Leptomycin B, NES-NLS-GFP accumulated in the nucleus (**Figure 3C**). Similarly, the cytoplasmic expression of mUBE3A-Iso2-GFP also shifted to a predominantly nuclear localization upon treatment with Leptomycin B (**Figure 3C**). In contrast, Leptomycin B treatment had no discernible influence on the nuclear localization of mUBE3A-Iso3. Therefore, mUBE3A-Iso2 gains entry into the nucleus but exhibits a net cytoplasmic localization because of its subsequently active export out of the nucleus due to the N-terminal extension.

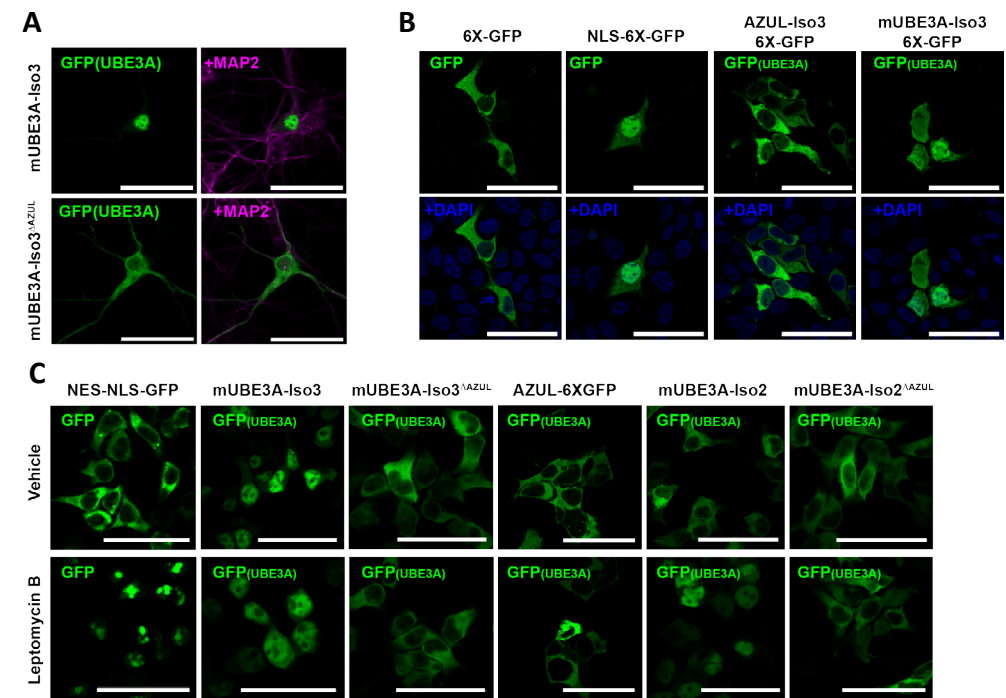


Figure 3. Nuclear localization of UBE3A requires the N-terminal AZUL domain.

A Hippocampal wild-type neurons derived from E16.5 embryos transfected at DIV4 with mUBE3A-Iso3 or mUBE3A-Iso3^{ΔAZUL} C-terminally tagged with GFP, were fixed and stained at DIV8 for MAP2. UBE3A-GFP expression was detected by direct fluorescence. Representative images from a minimum of 3 neuronal cultures derived from an average of 8 embryos with similar results obtained.

B HEK293T cells transfected with 6X-GFP, NLS-6X-GFP, AZUL-6X-GFP or mUBE3A-Iso3-6X-GFP stained with DAPI 30 hours after transfection. GFP-fused constructs were detected by direct fluorescence **C** Leptomycin B treatment (8 hours, 10 ng/ml) results in nuclear localization of mUBE3A-Iso2. HEK293T cells transfected for ~18h with NES-NLS-GFP, mUBE3A-Iso3-GFP, mUBE3A-Iso3^{ΔAZUL}-GFP, AZUL-6xGFP, mUBE3A-Iso2-GFP or mUBE3A-Iso2^{ΔAZUL}-GFP. **B-C** Representative images from 3 independent experiments with similar results obtained. **A-C**, scale bar: 50 μm.

We next reasoned that if the AZUL domain is indeed mediating UBE3A entry into the nucleus, then deletion of the AZUL domain should result in a cytoplasmic localization of UBE3A, even in the presence of Leptomycin B. Indeed, UBE3A-Iso2-ΔAZUL and UBE3A-Iso3-ΔAZUL displayed an exclusively cytosolic localization, even in the presence of Leptomycin B, confirming the

importance of the AZUL domain for nuclear import (**Figure 3C**). Moreover, Leptomycin B treatment did not change the cytosolic localization of AZUL-6xGFP (Figure 3C), consistent with our conclusion that the AZUL domain does not function as a *bona fide* NLS. Collectively, these data indicate that the AZUL domain is required for targeting UBE3A to the nucleus, and that the isoform-specific localization is achieved by the mUBE3A-Iso2-specific N-terminal extension, which promotes nuclear export.

Identification of PSMD4 as an UBE3A-AZUL binding protein

To identify *trans*-acting factors that participate in UBE3A targeting to the nucleus, we carried out an unbiased yeast two-hybrid screen with mUBE3A-Iso3 as bait (for details, see Methods). Screening of 69 million independent mouse adult brain cDNA clones resulted in the identification of four high-confidence interacting proteins, including two proteins previously suggested to interact with UBE3A — Ubch7 (also known as UBE2L3; the cognate E2 of UBE3A²¹) and PSMD4 (also known as RPN10 or S5a, a subunit of the 19S regulatory particle (RP) of the 26S proteasome)²² — and two novel interactors, nuclear NOP2/Sun RNA Methyltransferase Family Member 2 (NSUN2) and presynaptic Rabphilin 3A (**Supplementary Figure 3**). To determine whether these proteins bind to the N-terminus of UBE3A, we carried out yeast two-hybrid interaction assays. Notably, deletion of the AZUL domain selectively abrogated the ability of PSMD4 to bind UBE3A, while the interaction with the other identified proteins remained intact (**Supplementary Figure 3B**). The specific interaction of PSMD4 with the AZUL domain suggests that the PSMD4-UBE3A interaction may be important for the nuclear localization of UBE3A.

The AZUL domain of UBE3A is required to bind the proteasome

To further characterize the interaction between UBE3A and PSMD4, we carried out yeast two-hybrid and GST (Glutathione S-transferase) pull-down assays. We observed that the AZUL domain itself was both required and sufficient to bind PSMD4 in the two-hybrid assay (**Figure 4A**). In addition, GST pull-down experiments with bacterial expressed proteins showed that the interaction between the AZUL domain and PSMD4 is direct and does not require the presence of any other eukaryotic protein (**Figure 4B**; **Supplementary Figure 4**). Notably, mUBE3A-Iso2 bound to PSMD4 with comparable strength as mUBE3A-Iso3 (**Figure 4A**), indicating that the Iso2-

specific N-terminal extension does not interfere with the UBE3A-PSMD4 interaction, consistent with our finding that mUBE3A-Iso2 is imported into the nucleus prior to its targeted export.

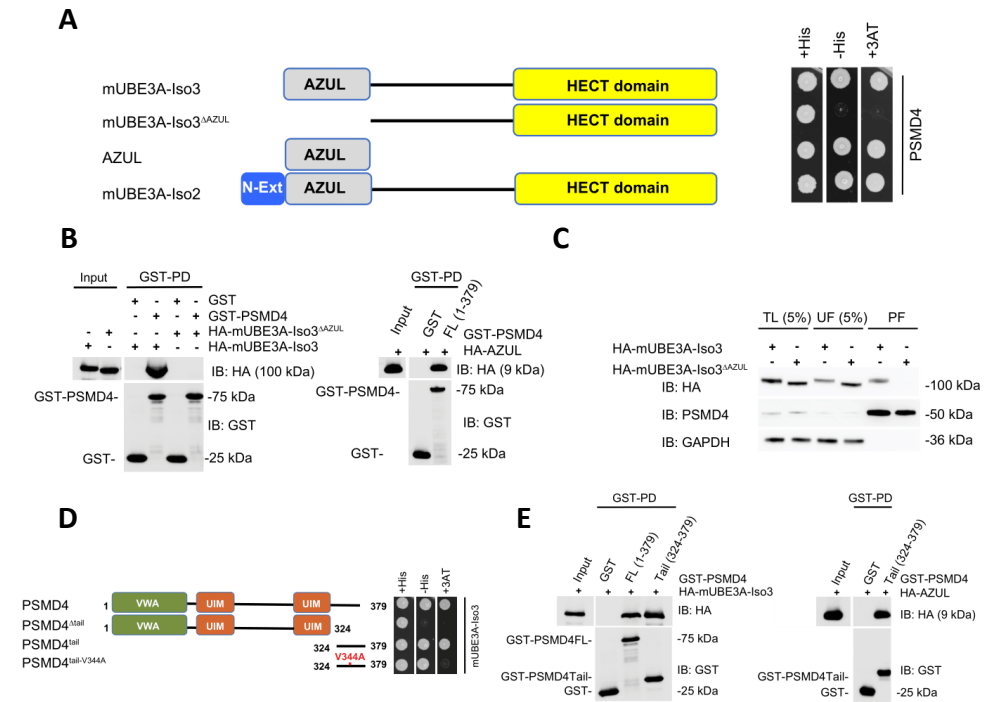


Figure 4. The AZUL domain of UBE3A is required to bind to PSMD4 and the proteasome.

A The interaction of mUBE3A with PSMD4 requires the UBE3A AZUL domain. Yeast two-hybrid interaction assay of the indicated UBE3A deletion constructs with full-length PSMD4 (for details, see legend to Figure S3). Representative data from 3 independent experiments with similar results obtained.

B GST (glutathione S-transferase) pull-down (PD) experiment to verify the interaction of the AZUL domain with PSMD4. Lysates of *E. coli* cells expressing HA-mUBE3A-Iso3, HA-mUBE3A-Iso3^{ΔAZUL} (left panel) or HA-AZUL (from Isoform 3, right panel) were incubated with GST-PSMD4^{FL} (full-length) bound to glutathione beads or GST only (negative control). Eluted proteins were analyzed by Western blot analysis using the indicated antibodies. The image has been cropped from a full Western blot (See Supplemental Figure 4 **A-C**). Representative data from a minimum of 2 independent experiments with similar results obtained.

C The AZUL domain is required to bind to the proteasome. Proteasomes were affinity purified from HEK293T^{ThRpn11-HTBH} cells expressing HA-mUBE3A-Iso3 or HA-mUBE3A-Iso3^{ΔAZUL}. Samples were analyzed by Western blot analysis using the

indicated antibodies. 5% of the total lysates (TL) and unbound fractions (UF) were loaded as compared to the affinity-purified proteasome fraction (PF). The image has been cropped from a full Western blot. (See Supplemental Figure 6 a-c). Representative data from 3 independent experiments with similar results obtained.

D The C-terminal tail of PSMD4 but not the ubiquitin interacting motif (UIM) is required and sufficient to bind mUBE3A. Yeast two-hybrid interaction assay of the indicated PSMD4 constructs with mUBE3A-Iso3. Indicated are the Von Willebrand factor type A (VWA) domain (green), the two UIMs (orange) and the Val344Ala point mutation (red) in the PSMD4 tail (amino acids 324-379). Representative data from 3 independent experiments with similar results obtained.

E Pull-down experiment to verify the interaction of the PSMD4 tail with the AZUL domain. PD of HA-mUBE3A-Iso3 with purified GST-PSMD4^{FL} or purified GST-PSMD4³²⁴⁻³⁷⁹ (left panel). Right panel shows PD of HA-AZUL (of mUBE3A-Iso3) with purified GST-PSMD4³²⁴⁻³⁷⁹. Samples were analyzed as described in the legend to panel **B**. The image has been cropped from a full Western blot. (See Supplemental Figure 6 d-f). Representative data from 2 independent experiments with similar results obtained.

To assess if the AZUL domain of UBE3A is required for proteasome association *in situ*, we affinity-purified proteasomes from HEK293^{RPN11-HTBH} cells, which express biotinylated RPN11, a subunit of the 19S regulatory particle. We found that approximately 5% of total (endogenous) UBE3A protein co-fractionated with affinity-purified proteasomes (**Supplementary Figure 5**). Proteasomes isolated from HEK293^{RPN11-HTBH} cells expressing HA-tagged mUBE3A-Iso3 or mUBE3A-Iso3-ΔAZUL revealed that mUBE3A-Iso3 lacking the AZUL domain does not associate with the proteasome (**Figure 4C; Supplementary Figure 6**). Together, these data show that the AZUL domain of UBE3A directly binds to PSMD4 and strongly suggest that UBE3A association to the proteasome is mediated by the interaction between its AZUL domain and PSMD4.

The C-terminus of PSMD4, but not the Ubiquitin Interacting Motif, is required for UBE3A binding

PSMD4 consists of an N-terminal von Willebrand factor type A (VWA) domain that mediates proteasome association²³, two Ubiquitin Interacting Motifs (UIMs)²⁴ and a C-terminal tail region (**Figure 4D**). The data obtained in the yeast two-hybrid screen suggested that the C-terminal 91 amino acids of PSMD4 (encompassing half of the second UIM and the tail region, amino acids 288-352; **Supplementary Figure 3**) is required for UBE3A interaction. Additional deletion analysis narrowed the critical UBE3A binding sequence down to amino acids 324-352 (**Supplementary Figure 4**). In support of this,

a construct lacking the C-terminal 55 amino acids (PSMD4Δtail; PSMD4 (1-324)) showed no interaction with UBE3A (**Figure 4D**). The importance of the PSMD4 C-terminal tail for UBE3A binding was confirmed by GST pull-down experiments, which showed that the C-terminal 55 amino acids of PSMD4 are necessary and sufficient to bind UBE3A through its AZUL domain (**Figure 4E; Supplementary Figure 6 D-F**).

Sequence alignments of PSMD4 tails from multicellular species showed a high sequence identity in the N-terminal half of the C-terminal tail comprising the UBE3A binding domain and a lower sequence identity in the C-terminal half (**Supplementary Figure 5**). Within the conserved N-terminal subdomain of the PSMD4 tail we identified a Valine residue (V344 in mouse PSMD4), which upon mutation to Alanine strongly reduced UBE3A interaction (**Figure 4D**). Together, these data define the minimal binding domains in PSMD4 and UBE3A required for their interaction.

The UBE3A-PSMD4 interaction is required for proper localization of UBE3A

Given the specific interaction of PSMD4 with the AZUL domain of UBE3A, we next investigated whether PSMD4 is indeed involved in regulating the subcellular localization of UBE3A. Since the localization of neuronal PSMD4 has not yet been reported, we first performed co-localization experiments in developing cortical neurons (**Figure 5A**). Consistent with a previous report¹¹, we observed that in immature neurons (DIV1 and DIV5) UBE3A is found in both the cytosol and the nucleus, whereas in more mature neurons (DIV12) UBE3A has a predominantly nuclear localization. Notably, the subcellular distribution of PSMD4 in the developing neurons is highly similar to that of UBE3A, showing both cytosolic and nuclear staining in DIV1 and DIV5 neurons and a predominantly nuclear staining in DIV12 neurons. This was confirmed by the strong correlation between the observed UBE3A and PSMD4 enrichment in the nucleus during *in vitro* development (Pearson's correlation coefficient $r=0.99$, $p=0.0087$) (**Figure 5B**). These data further establish PSMD4 as a potential candidate protein required for regulating nuclear UBE3A localization.

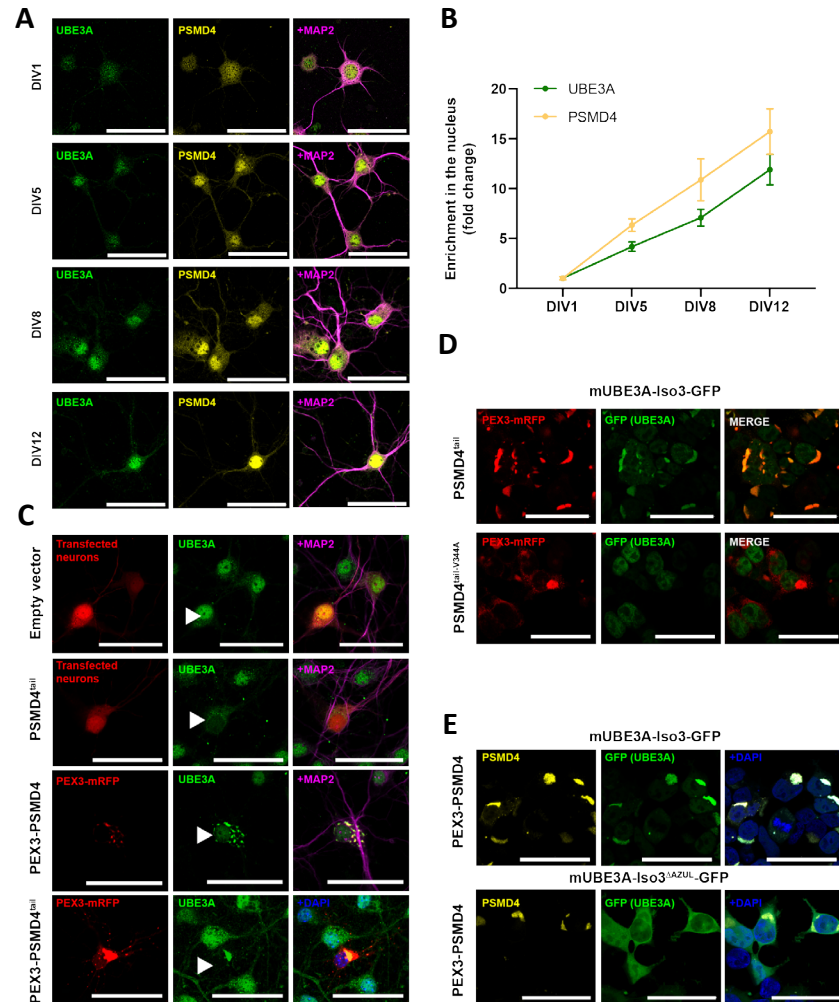


Figure 5. The UBE3A-PSMD4 interaction is required for nuclear localization of UBE3A.

A mUBE3A and PSMD4 show increased nuclear localization during neuronal maturation. P0-derived cortical neurons were cultured, fixed at the indicated DIV and stained for UBE3A, PSMD4 and MAP2. **B** Quantification of the Nuclear/Cytosolic (N/C) ratio of both UBE3A (green) and PSMD4 (yellow) during neuronal maturation. Ratios were normalized against the average N/C ratio for DIV1 in order to quantify the fold enrichment of UBE3A and PSMD4 in the nucleus. Time points represent independent experiments: DIV1 (n=12 cells), DIV5 (n=13), DIV8 (n=16), DIV12 (n=15). Bars shown represent mean \pm SEM. Pearson correlation coefficient ($r=0.99$, $p=0.0087$)

C Overexpression of the PSMD4 C-terminal tail (amino acids 324-379; PSMD4^{tail}) or the PSMD4 C-terminal tail fused to the peroxisomal membrane protein PEX3,

causes mislocalization of UBE3A. E16.5 derived hippocampal neurons were transfected at DIV7 with empty vector expressing td-TOMATO (upper panel), or with PSMD4 C-terminal tail (PSMD4^{tail}) and td-TOMATO under separate promoters (second panel), or with PEX3-mRFP-fused to PSMD4 (third panel), or with PEX3-mRFP fused to the PSMD4 C-terminal tail (bottom panel). Neurons were stained at DIV12 using UBE3A (green) and MAP2 (pink) antibodies or DAPI (blue). Transfected cells identified by td-TOMATO or mRFP expression are indicated by a white arrow.

D Localization of mUBE3A-Iso3 to PEX3-PSMD4^{tail} containing membrane structures is abrogated by the V344A mutation in the PSMD4 tail. HEK293T cells co-transfected with mUBE3A-Iso3-GFP, and PEX3-mRFP-PSMD4^{tail} or PEX3-mRFP-PSMD4^{tail-V344A} were fixed 20 hours after transfection and investigated for mRFP (red) and GFP (green) co-localization.

E Localization of mUBE3A-Iso3 to PEX3-PSMD4 containing membrane structures requires the AZUL domain of mUBE3A-Iso3. HEK293T cells co-transfected with PEX3-PSMD4 and mUBE3A-Iso3-GFP or mUBE3A-Iso3^{ΔAZUL}-GFP were fixed 20 hours after transfection and investigated for PSMD4 (yellow) and GFP (green) co-localization. Nuclei were stained with DAPI. **A, C-E** scale bar: 50 μ m. **C-E**. Representative images from 3 experiments with similar results obtained.

To obtain further evidence that PSMD4 mediates UBE3A nuclear targeting, we performed a competition experiment with the C-terminal tail of PSMD4 (amino acids 324-379). This protein fragment binds UBE3A, but lacks the VWA domain that is required for its association with the proteasome²³. Hence, overexpression of this peptide would presumably compete with endogenous PSMD4 for UBE3A binding and affect UBE3A localization. Indeed, overexpression of the PSMD4 C-terminal tail strongly shifted UBE3A towards a cytoplasmic localization (**Figure 5C**), strengthening the evidence that PSMD4 binding is necessary for UBE3A nuclear localization.

We next investigated if the interaction with PSMD4 is sufficient for dictating the subcellular localization of UBE3A. The N-terminal domain of the peroxisomal membrane protein PEX3 is sufficient to target proteins to peroxisomes²⁵. Therefore, we fused PSMD4 to the N-terminal amino acids 1-42 of PEX3 and included monomeric RFP as a fluorescent reporter (PEX3-mRFP-PSMD4). Neurons overexpressing PEX3-mRFP-PSMD4 showed, in addition to a weak nuclear UBE3A staining, a punctate fluorescence pattern of UBE3A, reminiscent of peroxisomal localization. In addition, UBE3A strongly co-localized with PEX3-mRFP-PSMD4, confirming that the PSMD4-UBE3A interaction is sufficient to re-direct UBE3A to the peroxisomal compartment (**Figure 5C**).

To determine if the minimal PSMD4-C-terminal tail region is sufficient to re-

direct the subcellular localization of UBE3A, neurons were transfected with a fusion protein in which the C-terminal tail of PSMD4 was fused to PEX3-mRFP (PEX3-mRFP-PSMD4-C). In neurons expressing this construct, mUBE3A-Iso3 was re-directed to structures also containing PEX3-mRFP-PSMD4-C terminal tail, and was virtually absent from the nucleus (**Figure 5C**). Co-localization of UBE3A and PEX3-mRFP was also observed in HEK293T cells in which we co-expressed GFP-tagged mUBE3A-Iso3 with PEX3-mRFP-PSMD4-C. In contrast, in cells expressing PEX3 fused to the PSMD4-C-tail^{V344A} mutant, UBE3A showed little co-localization with PEX3-mRFP-PSMD4-C-tail^{V344A}, and remained nuclear (**Figure 5D**). To test the requirement of the UBE3A-AZUL domain for the PEX3-PSMD4 interaction, HEK293T cells were co-transfected with PEX3-PSMD4 and UBE3A^{mIso3}-GFP with or without the AZUL domain. As expected, deletion of the AZUL domain strongly reduced co-localization with PEX3-PSMD4 (**Figure 5E**). These data collectively show that the PSMD4-UBE3A interaction (and more specifically, the PSMD4-C-tail with the UBE3A-AZUL domain) governs the nuclear localization of UBE3A.

An AS-associated missense mutation in the HECT domain causes mislocalization of UBE3A

Given that UBE3A is predominantly nuclear, we hypothesized that mislocalization of UBE3A might be an important pathophysiological mechanism in AS. If this hypothesis is correct, *UBE3A* mutations that affect PSMD4 binding should result in AS. Therefore, we used the two-hybrid system to screen for human AS-associated missense mutations that might affect the interaction with PSMD4. We included the two known AS mutations within the AZUL domain, as well as 10 additional missense mutations distributed broadly throughout *UBE3A* and covering the mutational hotspots that were recently identified²⁶ (**Figure 6A**). Only one missense mutation located in the HECT domain (p.Gly593Arg) showed a severely reduced interaction with PSMD4 in yeast two-hybrid (**Figure 6B; Supplementary Figure 7A**), although its *in vitro* interaction with PSMD4 appeared largely unaffected (**Supplementary Figure 7B-D**). This hitherto unreported mutation was identified as a *de novo* mutation in a carrier who shows the clinical features of AS, including developmental delay, microcephaly, wide-based gait, strabismus and gastrointestinal issues. In order to investigate the impact of the p.Gly593Arg mutation on UBE3A subcellular localization, we transfected HEK293T cells and hippocampal neurons with the homologous mouse variant mUBE3A-Iso3^{G590R} fused to GFP.

The G590R mutation exhibited UBE3A mislocalization to the cytosol, thereby emphasizing the importance of regions outside the AZUL domain for proper nuclear targeting and indicating the potential clinical significance of nuclear UBE3A for AS (**Figure 6C; Supplementary Figure 8A**).

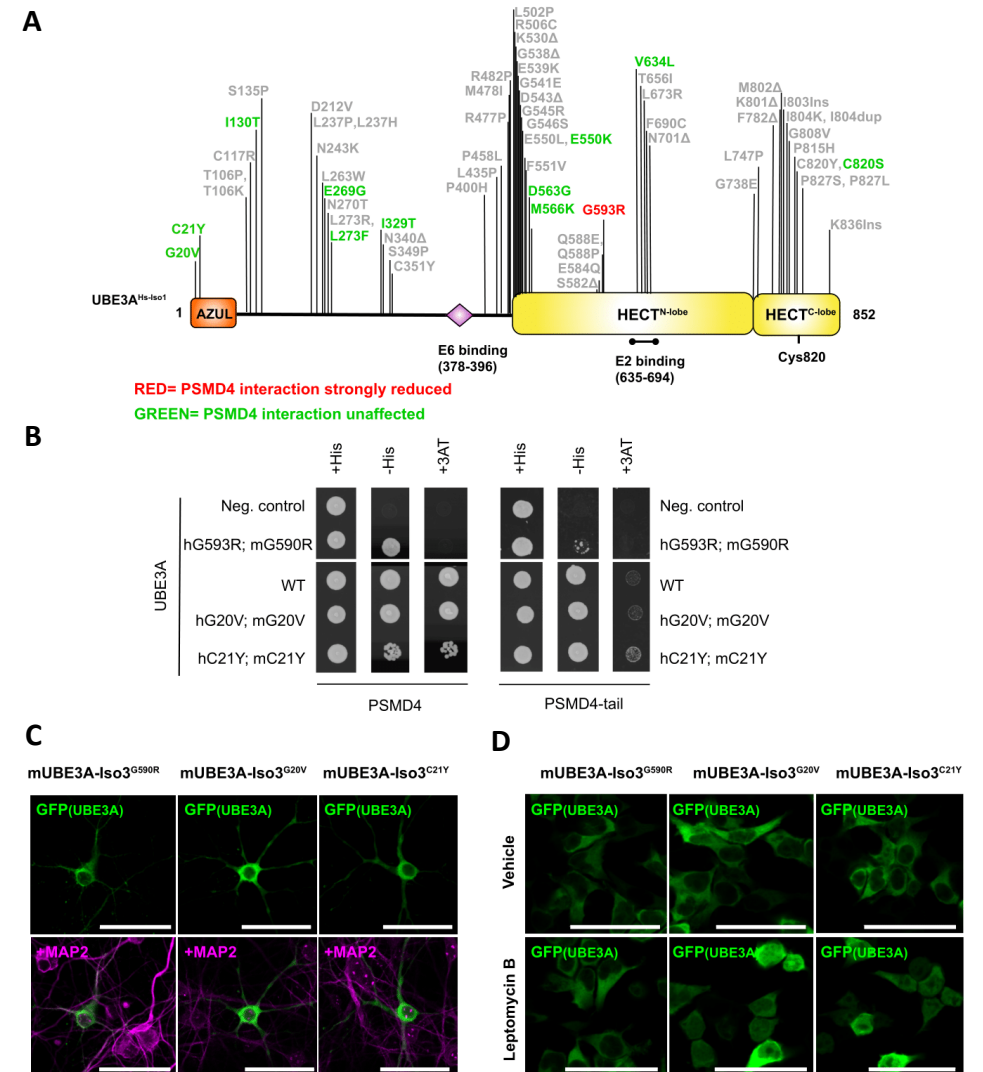


Figure 6. AS-associated missense mutations in the Zn-finger of the AZUL domain or the HECT domain disturb nuclear localization of UBE3A via distinct mechanisms.

A Schematic representation showing the location of patient-linked missense mutations in human UBE3A isoform 1 (accession: NP_570853.1). Mutations

tested in our study (colored) are distributed broadly throughout *UBE3A* and covering all mutational hotspots. The tested *UBE3A* mutations that did not affect interaction with PSMD4 are indicated in green, whereas the (only) mutation that abrogated the interaction is indicated in red. **B** The human p.G593R (mUBE3A-Iso3^{G590R}) mutation strongly reduces the interaction with PSMD4. The indicated patient-linked missense mutations were introduced at the analogous position in mUBE3A-Iso3. Mutations (indicated in the human (h) *UBE3A*-Iso1 and mouse (m) *UBE3A*-Iso3 numbering), were tested for strength of interaction with full-length PSMD4 or PSMD4 tail (amino acids 324-379) in a yeast two-hybrid spot assay. (Described in the legend of Supplemental Figure 3B; see also Supplemental Figure 5B). Data are representative of 3 independent experiments with similar results obtained.

C The AS-associated p.G20V, p.C21Y and p.G593R mutations (human *UBE3A* isoform 1 numbering) cause mislocalization of *UBE3A*. E16.5 derived hippocampal neurons transfected at DIV7 with mUBE3A-Iso3^{G20V}-GFP, mUBE3A-Iso3^{C21Y}-GFP or mUBE3A-Iso3^{G590R}-GFP (G593R in human *UBE3A*-Iso1), were fixed at DIV12 and stained with MAP2 antibody. *UBE3A* localization was assessed by direct GFP fluorescence. **D** The AS-associated p.G20V and p.C21Y affect nuclear retention. HEK293T cells transfected for ~18h with mUBE3A-Iso3^{G20V}-GFP, mUBE3A-Iso3^{C21Y}-GFP or mUBE3A-Iso3^{G590R}-GFP (G593R in human *UBE3A*-Iso1), were treated for 8 hours with 10 ng/ml of Leptomycin B or vehicle. Note that increased nuclear staining is observed in Leptomycin B treated cells expressing mUBE3A-Iso3^{G20V}-GFP and mUBE3A-Iso3^{C21Y}-GFP but not in treated cells expressing mUBE3A-Iso3^{G590R}-GFP. See also Supplemental Figure 5. **C-D**, scale bar: 50 μm; data are representative of a minimum of n=3 independent experiments with similar results obtained.

AS-associated missense mutations indicate that the Zn-finger function is essential for nuclear retention of *UBE3A*

We were surprised to find that the two missense mutations in the AZUL domain did not significantly affect PSMD4 binding either in yeast two-hybrid or the *in vitro* binding assay (**Figure 6B**; **Supplementary Figure 7**). One mutation (p.Cys21Tyr) eliminates Zn-binding by removing one of the obligate Zinc-coordinating cysteine residues¹⁸, whereas the other substitution (p.Gly20Val) affects a strictly conserved glycine residue (Gly20) preceding the Cys21^{27,28}. To determine whether these AS-associated missense mutations in the AZUL domain affect *UBE3A* localization, we introduced the analogous mutations separately in mouse mUBE3A-Iso3 fused to GFP (*UBE3A*-Iso3-GFP) and studied the subcellular distribution of these proteins (**Figure 6C**; **Supplementary Figure 8A**). Despite the ability of both mutants to bind to PSMD4, the p.Cys21Tyr and p.Gly20Val mutants both showed an exclusively cytosolic localization in hippocampal neurons and in HEK293T cells. A similar cytosolic distribution was found for the p.Cys21Tyr and p.Gly20Val *UBE3A*

mutants expressed in AS-derived mouse primary hippocampal neurons (**Supplementary Figure 8B**).

The ectopic cytoplasmic localization of p.Cys21Tyr and p.Gly20Val *UBE3A* mutants, despite their preserved binding to PSMD4, could suggest that *UBE3A* nuclear import is determined by its interaction with PSMD4, while nuclear retention is a PSMD4-independent mechanism that relies on the integrity of Zn-finger within the AZUL domain. To test this, we utilized Leptomycin B to block nuclear export. If the p.Cys21Tyr and p.Gly20Val *UBE3A* mutations impair nuclear import, treatment with Leptomycin B should not rescue the cytoplasmic mislocalization. In contrast, if the p.Cys21Tyr and p.Gly20Val *UBE3A* mutations impair nuclear retention, treatment with Leptomycin B should restore the nuclear localization. Indeed, consistent with a model whereby the integrity of the Zn-finger is necessary for maintaining nuclear retention, Leptomycin B treatment resulted in a partial shift of both mutant proteins from the cytosol to the nucleus (**Figure 6D**). In contrast, no effect of Leptomycin B treatment was observed on the cytosolic localization of the mUBE3A-Iso3^{G590R} mutant (homologous to the human p.Gly593Arg mutation), indicating that this mutant protein doesn't enter the nucleus. These findings indicate that nuclear localization of *UBE3A* is dependent on the two sequential steps of nuclear import and nuclear retention. This latter step requires the integrity of the Zn-finger of the AZUL domain. AS-associated mutations that affect either one of these steps result in the mislocalization of *UBE3A* to the cytosol.

UBE3A isoform-specific mice reveal the essential role of the nuclear *UBE3A* isoform

The mislocalization of *UBE3A* in specific AS patients suggests that mislocalization might be an important pathophysiological mechanism to cause AS. To examine the extent to which the nuclear versus cytosolic isoforms of *UBE3A* contribute to AS phenotypes, we generated two novel *Ube3a* mouse models. In one line, we mutated the first ATG (p.Met1X), which is the translational start site of *mUbe3a-Iso2*, resulting in a mouse that expresses only the short, nuclear-localized *UBE3A* isoform 3 (*Ube3a*^{mIso2/p+}, referred to as *Ube3a-iso2*^{KO}). In the second mouse line, we mutated the second ATG (p.Met22Ala), which is the start site of *mUbe3a-Iso3*, resulting in a mouse that expresses only the long, cytosolic *UBE3A* isoform 2 (*Ube3a*^{mIso3/p+}, referred to as *Ube3a-iso3*^{KO}) (**Figure 7A**).

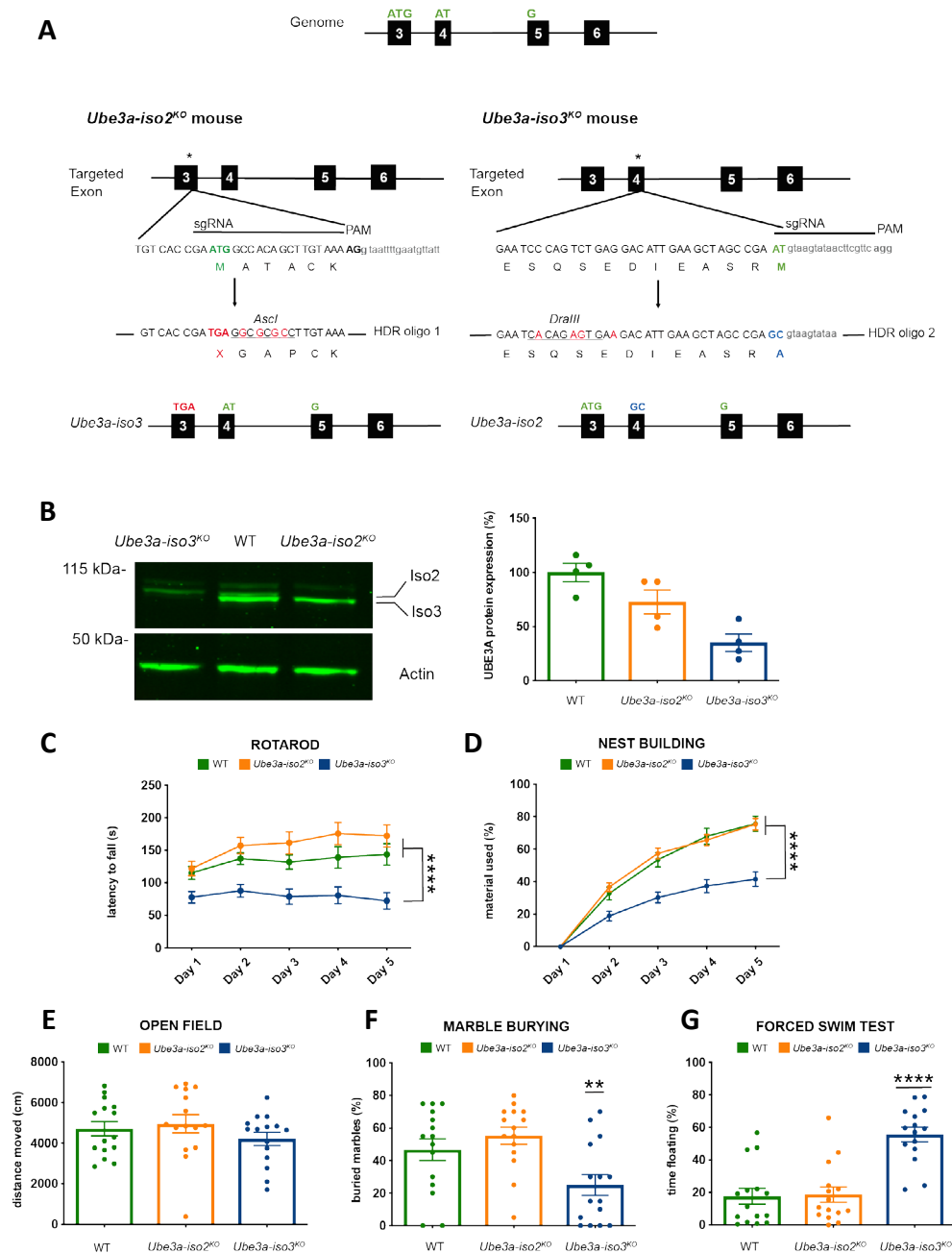


Figure 7. UBE3A isoform-specific mice reveal the essential role of the nuclear UBE3A isoform.

A Schematics depicting the generation of the *Ube3a-iso2^{KO}* mouse model (left)

where the first p.Met1 (ATG) in *Ube3a* exon 3 was replaced by a stop codon (TGA) resulting in the exclusive expression of mUBE3A-Iso3, and the generation of the *Ube3a-iso3^{KO}* mouse model (right) where the second p.Met22 (ATG) in *Ube3a* exon 4 was replaced by Ala (GCG) resulting in the exclusive expression of mUBE3A-Iso2. **B** Selective expression of mUBE3A isoforms in targeted mutants. Immunoblot analysis (left) and quantification (right) of the amount of mUBE3A present in lysates of cortex from *Ube3a-iso2^{KO}* and *Ube3a-iso3^{KO}* mice compared to WT mice ($n=4, 4, 4$ mice). Note that the amount of mUBE3A isoform expressed in the targeted mutants reflects the expression of endogenous isoform expression (see also Figure 2A; Supplemental Figure 2A). All data represent mean \pm SEM and are normalized against Actin. The image has been cropped from a full Western blot (See Supplemental Figure 9). **C-G** Behavioral characterization of wild-type (WT), *Ube3a-iso2^{KO}* and *Ube3a-iso3^{KO}* mice ($n=15, 15, 15$) in the 129S2B6/F1 background. **C** Accelerating rotarod. ($p=0.000048$) **D** Nest building. ($p=0.000006$) **E** Open field test. ($p=0.378$) **F** Marble burying test. ($p=0.003$) **G** Forced swim test. ($p=3.67E-07$) All data represent mean \pm SEM. Significant effects of genotype are indicated as ** $p<0.01$, **** $p<0.0001$. **C-D**, Two-way repeated-measures ANOVA (two-sided) with Bonferroni post hoc test. **E-G**, One-way ANOVA (two-sided) with Bonferroni post hoc test.

Western blot analysis of these UBE3A isoform specific lines confirmed that each line expresses only a single isoform, at levels comparable to the expression of mUBE3A-Iso2 and mUBE3A-Iso3 in wild-type mice (**Figure 7B; Supplementary Figure 9**). Moreover, levels of the non-coding *mUbe3a-Iso1* transcript¹⁵ were comparable to wild-type mice, although it should be noted that *mUbe3a-Iso1* transcript levels were barely detectable above background (**Supplementary Figure 1C**) and that this transcript has recently been retracted from the NCBI database because of insufficient evidence. We subjected the isoform-specific mice to a well-validated behavioral testing battery, for which we have recently shown robust phenotypes in AS model mice^{29,30}, including measures of locomotion, anxiety and repetitive/restrictive behavior. Importantly, *Ube3a-iso2^{KO}* and *Ube3a-iso3^{KO}* mutants, as well as littermate controls, were run as one single cohort in these tests, which allows for a better comparison between lines. We observed no phenotype of *Ube3a-iso2^{KO}* and *Ube3a-iso3^{KO}* mutants in the open field test (**Figure 7E; Supplementary Table 1**, for which we have previously shown that this is the weakest *Ube3a* phenotype³⁰). For all other behavioral tests examined, *Ube3a-iso3^{KO}* mutants were significantly different from both wild-type and *Ube3a-iso2^{KO}* mice (**Figure 7C-G; Supplementary Table 1**), and strongly resembled *Ube3a* knock-out mice^{29,30}. Taken together, these results suggest that UBE3A has a critical role in the nucleus, and the contribution of cytosolic UBE3A is

rather limited with respect to the mouse behavioral phenotypes.

Loss of nuclear UBE3A isoform results in synaptic changes that affect the excitation to inhibition balance

Given that *Ube3a-iso3^{KO}* mutants showed the behavioral phenotypes of AS model mice, we asked whether the loss of the nuclear UBE3A isoform leads to the same synaptic changes as those observed in AS model mice. We previously showed that loss of UBE3A results in marked changes of both inhibitory and excitatory inputs onto prefrontal cortex (PFC) layer 5 pyramidal neurons³¹. To assess if this is also the case in *Ube3a-iso3^{KO}* mutants, we recorded spontaneous excitatory postsynaptic currents (sEPSCs) and spontaneous inhibitory postsynaptic currents (sIPSCs) in PFC layer 5 pyramidal neurons. Replicating previous observations in AS model mice³¹, *Ube3a-iso3^{KO}* mutants exhibited a significantly higher sEPSC frequency and amplitude, as well as reduced sIPSC frequency and amplitude (Figure 8A-F). Hence, the ratios of sEPSC to sIPSC frequency and amplitude were strongly increased by the loss of the nuclear UBE3A isoform (Figure 8G-J), consistent with a marked shift in the synaptic excitation/inhibition balance. Taken together, these results indicate that loss of nuclear UBE3A affects synaptic function in a similar way as observed in AS model mice, which emphasizes the critical role of nuclear UBE3A in AS pathophysiology.

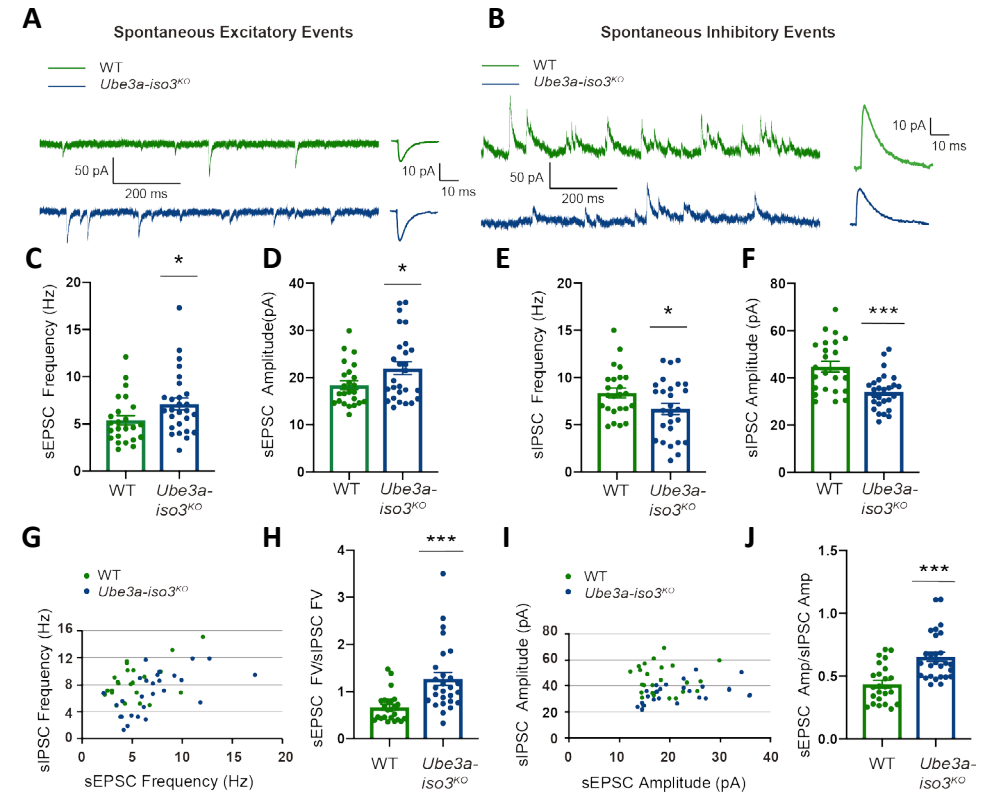


Figure 8. Loss of nuclear UBE3A isoform results in synaptic changes that affect the excitation to inhibition balance.

A Representative voltage clamp recordings of sEPSCs (left) and averages (right) from layer 5 pyramidal neurons, obtained by clamping the neuron at the reversal potential for synaptic inhibition (-70 mV) in wild-type (WT) (top) and *Ube3a-iso3^{KO}* mice (bottom). **B** Representative voltage clamp recordings of sIPSCs (left) and averages (right) of the same neuron from **A**, obtained by clamping the neuron at the reversal potential for synaptic excitation (0 mV) in WT (top) and *Ube3a-iso3^{KO}* mice (bottom). **C-F, H, J** Average data of electrophysiological analysis of WT and *Ube3a-iso3^{KO}* mice (n=24 cells, 27 cells, from 3 mice per genotype). **C** sEPSC Frequency (p=0.038). **D** sEPSC Amplitude (p=0.034). **E** sIPSC Frequency (p=0.039). **F** sIPSC Amplitude (p=0.00032). **G, I** Raster plot of all the cells included in the analysis. Each dot represents one cell, showing the frequency (**G**) and amplitude (**I**) of sEPSCs and sIPSCs. **H** Ratios of sEPSC to sIPSC frequency (p=0.00045). **J** Ratios of sEPSC to sIPSC amplitude (p=0.00033). All data represent mean \pm SEM. Student's t-test (two-sided). Significant effects are indicated as *p<0.05, ***p<0.001.

Discussion

PSMD4-mediated targeting of UBE3A to the nucleus

Consistent with previous publications⁹⁻¹³, we showed that UBE3A is highly enriched in the nucleus of mouse and human neurons. We further showed that the cytosolic/nuclear localization is dictated by the differential expression levels of the two UBE3A isoforms and we have identified the cis-acting elements and a trans-acting factor that regulates the nuclear targeting of UBE3A. Finally, we have demonstrated the importance of proper nuclear targeting of UBE3A for AS-related pathophysiology. Below we describe a detailed model for UBE3A localization and highlight the supporting evidence for key targeting steps (**Supplemental Figure 10**).

Distinct UBE3A domains are required for nuclear targeting

We found that both the long (Isoform 2) and short (Isoform 3) mouse UBE3A isoforms require their (N-terminal) AZUL domain for import into the nucleus. Deletion of the AZUL domain in both isoforms results in the cytosolic accumulation of UBE3A. Notably, in contrast to full-length mUBE3A-Iso3 fused to 6xGFP, the AZUL domain by itself was not sufficient to target 6xGFP to the nucleus, implying that other regions in UBE3A facilitate nuclear targeting. Indeed, we identified a region in the C-terminal HECT domain that may be an important determinant for UBE3A nuclear localization, since we found that the novel AS-associated p.G593R mutation abrogates nuclear entry of the protein. The exact mechanism by which this mutation prevents nuclear entry remains to be established, since this mutation interferes with PSMD4 binding *in vivo* (using the yeast two-hybrid assay) but shows normal binding to PSMD4 using *in vitro* binding assays. Notably, recent work on the folding of UBE3A revealed intra-molecular contacts between the N-terminus and the HECT domain of UBE3A³². Thus, we hypothesize that the intramolecular folding of UBE3A is required for nuclear targeting and that the p.G593R mutation disrupts proper folding of UBE3A, thereby preventing its import.

PSMD4 mediates the nuclear import of UBE3A

We found that the UBE3A AZUL domain binds PSMD4, a subunit of the RP of the proteasome that functions as the receptor for ubiquitinated proteins via its C-terminal UIMs²⁴. Although UBE3A is ubiquitinated itself, we showed that the interaction with PSMD4 does not require the UIMs but solely depends

on the C-terminal tail of PSMD4. Two independent experiments strongly support the notion that UBE3A binding to the C-terminal tail of PSMD4 is indispensable for UBE3A targeting to the nucleus: (1) Overexpression of the C-terminal tail of PSMD4 in neurons resulted in cytosolic accumulation of UBE3A, and (2) fusion of the C-terminal tail of PSMD4 to the peroxisomal membrane protein PEX3 redirected UBE3A to peroxisomes.

Interestingly, a previous study in *Drosophila* demonstrated a genetic interaction between PSMD4 and dUBE3A³³. Specifically, overexpression of dUBE3A led to an eye-degeneration phenotype, which was rescued by expression of a mutant form of PSMD4 that lacked the ability to bind to the proteasome. Although the precise mechanism of the rescue remains unknown, our data predict that the expression of the mutant PSMD4 might have mitigated the deleterious effects of dUBE3A overexpression by keeping it out of the nucleus.

Given that PSMD4 also lacks a typical nuclear localization signal (cNLS mapper³⁴) and is bound to the 19S RP of the 26S proteasome³⁵, it is likely that UBE3A associates via PSMD4 with the 19S RP or the 26S holoenzyme before import into the nucleus takes place. Consistent with this, we and others³⁶⁻⁴⁰ have found that a small fraction of endogenous UBE3A is associated with (affinity-purified) proteasomes and it has recently been shown that a preassembled RP and holoenzyme enter the nucleus⁴¹, suggesting that UBE3A uses a piggy-back type of mechanism to enter the nucleus.

The N-terminus of mUBE3A-Isoform 2 interferes with nuclear retention

We found that the differential localization of the long (Isoform 2) and short (Isoform 3) mouse UBE3A isoforms is determined by the 21 amino acid N-terminal extension specific to mUBE3A-Iso2. Notably, we found that this extension does not interfere with the binding of UBE3A to the C-terminus of PSMD4. Instead, we found that the N-terminal extension of mUBE3A-Iso2 interferes with nuclear retention of UBE3A.

A functional Zn-finger is required to retain mUBE3A-Isoform 3 in the nucleus

How is mUBE3A-Iso3 retained in the nucleus? One possibility is that mUBE3A-Iso3 selectively maintains its association with the proteasome within the nucleus. However, we think that this possibility is unlikely, since only a small fraction (5-10%) of UBE3A is associated with the proteasome in a biochemical fractionation, whereas 75-80% of UBE3A is located in the nucleus. Moreover,

we found that the two known human AS-associated Zn-finger mutations, one in the Zn-coordinating Cys residues (p.Cys21Tyr) and one in a preceding conserved glycine (p.Gly20Val), affect nuclear localization. Although *in vitro* binding assays did indicate a reduced interaction with PSMD4 as recently reported⁴², these mutations did not abrogate PSMD4 binding in the 2-hybrid assay. Leptomycin B experiments confirmed that these mutant proteins can be imported into the nucleus, implying that these mutations perturb nuclear retention instead of nuclear targeting. Thus, nuclear retention can be functionally separated from binding to PSMD4 (and hence the proteasome), and requires a functional Zn-finger. Taken together, this indicates that the AZUL domain has two dissociable functions: (1) nuclear import via a UBE3A Zn-finger-independent interaction with the proteasomal protein PSMD4, and (2) Zn-finger-dependent nuclear retention.

Given that DNA/RNA binding proteins often contain Zn-binding domains (called Zn-fingers)⁴³ it is tempting to speculate that nuclear retention of UBE3A is mediated by direct binding to DNA, but we can also not rule out that this domain is used to interact with other nuclear proteins. UBE3A has been shown to interact with a variety of nuclear proteins, including steroid hormone receptors and other co-regulators^{44,45}, and is recruited to the promoter region of the AR-responsive gene (PSA)⁴⁶.

The contribution of cytosolic and nuclear UBE3A to AS pathophysiology

A fundamental question is whether AS-associated pathophysiology is related to the function of UBE3A in the nucleus, cytosol, or both. We found that mice lacking the nuclear mUBE3A-Iso3 isoform showed all major behavioral phenotypes of AS model mice carrying a complete maternal deletion of UBE3A, while mice lacking the cytoplasmic mUBE3A-Iso2 isoform showed no discernible abnormalities. Moreover, our electrophysiological studies further indicated that loss of nuclear UBE3A cause the same synaptic deficits as we previously observed in AS model mice³¹, implying that the nuclear isoform is the most critical for AS-related pathophysiology. The recent report of three children with AS carrying a nearly identical missense mutation disrupting the translational start site of human UBE3A isoform 1 (homologue of mouse isoform 3) further strengthens the evidence that the nuclear isoform is particularly critical for the pathophysiology of AS⁴⁷. However, it is notable that the neurodevelopmental phenotype of these three individuals are milder than typical AS patients, suggesting that the contribution of cytosolic

UBE3A to AS pathophysiology is not entirely negligible.

There is a large body of literature that supports a role for UBE3A in transcriptional regulation, both in an ubiquitin ligase-dependent fashion as well as ligase-independent fashion. First, detailed immunohistochemical analysis of UBE3A subcellular localization in mouse neurons has revealed that nuclear UBE3A is associated with euchromatin-rich domains¹², which are generally considered to be transcriptionally-active regions. Second, it has been shown that UBE3A has a ubiquitin ligase-independent nuclear function⁴⁸. Moreover, overexpression of ligase-dead UBE3A fused to a NLS was shown to affect both social behavior as well as gene expression⁴⁹. Multiple studies have now shown that UBE3A also has a ligase-dependent role in transcription, by regulating the degradation of transcription complexes (extensively reviewed by⁵⁰). Hence, these findings support our notion that there may be an important AS-linked role of nuclear UBE3A in transcription regulation. In line with this, recent evidence suggests that Arc protein levels are regulated by UBE3A at the transcriptional level⁷. Future studies should therefore focus on the role of UBE3A in the nucleus, and how this relates to the pathophysiology of AS.

References

1. LaSalle, J. M., Reiter, L. T. & Chamberlain, S. J. Epigenetic regulation of UBE3A and roles in human neurodevelopmental disorders. *Epigenomics* **7**, 1213–1228 (2015).
2. Sell, G. L. & Margolis, S. S. From UBE3A to Angelman syndrome: a substrate perspective. *Front. Neurosci.* **9**, 322 (2015).
3. Scheffner, M. & Kumar, S. Mammalian HECT ubiquitin-protein ligases: biological and pathophysiological aspects. *Biochim. Biophys. Acta* **1843**, 61–74 (2014).
4. Judson, M. C. *et al.* GABAergic neuron-specific loss of Ube3a causes Angelman syndrome-like EEG abnormalities and enhances seizure susceptibility. *Neuron* **90**, 56–69 (2016).
5. Li, W. *et al.* Angelman syndrome protein Ube3a regulates synaptic growth and endocytosis by inhibiting BMP signaling in *Drosophila*. *PLoS Genet.* **12**, e1006062 (2016).
6. Greer, P. L. *et al.* The Angelman syndrome protein Ube3A regulates synapse development by ubiquitinating Arc. *Cell* **140**, 704–716 (2010).
7. Kuhnle, S., Mothes, B., Matentzoglou, K. & Scheffner, M. Role of the ubiquitin ligase E6AP/UBE3A in controlling levels of the synaptic protein Arc. *Proc. Natl. Acad. Sci. USA* **110**, 8888–8893 (2013).
8. Pignatelli, M. *et al.* Changes in mGlu5 receptor-dependent synaptic plasticity and coupling to homer proteins in the hippocampus of Ube3A hemizygous mice modeling Angelman syndrome. *J. Neurosci.* **34**, 4558–4566 (2014).
9. Dindot, S. V., Antalffy, B. A., Bhattacharjee, M. B. & Beaudet, A. L. The Angelman syndrome ubiquitin ligase localizes to the synapse and nucleus, and maternal deficiency results in abnormal dendritic spine morphology. *Hum. Mol. Genet.* **17**, 111–118 (2008).
10. Gustin, R. M. *et al.* Tissue-specific variation of Ube3a protein expression in rodents and in a mouse model of Angelman syndrome. *Neurobiol. Dis.* **39**, 283–291 (2010).
11. Miao, S. *et al.* The Angelman syndrome protein Ube3a is required for polarized dendrite morphogenesis in pyramidal neurons. *J. Neurosci.* **33**, 327–333 (2013).
12. Burette, A. C. *et al.* Subcellular organization of UBE3A in neurons. *J. Comp. Neurol.* **525**, 233–251 (2017).
13. Burette, A. C. *et al.* Subcellular organization of UBE3A in human cerebral cortex. *Mol. Autism* **9**, 54 (2018).
14. Yamamoto, Y., Huibregtse, J. M. & Howley, P. M. The human E6-AP gene (UBE3A) encodes three potential protein isoforms generated by differential splicing. *Genomics* **41**, 263–266 (1997).
15. Valluy, J. *et al.* A coding-independent function of an alternative Ube3a transcript during neuronal development. *Nat. Neurosci.* **18**, 666–673 (2015).
16. Wang, R. & Brattain, M. G. The maximal size of protein to diffuse through the nuclear pore is larger than 60kDa. *FEBS Letters* **581**, 3164–3170 (2007).
17. Ronchi, V. P., Klein, J. M., Edwards, D. J. & Haas, A. L. The active form of E6-associated protein (E6AP)/UBE3A ubiquitin ligase is an oligomer. *J. Biol. Chem.* **289**, 1033–1048 (2014).
18. Lemak, A., Yee, A., Bezsonova, I., Dhe-Paganon, S. & Arrowsmith, C. H. Zn-binding AZUL domain of human ubiquitin protein ligase Ube3A. *J. Biomol. NMR* **51**, 185–190 (2011).
19. Seibel, N. M., Eljouni, J., Nalaskowski, M. M. & Hampe, W. Nuclear localization of enhanced green fluorescent protein homomultimers. *Anal. Biochem.* **368**, 95–99 (2007).
20. Kudo, N. *et al.* Leptomycin B inactivates CRM1/exportin 1 by covalent modification at a cysteine residue in the central conserved region. *Proc. Natl. Acad. Sci. U.S.A.* **96**, 9112–9117 (1999).
21. Ronchi, V. P., Klein, J. M. & Haas, A. L. E6AP/UBE3A ubiquitin ligase harbors two E2~ubiquitin binding sites. *J. Biol. Chem.* **288**, 10349–10360 (2013).
22. Verma, R., Oania, R., Graumann, J. & Deshaies, R. J. Multiubiquitin chain receptors define a layer of substrate selectivity in the ubiquitin-proteasome system. *Cell* **118**, 99–110 (2004).
23. Sakata, E. *et al.* Localization of the proteasomal ubiquitin receptors Rpn10 and Rpn13 by electron cryomicroscopy. *Proc. Natl. Acad. Sci. USA* **109**, 1479–1484 (2012).
24. Young, P., Deveraux, Q., Beal, R. E., Pickart, C. M. & Rechsteiner, M. Characterization of two polyubiquitin binding sites in the 26 S protease subunit 5a. *J. Biol. Chem.* **273**, 5461–5467 (1998).
25. Soukupova, M., Sprenger, C., Gorgas, K., Kunau, W. H. & Dodt, G. Identification and characterization of the human peroxin PEX3. *Eur. J. Cell Biol.* **78**, 357–374 (1999).
26. Yi, J. J. *et al.* An Autism-linked mutation disables phosphorylation control of UBE3A. *Cell* **162**, 795–807 (2015).
27. Mueller, O. T. & Coovadia, A. Gene symbol: UBE3A. Disease: Angelman

- syndrome. *Hum. Genet.* **123**, 538 (2008).
28. Matsuura, T. *et al.* De novo truncating mutations in E6-AP ubiquitin-protein ligase gene (UBE3A) in Angelman syndrome. *Nat. Genet.* **15**, 74–77 (1997).
 29. Silva-Santos, S. *et al.* Ube3a reinstatement identifies distinct developmental windows in a murine Angelman syndrome model. *J. Clin. Invest.* **125**, 2069–2076 (2015).
 30. Sonzogni, M. *et al.* A behavioral test battery for mouse models of Angelman syndrome: a powerful tool for testing drugs and novel Ube3a mutants. *Mol. Autism* **9**, 47 (2018).
 31. Rotaru, D. C., van Woerden, G. M., Wallaard, I. & Elgersma, Y. Adult Ube3a Gene Reinstatement Restores the Electrophysiological Deficits of Prefrontal Cortex Layer 5 Neurons in a Mouse Model of Angelman Syndrome. *J. Neurosci.* **38**, 8011–8030 (2018).
 32. Sailer, C. *et al.* Structural dynamics of the E6AP/UBE3A-E6-p53 enzyme-substrate complex. *Nat. Commun.* **9**, 4441 (2018).
 33. Lee, S. Y. *et al.* Ube3a, the E3 ubiquitin ligase causing Angelman syndrome and linked to autism, regulates protein homeostasis through the proteasomal shuttle Rpn10. *Cell. Mol. Life Sci.* **71**, 2747–2758 (2013).
 34. Kosugi, S., Hasebe, M., Tomita, M. & Yanagawa, H. Systematic identification of cell cycle-dependent yeast nucleocytoplasmic shuttling proteins by prediction of composite motifs. *Proc. Natl. Acad. Sci. USA* **106**, 10171–10176 (2009).
 35. Kawahara, H. *et al.* Developmentally regulated, alternative splicing of the Rpn10 gene generates multiple forms of 26S proteasomes. *EMBO J.* **19**, 4144–4153 (2000).
 36. Besche, H. C., Haas, W., Gygi, S. P. & Goldberg, A. L. Isolation of mammalian 26S proteasomes and p97/VCP complexes using the ubiquitin-like domain from HHR23B reveals novel proteasome-associated proteins. *Biochem.* **48**, 2538–2549 (2009).
 37. Wang, X. *et al.* Mass spectrometric characterization of the affinity-purified human 26S proteasome complex. *Biochem.* **46**, 3553–3565 (2007).
 38. Scanlon, T. C. *et al.* Isolation of human proteasomes and putative proteasome-interacting proteins using a novel affinity chromatography method. *Exp. Cell Res.* **315**, 176–189 (2009).
 39. Tai, H.-C. Characterization of the brain 26S proteasome and its interacting proteins. *Front. Mol. Neurosci.* (2010). doi:10.3389/fnmol.2010.00012
 40. Martinez-Noel, G. *et al.* Identification and proteomic analysis of distinct UBE3A/E6AP protein complexes. *Mol. Cell. Biol.* **32**, 3095–3106 (2012).
 41. Pack, C.-G. *et al.* Quantitative live-cell imaging reveals spatio-temporal dynamics and cytoplasmic assembly of the 26S proteasome. *Nat. Commun.* **5**, 3396 (2014).
 42. Kühnle, S. *et al.* Angelman syndrome-associated point mutations in the Zn²⁺-binding N-terminal (AZUL) domain of UBE3A ubiquitin ligase inhibit binding to the proteasome. *J. Biol. Chem.* **293**, 18387–18399 (2018).
 43. Jantz, D., Amann, B. T., Gatto, G. J. & Berg, J. M. The design of functional DNA-binding proteins based on zinc finger domains. *Chem. Rev.* **104**, 789–799 (2004).
 44. Ramamoorthy, S. & Nawaz, Z. E6-associated protein (E6-AP) is a dual function coactivator of steroid hormone receptors. *Nucl. Recept. Sign.* **6**, e006 (2008).
 45. Reid, G. *et al.* Cyclic, proteasome-mediated turnover of unliganded and liganded ER α on responsive promoters is an integral feature of estrogen signaling. *Mol. Cell* **11**, 695–707 (2003).
 46. Khan, O. Y. *et al.* Multifunction steroid receptor coactivator, E6-associated protein, is involved in development of the prostate gland. *Mol. Endocrinol.* **20**, 544–559 (2006).
 47. Sadhwani, A. *et al.* Two Angelman families with unusually advanced neurodevelopment carry a start codon variant in the most highly expressed UBE3A isoform. *Am. J. Med. Genet. A* (2018). doi:10.1002/ajmg.a.38831
 48. Nawaz, Z. *et al.* The Angelman syndrome-associated protein, E6-AP, is a coactivator for the nuclear hormone receptor superfamily. *Mol. Cell. Biol.* **19**, 1182–1189 (1999).
 49. Krishnan, V. *et al.* Autism gene Ube3a and seizures impair sociability by repressing VTA Cbln1. *Nature* **543**, 507–512 (2017).
 50. Hokayem, El, J. & Nawaz, Z. E6AP in the brain: one protein, dual function, multiple diseases. *Mol. Neurobiol.* **49**, 827–839 (2013).

Acknowledgments

This work was funded by a joined NWO-ZonMw TOP grant (#91216045) to Y.E., B.D. and S.A.K. (to study the mechanism of nuclear UBE3A targeting), by grants from the Angelman Syndrome Foundation (ASF) to Y.E. (to generate and characterize isoform specific *Ube3a* mice) and B.D. (to identify novel targets and activators of UBE3A), by an Erasmus MC grant to Y.E. and S.A.K. (to study UBE3A localization in IPS cells) and by a grant from the Angelman Syndrome Alliance (ASA) to B.D, Y.E. and G.M.v.W. (to characterize UBE3A interacting proteins) and by a fellowship to M.S. from Associazione Angelman and FROM. We are grateful to Minetta Elgersma, Charlotte de Konink and Mehrnoush Aghadavoud Jolfaei for colony management and genotyping, to the Erasmus MC iPS Core Facility for reprogramming and characterization of human iPSC lines, to Lan Huang for providing the HEK293^{RPN11-HTBH} cells, to Casper Hoogenraad for providing the mRFP-PEX3 constructs, to Yana van der Weegen and Evelyn Hanemaaijer for construction of plasmids, to Noam Zelcer for providing material and technical support and to Ben Philpot, Matthew Judson and Minetta Elgersma for critical reading the manuscript and valuable advice.

Author Contributions

Conceptualization: Y.E., B.D., R.A.T., E.J.M. G.M.v.W, and S.A.K; Methodology: Y.E., B.D., R.A.T., M.S., S.N.V.B, G.M.v.W, and E.J.M; R.A.T. carried out mouse neuronal culturing and performed experiments involving confocal imaging and western blotting. M.S. carried out mouse behavior experiments, statistical analysis and contributed to confocal imaging and western blotting experiments. S.N.V.B. carried out yeast two hybrid assays and live confocal imaging experiments. F.I.Z. contributed to confocal imaging experiments and statistical analysis. A.M.P. contributed to confocal imaging experiments, statistical analysis and Western blotting. E.J.M. designed and generated the isoform specific mutant mice and quantified isoform specific RNA. M.v.d.B. made the constructs and performed the GST pull-down experiments. S.T.M., F.M.S.d.V. and S.A.K. contributed to human iPSC studies. J.S., J.M.K. and S.A.K contributed to human postmortem tissue studies. D.C.R. and L.M.C.K. performed and analyzed the electrophysiological recordings, and contributed to the writing of the results section on these experiments. H.H and M.W. contributed to patient recruitment, genotyping and phenotype/clinical data collection and analysis.

Writing - Original Draft: Y.E. and B.D.; Writing – Review & Editing: Y.E., B.D., S.A.K. and R.A.T; Supervision: Y.E., B.D., S.A.K., G.M.v.W, and E.J.M.; Funding acquisition: Y.E., B.D. and S.A.K.

Material and Methods

Cell lines, strains and tissue

HEK293T, HEK293T^{UBE3A-KO} and HEK293^{RPN11-HTBH} cells were cultured at 37°C in a 5% CO₂ humidified incubator in DMEM medium (Lonza) supplemented with 5% Pen/Strep and 10% (v/v) fetal calf serum.

HEK293T^{UBE3A-KO} were generated by CRISPR-Cas 9 technology as previously described⁵¹. Briefly, cells were co-transfected with pSC-TIA-p2A-Blast (generous gift of Prof. Dr. Noam Zelcer) and a gRNA (Table S1) cloned as a BbsI double stranded fragment into px330 (Table S2). Targeted cells were then selected with 5 µg/mL Blasticidin.

HEK293T^{RPN11-HTBH} cells were a generous gift of Dr. Huang and constitutively express an HTBH (6xhis-TEV-biotinylation signal-6xhis) tagged RPN11, a non-ATPase subunit of the 26S proteasome.

Mouse hippocampal, or cortical, primary neurons used for localization studies were isolated from E16.5 male and female wild-type FVB/NHSD embryo brains or from *Ube3a*^{m-/p+} (designated as 'AS' mice) and littermate control embryo brains in the 129S2B6F1/J background. Cells were cultured on poly-D-lysine coated glass coverslips at 37°C in a 5% CO₂ humidified incubator in neuron basal medium (NBM) supplemented with 1% pen strep (P/S), 1% Glutamax and 2% B27 (NBM+++).

iPSCs were derived from primary skin fibroblasts obtained from a 39-year-old female AS patient carrying a point mutation on the maternal allele of UBE3A (c.1730 G>A, p.W577*). The donor's caregiver provided written informed consent in accordance with the Medical Ethical Committee of the Erasmus University Medical Center. Stem cells were derived as described previously using a single, multicistronic lentiviral vector encoding OCT4, SOX2, KLF4 and MYC.25⁵². Quality control of iPSC clones was performed by karyotyping, real-time quantitative PCR and EB differentiation. Derivation and quality control of the Ctrl line (WT) as well as neuronal differentiation was previously described by Gunhanlar et al 2017⁵³. In short neural precursors cells (NPCs) were generated using an EB stage to induced neuroectoderm. To obtain human neurons, NPCs were plated on polyornithine/laminin-coated coverslips in neuronal differentiation medium. After 4 weeks of differentiation, only half of the medium of the cultures was replenished.

Neuronal cultures were differentiated for 6 weeks.

Postmortem brain tissue was obtained from participants enrolled naturalistically through an Erasmus MC postmortem tissue biobank. All procedures with human tissue were performed with the approval of the Medical Ethical Committee (IRB) of the Erasmus MC Rotterdam, including written consent of all subjects for brain donation in accordance with Dutch license procedures and the Declaration of Helsinki.

S. cerevisiae strains used for yeast two-hybrid analysis were Y187 (*MATα*, *ura3-52*, *his3-200*, *ade2-101*, *trp1-901*, *leu2-3, 112*, *gal4Δ*, *met*, *gal80Δ*, *URA3::GAL1UAS-GAL1_{TATA}-lacZ*; Clontech) and Y2H Gold (*MATα*, *ura3-52*, *his3-200*, *ade2-101*, *trp1-901*, *leu2-3, 112*, *gal4Δ*, *gal80Δ*, *met*, *MEL1*; Clontech). Cells were grown at 28°C in rich medium (YPAD; 2% (w/v) glucose, 2% (w/v) Bacto peptone, 1% (w/v) Bacto yeast extract and 40 mg/l adenine) or in minimal glucose medium containing 0.67% (w/v) Yeast Nitrogen Base (YNB) without amino acids (Difco), 2% (w/v) glucose and amino acids as required (20 mg/l uracil, 30 mg/l leucine, 20 mg/l tryptophan, 20 mg/l histidine, 40 mg/l adenine, 20 mg/l methionine) while shaking (200 rpm).

The *E. coli* strain BL21-GOLD (DE3) (B F⁻ *ompT hsdS(r_B⁻ m_B⁻) dcm⁺ Tet^R gal (DE3) endA Hte) was used for the expression experiments. Cells were grown at 37°C or 16°C in LB medium (1% (w/v) Bacto tryptone, 0.5% (w/v) Bacto yeast extract, 1% (w/v) NaCl) supplemented with 2% glucose, 50 mM Tris pH 8 and antibiotics as needed.*

Plasmid construction and DNA manipulation

PSMD4 and UBE3A constructs were amplified from mouse cDNA using a combination of forward and reverse primers as given in Supplementary Table 3, thereby introducing restriction sites at the 5' and 3' end of the gene fragment. PCR products were cloned by A-tailing into pGEMTeasy (Promega) and sequenced. For Y2H, PSMD4 constructs were cloned AscI-NotI into prey vector pGADT7mod, which is a derivative of pGADT7 (Clontech) containing a modified multiple cloning site. UBE3A constructs were cloned AscI-NotI into pYR22, a single copy bait vector, for yeast two hybrid assays and into a pEGFPn3 (Clontech) derived plasmid for expression in mammalian cells (pRA 196).

For the generation of C-terminally GFP-tagged constructs, the GFP open

reading was amplified with oligo's RA299 and RA300 using pEGFPn1 (Promega) as a template, thereby introducing a 5' SphI and a 3' NotI site. The resulting SphI-NotI GFP fragment was used in three fragment ligations with UBE3A AscI-SphI fragments (full length and deletions constructs) to generate in-frame UBE3A-GFP fusions in pRA196 (cut with AscI and NotI).

For GST pull-down experiments PSMD4 constructs were cloned in pGEX2TKmod, which is pGEX2TK (GE Healthcare) with a modified multiple cloning site⁵⁴. The PciI-NotI fragment encompassing full-length PSMD4 and the NcoI-NotI fragment harboring the PSMD4-C-tail (amino acids 324-379) were cloned in pGEX2TKmod digested with NcoI and NotI. The UBE3A fragments used in the GST pull-down experiments were cloned AscI-NotI into pYW5, which is a pRSF-Duet (Novagen) derived vector, thereby introducing a HA tag at their N-termini.

For the generation of the UBE3A point mutations described in this study a standard Quickchange site-directed mutagenesis protocol was employed (Stratagene).

Transfection of neurons

On the day of transfection, mouse hippocampal primary neurons were transferred in NBM supplemented with glutamine (500 μ M) and their conditioned medium was temporarily stored at 37 °C, 5% CO₂. 1.8 μ g of the desired constructs were complexed with Lipofectamine 2000 (Invitrogen 11668-019) and added to the neurons. After 1 hour incubation at 37°C in 5% CO₂, the medium was replaced by the conditioned medium previously stored. Neurons were fixed at the indicated time points.

Transfection of HEK293T cells

The day before transfection 0.2-0.4x10⁶ cells were seeded (on glass coverslips when required for imaging). On the day of transfection between 1.5 mg (for 1 well of a 12 well plate) and 2 mg (for 1 well of a 6 well plate) of DNA were diluted into DMEM serum free medium (100 ml for 1 well of a 12 well plate and 200ml for 1 well of a 6 well plate). Polyethylenimine (PEI, Polysciences Inc 23966) was added to the DNA mix in a ratio DNA (mg): PEI (mg) of 1:3 and the DNA mix was incubated for 15 min. Fresh DMEM (10% FKS, 5% P/S) was added to the HEK293T cells and the DNA mix was added drop-wise to each well. The medium was refreshed after 4-6 hours to prevent PEI toxicity.

Yeast two-hybrid screen

To identify proteins that interact with UBE3A we performed a yeast two-hybrid (Y2H) screen. Approximately 69 x 10⁶ mouse brain cDNA prey clones were screened against a version of UBE3A deleted of its C-terminal six amino acids (UBE3A Δ C6). This C-terminal deletion prevents the E3 ligase from transferring ubiquitin moieties from the active site Cys residue of the HECT domain to bound targets⁵⁵ thereby minimizing interference due to target ubiquitination and/or degradation. Four high confidence interacting proteins were identified in this screen (**Supplemental Figure 3A**) of which two proteins were previously suggested to interact with UBE3A: Ubch7 (also known as UBE2L3; the cognate E2 of UBE3A; 2 clones) and PSMD4 (also known as RPN10 or S5a; 7 clones of which 6 independent). The two novel UBE3A interactors identified were nuclear NOP2/Sun RNA Methyltransferase Family Member 2 (NSUN2; 13 clones of which 7 independent) and presynaptic protein Rabphilin 3A (2 clones). Reanalysis in the Y2H assay showed that all four proteins interacted with full-length mUBE3A-Iso3 and that only PSMD4 lost its interaction with UBE3A when the AZUL domain was deleted (**Supplemental Figure 3B**).

Yeast two-hybrid assay

Yeast two-hybrid assays were performed essentially as described previously⁵⁶ using *S. cerevisiae* strains Y187 and Y2H Gold. Briefly, Y187 cells transformed with the bait constructs (mouse E6AP constructs) and Y2H Gold cells transformed with the prey constructs (mouse PSMD4 constructs), were selected on minimal agar plates lacking tryptophan or leucine, respectively. Following an O.N. (16h) incubation in selective minimal medium (while shaking, 200 rpm), 2x10⁶ cells of each transformed strain (1:1 ratio) were mated in 2X-YPAD for 24 hrs while shaking (50 rpm) at 28°C. The so obtained diploids were then grown on minimal glucose plates lacking both tryptophan and leucine for 48-72h. Selected colonies were cultured for 16 hrs in minimal glucose medium lacking tryptophan and leucine, re-inoculated at an OD₆₀₀ of 0.2 and grown till an OD₆₀₀ of 1. Cells were then washed with sterile water and serially diluted so as to plate from 10² to 10⁵ cells/spot on minimal glucose agar lacking tryptophan and leucine, and with or without histidine. Minimal glucose agar plates lacking tryptophan, leucine and adenine were used to determine the strength of interaction. Plates were incubated for 4 days at 28°C before analysis.

GST pull-down assay

E. coli BL21-GOLD (DE3) (Agilent 230246) cells transformed with bacterial expression constructs were grown overnight at 37°C in LB medium supplemented with 2% glucose, 50 mM Tris (pH 8) and antibiotics as needed. The next morning cells were inoculated at an OD₆₀₀ of 0.2 and grown at 16°C to an OD₆₀₀ of 0.7. Cells were then induced by the addition of 0.5 mM Isopropyl β-D-1-thiogalactopyranoside (IPTG, Invitrogen Life Technologies 15529-019) and further grown at room temperature for 3-4 hours (for the GST constructs) or at 16°C for 16-18 h (for the UBE3A constructs). Pelleted cells were lysed in cold lysis buffer (50 mM Sodium-phosphate pH 8.0, 150 mM NaCl, 5% (v/v) glycerol, 5 mM 2-Mercaptoethanol, 1 mM PMSF (Sigma P7626), RNase [0.01 mg/ml], DNase [0.01 mg/ml] with protease inhibitor cocktail (Roche) by sonication (Sanyo soniprep). Debris were removed by centrifugation (13,000 xg, 30 min) and the supernatant was filtered through a 0.45 μm filter. IGEPAL CA-630 (Sigma I3021) was added (0.5% w/v final concentration) and the cleared lysate containing the GST-PSMD4 fusion protein or GST alone (control) was incubated with Glutathione Sepharose beads (GE Healthcare) for 2 hours at 4°C (end-over-end). After three wash steps with lysis buffer containing 0.5% IGEPAL CA-630, equal amounts of the second cleared lysate containing HA-UBE3A was added to the beads and incubation was continued for 1 hour at 4°C. Beads were washed three times with lysis buffer containing 0.5% IGEPAL CA-630, and elution was carried out by heating the beads in 1x Laemmli sample buffer (62.5 mM Tris-HCl pH 6.8, 2% SDS, 10% glycerol, 0.004% bromophenol blue) supplemented with EDTA (1mM) and DTT (50mM) prior to SDS-polyacrylamide gel electrophoresis (PAGE). Total lysates and elutions were analyzed by Western blotting using the appropriate antibodies.

26S Proteasome purification

The stable HEK293 cell line expressing Rpn11-HTBH was a generous gift of Dr. Huang (University of California, Irvine). Rpn11-HTBH cells were transfected with UBE3A and PSMD4 constructs using JetPRIME. For each purification experiment a full six well plate of transfected hRpn11-HTBH cells was used and approximately 500ng of DNA were transfected per well. Cells were washed in PBS and incubated for 3-5 minutes with TrypLE. The cell pellets were then collected and lysed in 1 ml of buffer A [100 mM sodium chloride, 50 mM sodium phosphate, 10% (v/v) glycerol, 5 mM ATP, 1 mM DTT, 5

mM MgCl₂, 1x protease inhibitor cocktail (Roche), and 0.5% (v/v) IGEPAL CA-630 (pH 7.5)]. The lysates were centrifuged at 13,000 rpm for 15 min and a sample of the supernatant was taken ("total lysate"). The remaining supernatant was incubated with streptavidin resin (Thermo Fisher Pierce 20349) overnight at 4°C (end-over-end). Next, the streptavidin beads were collected by centrifugation and the supernatant (unbound fraction) was saved. The streptavidin beads were then washed 3 times with 20 bed volumes of lysis buffer and bound proteins were eluted by incubation at 95°C for 5 min with 2x Laemmli sample buffer.

Western blot analysis

For Western blot analysis approximately 20μg of total protein lysates per sample were separated by SDS-PAGE and transferred onto nitrocellulose membranes. Next, membranes were blocked in TBS (10 mM Tris-HCl [pH 8.0], 150 mM NaCl) containing 5% (w/v) powdered milk for 1 hour at room temperature, washed 3 times in TBS-T (TBS with 0.1% Tween-20, Sigma P1379) and incubated at 4°C over-night, rotating end-over-end, with the primary antibody dissolved in TBS-T with 2% (w/v) milk solution. The day after membranes were washed 3 times for 10 minutes with TBS-T and incubated with the secondary antibody dissolved in TBS-T with 2% (w/v) milk for 1 hour. At the end of the incubation, membranes were washed 3 times for 10 minutes with TBS and analyzed by either measuring enhanced chemiluminescence (ECL) or infrared fluorescence (Li-Cor).

Quantification of the Western blots

Quantification of proteins was done using a Odyssey CLx imager and Odyssey 3.0 software (LI-COR Biosciences).

To measure the total amount of UBE3A and the relative amounts of the UBE3A isoforms in tissue of WT, UBE3A isoform-specific mice and human postmortem brain material, the signal obtained from the bands of interest on the Western blots were corrected for background and then normalized using the signal of endogenous actin as reference. The relative amounts of the UBE3A isoforms are given as percentage of the total UBE3A present in WT mice (or human brain material).

Fluorescence microscopy

The following fixation and staining protocols were applied to hippocampal

neurons, cortical neurons and HEK293T cells:

After medium aspiration, cells plated on glass coverslips were incubated with 0.5 ml of 4% PFA/ 4% Sucrose at room temperature for 10 min. Fixed cells were washed 3 times for 5 minutes in PBS at room temperature. Coverslips were incubated over-night at 4°C with the required primary antibody dissolved in GDB solution (0.1% (w/v) gelatin, 0.3% (v/v) Triton X-100, 450 mM NaCl, 16 mM phosphate buffer pH 7.4) at the concentrations indicated by the manufacturer. The day after coverslips were washed 3 times for 5 minutes in PBS at room temperature and incubated 1 hour at room temperature with the required secondary antibody dissolved in GDB solution. Coverslips were washed 2 times for 5 minutes in PBS and incubated in a PB (phosphate buffer, 0.2 M)-DAPI (4',6-diamidino-2-phenylindole, 300nM final concentration, Thermo Fisher Scientific D3571) solution for 10 min at room temperature if required. Coverslips were rinsed briefly in milliQ water and mounted on glass slides using MOWIOL.

Human neurons were fixed and staining using 4% formaldehyde in phosphate-buffered saline (PBS). Primary antibodies were incubated overnight at 4°C in labeling buffer containing 0.05 M Tris, 0.9% NaCl, 0.25% gelatin and 0.5% Triton-X-100 (pH 7.4). Immunofluorescence for human tissue was performed as previous described⁵⁷ with minor alterations. Briefly, human frontal cortex blocks were post-fixed for 48 hours in ice-cold, fresh 4% paraformaldehyde (PFA, 0.1 M phosphate buffer, pH 7.3) at 4°C. Tissue was subsequently transferred to 10% sucrose (0.1 M phosphate buffer, pH 7.3) and stored overnight at 4°C. Embedding was performed in 12% gelatin/10% sucrose, with fixation in 10% PFA/30% sucrose solution for 2 hours at room temperature and overnight immersion in 30% sucrose at 4°C. Serial 40 µm sections were collected along the rostrocaudal axis using a freezing microtome (SM 2000R; Leica, Wetzlar, Germany) and stored until further use. Free-floating sections were washed thoroughly with PBS before being incubated in sodium citrate (10 mM) at 80°C for 45 minutes and rinsed with PBS. Sections were pre-incubated with a blocking PBS buffer containing 0.5% Triton X-100 and 5% bovine serum albumin (BSA) for 1 hour at room temperature. Primary antibody labeling was performed in PBS buffer containing 0.5% Triton X-100 and 1% BSA for 72 hours at 4 °C. Following primary antibody labeling, sections were washed with PBS and incubated with corresponding Alexa conjugated secondary antibodies in PBS buffer

containing 0.5% Triton X-100, 1% BSA for 5 hours at room temperature. Nuclear staining was performed using DAPI (1:10000).

All images were acquired using the LSM700 confocal microscope (Zeiss).

Quantification of fluorescence intensity

Image analysis and quantification were performed with Fiji software. To measure UBE3A and PSMD4 co-localization level, Raw Integrated Density (RawIntDen) was measured for both UBE3A and PSMD4 staining in the nucleus and in the cytoplasm using DAPI and MAP2 staining as a nuclear and a cytoplasmic reference (mask), respectively. For each image, the Nuclear/Cytoplasmic ratio was calculated using the average nuclear and cytoplasmic RawIntDen and normalized against the average Nuclear/Cytoplasmic ratio for DIV1, resulting in the calculation of the fold increase of protein levels in the nucleus during *in vitro* development.

Quantification of *Ube3a-iso1* transcripts

Total RNA was isolated from adult mouse cortex of WT, *Ube3a-iso2^{KO}* and *Ube3a-iso3^{KO}* mice (RNeasy, Qiagen). cDNA was generated (iScript select, Bio-Rad) using specific RT primers situated in exon 11b (see **Supplemental Figure 1**), exon 13 in addition to a primer in Gapdh (internal control), and subjected to QPCR (SYBR Green PCR Master Mix; Applied biosystems). QPCR primers were chosen spanning the exon 10/11a junction and a second reverse primer in exon 11b (exon 10/11b). The DDCq method was applied to determine relative transcript levels.

Generation of *Ube3a-iso2^{KO}* and *Ube3a-iso3^{KO}* mice

To generate mice expressing only the long form of mUBE3A-Iso2, we genome edited the ATG encoding the methionine initiating the translation of the short mUBE3A-Iso3 isoform by mutating this to a GCG encoding an alanine. The first 2 nucleotides of the ATG is located at the 3' end of exon 4 (NM_011668) and a gRNA was designed using the online CRISPR design tool (<http://crispr.mit.edu>) to target a sequence just downstream of the target AT sequence. A pair of oligos for the gRNA were hybridized and ligated into BbsI digested pSpCas9 (BB)-2A-GFP ; Addgene plasmid #48138⁵⁸. A 200 nt single stranded oligonucleotide (ssODN, Integrated DNA technologies) for the HDR-mediated genome editing was designed to include the mutation

to the ATG (AT to GC) and a silent diagnostic DraIII restriction endonuclease site. The plasmid and ssODN were each diluted to a final concentration of 10ng/ul in injection buffer (10 mM Tris/0.1 mM EDTA pH 7.5) and used for pronuclear injections of mouse zygotes. This resulted in *Ube3a*^{mIso3/p+} mice (*Ube3a*^{em1Yelg}; MGI 6158669; in this study referred to as *Ube3a-iso3*^{KO} mice), in the C57BL/6J (Charles River) background.

The same approach was used to generate the mouse solely expressing the short mUBE3A-Iso3, using a gRNA to target the methionine encoding ATG in exon 3 (NM_011668) initiating the translation of the short mUBE3A-Iso3 isoform, and a ssODN in which the ATG was replaced with a TGA stop codon and a silent Ascl restriction site for diagnostic purposes. DNA obtained from the founder pups were used for PCR amplification using primers flanking the targeted site and subjected to Sanger sequence analysis. This resulted in *Ube3a*^{mIso2/p+} (*Ube3a*^{em2Yelg}; MGI 6158671; in this study referred to as *Ube3a-iso2*^{KO} mice), in the C57BL/6J (Charles River) background.

Ube3a-iso2^{KO} and *Ube3a-iso3*^{KO} mice were maintained for 3-8 generations in C57BL/6J (Charles River) background by crossing male *Ube3a*^{pIso2KO/m+} or *Ube3a*^{pIso3KO/m+} mice in C57BL/6J background with female wild-type mice in C57BL/6J background. For behavioral experiments, female *Ube3a*^{pIso2KO/m+} or *Ube3a*^{pIso3KO/m+} mice in C57BL/6J background were bred with WT male in the 129S2/SvPasCrl background to yield *Ube3a*^{mIso2/p+} (referred to as *Ube3a-iso2*^{KO} mice) or *Ube3a*^{mIso3/p+} (referred in the manuscript as *Ube3a-iso3*^{KO} mice) and their WT littermates in the F1 hybrid 129S2-C57BL/6J background (*Ube3a-iso2*^{KO}=15, littermate wild-type=8; *Ube3a-iso3*^{KO}=15, littermate wild-type=7).

Mouse husbandry

Mice were housed in individually ventilated cages (IVC; 1145T cages from Techniplast) in a barrier facility. Mice were genotyped when they were 4-7 days old, and re-genotyped at the completion of the experiments. All animals were kept at 22±2°C with a 12 hours dark and light cycle, and were tested in the light period, provided with mouse chow (801727CRM(P) from Special Dietary Service) and water *ad libitum*. During behavioral testing, mice were group-housed (2-4), except (in rare cases) when fighting between males was observed and during the nest building and forced swim test. All animal experiments were conducted in accordance with the European Commission

Council Directive 2010/63/EU (CCD approval AVD101002016791).

Behavioral test battery

All behavioral experiments were performed during the light period of the light/dark cycle. Both male and female mice at the age of 9-14 weeks were used for the experiments. Mice were acclimatized to the testing room for 30 minutes before each behavioral performance. All behavioral testing and scoring were performed by an experimenter blind to genotype. Behavioral tests were run as previously described^{29,30}, and as listed below.

Accelerating rotarod. Motor capabilities were tested by placing the mice on the accelerating rotarod (4-40 rpm, in 5 minutes; model 7650, Ugo Basile Biological Research Apparatus, Varese, Italy). Mice were tested twice per day with a 45-60 min inter-trial interval for 5 consecutive days (same hour every day). For each day, the average time spent on the rotarod was calculated, or the time until the mouse made 3 consecutive wrapping / passive rotations on the rotarod (latency in seconds). Maximum duration of a trial was 5 min.

Open Field test. Mice were individually placed in a brightly lit 110 cm diameter circular open field and allowed to move for 10 min. The total distance moved by each mouse in the open arena was recorded by an infrared camera (Noldus® Wageningen, NL) connected to the EthoVision® software (Noldus® Wageningen, NL), and the final outcome is indicated as distance moved in meters.

Marble burying test. Open makrolon (polycarbonate) cages (50x26x18 cm) were provided with 4 cm of bedding material (Lignocel® Hygenic Animal Bedding, JRS). On top of the bedding material 20 blue glass marbles were placed in an equidistant 5 x 4 grid and the animals were free to access to the marbles for 30 minutes. Once the time was run out, the mice were gently removed from the cage. The outcome measured is the number of buried marbles, which were scored as buried when covered more than 50% by bedding material.

Nest Building test. Mice were single housed for a period of 5 to 7 days before the start of the experiment. Successively, the used nesting material was replaced with around 11 grams (11±1) of compressed extra-thick blot filter

paper (Bio-rad®) was added to the cage. The amount of the unused nest material was weighed and noted every day for a consecutive of 5 days, each day at the same hour.

Forced swim test. Mice were placed in a cylindrical transparent tank (27cm high and 18cm diameter) filled with water (26±1 degrees Celsius) 15 cm deep for 6 min. The outcome measured is the time in seconds in which the mouse was immobile. The latency of immobility was only assessed during the last 4 min of the test. The mouse was considered to be immobile when he stopped to move, making only movements necessary to keep its head above water.

Electrophysiology

Mice, both males and females of about 10 weeks old, were decapitated under Isoflurane anesthesia, and brains quickly removed and immersed in ice-cold, modified ACSF containing the following (in mM): 125 NaCl, 3 KCl, 1.25 NaH₂PO₄, 26 NaHCO₃, 10 glucose, 7 MgSO₄, and 0.5 CaCl₂, pH 7.3–7.4 when bubbled with 95% O₂–5% CO₂. Next, coronal PFC slices (300 µm) were made and immediately placed in an incubation chamber filled with normal ACSF containing (in mM): 125 NaCl, 3 KCl, 1.25 NaH₂PO₄, 26 NaHCO₃, 10 glucose, 1 MgSO₄, and 2 CaCl₂, pH 7.3–7.4 when bubbled with 95% O₂–5% CO₂. Slices were incubated for about 10–15 min at 35°C followed by stabilization at room temperature, in the same solution, for at least 60 min before they were transferred to the recording chamber. The recording chamber was superfused at a flow rate of 2 ml/min with normal ACSF. Chamber temperature was adjusted to 28–30°C.

Cells were visualized using a Nikon microscope equipped with infrared illumination and differential interference contrast video microscopy. Data was obtained using Multiclamp 700B amplifiers (Axon Instruments, CA, USA). Signals were low-pass filtered at 4 kHz and digitized at 20 kHz using Digidata acquisition interfaces and Clampex software. Whole-cell voltage clamp recordings were obtained from layer 5 pyramidal cells in the infralimbic, or prelimbic regions of the mouse medial frontal cortex, here collectively referred to as the mPFC. The pipette capacitance was compensated and series resistance was continuously monitored but was not compensated. Only recordings with a stable series resistance of less than 15 MΩ were used for analysis. Patch electrodes (2–3 MΩ) were backfilled with internal solution, contained the following (in mM): Cs-gluconate 125, CsCl 2.5, NaCl

4, HEPES 10, EGTA 1, MgATP 2, NaGTP 0.3, and Na-phosphocreatine 2. The pH was adjusted to 7.2–7.4 using KOH. To recover the morphology of the recorded neurons, biocytin (5mg/ml) was included in the patch pipette. For each neuron we obtained both spontaneous excitatory (sEPSC) and inhibitory (sIPSC) currents by voltage clamping the neurons at the reversal potential of GABA(A) and glutamate receptors respectively. sEPSCs, recorded at -70 mV and sIPSC, recorded at 0 mV, were detected using Mini analysis software (Synaptosoft Inc., NJ, USA). To analyze the frequency, events were counted over 5 minutes of recording. To obtain the average events, for each cell, at least 100 non-overlapping events were detected and averaged. The peak amplitude of the average sEPSC, and sIPSC was measured relative to the baseline current.

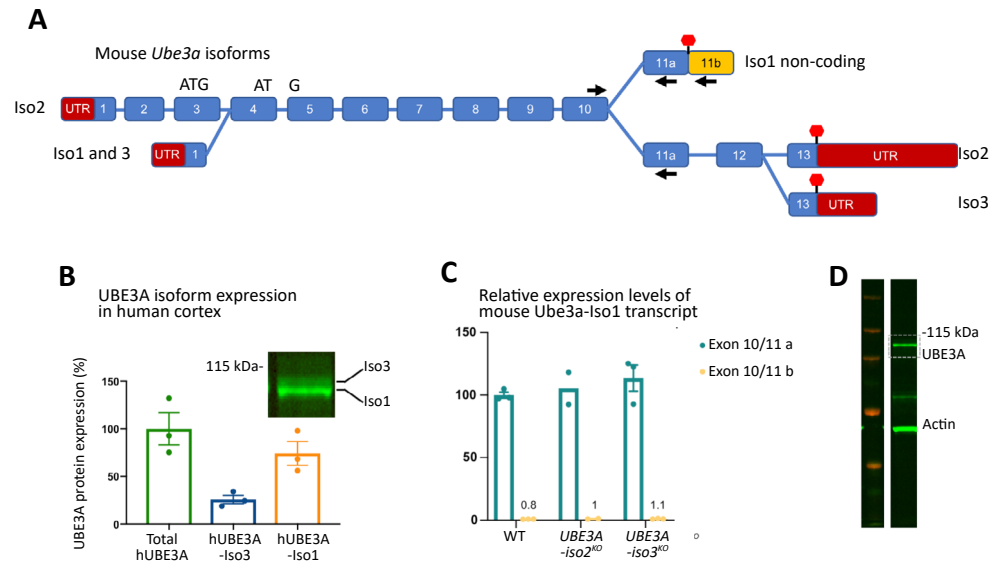
Statistics & Reproducibility

All experiments described in this study have been independently repeated a minimum of three times, except for the experiments in **Figure 4B,e** and **Supplementary Figure 7B**, which were repeated twice.

All mouse behavioral data were statistically analyzed using IBMS SPSS software. Rotarod and nest building tests were analyzed with a factorial repeated measure ANOVA test, while open field, marble burying and forced swim test were analyzed with a 1-way ANOVA test. Student t test was performed for electrophysiological data. Pearson r correlation test was performed to test colocalization between PSMD4 and UBE3A proteins. Behavioral data were tested for normality with the Kolmogorov-Smirnov and Shapiro-Wilk statistic test, and adjustment for multiple comparisons were performed using the Bonferroni post-hoc test. Electrophysiological data distribution was assumed to be normal but this was not formally tested. Electrophysiological and mouse behavioral data are presented as mean ± SEM in all figures. *P* values lower than 0.05 were considered significant. For all tests, statistical significance of genotype was denoted by *p*<0.05 (*), *p*<0.01(**), *p*<0.001(***), *p*<0.0001(****). For the behavioral studies, sample sizes were previously calculated using a large cohort of *Ube3a*^{m-/p+} mice³⁰. For the electrophysiological studies, our sample sizes were similar to those reported in our previous study using *Ube3a*^{m-/p+} mice³¹. No animal or sample was excluded from the analysis. Experiments were randomized with respect to genotypes and treatments, and control experiments (e.g. vehicle or wild-type construct) were interleaved with the experimental conditions. The

investigators were blind to the genotype/treatment during the experiments and outcome assessment.

Supplementary Information



Supplementary Figure 1

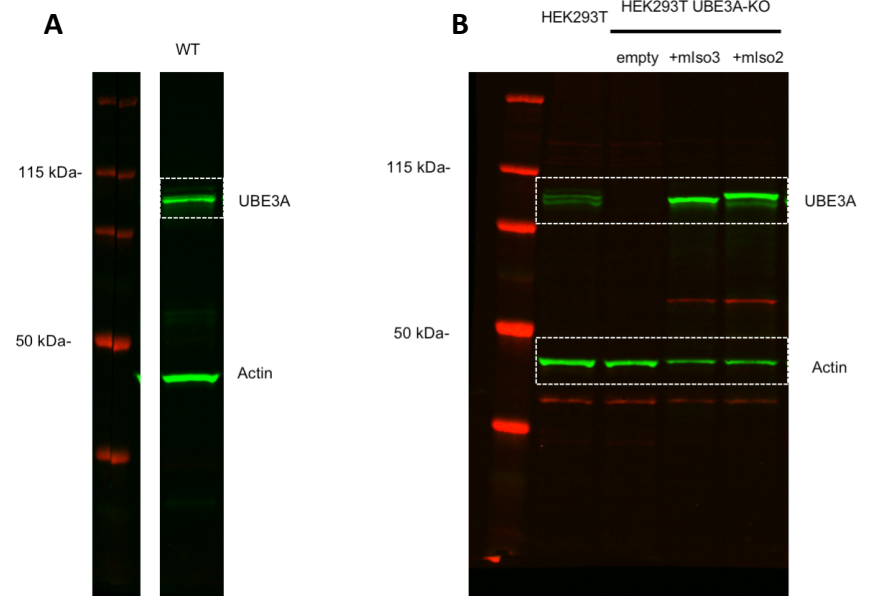
UBE3A isoform expression in mouse and human brain.

A Mouse genomic structure of the *Ube3a* locus indicating the annotated splice variants relative to the longest isoform (Iso 2; NCBI Reference Sequence: NM_011668.3). ATG refers to the initiation codon in exon 3 (UBE3A iso2 protein) and to the initiation codon at the border of exons 4/5 (UBE3A iso3 protein). *mUbe3a-Iso1* (NCBI Reference Sequence: NM_173010.3) is a non-coding transcript, but note that this RefSeq has been removed from the NCBI database because of insufficient support for this transcript.

B Quantification of hUBE3A-Iso3 and hUBE3A-Iso1 of three independent human post-mortem cortical (PFC) lysates. Inset shows a representative UBE3A immunoblot. The image is vertically stretched to separate the isoform bands for better quantification. Data are shown as the mean \pm SEM. $n=3$ biologically independent samples.

C Quantification of *mUbe3a*-Iso1 RNA transcript in wild-type and isoform specific mutant mice. qPCR was performed on cDNA generated from total cortex RNA obtained from WT ($n=3$ mice), *mUbe3a-Iso2*^{KO} ($n=2$ mice) and *mUbe3a-Iso3*^{KO} ($n=3$ mice) mice, by using a reverse primer in exon 11b and exon 13, to determine the relative level of isoform 1 transcripts. The level of exon 10- exon 11a containing transcripts was set at 100%. The relative amount of transcripts containing exon 10-11a-11b was determined using the same forward primer in exon 10 and a reverse in Exon 11b. Note that the levels of *mUbe3a*-Iso1 are very low compared to total *Ube3a* mRNA. Data are shown as the mean \pm SEM.

D Full Western blot used for Supplementary Figure 1B.

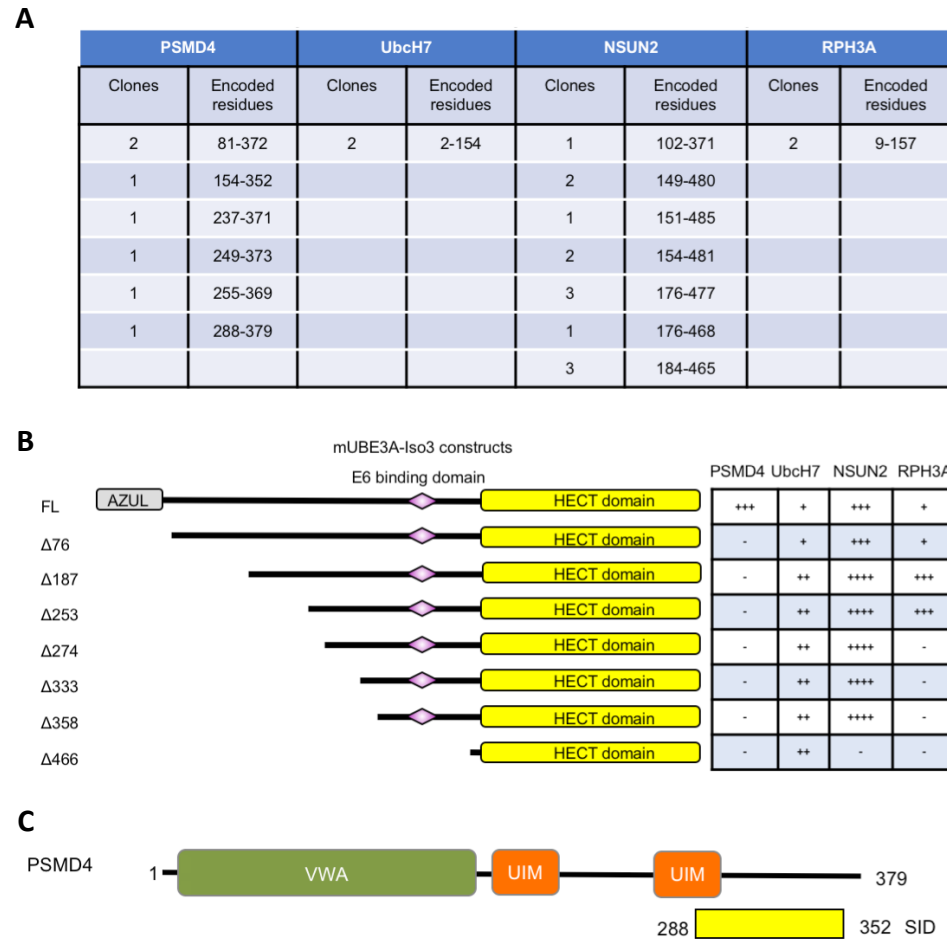


Supplementary Figure 2

Full Western blots from Figures 2a,c.

A Full Western blot used for Figure 2A showing the mUBE3A-Iso2 and mUBE3A-Iso3 isoforms.

B Full Western blot used for Figure 2C showing heterologously expressed mUBE3A isoforms in HEK293T cells.



Supplementary Figure 3

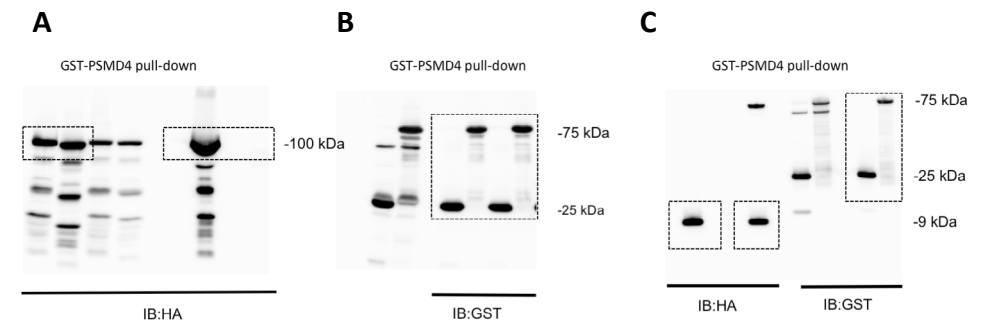
Identification of PSMD4 as binding partner of UBE3A by yeast two-hybrid screening.

A Screening for UBE3A interacting proteins. Mouse UBE3A-Iso3 lacking the C-terminal 6 amino acids was fused in frame to the LexA DNA-binding domain and a custom yeast two-hybrid screen (Hybrigenics) was performed against 69 million independent mouse adult brain cDNA clones, fused to the Gal4 activation domain. Twenty-four high confidence clones, which activated multiple reporter genes, encoding four different proteins were isolated: PSMD4 (also known as Rpn10 or S5a), UbcH7 (cognate E2 of UBE3A), and two novel UBE3A binding proteins, NSUN2 and RPH3A.

B Mapping of the binding sites on UBE3A with the four identified proteins. The full-length mUBE3A-Iso3 (FL) interacts strongly with PSMD4 and NSUN2 while the interaction with RPH3A and UbcH7 is relatively weak. Deletion of the UBE3A AZUL domain ($\Delta 76$, the domain required for nuclear localization of mUBE3A-Iso3)

results in loss of interaction with PSMD4 while interaction with the other three binding partners is unaffected. Upon further deletion the interaction with RPH3A ($\Delta 274$) and NSUN2 ($\Delta 466$) is also lost, showing that the three binding partners, PSMD4, NSUN2 and RPH3A, interact with different regions in the N-terminal domain of UBE3A. All N-terminal deletion constructs harbor the HECT domain, which is the binding site for UbcH7, and therefore the interaction with UbcH7 is unaffected. Strength of interaction was determined by spotting serial dilutions of yeast cells co-transformed with bait and prey plasmids on solid medium plates without histidine or without histidine and containing 10 mM 3-AT (3-amino triazol; inhibitor of the HIS3 gene product), or without histidine and containing 20 mM 3-AT or on medium lacking adenine. ‘-,’ indicates no growth on His-plates (no interaction); +, growth on His- plates (weak interaction); ++, growth on His- +10 mM 3AT plates (medium strength interaction); +++, growth on His- + 20 mM 3AT (strong interaction); +++, growth on plates lacking adenine (Ade-) (very strong interaction).

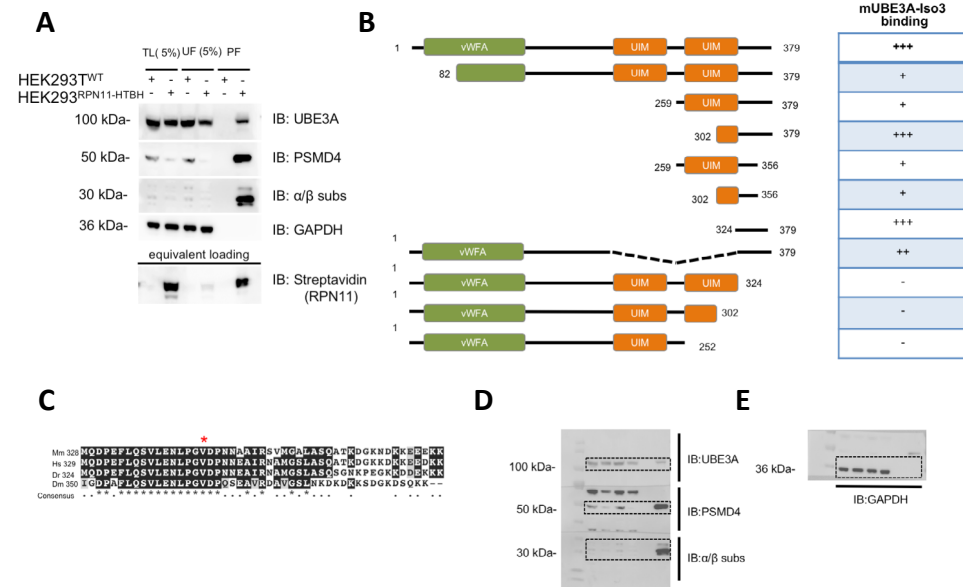
C Graphical representation of the Selected Interaction Domain (SID) of PSMD4, based on the shared overlap of the 6 independently identified PSMD4 clones in the two-hybrid screen (see panel A). Indicated are the von Willebrand factor type A domain (VWA; green) and the two Ubiquitin Interacting Motifs (UIMs) of PSMD4. The SID encompasses approximately half of the second UIM and most of the C-terminal tail (amino acids 288-352).



Supplementary Figure 4

Full Western blots from Figures 4b.

A-B Full Western blots used for Figure 4B showing the pull-down (PD) experiment verifying the interaction of the AZUL domain with PSMD4.



Supplementary Figure 5

Association of endogenous UBE3A with proteasomes and identification of the regions in PSMD4 required for interaction with UBE3A.

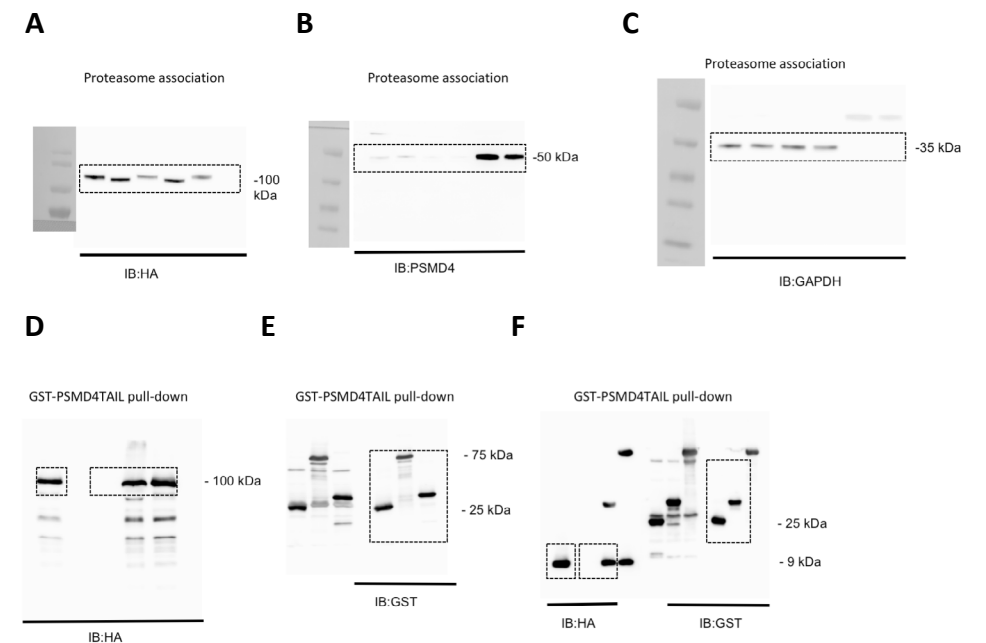
A Association of endogenous UBE3A with proteasomes. Affinity purification of proteasomes from HEK293T^{RPN11-HTBH} cells stably expressing biotinylated Rpn11 (subunit of the 19S regulatory particle) and wild-type HEK293T (control) cells using streptavidin beads. The fractions were analyzed by SDS-PAGE and immunoblotting with the indicated antibodies. 5% of the total lysates (TL) and unbound fractions (UF) were loaded as compared to the affinity-purified proteasome fractions (PF) in all immunoblots, except for the streptavidin immunoblot where equivalent volumes of each fraction were loaded. The UBE3A immunoblot shows that approximately 5% of total, endogenous, UBE3A is recovered in the proteasome fraction (PF) derived from HEK293T^{RPN11-HTBH} cells, but is absent in the PF from control HEK293T cells. The HEK293T^{RPN11-HTBH} derived PF is highly enriched for the α/β subunits of the 20S core particle and PSMD4, a subunit of the 19S regulatory particle, demonstrating that the 20S core particle is recovered together with the 19S regulatory particle. Affinity-purified proteasomes contain very little cross-contaminating proteins as shown by the absence of GAPDH, an abundant cytosolic protein, in the PF fraction. The streptavidin immunoblot shows the high recovery of biotinylated RPN11, which was used as the affinity tag to pull-down proteasomes. Data are representative blots from three independent experiments with similar results obtained.

B Yeast two-hybrid analysis of the UBE3A-PSMD4 interaction. The indicated PSMD4 deletion constructs in a prey vector were tested against mUBE3A-Iso3 in a bait vector. Neither the deletion of the VWA domain nor the UIM domains

of PSMD4, either separately or in combination, abrogates the interaction with UBE3A, indicating that these structural domains in PSMD4 are not required for UBE3A interaction. Strength of interaction was determined as described in the legend to Supplemental Figure 3B.

C Multiple sequence alignment of PSMD4 tails from multicellular species (BoxShade 3.21 software): *Mus musculus* (Mm); *Homo sapiens* (Hs); *Danio rerio* (Dr); *Drosophila melanogaster* (Dm). Residues that are identical in at least three proteins are shaded black, while similar residues are shaded grey. Indicated by a red asterisk is the strictly conserved valine residue (V344 in mouse) that was mutated in this study. Data are representative blots from three independent experiments with similar results obtained.

D-E Full Western blots used for Supplementary Figure 5a showing the association of endogenous UBE3A with proteasomes.

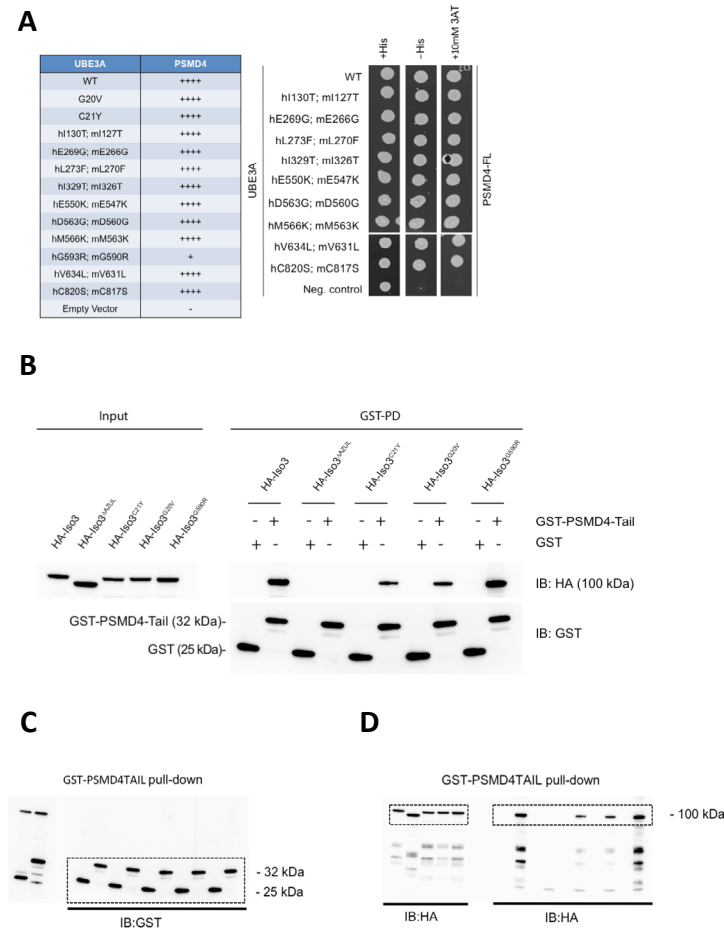


Supplementary Figure 6

Full Western blots used for Figures 4c,e.

A-C Full Western blot used for Figure 4C showing that the AZUL domain is required for binding of UBE3A to the proteasome.

D-F Full Western blot used for Figure 4E showing the pull-down (PD) experiment verifying the interaction between the PSMD4-tail and the AZUL domain.



Supplementary Figure 7

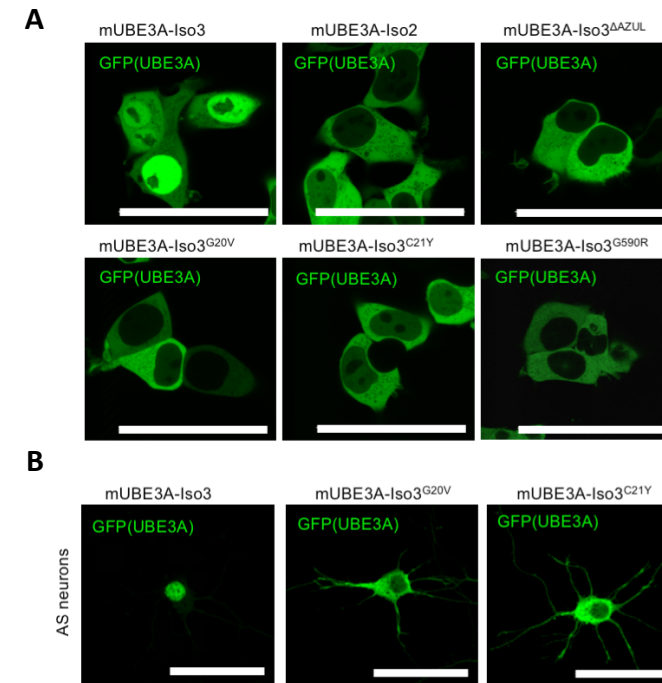
Interaction PSMD4 with AS-associated missense mutations in UBE3A.

A Two-hybrid interaction analysis of PSMD4 with selected AS-associated missense mutations which are distributed broadly throughout UBE3A and covering all mutational hotspots (see Figure 6). Mutations are indicated in the human (h) UBE3A-Iso1 and mouse (m) UBE3A-Iso3 numbering, but were all assessed in mUBE3a-Iso3. Only the hUBE3AG593R/mUBE3AG590R mutant shows a strongly reduced interaction with PSMD4. The interaction of wild-type (WT) mUBE3a-Iso3 is shown as control. Strength of interaction as indicated in the left column, was determined in a spot assay on selective growth media, as described in the legend to Supplemental Figure 3B. A representative yeast two-hybrid spot assay is shown on the right. Representative data from 3 independent experiments with similar results obtained.

B Pull-down (PD) experiment to verify the interaction of the PSMD4-tail with the AS-associated p.G20V, p.C21Y and p.G593R mutations (human UBE3A isoform 1 numbering). GST pull-down experiments were performed on lysates of *E. coli* cells expressing HA-mUBE3A-Iso3FL, HA-mUBE3A-Iso3ΔAZUL, HA-mUBE3A-

Iso3G20V, HA-mUBE3A-Iso3C21Y or HA-mUBE3A-Iso3G590R (G593R in human UBE3A-Iso1). Lysates were incubated with GST-PSMD4324-379 (GST-PSMD4 tail) bound to glutathione beads or GST only (negative control). Eluted proteins were analyzed by immunoblotting using the indicated antibodies (right panels). Inputs (5%) are shown in the left panel. Representative data from 2 independent experiments with similar results obtained.

C-D Full Western blot used for Supplementary Figure 7B showing the pull-down (PD) experiment to verify the interaction of the PSMD4-tail with the AS-associated p.G20V, p.C21Y and p.G593R mutations (human UBE3A isoform 1 numbering).



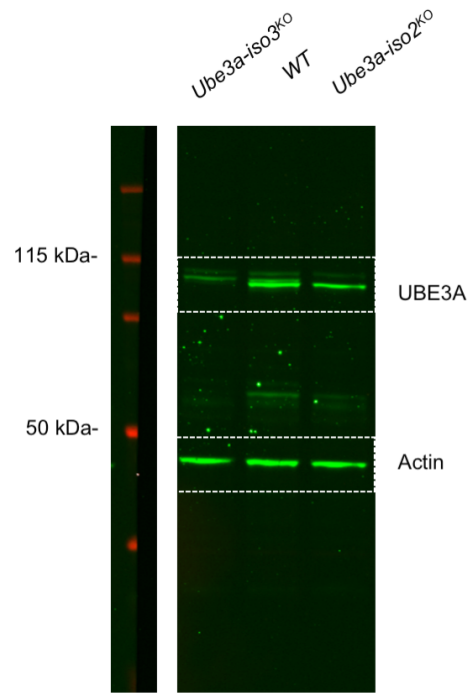
Supplementary Figure 8

AS-associated missense mutations in the Zn-finger of the AZUL domain and in the HECT domain disturb nuclear localization of UBE3A via distinct mechanisms.

A Localization of UBE3A isoforms and AS-linked UBE3A mutants in HEK293T cells. Cells transfected with the indicated UBE3A-GFP constructs were imaged by live cell confocal microscopy approximately 48 hours after transfection. Data are representative images from three independent experiments with similar results obtained.

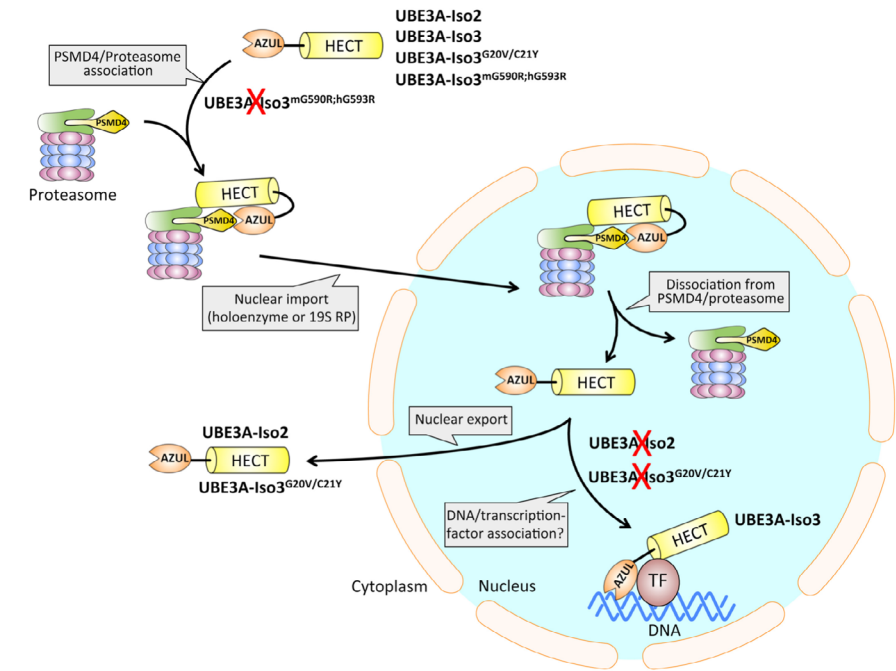
B AS-associated Zn-finger mutations p.G20V and p.C21Y abrogate nuclear localization. Mouse E16.5 derived hippocampal AS neurons transfected at DIV5 with mUBE3A-Iso3^{G20V}, mUBE3A-Iso3^{C21Y} or mUBE3A-Iso3 (WT) were fixed at DIV7.

A-B, scale bar: 50 μm. Data are representative images from three independent experiments with similar results obtained.



Supplementary Figure 9
Full Western blot used for Figure 7B.

Full Western blot for Figure 7B showing selective expression of mUBE3A isoforms in targeted mutants.



Supplementary Figure 10
Model for UBE3A localization.

Nuclear localization of UBE3A is controlled by two steps: (1) PSMD4 mediated import into the nucleus of both isoforms (mediated by the AZUL domain, as well as sequences in the HECT domain which may be required for proper folding) and (2) selective retention of the mUBE3A-Iso3 isoform in the nucleus by means of a functional Zn-finger. The N-terminal extension of mUBE3A-Iso2 interferes with nuclear retention. The AS-associated p.G20V, p.C21Y and p.G593R mutations (human UBE3A isoform 1 numbering; mouse UBE3A-Iso3 p.G590R) cause mislocalization of UBE3A by either affecting import in the nucleus (p.G593R) or by affecting nuclear retention (p.G20V, p.C21Y). See discussion for more details about this model. TF: transcription factor.

Supplementary Table 1, 2, 3 of this Chapter are available at the following DOI link: [10.1038/s41593-019-0425-0](https://doi.org/10.1038/s41593-019-0425-0).

Supplemental References:

51. Loregger, A. *et al.* Haploid Mammalian Genetic Screen Identifies UBXD8 as a Key Determinant of HMGCR Degradation and Cholesterol Biosynthesis. *Arterioscler. Thromb. Vasc. Biol.* **37**, 2064–2074 (2017).
52. Warlich, E. *et al.* Lentiviral vector design and imaging approaches to visualize the early stages of cellular reprogramming. *Mol. Ther.* **19**, 782–789 (2011).
53. Gunhanlar, N. *et al.* A simplified protocol for differentiation of electrophysiologically mature neuronal networks from human induced pluripotent stem cells. *Mol. Psych.* **23**, 1336–1344 (2018).
54. Verschueren, E. *et al.* Evolution of the SH3 Domain Specificity Landscape in Yeasts. *PLoS ONE* **10**, e0129229 (2015).
55. Huibregtse, J. M., Scheffner, M., Beaudenon, S. & Howley, P. M. A family of proteins structurally and functionally related to the E6-AP ubiquitin-protein ligase. *Proc. Natl. Acad. Sci. U.S.A.* **92**, 5249 (1995).
56. Nelson, J. K. *et al.* The Deubiquitylase USP2 Regulates the LDLR Pathway by Counteracting the E3-Ubiquitin Ligase IDOL. *Circ. Res.* **118**, 410–419 (2016).
57. Amin, N. *et al.* A rare missense variant in RCL1 segregates with depression in extended families. *Mol. Psych.* **23**, 1120–1126 (2018).
58. Ran, F. A. *et al.* Genome engineering using the CRISPR-Cas9 system. *Nat Protoc* **8**, 2281–2308 (2013).

CHAPTER 7
General Discussion



General Discussion

Neurodevelopmental disorders encompass a broad spectrum of phenotypes with potential contributions from a large number of genes ¹. Mice and humans are 80 million years apart in evolution, but most of the protein-coding genes are highly conserved ². Because of this, mouse models have been used extensively for modeling human diseases, and for understanding the molecular mechanisms that underlie the formation of differentiated neurons, synapses and the tightly controlled functional neuronal networks. As discussed in **Chapter 1**, one of these neurodevelopmental disorders is Angelman Syndrome (AS), a debilitating disease that is caused by the loss of functional maternally-derived UBE3A protein ^{3,4}. The role of this protein in the pathophysiology of the disease is not known yet and multiple labs are trying to unveil it. The genetic contribution of *UBE3A* in the development of AS encouraged, and still encourages, the development of mutant mouse models, to advance our understanding of biological mechanisms underlying behaviors which are affected in the syndrome.

Mouse models of human neurodevelopmental disorders should be designed optimizing two important key aspects: construct validity, which is the similarity to the underlying causes of the disease, and face validity, which is the resemblance to the human symptoms ⁵.

In **Chapter 2** we extensively explored the robustness of the phenotypes observed in the AS mouse model. The development of treatments for any neurodevelopmental disorder (NDD) including AS heavily relies on the ability to test the efficacy of drugs in mouse models that show reliable, and preferably clinically relevant phenotypes. As previously mentioned, the most commonly used mouse model in AS research, is the one generated by the Beaudet lab in 1998 (*Ube3a^{tm1Alb}*) and is also the main *Ube3a* mouse line tested in **Chapter 2** and **3** of this thesis ⁶. This mouse line together with the recently generated *Ube3a^{mE113X/p+}* (*Ube3a^{tm2Yelg}*) line ⁷, is lacking UBE3A expression, like in AS patients (good construct validity). Moreover, several studies together with **Chapter 2** reported that the mouse model generated by the Beaudet lab captures many key neurological features of the disorder (*e.g.* epilepsy, motor deficits, abnormal EEG), as well as some of the behavioral abnormalities (*e.g.* abnormal sleep patterns, increased anxiety, repetitive behavior ^{6,8-11}). This good face validity reported in **Chapter 2**, but also in many other studies encouraged us to develop a set of behavioral tests that could be useful to

investigate not only the efficiency of potential drugs, but also the robustness of the behaviors that can be useful to test multiple *Ube3a* mouse lines.

The behavioral test battery described in **Chapter 2** covers behavioral paradigms that assess domains of motor performance, anxiety, repetitive behavior and seizure susceptibility, which are all relevant clinical phenotypes of AS. Moreover, one of the most important aspects of the study, is the finding about the robustness of the analyzed behavioral tasks. The test battery with its AS related phenotype has been replicated not only in 8 independent experiments done by 5 different operators, but also in multiple *Ube3a* mouse lines. Thanks to the meta-analysis described in **Chapter 2**, we are now aware of the robustness/weakness of each of the phenotypes (especially in F1 hybrid 129S2-C57BL/6J background).

When it comes to finding the right therapeutic approach not only for AS, but for all neurodevelopmental disorders, there is an urgent need of robust clinically relevant behavioral phenotypes that can help researchers address clinically relevant questions.

Together with the concepts of construct and face validity, another type of validity that must be discussed is the predictive validity, which is about the expected responses to treatments that are effective in the human condition ⁵. Again, the test battery performed with AS mice has been proven to be extremely important in terms of drug validation. Indeed, in **Chapter 2** and **3** we tested the translational value of the behavioral test battery re-evaluating three drugs that were previously tested in clinical trials involving individuals with AS: Minocycline (trial register NCT01531582 ¹² and NCT02056665 ¹³), Levodopa (trial register NCT01281475 ¹⁴) and Gaboxadol (trial register NCT02996305). On one hand, the negative outcomes observed administering Minocycline and Levodopa in clinical trials have been clearly confirmed with the test battery. On the other hand, with regards to Gaboxadol, AS treated mice showed an improvement when tested on the rotating rod, showing a parallel with the human condition.

Given the validity of the AS mouse model and robustness of the standardized test battery, we tried to further address another important clinical question. Promising treatment strategies for AS are directed at unsilencing paternal *UBE3A* gene inactivation ¹⁵. However, for such strategies to be successful, it is important to know when such a treatment should start, and how much UBE3A expression is needed for normal brain development. Previous studies from the Elgersma lab showed that early embryonic *Ube3a* gene reactivation

(E0) results in full phenotypic rescue, whereas a phenotypic rescue was rather limited when *Ube3a* gene expression was induced three weeks after birth¹⁶.

In **Chapter 4** we further delineated the critical period for UBE3A expression during early brain development. In addition, we investigated the importance of embryonic UBE3A expression from the paternal allele in mice with or without maternal UBE3A expression. In other words, we tried to investigate to what extent is bi-allelic UBE3A expression during pre-natal development needed for normal brain development. With the use of the test battery and of a new inducible AS mouse model (*Ube3a^{tm1Yelg}* crossed with Tg(Nes-cre)1Kln) we observed a full rescue of the AS mouse model phenotypes when maternal *Ube3a* gene reactivation was induced around the onset of the last trimester, narrowing down the critical therapeutic window (E12.5-P21). Moreover, we found only a limited effect of silencing UBE3A expression from the paternal allele in AS mice. Combined with previous studies^{6,9,16–18}. **Chapter 4** provides further important information for designing optimal treatment strategies that are aimed at reinstating UBE3A expression in individuals with AS.

While **Chapter 4** is more focused on the function and the importance of having UBE3A expression *during* brain development, **Chapter 5** investigates the function of UBE3A in adulthood. Angelman Syndrome is well known to be a neurodevelopmental disorder, which occurs when UBE3A is missing during brain development. However, **Chapter 5** gives reasons to believe that UBE3A exerts its role not only during brain development, but in a limited way also *after* brain development. As previously mentioned, there are multiple efforts in development to treat Angelman syndrome by reinstating UBE3A expression, either transiently or enduringly^{15,19–21}. Together with Silva Santos' study, **Chapter 4** and **5** highlights that there is likely to be clinical benefit by having enduring UBE3A reinstatement, and that transient UBE3A reinstatement during a critical window of early development is likely to prevent most adverse Angelman syndrome phenotypes. Interestingly, there are a number of phenotypes that seem to be unlinked to a strict critical window. In 2015 Silva Santos showed that Long Term Potentiation (LTP) phenotype has no critical window in which it can be rescued¹⁶. Since LTP is the persistent strengthening of synapses during learning processes, this might suggest that cognitive functions that are affected in AS can be rescued at any time, taking advantage from a transient reinstatement even after brain development. Unfortunately, the test battery does not include a robust

cognitive phenotype that can address this point, limiting the conclusions that can be drawn. Another phenotype that must be mentioned is the forced swim test impairment. This behavior requires the presence of UBE3A not only during brain development, but also afterwards in adulthood, while the mouse is performing the task. We actually do not know how we can translate this phenotype to the human condition, but this is an extremely important aspect in terms of therapy. These findings provide important considerations for upcoming clinical trials in which *UBE3A* gene expression is reactivated, giving more information about when *UBE3A* reinstatement should start and for how long *UBE3A* expression should be maintained.

Finally, **Chapter 6** provides for the first time a new viewpoint on how loss of UBE3A is correlated to AS. Previous literature has established that the synapses of AS mouse models function suboptimally, and this deficit might underlie the severe neurodevelopmental delay observed in AS^{22–28}. Since UBE3A is present in synapses, most of the research on UBE3A has focused on its role in the synapse, but its precise role remained elusive. However, as shown in **Chapter 6**, UBE3A is also present in other subcellular locations, in particular, it is highly abundant in the nucleus. **Chapter 6** is again a good demonstration of the contribution of mouse models to the understanding the molecular mechanisms underlying the pathophysiology of NDDs. With the use of the test battery and especially the development of two new AS mouse models that either express the nuclear form of UBE3A or the cytosolic one, we have been able to show that the nuclear isoform of UBE3A is extremely important for normal brain development. Consistent with an important role of UBE3A in the nucleus, **Chapter 6** suggests that mice which specifically lack the mainly nuclear UBE3A, highly resembled AS mice that lack UBE3A altogether. Interestingly, beside showing behavioral deficits, the synapses of these mice were no longer functioning properly. Several studies suggest that increased excitability is a common feature across neuronal networks from AS mice^{7,29–31} and this is also what we can observe in mice lacking the nuclear form of UBE3A. In contrast, mice that lacked the cytosolic UBE3A appeared unaffected. The recent study reporting 3 AS children affecting the translational start site of human UBE3A isoform 1, further strengthens our hypothesis that the UBE3A ligase exerts important functions in the nucleus (manuscript under review). Given this discovery, future studies should be aimed at elucidating the precise role of the enzyme in the nucleus and how this role relates to the pathophysiology of AS, if in a ubiquitin ligase-

dependent or -independent way or both.

The data obtained with the AS mouse models reported in this thesis highlights important knowledge gained in the field of AS, but still there are some limitations and open questions that need to be discussed and addressed in future studies.

As reported in **Chapter 1** and **2**, one of the key characteristics of AS is intellectual disability. Despite profound cognitive impairments observed in individuals with AS, learning deficits in the AS mouse model are rather mild and the test battery lacks the presence of a cognitive task. Cognition is usually evaluated in rodent models of neurological disorders via the assessment of memory and learning through tasks like the Morris water maze or the fear conditioning test. Several studies have reported learning deficits in AS mice by using the Morris water maze test^{19,32,33}. However, as reported in **Chapter 2** we found that a large number of mice are needed to detect significant differences and results varied strongly among experimenters, making this behavioral task too weak to draw any strong conclusions. The same counts for the fear conditioning test, the outcome of which is very inconsistent even when using the same AS mouse strain, but in different labs and by different experimenters^{6,10,34–37}. In terms of drug testing, this limitation can be quite crucial. Again, the data of Santos and colleagues indicate that the hippocampal LTP shown to be decreased in AS mice has no critical window, suggesting that cognitive phenotypes may be rescued at any time¹⁶. Since we are missing a valid cognitive test, little can be said with preclinical models for example about the power of potential drugs aimed to rescue the cognitive phenotypes observed in AS. Therefore, this is an important aspect that must be addressed with a valid behavioral task which is now missing in the test battery. Beside the Morris Water Maze and the fear conditioning tests, there are many more cognitive paradigms available for assessment of mouse cognition³⁸. A few of these tests that might be included in the test battery and can be useful to investigate cognitive abilities in AS mice are passive and active avoidance tests. These simple tasks are commonly used to examine various memory functions in mice, including acquisition, short-term or working memory, consolidation, and long-term memory³⁸. However, active avoidance tests require a long period of training that is not in line with the idea of quick preclinical drug testing. Another cognitive task that might be used and further standardized in the context of AS is the novel object

discrimination test which permits rapid screening of recognition memory in mice^{7,30–32,39–44}. Passive avoidance tests and novel object recognition tasks are not going to cover all the aspects of cognitive functions, but can provide greater insights into the gene contribution to the AS disorder and can be helpful evaluating potential drug candidates in the pre-clinical model system. Another limitation that has been briefly touched upon in **Chapter 2** is the fact that most of the discovery on AS are based on the use of the *Ube3a*^{tm1Alb} mouse model, in which the only *Ube3a* gene is missing. However, in the context of construct validity, this UBE3A-centric mouse model might not be the only one to be considered to investigate the causes of the disorder. The mutant mouse model (already existing) that should be further investigated is the AS mutant mice with a 1.6-Megabase (Mb) chromosomal deletion from *Ube3a* to *Gabrb3*⁴⁵. This is due to the fact that majority of AS patients have large deletions of the chr15q11-13 region. These mice with maternal, but not the paternal megabase deletion, showed most of the AS related phenotypes like increased spontaneous seizure activity, abnormal EEG, motor, learning and memory impairments, as well as anxiety and abnormal social behavior⁴⁵. Despite the fact that this model is structurally closer to AS deletion mutations encountered in humans (therefore it has better construct validity), very few studies described its potential in understanding the cause underlying AS and in investigating putative effective therapeutics. Further studies using the AS deletion mouse model should be encouraged.

Chapter 6 focused on the need of UBE3A in the nuclear compartment. However, two other important questions must be further addressed. The first one is about the importance of UBE3A in the synaptic compartment, and in particular which brain areas can explain not only the observed behavioral phenotypes, but also the reported neuronal excitation/inhibition imbalance present in AS^{7,31,32,40–44,46}; the second one is about the amount of UBE3A needed in the different cellular compartments.

Aforementioned, it is generally accepted that UBE3A functions as an E3 ubiquitin ligase which links ubiquitin moieties to its protein targets, labelling them for proteasomal degradation, modifying their localisation or impacting their function. With regards to the synaptic compartment, there is indeed a list of direct interactors of UBE3A that might explain the observed neuronal excitation/inhibition imbalance. In hippocampal slices of AS mice, the absence of UBE3A protein results in an increase in synaptic

small-conductance potassium channel 2 (SK2) levels, which leads to tonic inhibition of the NMDA receptor (NMDAR) with impairment of LTP. When in action, UBE3A facilitates SK2 internalization from the synaptic membrane by endocytosis. However, in the context of AS, SK2 hippocampal functionality is missing³⁶. In 2012, Egawa and colleagues showed that tonic inhibition is decreased in granule cells⁴³ and that this is linked to reduced degradation and activity of the GABA (GAT1) transporter. Finally, another important factor for synaptic development which is misregulated in AS is the RhoA guanine nucleotide exchange factor, Ephexin5. This factor negatively regulates excitatory synapse development and it has been found to be degraded after UBE3A ubiquitination⁴⁷. Thus, these synaptic interactors of UBE3A suggest that UBE3A not only has a function in the nucleus as suggested in **Chapter 6**, but also has critical functions in the cytoplasmic compartment, especially in terms of synapse development.

With regards to the function of UBE3A in different brain areas, we must consider that in AS, loss of UBE3A expression occurs in all neurons of the central nervous system^{22,41}. Hippocampus, cortex and cerebellum are the main brain areas that have been investigated in the context of the AS pathology. However, the specific contribution of the different regions of the brain like hippocampus (mainly involved in memory formation and linked to cognitive deficits), cortex and cerebellum (main contributors of motor abilities) to the disease remains difficult to be distinguished.

With regards to the second question, it is important to notice that in **Chapter 6** we showed that in physiological conditions approximately 80% of the total protein is nuclear, while approximately 20% of UBE3A is cytosolic. The UBE3A isoform 3 KO mouse recapitulates all the AS phenotypes, and is missing the majority (80%) of the protein. This is on one hand very interesting, but on the other hand immediately puts forward another question: what if the behavioral phenotypes observed in this model are not only caused by the specific loss of UBE3A from the nuclear compartment, but also by the loss of most UBE3A present in the cell? It is quite interesting that the mouse model lacking 20% of (cytosolic) UBE3A does not show any behavioral phenotypes in the context of the test battery, suggesting that 80% of UBE3A might be enough to fulfill all its biological functions in the cell. While this is mere speculation, it might be interesting to develop a new mouse model that exactly addresses this point. Two possible mouse models that would allow us to address this question come to mind. The first is an AS mouse model

that expresses 20% of nuclear UBE3A (and no cytosolic UBE3A), the second, and possibly even better model, is an AS mouse that expresses no nuclear UBE3A and has increased levels of cytosolic UBE3A amounting to 80% of the normal (wild type) UBE3A levels. With these mouse models we should be able to disentangle the contribution of the total amount of UBE3A needed in the cell from the localization specific contribution to the development of AS phenotypes.

In summary many questions, both scientifically and clinically relevant have been addressed with the use of multiple AS mouse models. From these studies, it is even more clear that UBE3A expression must be tightly regulated both in time and space, and the development of other AS mouse models and behavioral tasks should be encouraged in order to first further understand the molecular mechanism underlying AS and then to develop therapeutic approaches able to help the majority of AS affected patients.

References

1. Martens, G. & van Loo, K. Genetic and Environmental Factors in Complex Neurodevelopmental Disorders. *Current Genomics* **8**, 429–444 (2009).
2. Comparative Genomics | Learn Science at Scitable. Available at: <https://www.nature.com/scitable/knowledge/library/comparative-genomics-13239404/>. (Accessed: 2nd March 2020)
3. Williams, C. A., Frias, J. L. & Opitz, J. M. The Angelman (“Happy Puppet”) syndrome. *American Journal of Medical Genetics* **11**, 453–460 (1982).
4. Kishino, T., Lalande, M. & Wagstaff, J. UBE3A/E6-AP mutations cause Angelman syndrome. *Nature Genetics* **15**, 70–73 (1997).
5. Nestler, E. J. & Hyman, S. E. Animal models of neuropsychiatric disorders. *Nature Neuroscience* **13**, 1161–1169 (2010).
6. Jiang, Y. hui *et al.* Mutation of the Angelman ubiquitin ligase in mice causes increased cytoplasmic p53 and deficits of contextual learning and long-term potentiation. *Neuron* **21**, 799–811 (1998).
7. Wang, T., van Woerden, G. M., Elgersma, Y. & Borst, J. G. G. Enhanced Transmission at the Calyx of Held Synapse in a Mouse Model for Angelman Syndrome. *Frontiers in Cellular Neuroscience* **11**, 1–19 (2018).
8. Allensworth, M., Saha, A., Reiter, L. T. & Heck, D. H. Normal social seeking behavior, hypoactivity and reduced exploratory range in a mouse model of Angelman syndrome. *BMC genetics* **12**, 7 (2011).
9. Miura, K. *et al.* Neurobehavioral and Electroencephalographic Abnormalities in Ube3aMaternal-Deficient Mice. *Neurobiology of Disease* **9**, 149–159 (2002).
10. Huang, H.-S. *et al.* Behavioral deficits in an Angelman syndrome model: effects of genetic background and age. *Behavioural brain research* **243**, 79–90 (2013).
11. Born, H. A. *et al.* Strain-dependence of the Angelman Syndrome phenotypes in Ube3a maternal deficiency mice. *Scientific reports* **7**, 8451 (2017).
12. Grieco, J. C. *et al.* An open-label pilot trial of minocycline in children as a treatment for Angelman syndrome. *BMC neurology* **14**, 232 (2014).
13. Ruiz-Antorán, B. *et al.* Randomized Clinical Trial, Placebo Compared To Evaluate The Efficacy And Safety of Minocycline In Angelman Syndrome (A-Manece Study). *Clinical Therapeutics* **37**, e154–e155 (2015).
14. Tan, W. H. *et al.* A randomized controlled trial of levodopa in patients with Angelman syndrome. *American Journal of Medical Genetics, Part A* 1–9 (2017). doi:10.1002/ajmg.a.38457
15. Meng, L. *et al.* Towards a therapy for Angelman syndrome by targeting a long non-coding RNA. *Nature* **518**, 409–12 (2014).
16. Silva-Santos, S. *et al.* Ube3a reinstatement identifies distinct developmental windows in a murine Angelman syndrome model. *Journal of Clinical Investigation* **125**, 2069–2076 (2015).
17. Gu, B. *et al.* Ube3a reinstatement mitigates epileptogenesis in Angelman syndrome model mice. *The Journal of Clinical Investigation* **129**, 163–168 (2019).
18. Heck, D. H., Zhao, Y., Roy, S., Ledoux, M. S. & Reiter, L. T. Analysis of cerebellar function in Ube3a-deficient mice reveals novel genotype-specific behaviors. doi:10.1093/hmg/ddn117
19. Daily, J. L. *et al.* Adeno-associated virus-mediated rescue of the cognitive defects in a mouse model for Angelman syndrome. *PloS one* **6**, e27221 (2011).
20. Huang, H.-S. *et al.* Topoisomerase inhibitors unsilence the dormant allele of Ube3a in neurons. *Nature* **481**, 185–189 (2011).
21. Meng, L. *et al.* Truncation of Ube3a-ATS Unsilences Paternal Ube3a and Ameliorates Behavioral Defects in the Angelman Syndrome Mouse Model. *PLoS Genetics* **9**, (2013).
22. Dindot, S. V., Antalffy, B. A., Bhattacharjee, M. B. & Beaudet, A. L. The Angelman syndrome ubiquitin ligase localizes to the synapse and nucleus, and maternal deficiency results in abnormal dendritic spine morphology. *Human Molecular Genetics* **17**, 111–118 (2008).
23. Yashiro, K. *et al.* Ube3a is required for experience-dependent maturation of the neocortex. *Nature Neuroscience* **12**, 777–783 (2009).
24. Greer, P. L. *et al.* The Angelman Syndrome Protein Ube3A Regulates Synapse Development by Ubiquitinating Arc. *Cell* **140**, 704–716 (2010).
25. Sato, M. & Stryker, M. P. Genomic imprinting of experience-dependent cortical plasticity by the ubiquitin ligase gene Ube3a. *Proceedings of the National Academy of Sciences of the United States of America* **107**, 5611–5616 (2010).
26. Miao, S. *et al.* The Angelman syndrome protein Ube3a is required for polarized dendrite morphogenesis in pyramidal neurons. *The Journal of neuroscience : the official journal of the Society for Neuroscience* **33**, 327–33 (2013).
27. Yi, J. J. J. *et al.* An Autism-Linked Mutation Disables Phosphorylation Control

- of UBE3A. *Cell* **162**, 795–807 (2015).
28. Kim, H., Kunz, P. A., Mooney, R., Philpot, B. D. & Smith, S. L. Maternal Loss of Ube3a Impairs Experience-Driven Dendritic Spine Maintenance in the Developing Visual Cortex. *Journal of Neuroscience* **36**, 4888–4894 (2016).
 29. Sidorov, M. S. *et al.* Enhanced Operant Extinction and Prefrontal Excitability in a Mouse Model of Angelman Syndrome. *The Journal of neuroscience : the official journal of the Society for Neuroscience* **38**, 2671–2682 (2018).
 30. Rotaru, D. C., van Woerden, G. M., Wallaard, I. & Elgersma, Y. Adult Ube3a gene reinstatement restores the electrophysiological deficits of prefrontal cortex layer 5 neurons in a mouse model of angelman syndrome. *Journal of Neuroscience* (2018). doi:10.1523/JNEUROSCI.0083-18.2018
 31. Kaphzan, H., Buffington, S. A., Jung, J. I. I., Rasband, M. N. & Klann, E. Alterations in Intrinsic Membrane Properties and the Axon Initial Segment in a Mouse Model of Angelman Syndrome. *The Journal of neuroscience : the official journal of the Society for Neuroscience* **31**, 17637–48 (2011).
 32. van Woerden, G. M. *et al.* Rescue of neurological deficits in a mouse model for Angelman syndrome by reduction of alphaCaMKII inhibitory phosphorylation. *Nature neuroscience* **10**, 280–282 (2007).
 33. Huang, H. S. *et al.* Behavioral deficits in an Angelman syndrome model: Effects of genetic background and age. *Behavioural Brain Research* **243**, 79–90 (2013).
 34. Hethorn, W. R. *et al.* Reelin supplementation recovers synaptic plasticity and cognitive deficits in a mouse model for Angelman syndrome. *The European journal of neuroscience* **41**, 1372–80 (2015).
 35. Baudry, M. *et al.* Ampakines promote spine actin polymerization, long-term potentiation, and learning in a mouse model of Angelman syndrome. *Neurobiology of Disease* **47**, 210–215 (2012).
 36. Sun, J. *et al.* UBE3A Regulates Synaptic Plasticity and Learning and Memory by Controlling SK2 Channel Endocytosis. *Cell reports* **12**, 449–61 (2015).
 37. Sun, J. *et al.* mTORC1–S6K1 inhibition or mTORC2 activation improves hippocampal synaptic plasticity and learning in Angelman syndrome mice. *Cellular and Molecular Life Sciences* **73**, 4303–4314 (2016).
 38. Rodriguiz, R. M. & Wetsel, W. C. Assessments of cognitive deficits in mutant mice. in *Animal Models of Cognitive Impairment* 223–282 (CRC Press, 2006). doi:10.1201/9781420004335.ch12
 39. Lueptow, L. M. Novel Object Recognition Test for the Investigation of Learning and Memory in Mice. *Journal of visualized experiments : JoVE* (2017). doi:10.3791/55718
 40. Wallace, M. L., Burette, A. C., Weinberg, R. J. & Philpot, B. D. Maternal Loss of Ube3a Produces an Excitatory/Inhibitory Imbalance through Neuron Type-Specific Synaptic Defects. *Neuron* **74**, 793–800 (2012).
 41. Judson, M. C., Sosa-Pagan, J. O., Del Cid, W. a., Han, J. E. & Philpot, B. D. Allelic specificity of Ube3a expression in the mouse brain during postnatal Development. *Journal of Comparative Neurology* **522**, 1874–1896 (2014).
 42. Judson, M. C. *et al.* GABAergic Neuron-Specific Loss of Ube3a Causes Angelman Syndrome-Like EEG Abnormalities and Enhances Seizure Susceptibility. *Neuron* **90**, 56–69 (2016).
 43. Egawa, K. *et al.* Decreased Tonic Inhibition in Cerebellar Granule Cells Causes Motor Dysfunction in a Mouse Model of Angelman Syndrome. *Science Translational Medicine* **4**, 163ra157–163ra157 (2012).
 44. Bruinsma, C. F. *et al.* Dissociation of locomotor and cerebellar deficits in a murine Angelman syndrome model. 1–11 doi:10.1172/JCI83541.(EMG)
 45. Jiang, Y. H. *et al.* Altered ultrasonic vocalization and impaired learning and memory in Angelman syndrome mouse model with a large maternal deletion from Ube3a to Gabrb3. *PLoS ONE* **5**, e12278 (2010).
 46. Rotaru, D. C., van Woerden, G. M., Wallaard, I. & Elgersma, Y. Adult Ube3a Gene Reinstatement Restores the Electrophysiological Deficits of Prefrontal Cortex Layer 5 Neurons in a Mouse Model of Angelman Syndrome. *The Journal of neuroscience : the official journal of the Society for Neuroscience* **38**, 8011–8030 (2018).
 47. Margolis, S. S. *et al.* EphB-mediated degradation of the RhoA GEF Ephexin5 relieves a developmental brake on excitatory synapse formation. *Cell* **143**, (2010).

Appendix

Summary
Samenvatting
Publications
Curriculum Vitae
PhD Portfolio



Summary

The overall aim of this thesis is to investigate how the use of mouse models can be useful to address several questions relevant to both clinical and fundamental research with respect to Angelman Syndrome (AS). AS is a rare neurodevelopmental disorder caused by the loss of function of the maternal ubiquitin protein ligase E3A (UBE3A), an enzyme involved in the ubiquitination of other proteins. Individuals with AS are characterized by several clinical features like intellectual disability, impaired motor coordination, epilepsy and behavioral abnormalities including autism spectrum disorder features. Studying AS mice shed light on the pathophysiology of Angelman syndrome and reveals potential therapeutic approaches (**Chapter 1**), which are the focus of this thesis.

Chapter 2 describes a battery of behavioral tests, that assess phenotypes covering motor performance, repetitive behavior, anxiety, and seizure susceptibility of AS mice. In this Chapter we combined data of eight independent experiments involving more than 100 AS mice. Using a meta-analysis, we determined the statistical power of the subtests, and the effect of putative confounding factors. We evaluated the robustness of these phenotypes when tested in a standardized manner, which turned out to be useful not only to test pharmaceutical compounds, but also to test different AS mouse models.

Chapter 2 and its addendum **Chapter 3** focus on the use of this behavioral test battery to assess the efficacy of drugs like Minocycline, Levodopa and Gaboxadol which were recently tested in clinical trials of AS. Interestingly, in agreement with the clinical trial results, we found that Minocycline and Levodopa treatment of *Ube3a* mice did not show any sign of improved performance in our test battery. In contrast, Gaboxadol data confirms a possible benefit for Gaboxadol treatment for AS for some of the phenotypes, and emphasizes the translational value of the mouse behavioral testing battery.

Chapter 4 further investigates the critical window for therapeutic intervention in AS, giving also more insights about the function of the paternal *Ube3a* allele in the disease. In neurons, UBE3A expression is tightly regulated by a mechanism of imprinting which suppresses the expression of the paternal UBE3A allele. In mice, full silencing of the paternal allele is achieved in the early perinatal period. Promising treatment strategies for AS are directed at

unsilencing paternal UBE3A gene inactivation. However, for such strategies to be successful, it is important to know when such a treatment should start, and how much UBE3A expression is needed for normal brain development. Previous studies in conditional mouse models of AS suggested that early UBE3A expression is required to rescue the behavioral phenotypes of the AS mouse model. These studies showed that early embryonic *Ube3a* gene reactivation results in full phenotypic rescue, whereas a phenotypic rescue was rather limited when *Ube3a* gene expression was induced three weeks after birth. In Chapter 4, we observed a full rescue of AS-related behavioral phenotypes when gene activation was induced prenatally around the last week of mouse pregnancy, and that approximately 50% UBE3A expression throughout pregnancy is sufficient for normal brain development.

Chapter 5 looks specifically at the role of UBE3A *after* development. Previous studies, as well as **Chapter 4**, examined the functional role of *Ube3a* during embryonic development, giving insights about when *Ube3a* gene reactivation should start to observe the best benefits and phenotype rescues. In **Chapter 5** we examined how long does UBE3A protein need to be expressed in order to fulfill all its biological functions. By deleting the *Ube3a* gene at three ages spanning brain maturation, we emphasized that UBE3A critically impacts early brain development, but plays a more limited role in adulthood. Early embryonic deletion of *Ube3a* recapitulated all behavioral deficits of AS mice. In contrast, *Ube3a* gene deletion at 3 or 12 weeks of age did not have a significant effect on most behavioral tasks, and did not increase seizure sensitivity. Altogether, our findings provide important considerations for upcoming clinical trials in which UBE3A gene expression is reactivated, and suggest that even transient UBE3A reinstatement during a critical window of early development is likely to prevent most adverse Angelman syndrome phenotypes. However, sustained UBE3A expression into adulthood is probably needed for optimal clinical benefit.

Chapter 6 describes a new pathophysiological mechanism underlying AS and stresses the importance of UBE3A subcellular localization in the AS pathogenicity. The two major isoforms of UBE3A exhibit a highly distinct nuclear versus cytoplasmic subcellular localization. By using UBE3A isoform specific mouse models, we showed that the lack of the nuclear UBE3A isoform recapitulates the behavioural and electrophysiological phenotypes of AS mice, whereas mice harbouring a targeted deletion of the cytosolic isoform were unaffected. We identified AS-associated UBE3A missense

mutations that can interfere with either the nuclear targeting (regulated through direct binding to PSMD4/RPN10) or nuclear retention of UBE3A, further suggesting that the nuclear UBE3A isoform is the most critical for AS pathogenicity. Altogether, our data offer for the first time a new viewpoint on the importance of UBE3A in the nucleus.

Samenvatting

Het doel van dit proefschrift is aantonen hoe het gebruik van muismodellen kan bijdragen aan het beantwoorden van zowel klinische als fundamentele vragen met betrekking tot ernstige neurologische ontwikkelingsstoornissen, zoals in dit geval Angelman syndroom (AS). AS is een zeldzame hersenontwikkelingsstoornis die veroorzaakt wordt door een defect in het maternale ubiquitine eiwit ligase E3A (UBE3A). De exacte rol van UBE3A in de ontwikkeling van hersenen is niet bekend. Individuen met AS vertonen verscheidene klinische karakteristieken, waaronder verstandelijke beperkingen, slechte motor coördinatie, epilepsie en gedragsstoornissen, zoals autisme. Het gebruik van AS-muismodellen heeft, naast inzicht in de pathologie van AS, ook de mogelijkheid opgeleverd om potentiële therapieën te bestuderen (**hoofdstuk 1**), wat tevens ook de focus is van dit proefschrift. In **hoofdstuk 2** wordt ingegaan op een reeks van muis gedragsexperimenten die gericht zijn op het onderzoeken van fenotypes met betrekking tot motorfunctie, repetitief gedrag, angst en gevoeligheid voor epileptische aanvallen in AS muizen. In dit hoofdstuk is data van acht onafhankelijke experimenten gecombineerd met in totaal meer dan 100 AS muizen (ook wel *Ube3a* muizen genoemd). Met een meta-analyse is een statistische power vastgesteld voor de sub-experimenten en de daarbij horende mogelijke cofactoren. Dit onderzoek bleek van grote waarde te zijn niet alleen om farmaceutische componenten te bestuderen, maar ook om verschillende AS-muismodellen te onderzoeken, en is een belangrijke component voor alle artikelen in dit proefschrift.

In **hoofdstuk 2** en **hoofdstuk 3** wordt ingegaan op het gebruik van dezelfde reeks muis-gedragsexperimenten om de effectiviteit van medicijnen te bepalen die recent getest zijn binnen de AS kliniek, waaronder Minocycline, Levodopa en Gaboxadol. Opvallend was dat, net als in de klinische testen, Minocycline en Levodopa behandelingen geen effect hadden op de *Ube3a* muizen. Dit in tegenstelling tot Gaboxadol dat een positief effect had op sommige fenotypes binnen de gedragsreeks en daarmee de translationele waarde van dit soort onderzoek benadrukt.

In **hoofdstuk 4** wordt de kritische periode onderzocht voor een therapeutische interventie binnen AS waarbij ook inzicht is verkregen in de functie van het paternale *Ube3a* allel. In neuronen is UBE3A-eiwit expressie strikt gereguleerd door een mechanisme dat “imprinting” wordt genoemd, hierbij wordt de

expressie van het paternale allel in dit geval onderdrukt. In muizen duurt deze onderdrukking voort tot in de vroege perinatale periode. Een veelbelovende behandelingsmethode voor AS is het activeren van dit normaliter onderdrukte paternale *UBE3A* allel. Echter, om succesvol te kunnen zijn, is het van groot belang om te weten wanneer er behandeld moet worden en hoeveel eiwit er uiteindelijk tot expressie moet worden gebracht om het brein normaal te kunnen laten functioneren. Voorgaande studies met conditionele AS knock-out muizen, suggereren dat vroege embryonale expressie van *UBE3A* nodig is om normaal te ontwikkelen. Deze studies toonden aan dat reactivatie van het *Ube3a* gen tijdens de vroege embryonale periode resulteerde in volledig gedragsherstel, wat niet het geval is wanneer het gen werd geactiveerd drie weken na de geboorte. In hoofdstuk 4 vonden wij volledig herstel van de AS gerelateerde gedragsfenotypes wanneer gen activatie geïnduceerd werd rond de start van de laatste week van de muis zwangerschap, en dat ca. 50% *UBE3A* expressie gedurende de gehele zwangerschap voldoende is voor normale hersenontwikkeling.

In **hoofdstuk 5** wordt specifiek gekeken naar de rol van *UBE3A* na de ontwikkeling. In eerder onderzoek, waaronder ook hoofdstuk 4, is de functionele rol van *Ube3a* tijdens embryonale ontwikkeling onderzocht, wat tot verdere inzichten heeft geleid wanneer activatie van het *Ube3a* gen nodig is om het beste resultaat te bereiken. Door het *Ube3a* gen te verwijderen op drie verschillende leeftijden tijdens de ontwikkeling van de hersenen van de muis, laten we in hoofdstuk 5 zien dat *UBE3A* voornamelijk belangrijk is tijdens de vroege hersenontwikkeling en een kleinere rol speelt in het volwassen stadium. Deletie van het gen tijdens de embryonale periode resulteerde in een volledige AS fenotype. Wanneer gen deletie echter in 3 tot 12 weken oude muizen plaatsvond, had dit slechts een gering effect op het fenotype. Samenvattend tonen onze bevindingen aan dat het van groot belang is dat een gen activatie therapie zo spoedig mogelijk gestart wordt. Om een optimaal klinisch effect te bereiken is behandeling tot in volwassenheid waarschijnlijk nodig.

In **hoofdstuk 6** wordt een nieuw pathologisch mechanisme van AS beschreven, waarbij het belang benadrukt wordt van de juiste *UBE3A* subcellulaire lokalisatie. De twee voornaamste isovormen van *UBE3A* verschillen van elkaar in nucleaire versus cytoplasmatische subcellulaire lokalisatie. Met behulp van *UBE3A* isovorm- specifieke muismodellen tonen wij aan dat het ontbreken van de nucleaire *UBE3A* isovorm de meeste overeenkomsten geeft

met AS muizen wanneer we kijken naar gedrags- en elektrofysiologische fenotypes. Muizen waarbij de cytoplasmatische isovorm mist, gedragen zich echter normaal. Missense mutaties in het *UBE3A* gen gerelateerd aan AS, die interfereren met het transport van *UBE3A* naar de kern (gereguleerd door *PSMD4/RPN10*) of interfereren met het verblijf in de kern, benadrukken het belang van de rol van *UBE3A* in de celkern.

Publications

Present Thesis:

Avagliano Trezza R*, **Sonzogni M***, Bossuyt SNV*, Zampeta FI, Punt AM, van den Berg M, Rotaru DC, Koene LMC, Munshi ST, Stedehouder J, Kros JM, Williams M, Heussler H, de Vrij FMS, Mientjes EJ, van Woerden GM, Kushner SA, Distel B, Elgersma Y (2019) Loss of nuclear UBE3A causes electrophysiological and behavioral deficits in mice and is associated with Angelman syndrome. *Nature Neuroscience*. 22(8):1235-1247.

Sonzogni M, Hakonen J, Bernabé Kleijn M, Silva-Santos S, Judson MC, Philpot BD, van Woerden GM, Elgersma Y (2019) Delayed loss of UBE3A reduces the expression of Angelman syndrome-associated phenotypes. *Molecular Autism*. 10:23.

Sonzogni M*, Wallaard I*, Santos SS*, Kingma J, du Mee D, van Woerden GM, Elgersma Y (2018) A behavioral test battery for mouse models of Angelman syndrome: a powerful tool for testing drugs and novel *Ube3a* mutants. *Molecular Autism*. 9:47.

Sonzogni M, Zhai P, Mientjes EJ, van Woerden GM, Elgersma Y (2020) Assessing the requirements of perinatal UBE3A expression for rescue of behavioral phenotypes in a mouse model for Angelman Syndrome. (*Provisionally accepted for Molecular Autism*).

Not in Thesis:

Zampeta FI, **Sonzogni M***, Niggli E*, Lendemeijer B, Smeenk H, de Vrij FMS, Kushner SA, Distel B, Elgersma Y (2020) Conserved UBE3A subcellular distribution between human and mice is facilitated by non-homologous isoforms. (*Submitted to Nature Communications*)

* These authors contributed equally

Curriculum vitae

Monica Sonzogni was born on June 22nd 1990 in Bergamo, Italy. In 2009 after graduating from high school at Liceo Scientifico Lorenzo Mascheroni in Bergamo, she decided to follow the 3 years bachelor program in Biotechnology (School of Sciences) at the University of Milano-Bicocca in Milan (Italy). After graduating from the bachelor program, she decided to continue her academic experience attending the master course of Biotechnology in Medicine (School of Medicine and Surgery) at the University of Milano-Bicocca in Monza (Milan). During the 2 years of master she worked on the study of a rare cardiac genetic disease at the Department of Medical Genetic of the Papa Giovanni XXIII Hospital in Bergamo and the at the Department of Cardiology and Pneumology of the George August University in Goettingen (Germany). At the end of her master in 2015, the author moved to Rotterdam (The Netherlands), where she started her PhD at the Department of Neuroscience at the Erasmus Medical Center under the supervision of Prof. Dr.Ype Elgersma. Her main research activity is presented in this thesis.

PhD Portofolio

Name: Monica Sonzogni
 PhD period: 2015-2019
 Department: Neuroscience
 Promotor: Prof. Dr. Ype Elgersma
 Co-Promotor: Dr. Ben Distel
 Research School: Research School of Neuroscience (ONWAR)

PhD Training**Year**

Course on Laboratory Animal Science (Article 9)	2016
Neuropsychopharmacology	2017
Biomedical English Writing and Communication	2018
Statistic in Neuroscience	2018
Scientific Integrity	2019

Conferences

4th International Angelman Syndrome Scientific Conference, Liverpool (UK)	2015
Dutch Neuroscience meeting, Lunteren (NL) (poster presentation)	2016
European Neuroscience meeting (FENS), Berlin (DE) (poster presentation)	2018
6th International ASA (Angelman Syndrome Alliance) Scientific Conference, Hamburg (DE) (oral presentation)	2018
Bergamo Scienza, Bergamo (IT) (selected speaker)	2019

Seminars and workshops

Neuroscience Department seminar series, Rotterdam (NL)	2015-2019
ONWAR Annual PhD meeting, Zeist (NL) (poster presentation)	2016-2018
ONWAR Annual PhD meeting, Zeist (NL)(oral presentation)	2019

Teaching/Thesis Supervision

Mireia Bernabè Kleijn (Biology and Medical laboratory Sciences_Hogeschool Leiden)	February 2017-December 2017
---	-----------------------------

Acknowledgments

When I arrived in Holland 5 years ago, I never thought of living such an experience as the one I had during my doctorate. I arrived as a girl, afraid and insecure of what the path in Rotterdam was going to be, spending days in the lab with perfect strangers.

These perfect strangers have become a family to me, whom I will forever be grateful to welcoming me and accompanying me with much love during my stay abroad.

Ype, my biggest thanks go to you because you believed in me from day one, despite my perhaps excessive sensitivity and at times of insecurity. During my interview you said: "Once you will be done with your PhD, you will be a different person". You were right. Thanks to the opportunity you have given me, I developed not only scientifically but I also grow as a person. There are not enough words to say how much this experience changed my life. I will always be grateful that you let me be part of your lab.

Dear Ben, or as we were sometimes saying in the lab 'Uncle Ben', I will always admire your passion and love for science. Thanks for the precious suggestions you gave me over the years of my PhD. You have been a real mentor.

I am extremely grateful to my reading committee: Dr. F.M.S. de Vrij, Prof. dr. R. Willemsen and Prof. dr. J.R. Homberg for the time dedicated to the evaluation of this thesis.

Ilse, I have always admired your attention to details and your dedication. I could not have asked for a better colleague while doing all the shared experiments. How many times we spent together with ups and down... This thesis is also the fruit of your precious work and you must be proud of it!

Linda, as I told you once, the first time I saw you I was not sure if you liked me. Now, after all these years spent together, I can say that I found a real friend in you, a genuine person always ready to help me when needed. I really wish you all the best!

Edwin and Diana, you have been my point of reference within the lab. I truly

believe that you are the key to the harmony in the lab. I will forever miss the ironic and *gezellig* moments we spent together.

Rossella and Stijn, like a sister and a brother you arrived in the lab adding a bit of spark. I am lucky to have worked with you during this life experience and to have built a precious friendship with you.

Mattijs and Isabella, you were the last PhD students that I got to know in the lab, but since day one you both showed how much passion and love you have for science. I learned a lot from both of you and you must be proud of the projects you are pursuing.

Minetta and Mehrnoush, I truly believe that the lab without your tremendous amount of experience and professionalism will be lost. Thanks for your patience and for being there for help while planning all the mouse related projects.

A special thanks goes to all the students that I supervised and worked with. It was a pleasure to see how much you enjoyed to work on all the different projects.

Marielle, in your little office you have been my never-ending support, always with a smile from the beginning to the end of my PhD. Thanks a lot for all your help!

Thanks to the Van Woerden lab, to Geeske, Martina and Charlotte for the critical suggestions and support in projects shared together.

Many thanks also to the Kushner lab, Steven and Femke, for your precious contributions to our research projects and for sharing with us your excellent expertise.

Simona e Vincenzo, grazie a voi il mondo era un po' più piccolo e casa più vicina.

Ilaria, sono fortunata ad averti incontrato. Come un raggio di sole dall'Italia mi hai donato positività, motivandomi e spronandomi. Cara amica, ti ammi-

ro: sei una scienziata e una madre modello, un esempio da seguire.

Un sincero grazie va alla fondazione FROM (Fondazione per la Ricerca Ospedale di Bergamo) e all'Associazione Angelman, in particolar modo a Roberta e Luca, splendidi genitori che mai hanno smesso di supportare il lavoro che ho svolto e che, attraverso innumerevoli attività di volontariato, sono riusciti a finanziare diversi progetti di ricerca, volti a trovare la giusta terapia contro la sindrome di Angelman.

Alla mia famiglia e a mia madre, che ha sempre creduto in tutte le mie scelte. Ti sono grata, mamma, perché, in questi ultimi anni passati all'estero e lontano da casa, mi sei stata incessantemente vicina, facendoti pure confidente e psicologa, lenendo la mia malinconia. Essere madre non penso sia semplice, ma spero, un giorno, di essere alla tua altezza.

Infine, un grazie speciale a mio marito, che, sapendo bene la sofferenza e le difficoltà a cui sarebbe andato incontro, ha accolto la mia volontà di partire, attendendo, pazientemente e in silenzio, il mio ritorno. Jacopo, poche persone sarebbero state in grado di fare ciò che noi abbiamo fatto, di costruire, nonostante la distanza, un amore così grande. Ora siamo vicini, una famiglia e se sono riuscita a raggiungere questo traguardo è anche per merito tuo.

